USGS
science for a changing world

Recent U.S. Geological Survey Studies in the Tintina Gold Province, Alaska, United States, and Yukon, Canada—Results of a 5-Year Project

Scientific Investigations Report 2007–5289

U.S. Department of the Interior
U.S. Geological Survey

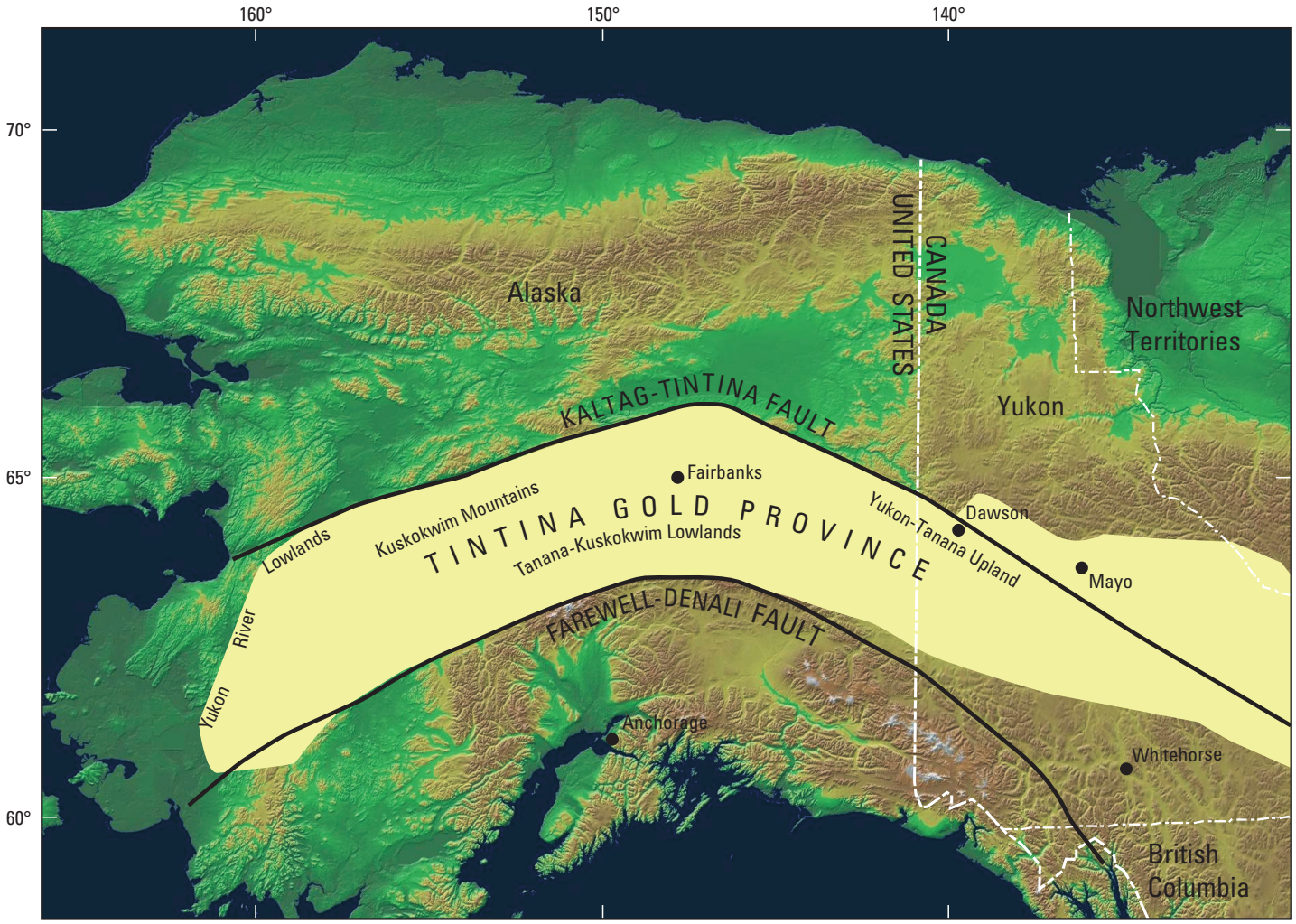

Landsat-based shaded-relief map of the Tintina Gold Province in Alaska and Yukon (courtesy of Craig J.R. Hart, University of Western Australia, Crawley).

Cover. View of a portion of the Black Mountain tectonic zone (ridge in background) looking northeast across the Tibbs Creek drainage within the Yukon-Tanana Upland. This zone, the subject of chapter D of this report, is the locus of almost all of the mineralized base and precious metal veins in the Big Delta B–1 quadrangle. The zone is characterized by complex faulting, shearing, intrusions, and zones of gold and antimony mineralization (photograph by Larry P. Gough).

Recent U.S. Geological Survey Studies in the Tintina Gold Province, Alaska, United States, and Yukon, Canada—Results of a 5-Year Project

Edited by Larry P. Gough and Warren C. Day

Scientific Investigations Series 2007–5289

U.S. Department of the Interior
U.S. Geological Survey

U.S. Department of the Interior
KEN SALAZAR, Secretary

U.S. Geological Survey
Marcia K. McNutt, Director

U.S. Geological Survey, Reston, Virginia: 2010

For more information on the USGS—the Federal source for science about the Earth, its natural and living resources, natural hazards, and the environment, visit http://www.usgs.gov or call 1-888-ASK-USGS

Suggested citation:
Gough, L.P., and Day, W.C., eds., 2010, Recent U.S. Geological Survey studies in the Tintina Gold Province, Alaska, United States, and Yukon, Canada—Results of a 5-Year Project: U.S. Geological Survey Scientific Investigations Report 2007–5289, 148 p.

Tintina Gold Province Project — Editors' Preface and Overview

By Larry P. Gough and Warren C. Day

This report presents summary papers of work conducted between 2002 and 2007 under a 5-year project effort funded by the U.S. Geological Survey Mineral Resources Program, formerly entitled "Tintina Metallogenic Province: Integrated Studies on Geologic Framework, Mineral Resources, and Environmental Signatures." As the project progressed, the informal title changed from "Tintina Metallogenic Province" project to "Tintina Gold Province" project, the latter being more closely aligned with the terminology used by the mineral industry. As Goldfarb and others explain in the first chapter of this report, the Tintina Gold Province (TGP) is a convenient term used by the mineral exploration community for a "region of very varied geology, gold deposit types, and resource potential."

The TGP encompasses roughly 150,000 square kilometers (km^2), bounded by the Kaltag-Tintina fault system on the north and the Farewell-Denali fault system on the south. It extends westward in a broad arc, some 200 km wide, from northernmost British Columbia, through the Yukon, through southeastern and central Alaska, to southwestern Alaska (fig. 1; Goldfarb and others, 2000; Smith, 2000). The climate is subarctic and, in Alaska, includes major physiographic delineations and ecoregions such as the Yukon-Tanana Upland, Tanana-Kuskokwim Lowlands, Yukon River Lowlands, and the Kuskokwim Mountains (Nowacki and others, 2002).

Although the TGP is historically important for some of the very first placer and lode gold discoveries in northern North America, it has recently seen resurgence in mineral exploration, development, and mining activity. This resurgence is due to both new discoveries (for example, Pogo and Donlin Creek) and to the application of modern extraction methods to previously known, but economically restrictive, low-grade, bulk-tonnage gold resources (for example, Fort Knox, Clear Creek, and Scheelite Dome; see Chapter A by Goldfarb and others in this volume). In addition, the TGP hosts numerous other mineral deposit types, possessing both high and low sulfide content, which are currently not in development.

Until the recent increase in exploration activity at the huge Pebble porphyry copper-gold deposit near Iliamna Lake in 2001, by far most of the exploration dollars spent over the past decade, in Alaska and the Yukon for the identification of new gold resources, have been in the TGP. Chapters A and C of this report present new research that improves our understanding of the regional tectonic and hydrologic processes that localized these low-grade, high-tonnage gold resources. Chapter B describes the tectonic setting and metallogenesis of volcanogenic massive sulfide deposits in the Bonnifield mining district south of Fairbanks and provides the geologic framework for Chapters E and J.

The TGP covers a vast region with very limited road or navigable river access. Thus, remote sensing techniques are critical for characterizing the geologic framework for the region. Geophysical studies, such as aeromagnetic surveys employed to help define the Black Mountain tectonic zone described in Chapter D, are often the only technique available to rapidly detect major tectonic features at the regional scale. Chapter E presents the results of satellite-borne remote sensing techniques using the Advanced Spaceborne Thermal Emission and Reflection Radiometer (ASTER) sensor mapping of hydrothermal alteration patterns associated with volcanogenic massive sulfide and porphyry deposits in the Bonnifield mining district. The technique detected some of the known mineral deposits in the region, as well as mineralogically similar targets that may represent potential undiscovered deposits. The research presented demonstrates that the ASTER technique is an extremely powerful tool for remotely characterizing the bedrock mineralogy, and hence, rock type, in areas with minimal to no vegetation cover within the TGP.

In addition, geochemical, hydrogeochemical, and biogeochemical signatures are presented for both regional, unmineralized areas, and more localized deposit-specific areas throughout the TGP. Sampled media include soils, sediments, surface water, ground water, and vegetation. These signatures are interpreted in the context of bedrock mineralogy and geochemistry, weathering, and soil-forming processes, as well as bioavailability considerations. The information obtained assists in understanding the transport and mobility of trace elements—some of which are important in an environmental context. The environmental signature studies were designed to incorporate the expertise and research capabilities of several disciplines. All such studies rely on an understanding of the geologic and hydrogeologic framework of the region.

Chapter F demonstrates a creative approach using aufeis ("ice" fields localized in drainage basins) as an unconventional proxy for the location of faults along high-gradient alpine drainages. The concept is that aufeis is an accumulation of winter ice, up to several meters thick, along stream and river valleys in arctic and subarctic environments, and is preferentially associated with high-gradient streams. This aufeis formed as a result of discharge of ground water from beneath a permafrost layer within the stream channels. Recent bedrock geologic mapping of the Big Delta B–2 quadrangle indicates that the streams in which aufeis occurs are underlain by throughgoing, high-angle brittle faults, suggesting that the faults are hydraulically conductive to ground water flow. Minor or no aufeis accumulations were observed contemporaneously in other drainage valleys where no extensive fault structures have been mapped, implying that aufeis formation results from more than a topographic effect or discharge from bank storage. Thus, the presence of thick and extensive aufeis in high-gradient streams may be a useful aid to identifying geologic structures in arctic and subarctic climates.

Epigenetic gold deposits are the principal exploration targets within the TGP at this time. Characterizing the geochemical dispersion of pathfinder elements associated with mineralizing systems in the natural environment is a powerful exploration tool. Chapter G synthesizes the efforts to study the natural dispersion of the pathfinder elements arsenic (As) and antimony (Sb) associated with several epigenetic gold mineralizing systems in the TGP. Arsenic and antimony also have garnered attention from the scientific community and the general public due to their potential toxicity. Understanding the fundamental geochemical controls on the natural and anthropogenic distribution of arsenic and antimony in the environment is critical for both mineral exploration and human health communities. This study found that the mobility of arsenic and antimony is controlled primarily by the local reduction-oxidation reaction (redox) environment, with arsenic being less mobile in oxidized surface waters relative to antimony, and arsenic more mobile in reduced ground waters.

A broad approach to landscape geochemistry is presented in Chapter H, which investigates the geochemical linkage among stream waters, streambed sediments, soils, and vegetation with that of regional bedrock. This study provides important premining data for any future mineral development in the Goodpaster River watershed, which lies in the heart of the Yukon Tanana Upland of east-central Alaska. A more focused study is provided in Chapter I, which characterizes the geochemical signature of a volcanogenic massive sulfide (VMS) deposit in the Bonnifield district of central Alaska. The Red Mountain base-metal deposit is a rare, natural laboratory that allows study of an acid-generating, metal-leaching VMS mineral deposit exposed in an undisturbed environment. Dissolution of pyrite and associated secondary reactions under near-surface, oxidizing conditions are the primary causes for the acid generation and metal leaching of the rocks at Red Mountain. However, the acidic waters mix with surrounding alkaline waters that have interacted with carbonate veinlets, resulting in self-mitigation via dilution, neutralization, and attendant co-precipitation. This process limits downstream hydrogeochemical evidence of the deposit to within a few kilometers. Chapter J reports on the occurrence and biogeochemistry of unusual plant species, and of their supporting sediment and soils, in the area of the Red Mountain deposit. Field studies of these occurrences are important for understanding the habitat requirements of rare or unusual species and for a full appreciation of the ecology and biogeochemical diversity of mineralized areas.

Finally, Chapter K is a bibliographic listing of all reports that have been published by USGS personnel since inception of the TGP project in 2002. As noted in the acknowledgments, many of the reports are the result of the work with colleagues from other government agencies as well as academia and industry.

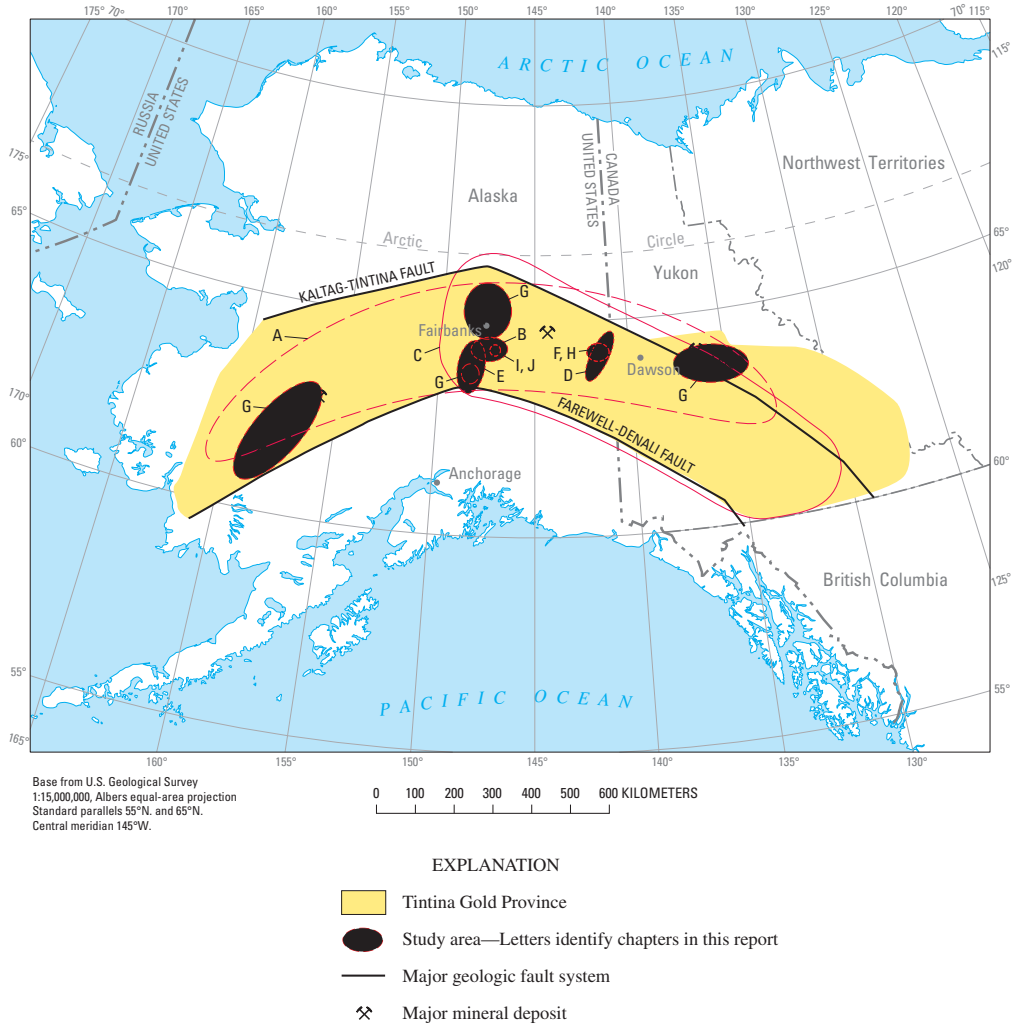

Figure 1. Study areas within the Tintina Gold Province of Alaska and Yukon covered by the individual chapters (letters) in this compilation (see table of contents).

Acknowledgments

We would especially like to thank the following list of key agencies, universities, and industries that provided valuable logistical and technical assistance during both the field work and data interpretation phases of this effort:

Alaska Department of Natural Resources
- Division of Geological and Geophysical Surveys
- Division of Mining, Land and Water
- Division of Forestry

Alaska Department of Environmental Conservation
Avalon Gold Corporation
Calista Corporation
Doyon, Ltd.
Fairbanks Gold Mining, Inc.
Grayd Resource Corporation
Geo-Watersheds Scientific
NovaGold Resources, Inc.
Pacific Alaska Resources Company
Pacific Rim Geological Consulting
Teck Cominco, Ltd.
TNR Resources, Ltd.
University of Alaska, Anchorage
University of Alaska, Fairbanks
University of Colorado, Boulder
University of Western Australia
U.S. Bureau of Land Management
U.S. Department of Agriculture, Natural Resources Conservation Service
U.S. Geological Survey, Mineral Resources Program
U.S. National Park Service
- Denali National Park and Preserve
- Yukon-Charley Rivers National Preserve

Yukon Geological Survey

References Cited

Goldfarb, R.J., Hart, C.J.R., Miller, M.L., Miller, L.D., Farmer, G.L., and Groves, D.I., 2000, The Tintina gold belt: a global perspective, *in* Tucker, T.L., and Smith, M.T., eds., The Tintina gold belt—Concepts, exploration and discoveries: British Columbia and Yukon Chamber of Mines Special Volume 2, p. 5–34.

Nowacki, G.J., Spencer, Page, Fleming, Michael, Brock, Terry, and Jorgenson, Torre, 2002, Unified ecoregions of Alaska, 2001: U.S. Geological Survey Open-File Report 02–297, scale 1:4,000,000.

Smith, M.T., 2000, The Tintina gold belt: an emerging gold district in Alaska and Yukon, *in* Tucker, T.L., and Smith, M.T., eds., The Tintina gold belt—Concepts, exploration, and discoveries: British Columbia and Yukon Chamber of Mines Special Volume 2, p. 1–3.

Contents

[Letters designate the chapters]

Conversion Factors and Notes

Multiply	By	To obtain
	Length	
centimeter (cm)	0.3937	inch (in.)
millimeter (mm)	0.03937	inch (in.)
meter (m)	3.281	foot (ft)
kilometer (km)	0.6214	mile (mi)
	Area	
square kilometer (km^2)	247.1	acre
	Volume	
liter (L)	33.82	ounce, fluid (fl. oz)
cubic meter (m^3)	35.31	cubic foot (ft^3)
ounce, fluid (fl. oz)	0.02957	liter (L)
	Pressure	
kilobar	1000	kilopascal (kPa)
	Flow rate	
cubic meter per second (m^3/s)	35.31	cubic foot per second (ft^3/s)
liter per second (L/s)	15.85	gallon per minute (gal/min)
	Mass	
microgram (µg)	0.00000003527	ounce avoirdupois (oz)
milligram (mg)	0.00003527	ounce avoirdupois (oz)
gram (g)	0.03527	ounce avoirdupois (oz)
megagram (Mg) = metric ton (t)	1.102	ton, short (2,000 lb)
megagram (Mg) = metric ton (t)	0.9842	ton, long (2,240 lb)
	Density	
kilogram per cubic meter (kg/m^3)	0.06242	pound per cubic foot (lb/ft^3)
	Ore grade	
gram per metric ton (g/t)	0.032	ounce avoirdupois, per ton (oz/ton)
ounce avoirdupois, per ton (oz/ton)	31.25	gram per metric ton (g/t)

Temperature in degrees Celsius (°C) may be converted to degrees Fahrenheit (°F) as follows:

°F=(1.8×°C)+32

Specific conductance is given in microsiemens per centimeter at 25 degrees Celsius (µS/cm at 25 °C).

Concentrations of chemical constituents in water are given either in milligrams per liter (mg/L), micrograms per liter (µg/L), or parts per million (ppm).

Concentrations of chemical constituents in soil are given in milligrams per kilogram (mg/kg).

Geology and Origin of Epigenetic Lode Gold Deposits, Tintina Gold Province, Alaska and Yukon

By Richard J. Goldfarb, Erin E. Marsh, Craig J.R. Hart, John L. Mair, Marti L. Miller, and Craig Johnson

Chapter A of
Recent U.S. Geological Survey Studies in the Tintina Gold Province, Alaska, United States, and Yukon, Canada—Results of a 5-Year Project

Edited by Larry P. Gough and Warren C. Day

Scientific Investigations Report 2007–5289–A

U.S. Department of the Interior
U.S. Geological Survey

Contents

Figures

Tables

Geology and Origin of Epigenetic Lode Gold Deposits, Tintina Gold Province, Alaska and Yukon

By Richard J. Goldfarb,[1] Erin E. Marsh,[1] Craig J.R. Hart,[2] John L. Mair,[3] Marti L. Miller,[1] and Craig Johnson[1]

Abstract

More than 50 million ounces of lode gold resources have been defined in the previous 15 years throughout accreted terranes of interior Alaska and in adjacent continental margin rocks of Yukon. The major deposits in this so-called Tintina Gold Province formed around 105 to 90 million years ago in east-central Alaska and Yukon, and around 70 million years ago in southwestern Alaska, late in the deformational history of their host rocks. All gold deposits studied to date formed from CO_2-rich and ^{18}O-rich crustal fluids, most commonly of low salinity. The older group of ores includes the low-grade intrusion-related gold systems at Fort Knox near Fairbanks and those in Yukon, with fluids exsolved from fractionating melts at depths of 3 to 9 kilometers and forming a zoned sequence of auriferous mineralization styles extending outward to the surrounding metasedimentary country rocks. The causative plutons are products of potassic mafic magmas generated in the subcontinental lithospheric mantle that interacted with overlying lower to middle crust to generate the more felsic ore-related intrusions. In addition, the older ores include spatially associated, high-grade, shear-zone-related orogenic gold deposits formed at the same depths from upward-migrating metamorphic fluids; the Pogo deposit is a relatively deep-seated example of such. The younger gold ores, restricted to southwestern Alaska, formed in unmetamorphosed sedimentary rocks of the Kuskokwim basin within 1 to 2 kilometers of the surface. Most of these deposits formed via fluid exsolution from shallowly emplaced, highly evolved igneous complexes generated mainly as mantle melts. However, the giant Donlin Creek orogenic gold deposit is a product of either metamorphic devolatilization deep in the basin or of a gold-bearing fluid released from a flysch-melt igneous body.

Introduction

During the previous 5 years, we have carried out geological and geochemical studies of the major lode gold deposits in interior Alaska and adjacent Yukon, Canada. This area, termed the Tintina Gold Province (TGP), is a region of important new mineral discoveries and exploration interest. Our investigations included detailed descriptions of mineralization styles, mineralogical assemblages, geochemical signatures, and geochronological relations. Igneous rocks that are spatially and temporally associated with the deposits were studied in regard to their genesis and possible relation to the gold-bearing hydrothermal systems. Detailed fluid-inclusion and stable-isotope ore-genesis work was carried out to place geochemical constraints on the ore-forming fluids. Local ore-deposit models for the gold deposit types within the TGP were constructed from the data collected during the research program.

Overview and History of the Tintina Gold Province

The TGP is an area of greater than 150,000 square kilometers (km^2) that includes much of interior Alaska and adjacent parts of central Yukon (fig. A1; Goldfarb and others, 2000; Smith, 2000; see figure 1 of Editors' Preface and Overview). In Alaska, this highly mineralized province includes the area between the regional-scale Kaltag-Tintina and Denali-Farewell fault systems. Where the province continues to the east in Yukon, it is located northeast of the Kaltag-Tintina fault system. This vast region is defined by more than 15 individual gold belts and districts, which traditionally were mainly mined for their placer resources. Recently, however, many of these belts and districts have begun to be recognized for their lode gold potential.

This broad and arc-shaped region, which is about 2,000 km in length and continues from Yukon to southwestern Alaska, was first referred to as the Tintina Gold Belt in 1997 by many company geologists. It was mainly a promotional term for a region of highly varied geology, gold deposit types,

[1]U.S. Geological Survey.

[2]Mineral Deposit Research Unit, The University of British Columbia.

[3]Geoinformatics Exploration Inc., Australia.

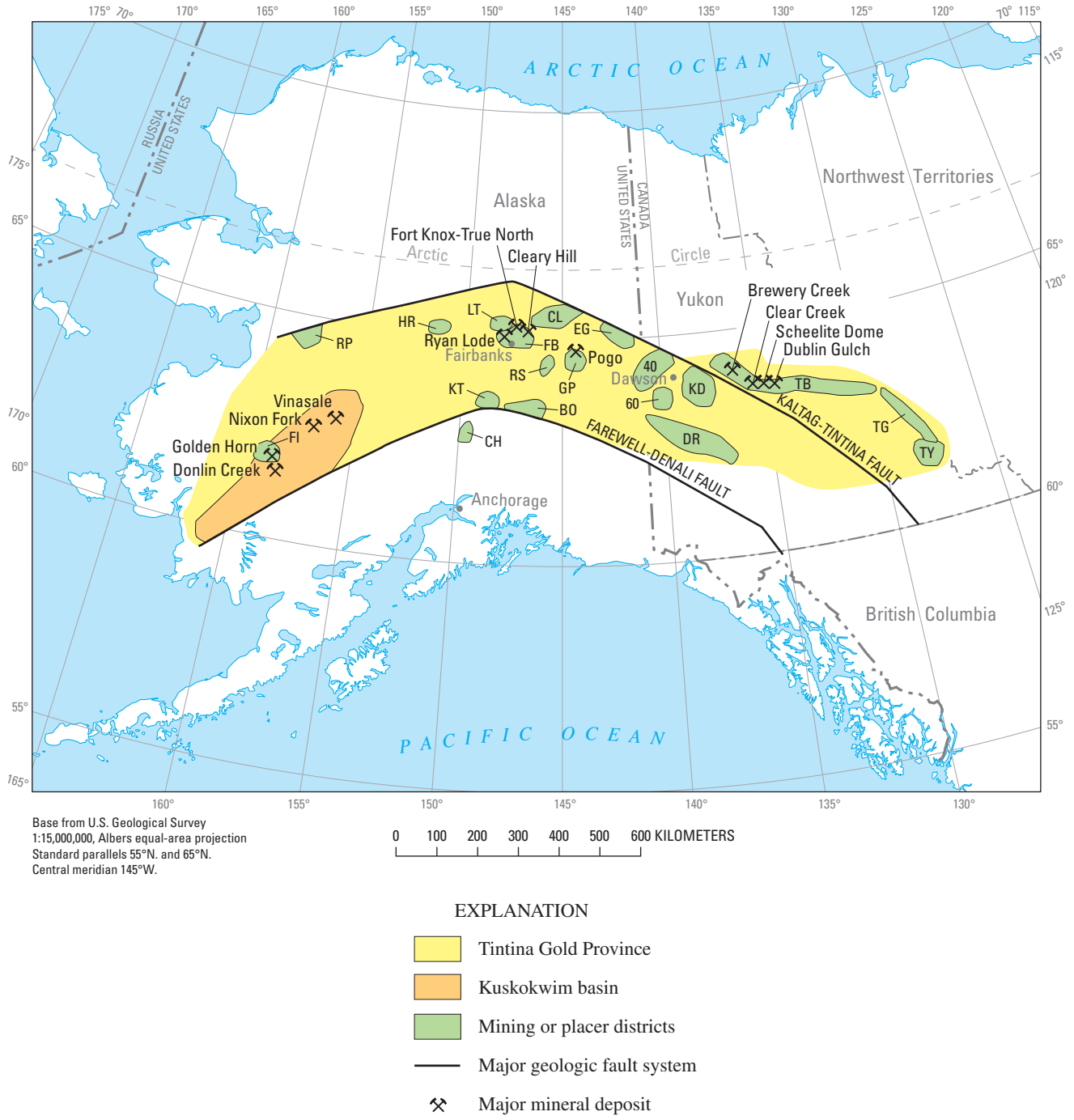

Figure A1. Main gold districts of the Tintina Gold Province of interior Alaska and adjacent Yukon, Canada. The districts are all known for their historic placer gold production, but many areas, notably the Kuskokwim, Fairbanks, Goodpaster, and Tombstone regions, have seen high levels of exploration and concomitant discovery and development during the last 15 years. Mining or placer district names abbreviated as follows: 40, Fortymile; 60, Sixtymile; BO, Bonnifield; CH, Chulitna; CL, Circle; DR, Dawson Range; EG, Eagle; FB, Fairbanks; FI, Flat-Iditarod; GP, Goodpaster; HR, Hot Springs-Rampart; KD, Klondike; KT, Kantishna; LT, Livengood-Tolvana; RP, Ruby-Poorboy; RS, Richardson; TB, Tombstone; TG, Tungsten; TY, Tay River (after Hart and others, 2002).

Figure A2. *A*, Underground development of the high-grade, flat-lying gold orebodies at the Pogo deposit, Goodpaster district, began in 2006. *B*, The first large-scale lode gold development in the Tintina Gold Province was at the Fort Knox deposit near Fairbanks, where low-grade gold ore has been mined since 1996 by open pit methods.

and significant resource potential. Because it was really not a distinct belt and was composed of numerous mineral districts of differing ages and characteristics, Hart and others (2002) argued that it simply be viewed as a large gold province within the northern North American Cordillera and termed the region the TGP. Most significantly, the province includes the Clear Creek, Scheelite Dome, Dublin Gulch, and Brewery Creek deposits of central Yukon; the Fairbanks and Goodpaster gold districts of east-central Alaska; and the lodes of the Kuskokwim basin of southwestern Alaska.

Exploration in the eastern part of the TGP began near the turn of the 20th century. At about the time of the great Klondike (in Yukon) gold rush of 1898, placer gold fields were identified in the eastern part of the TGP, both to the east of the Klondike at Scheelite Dome, Dublin Gulch, and Clear Creek (1894-1901) and to the west in the Fairbanks district of Alaska (1901). Those in the Fairbanks district yielded more than 8 million ounces (Moz) of gold during the 1900s, with other significant (0.5-1.0 Moz of gold each) east-central Alaskan placer districts (fig. A1) including Circle, Fortymile, Eagle, Circle Hot Springs-Rampart and Livengood-Tolvana (Goldfarb and others, 1997). The Yukon placer fields in the TGP were all small; the largest is probably Clear Creek, and it has yielded only 130,000 oz of gold (Allen and others, 1999). Historical lode production had been minor; through the mid-1990s, there was almost no lode gold production from Yukon (Hart and others, 2002) and only a few hundred thousand ounces of gold were mined from a few small, high-grade (10-30 grams per metic ton (g/t) gold) quartz vein systems near Fairbanks (McCoy and others, 1997). However, recent exploration and development of the high-grade Pogo deposit within the Goodpaster district (figs. A1, A2*A*; Smith and others, 1999), located about 150 km southeast of Fairbanks, has led to the start of mining of a 5.6 Moz gold resource late in 2006.

Technological advances during the last decade and favorable existing infrastructure (Mueller and others, 2004) have allowed for the economically successful recovery of large volumes of gold ore for the first time in the eastern Alaska-Yukon region from material with grades of less than 1 g/t of gold (table A1). In 1996, the Fort Knox deposit, located 20 km northeast of Fairbanks, was put into production as a low-grade, bulk-tonnage resource (fig. A2*B*). It has so far yielded more than 4.5 Moz of gold, and has at least 4.6 Moz of gold remaining (Bakke, 1995; Bakke and others, 2000; Kinross Gold Corporation, 2009). During the previous 10 years, the Scheelite Dome, Dublin Gulch, and Clear Creek properties have been continually evaluated for similar bulk-tonnage gold resources. The nearby Brewery Creek deposit was mined for almost 250,000 oz of gold between 1995 and 2002, from shallow oxidized ore zones where refractory gold had been naturally liberated into a form that could be heap leached (Hart and others, 2002).

The first exploration recorded within the western part to the TGP was by Russian prospectors in the Kuskokwim basin in the early 1800s. They discovered the first among many small mercury- and antimony-bearing quartz vein systems that are located throughout southwestern Alaska (Bundtzen and Miller, 1997). Between 1901 and 1916, placer gold accumulations were discovered in many parts of southwestern Alaska, and the resulting districts in the westernmost part of the TGP yielded slightly more than 3 Moz of gold during the subsequent 100 years. A very small amount of gold was recovered from gold-bearing quartz veins at the Golden Horn deposit in the Flat-Iditarod district between 1922 and the mid-1980s (Bull, 1988). U.S. Geological Survey work in the mid-1980s indicated significant gold concentrations in many of the mercury and antimony deposits in the central Kuskokwim basin (Gray and others, 1990), and isotope and fluid-inclusion studies indicated that hydrothermal fluids responsible for

Table A1. Major lode gold resources of the Tintina Gold Province (updated from Hart and others, 2002).

[Abbreviations: Moz, million ounces; g/t, grams per metric ton]

Deposit	Location	Endowment (Moz)	Grade (g/t)	Production to date (Moz)
Donlin Creek	Kuskokwim basin	31.7	2.91	none
Fort Knox	Fairbanks district	9.2	0.93	4.6
Pogo	Goodpaster district	5.6	18.9	1.2
Dublin Gulch	Selwyn basin	1.96	0.916	none
Cleary Hill	Fairbanks district	1.6	34.0	0.5
Shotgun	Kuskokwim basin	1.1	0.93	none
Vinasale	Kuskokwim basin	0.92	2.4	none
Brewery Creek	Selwyn basin	0.85	1.44	0.27
True North	Fairbanks district	0.79	1.69	0.44

formation of these mineral deposits were typical of those that form many lode gold deposits (Goldfarb and others, 1990). Since that work, significant gold resources at historic stibnite prospects have been delineated at Vinasale Mountain and particularly Donlin Creek (table A1), with the latter being one of the world's largest gold deposits known to date.

Geology and Gold Deposits of Central Yukon

The Yukon part of the TGP (fig. A3) is underlain by Neoproterozoic to Early Carboniferous continental margin rocks of the Selwyn basin, a fault-controlled depression developed on the edge of the North American craton. Gold deposits are hosted by phyllite, psammite, calc-phyllite, conglomerate, and marble of the Neoproterozoic to Early Cambrian Hyland Group (Murphy and others, 1993). Middle Jurassic to Early Cretaceous folding, thrusting, and lower greenschist-facies metamorphism of these rocks reflects seaward accretion of terranes along the continental margin. A 750-km-long belt of mainly felsic intrusions, termed the Tombstone-Tungsten belt (TTB), was emplaced into these rocks around 96 to 90 million years ago (Ma) and approximately 8 to 10 million years (m.y.) subsequent to final deformation (Hart, Mair, and others, 2004).

The notably reduced igneous rocks (Thompson and Newberry, 2000; Hart, 2007) of the TTB can be divided into the informally named Mayo, Tungsten, and Tombstone suites (Hart, Mair, and others, 2004). Most of the gold deposits, including those at Scheelite Dome, Clear Creek, and Dublin Gulch, are associated with the subalkaline, metaluminous to slightly peraluminous monzogranites to quartz monzonites, with minor granodiorite, of the Mayo suite. Isotopic data indicate that these rocks of the Mayo suite, as is common in many postcollisional settings, represent a mixture between potassic magmas that were generated in the subcontinental lithospheric mantle (SCLM) and those formed in the overlying lower to middle crust (John L. Mair, Geoinformatics Exploration, Inc., unpub. data, 2008). Emplacement of the more felsic and fractionated, weakly peraluminous, monzogranites and granites of the Tungsten suite, mainly generated from melted continental crust, is associated with formation of world-class tungsten skarn deposits at the easternmost end of the TGP. The least reduced, metaluminous, predominantly syenites of the Tombstone suite, generated from enriched SCLM, are associated with more copper-rich gold occurrences and, in addition, with the gold ores that were mined at Brewery Creek.

The Clear Creek gold deposits consist of auriferous sheeted quartz veins (fig. A4*A*) that cut six stocks of the Mayo suite and, to a lesser degree, are hosted by the surrounding 3- to 5-km-wide zones of hornfels rocks (Marsh and others, 1999, 2003). The veins contain 1 to 2 percent pyrite and arsenopyrite, with lesser pyrrhotite, scheelite, and bismuthinite. The more gold-rich veins may contain greater than 1 percent arsenic, and 100 to 1,000 parts per million (ppm) of both tungsten and bismuth. Gold to silver ratios range from 1:1 to 5:1. Individual veins are generally 0.2 to 5 centimeters (cm) wide and tens of meters long. Vein densities are 3 to 5 veins per meter. Narrow alteration envelopes of quartz, potassium feldspar, and biotite, with some sericite, pyrite, chalcopyrite, hematite, and calcite, surround the quartz veins. Tourmaline and albite are also present in some of the veins. Several small tungsten-tin and tungsten-gold skarns occur where the country rocks are more calcareous. Dates on the stocks by U-Pb techniques are around 91.5 Ma; $^{40}Ar/^{39}Ar$ ages from vein-related micas are around 90 Ma.

The main part of the Dublin Gulch deposit is localized within the apical zone of a granodiorite stock of the Mayo suite (Maloof and others, 2001; Hart and others, 2002). The 600×400-meter (m) area hosts steep, sheeted quartz-feldspar extensional veins (fig. A4*B*), each a few centimeters in width, containing gold, molybdenite, lead-bismuth-antimony sulfo-

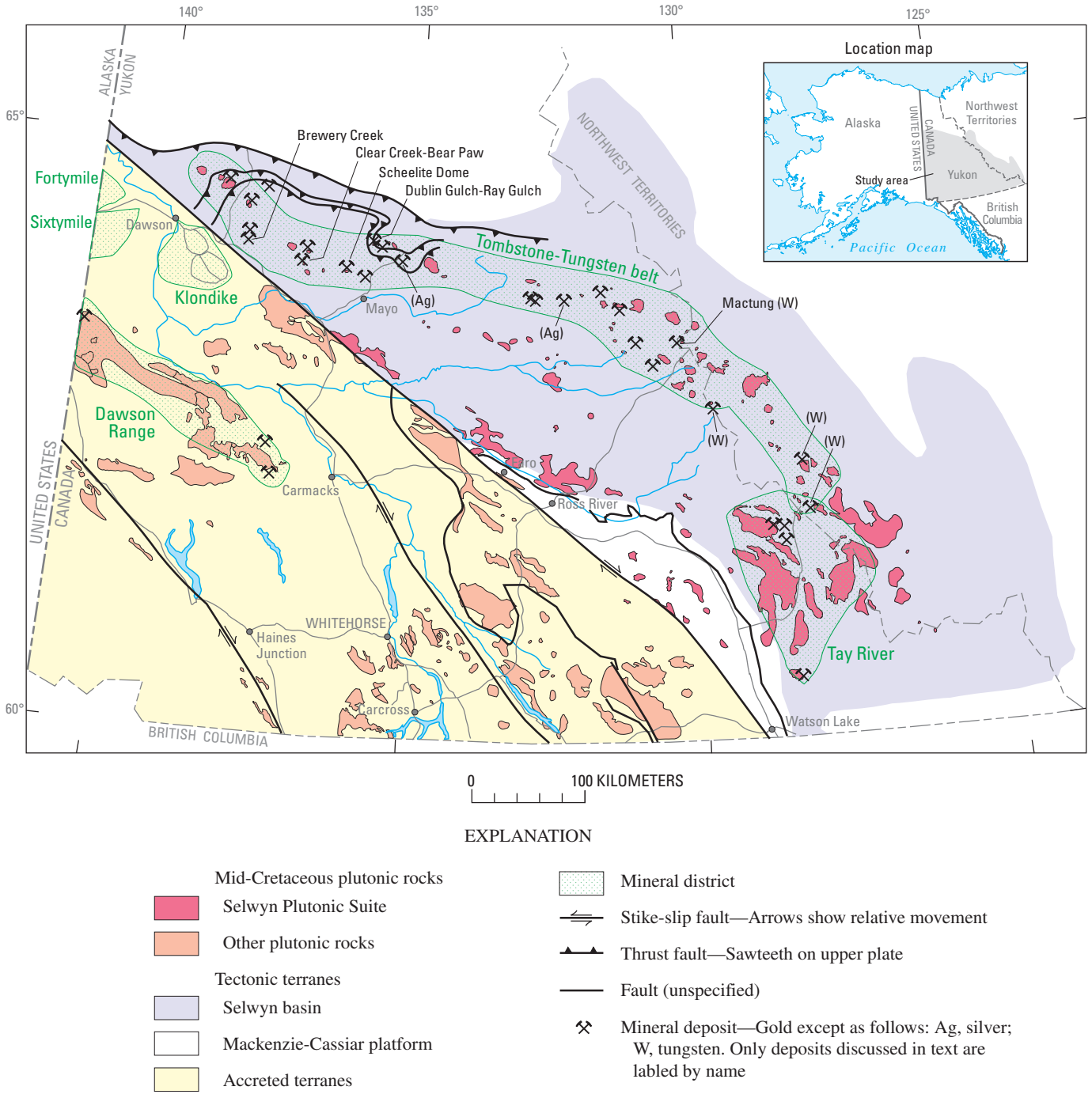

Figure A3. Gold, sliver, and tungsten deposits of the Tombstone-Tungsten magmatic belt in Yukon define the easternmost part of the Tintina Gold Province.

salts, galena, and bismuthinite; alteration phases include albite, potassium feldspar, sericite, carbonate, and chlorite. The deposit is within a few kilometers of the Ray Gulch tungsten skarn deposit, and silver- and lead-bearing veins are in more distal locations. Both pluton emplacement and vein formation are around 94 to 93 Ma (Selby and others, 2003).

In contrast to the other Yukon deposits, the gold occurrences at Scheelite Dome are dominantly hosted by hornfels and are more diverse in style (Mair and others, 2000, 2006). Gold is common in reduced skarns, quartz-feldspar-carbonate veins, and as disseminations in areas of carbonate- and sericite-altered country rocks, mainly in a 10×3-km east-trending zone. The extensional veins are 0.5 to 3 cm wide, and have densities of about 10 veins per meter. In addition to gold, they contain arsenopyrite, pyrite, quartz, albite, ankerite, microcline, muscovite, and tourmaline. Consistent geo-

Figure A4. *A*, Typical gold- and scheelite-bearing, sheeted quartz±feldspar±muscovite veins cutting granite at Dublin Gulch occurrence in Yukon. *B*, Gold-bearing sheeted veins from Dublin Gulch with potassium-feldspar-rich alteration envelope and low-sulfide, quartz-rich infill. *C*, Highly fractured and veined ore from Fort Knox showing dominant "sheeted" veins, and intersecting cross-veins. This is unlike typical stockworks in porphyry deposits. The larger central vein also contains alkalic feldspar. Note the limited alteration selvages adjacent to the veins.

chemical anomalies for bismuth, tellurium, and tungsten also characterize the veins. Alteration selvedges on the walls of the veins include muscovite, carbonate, quartz, and sulfide mineral phases. Locally, gold and scheelite are present in sheeted veins in the monzogranite to quartz monzonite igneous rocks. $^{40}Ar/^{39}Ar$ dates on gold-related hydrothermal biotite are within 2 m.y. of the 94.59±0.90 Ma U-Pb crystallization age for the igneous rocks. Small silver-, antimony-, lead-, and (or) zinc-bearing quartz vein occurrences surround the Scheelite Dome gold-bearing occurrences.

Geology and Gold Deposits of East-Central Alaska

The east-central Alaskan part of the TGP (fig. A5) is underlain by medium- to high-grade metamorphic rocks, which include those of the widespread Fairbanks-Chena assemblage (Dusel-Bacon and others, 2006). Neoproterozoic to middle Paleozoic protoliths for the metamorphic rocks are mainly clastic sedimentary rocks, with lesser carbonate and magmatic units (Foster and others, 1994). Regional metamorphism likely occurred in the Late Jurassic to Early Cretaceous. The country rocks have been widely intruded by Early Cretaceous felsic to intermediate batholiths, stocks, and dikes. Similar to those of Yukon, these igneous rocks are reduced, have low ferric-to-ferrous ratios (less than 1), and are of low magnetic susceptibility (Hart, Goldfarb and others, 2004). In the Fairbanks area, they occur as shallowly emplaced (less than 3 to 5 km), 94 to 90 Ma isolated domal bodies; in the Goodpaster district, they are more deeply emplaced (5 to 9 km, Dillworth, 2003), widespread 113 to 102 Ma batholiths and 99 to 95 Ma smaller bodies (Day and others, 2007).

In the Fairbanks district, the Fort Knox deposit is located in the apex of a variably porphyritic, monzogranite to granodiorite stock (fig. A2*B*; Bakke, 1995). The gold occurs in steeply dipping, commonly sheeted, quartz-potassium-feldspar veins and in planar quartz veins that occur along later gently to moderately dipping shear zones cutting the igneous rocks (fig. A4*C*). High fineness gold in the veins is commonly intergrown with native bismuth, bismuthinite, and tellurobismuth (McCoy and others, 1997). Total sulfide volumes are much less than 1 percent and include phases such as pyrite, pyrrhotite, arsenopyrite, scheelite, and molybdenite. Alteration phases include potassium feldspar, albite, biotite, sericite, and ankerite. An Re-Os date on hydrothermal molybdenite of 92.4±1.2 Ma is identical to the crystallization age of the Fort Knox stock (Selby and others, 2002). Isotopic data from the ore-hosting stock at Fort Knox indicate an origin similar to Cenomanian magmas in Yukon, reflecting both mantle and crustal contributions (Haynes and others, 2005).

Numerous smaller gold deposits are also spread throughout the Fairbanks district (fig. A6; Goldfarb and others, 1997; McCoy and others, 1997; Bakke and others, 2000; Hart and others, 2002). The True North deposit (figs. A5, A6), originally prospected 100 years earlier as an antimony prospect, was mined for gold at a small scale, providing additional feed for the Fort Knox mill, from 2001 to 2005. This deposit, located about 20 km northwest of Fort Knox, comprises gold in quartz veinlets, disseminations, and breccia along a shallow thrust in carbonaceous felsic schist. The fine-grained gold is associated with pyrite, arsenopyrite, and stibnite. Igne-

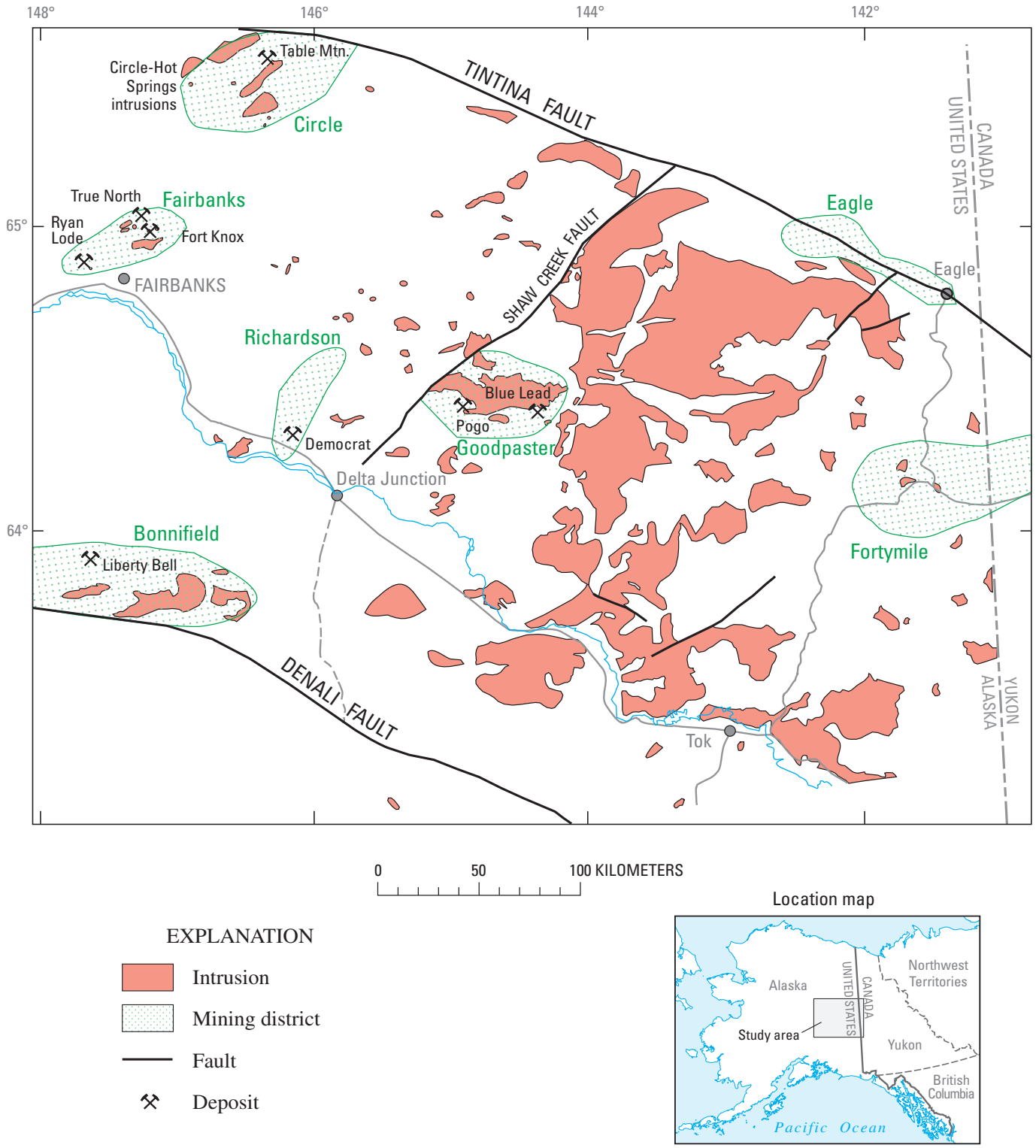

Figure A5. Gold districts (pattern) of the Tintina Gold Province in east-central Alaska and spatially associated reduced mid-Cretaceous igneous rocks (shaded) (from Hart and others 2002).

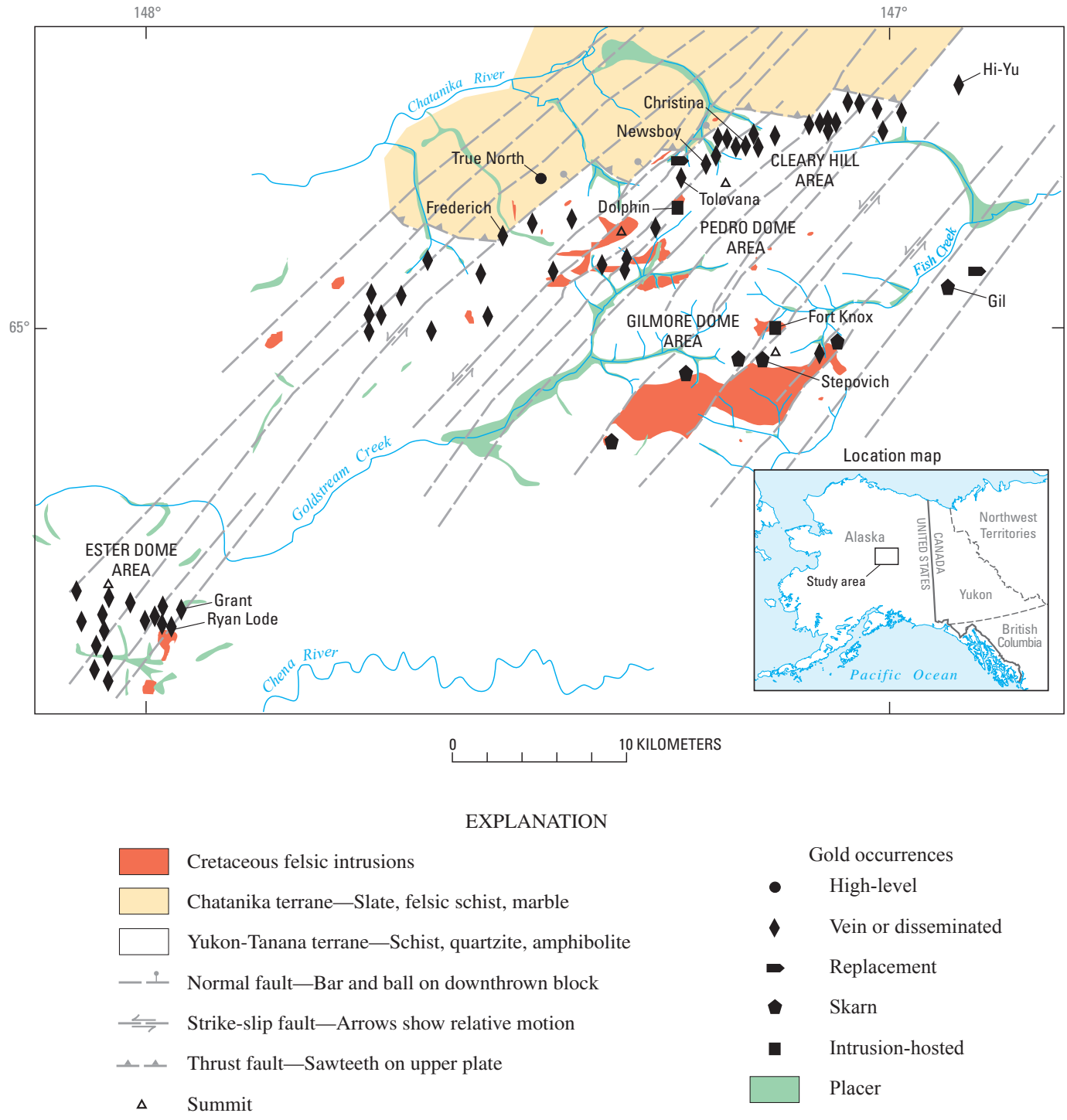

Figure A6. Gold deposits of the Fairbanks district (from Hart and others, 2002).

ous rocks are not recognized at the deposit. The Gil deposit, about 10 km east of Fort Knox, is a sheeted gold-bearing vein system in calc-silicates that likely formed above an as-yet-unroofed pluton intruding schist; other small and subeconomic tungsten skarns also occur in the same area. Many shear-hosted gold-bearing quartz veins, typically dominated by arsenopyrite, occur throughout the district (fig. A7). The largest, the Ryan Lode, occurs along the sheared margin of a tonalite stock. The majority of the schist-hosted deposits (for example, Grant, Cleary Hill, Newsboy, Hi-Yu, Christina, Tolovana) are along steeply dipping, northeast- or northwest-trending fault zones and have characteristic quartz-sericite-ankerite alteration haloes. $^{40}Ar/^{39}Ar$ dates on micas of 89 to 88 Ma for Ryan Lode (McCoy and others, 1997) and 103 Ma for Hi-Yu (R.J. Goldfarb, unpub. data, 2007), as well as a preliminary Re-Os sulfide date of 92 Ma for Tolovana (R.J.

Figure A7. Small shear-hosted gold vein system at the Tolovana deposit, Fairbanks district.

Goldfarb, unpub. data, 2007), suggest that the schist-hosted deposits both overlap and predate Cretaceous magmatism in the district.

High-grade, low-angle, multiphase, shear-hosted veins (fig. A2*A*) cutting mainly gneiss units (Day and others, 2003) and averaging 7 m in thickness with an areal extent of as much as 1.4×0.7-km (Smith and others, 1999; Rhys and others, 2003) were discovered at Pogo in 1996. Sulfide phases, comprising about 3 percent of the veins, include arsenopyrite, pyrite, pyrrhotite, loellingite, chalcopyrite, molybdenite, and bismuth- and tellurium-bearing phases. Alteration phases include biotite, quartz, sericite, potassium feldspar, ferroan dolomite, and chlorite. Reduced granites and tonalities of the Goodpaster batholith, located a few kilometers north of Pogo and comprising mainly crustal melts (in contrast to those at Fort Knox and in Yukon), were intruded around 109 to 103 Ma, during the final stages of regional metamorphism and deformation (Dilworth and others, 2007). Igneous activity thus overlaps with the 104.2 Ma mineralization age as determined by Re-Os analysis of ore-related molybdenite (Selby and others, 2002). Other small gold prospects in the Goodpaster area (Shawnee Peak, Prospect 4021), however, have Re-Os ages of around 95 Ma (Hart and others, 2002).

Geology and Gold Deposits of Southwestern Alaska

The far western end of the TGP (fig. A8) is underlain by Late Cretaceous clastic rocks of the Kuskokwim Group (Decker and others, 1994; Miller and others, 2002). These approximately 95 to 77 Ma sandstones and shales filled a northeast-trending, strike-slip basin between a series of older amalgamated terranes. Regional deformation was initiated in the Late Cretaceous and exposed rocks show evidence of only the lowest grades of regional metamorphism. Widespread, mainly intermediate, calc-alkaline volcanic-plutonic complexes formed throughout the region between 76 and 63 Ma. These metaluminous igneous rocks are a part of a very broad (550 km long), subduction-related arc formed from crustally contaminated mantle melts (Moll-Stalcup, 1994). A second set of intrusive rocks is manifest by approximately 75 to 65 Ma felsic to intermediate, peraluminous, hypabyssal granite porphyry dikes and plugs that are most likely melted Kuskokwim Group rocks (Miller and Bundtzen, 1994). Both intrusive suites are spatially associated with gold resources (Bundtzen and Miller, 1997; Miller and others, 2007).

The giant Donlin Creek gold deposit (fig. A9) occurs as a series of prospects localized within an 8×3-km swarm of the hypabyssal granite porphyry dikes (Goldfarb and others, 2004). Thin quartz veinlets, with lesser dolomite and ankerite, fill brittle extensional fractures within the igneous rocks. Fine-grained pyrite, arsenopyrite, and stibnite comprise 3 to 5 percent of the mineralized rock; orpiment, realgar, cinnabar, native arsenic, and graphite are also present. Gold is almost exclusively a refractory phase in the arsenopyrite. In contrast to many of the gold resources elsewhere in the TGP, bismuth, tellurium, and tungsten do not occur in anomalously high concentrations in the Donlin Creek orebody. Sericitization, carbonatization, and sulfidation are common in the veinlet wallrocks. $^{40}Ar/^{39}Ar$ dating of hydrothermal micas suggests veining occurred within a few million years after intrusion of the 75 to 69 Ma dike host rocks. Isotopic data indicate the source magma for the dikes was mainly of crustal origin, probably sediments of the lower parts of the Kuskokwim basin that were subjected to a localized domain of elevated crustal heat flow. A few other gold occurrences in this part of the TGP, including that at Vinasale Mountain, appear to be localized in similar peraluminous dike systems.

A series of gold occurrences in the Shotgun Hills are associated with weakly metaluminous to strongly peraluminous granite to granodiorite stocks and dikes, some of which are porphyritic and locally fractionated to quartz-feldspar porphyry dikes. The Shotgun gold deposit is situated near the apex of one such evolved quartz-feldspar porphyry phase. It occurs as 0.5- to 5-cm-wide stockworks of auriferous quartz

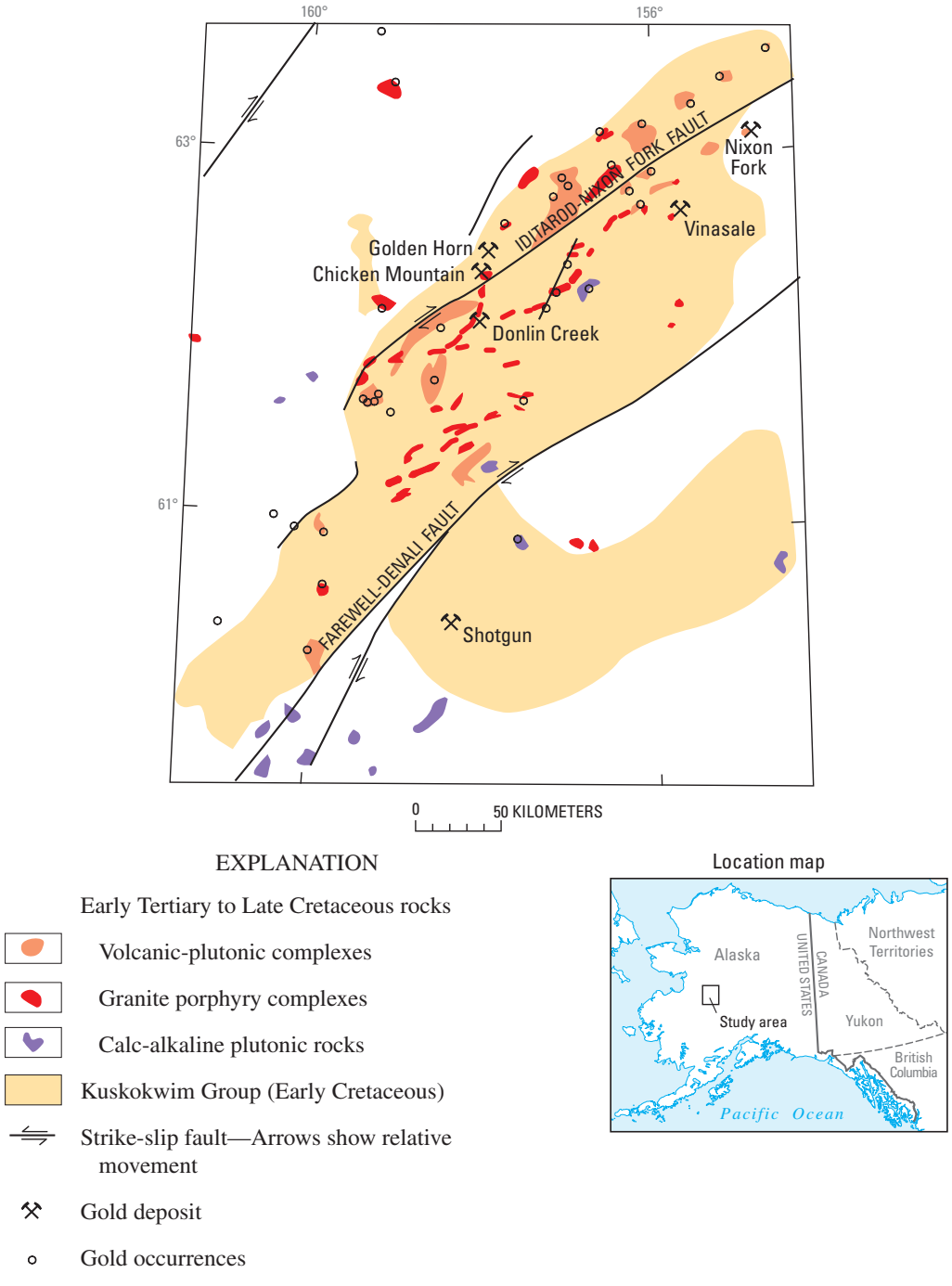

Figure A8. Main lode gold resources in the western end of the Tintina Gold Province (after Bundtzen and Miller, 1997; Hart and others, 2002).

veinlets (Rombach and Newberry, 2001). The veinlets contain less than 1 percent sulfides that are dominated by gold-bearing arsenopyrite commonly associated with pyrite, pyrrhotite, and chalcopyrite, and also loellingite and bismuth-, tellurium-, and tungsten-rich mineral phases. Gold grades tend to correlate with abundance of albite alteration. Tourmaline and quartz commonly cement brecciated porphyry and hornfels rocks. The igneous host rock is dated as 69±1 Ma (Rombach and Newberry, 2001). Isotopic data indicate that this igneous rock has a source in common with those of the other volcanic-plutonic complexes throughout the Kuskokwim region, which is most likely evolved mafic to intermediate mantle melts (J.L. Mair, unpub. data, 2007).

In addition to the Shotgun Hills, important gold resources are associated with other relatively evolved, metaluminous intrusive phases of the volcanic-plutonic complexes that are scattered elsewhere in this part of the TGP. These include auriferous quartz stockworks in monzonite at the Golden Horn deposit in Flat (Bull, 1988) and auriferous skarns at Nixon Fork (Newberry and others, 1997). Where the igneous rocks in these complexes are the most evolved (syenitic to monzonitic), silver-, bismuth-, and tin-rich veins appear to be more dominant than gold-bearing veins.

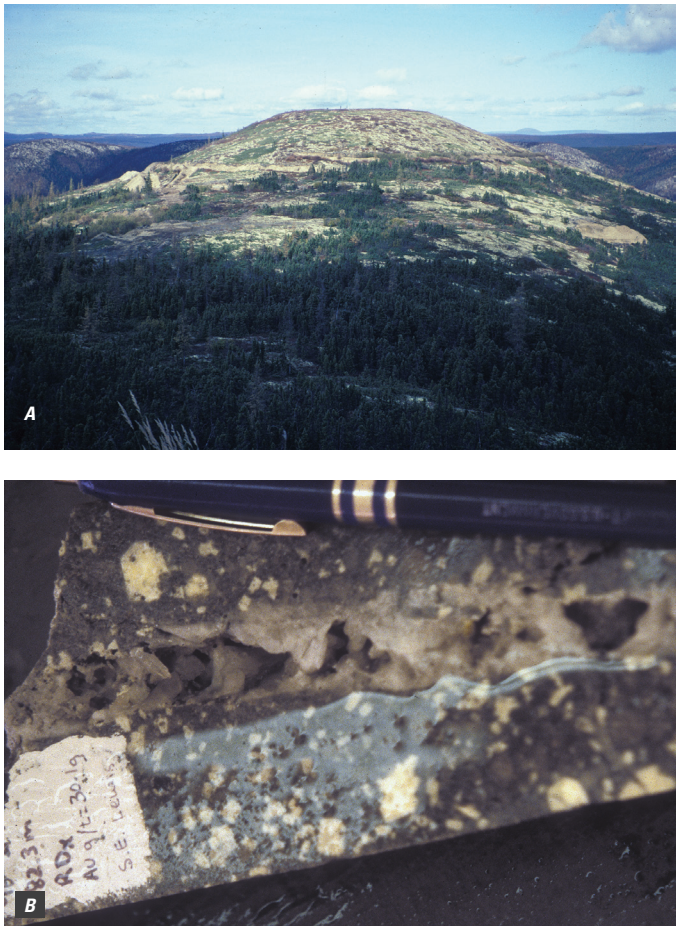

Figure A9. *A*, Aerial photograph of the Donlin Creek deposit area that is centered on a seriees of topographic domes in the Kuskokwim Mountains region of southwestern Alaska. *B*, Most of the mineralization at the Donlin Creek gold deposit occurs in these narrow, vuggy quartz-carbonate veinlets within an igneous dike-sill complex. The igneous host rocks are mainly rhyodacitic in composition, and sometimes porphyritic, as shown here.

Geochemical Constraints on Gold Ore-Forming Fluids

Fluid-Inclusion Studies

Fluid-inclusion microthermometric studies of ore-bearing quartz have allowed for definition of the pressure, temperature, and chemical composition of the ore-forming solutions responsible for the main gold resources in the TGP (table A2). Those gold deposits hosted by and within the surrounding hornfels of the mid-Cretaceous plutons (Fort Knox, Dublin Gulch, Scheelite Dome, Clear Creek) typically developed from low to moderate salinity (≤12 weight percent NaCl equivalent), gas-rich (typically ≥15-20 mole percent CO_2) fluids at temperatures of 290°C to 380°C, and pressures of 1 to 2 kilobars (kb) (or 3.5 to 7 km depth); the Dublin Gulch veins appear to have been slightly cooler, and the Scheelite Dome veins are likely slightly deeper in origin relative to the others. Available data indicate that other mid-Cretaceous gold deposits hosted by metamorphic rocks in the Fairbanks and Goodpaster districts have the same gas-rich, low to moderate salinity fluid type. Pogo and adjacent prospects in the Goodpaster district show indications of being the most deeply formed and hottest among the TGP gold ore systems. In contrast to the gold deposits in the eastern part of the TGP, the Late Cretaceous Donlin Creek and Shotgun deposits in southwestern Alaska formed within the upper 1 to 2 km of the crust; Shotgun is also characterized by an anomalously high-salinity hydrothermal fluid.

Laser-ablation inductively coupled plasma-mass spectrometry (ICP-MS) microanalysis was applied to fluid inclusions in ore-stage quartz to obtain quantitative estimates of any significant differences in the relative abundances of a variety of trace elements in the hydrothermal solutions of the various gold deposits of the TGP (Marsh and others, 2005). Single fluid inclusions from intrusion-hosted, gold-bearing quartz-feldspar veins at Fort Knox were analyzed simultaneously for many major, minor, and trace element relative concentrations. Element ratio measurements (all to Na) range from 0.01 to 0.06 for arsenic and 0.004 to 0.03 for antimony in Fort Knox intrusion-hosted quartz veins, but one extremely gold-rich quartz-feldspar vein had a ratio as high as 0.37 for arsenic. In addition, whereas most bismuth ratios were less than or equal to 0.01, one inclusion within the quartz-feldspar vein had a ratio of 0.67. Base metal ratios were consistently less than 0.01 for lead, and 0.01 to 0.05 for copper and zinc. Similar values characterized fluid inclusions from sheeted veins within the stocks at Scheelite Dome and Clear Creek, but inclusions from auriferous veins in adjacent hornfels at Scheelite Dome commonly showed arsenic, lead, and antimony ratios of greater than 1. Data from reconnaissance examination of several other significant gold deposits that are not hosted by the reduced approximately 90 Ma stocks were compared and contrasted with those data from the Fort Knox and Yukon deposits. Analysis of a few of the inclusions from the Pogo deposit showed no obvious distinction from those that typified the intrusion-hosted deposits. At Donlin Creek, inclusions from the main gold resource exhibited highly anomalous ratios of 4 to 15 for arsenic and 3 to 5 for iron, and elevated ratios of 0.1 to 0.3 for antimony, whereas those from the subeconomic Dome property at the northern margin of the Donlin Creek mineralized zone were 0.004 to 0.016, 0.026 to 0.079, and 0.001 to 0.003, respectively. It is unclear as to whether the Donlin Creek ore fluids were indeed exceptionally anomalous or if perhaps significant dissolution of abundant fine-grained arsenic- and antimony-bearing sulfide phases within the quartz veinlets occurred.

Noble-Gas Studies

Noble-gas isotopes were determined for samples of quartz vein material from gold deposits of the TGP. Helium-

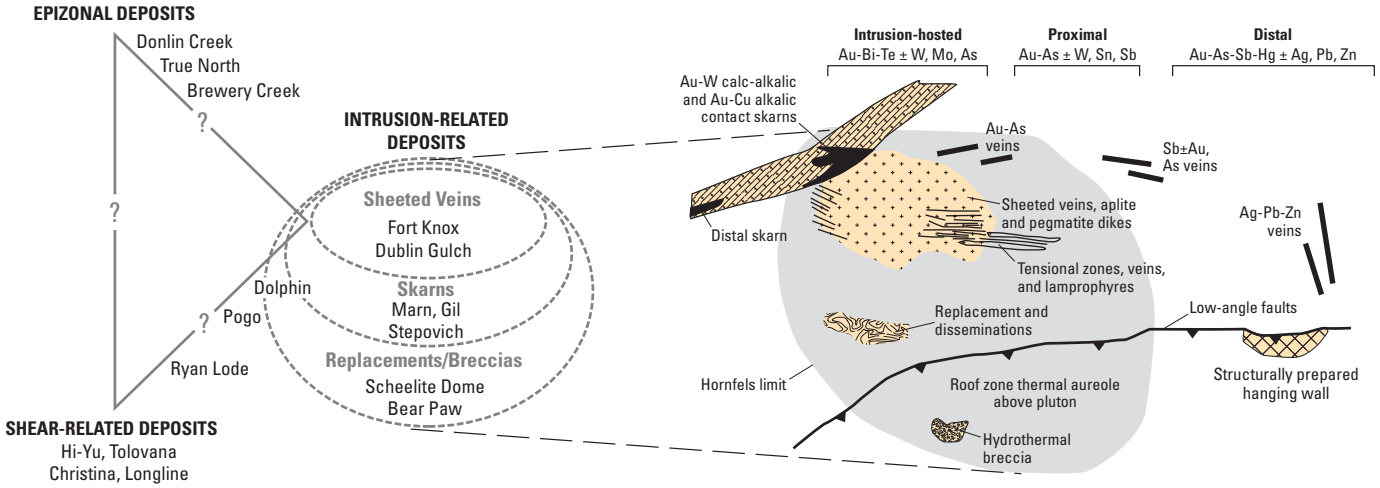

Figure A10. Intrusion-related gold systems in the Tintina Gold Province are characterized by a model that has differing deposit styles, metallogeny, and geochemistry surrounding a causative mid-Cretaceous igneous body. Other shear-related ore deposits, although spatially and temporally associated with mid-Cretecous plutons, are more like classic orogenic gold deposits. Shallowly formed epizonal deposits are more difficult to classify and remain controversial regarding their genesis. (After Hart and others, 2002.)

isotope ratios have *R/Ra* (where *R* is the measured $^{3}He/^{4}He$ ratio and *Ra* the atmospheric ratio) values that varied from less than 0.1 for Pogo to greater than 15 for Clear Creek. Preliminary helium data suggest that deposits in Yukon (Clear Creek, Scheelite Dome) have a definite mantle contribution, whereas ore-forming fluids in the TGP deposits sampled in Alaska (Fort Knox, Pogo, Donlin Creek) are dominated by helium with a crustal origin. The $^{40}Ar/^{36}Ar$ ratios from Donlin Creek are close to those for air (295.5) and indicate contamination by air-saturated ground waters in this relatively shallowly formed ore deposit. The other studied gold deposits in east-central Alaska and adjacent Yukon have typical ratios of approximately 500, suggesting a consistent gas source added from the crust or mantle (see Allegre and others, 1987).

Stable-Isotope Studies

Stable-isotope data are consistent with deep crustal sources for major ore-fluid components. Oxygen-isotope data (table A2) for ore-bearing quartz in all gold deposits typically are in the range of 12 to 19 parts per thousand (per mil), indicating a fluid of magmatic or metamorphic source, but with little, if any, contribution from meteoric sources. Nitrogen-isotope data from the Christina deposit in the Fairbanks district suggest that at least the ore fluids for the sedimentary rock-hosted gold-bearing vein deposits in this specific area are of metamorphic origin (Jia and others, 2003). Large variations in sulfur-isotope data (table A2) reflect variable crustal reservoirs for the sulfur that transports the gold ore in the hydrothermal solutions. Extremely negative values for sulfur isotopes for sulfide minerals at Donlin Creek, in the hornfels-hosted veins at Clear Creek, and at Scheelite Dome reflect the highly reduced nature of the sedimentary rocks that provide sulfur to the hydrothermal fluids.

Genesis of Lode Gold Deposits

Geological, geochronological, and geochemical data suggest that both magmatic and metamorphic models can be applied to explaining the distribution of gold resources across the TGP (Goldfarb and others, 2005). Most of the small and widely distributed, approximately 105 to 90 Ma shear zone-related, gold-bearing quartz veins in the Fairbanks (fig. A7) and Goodpaster (fig. A2*A*) districts are best classified as orogenic gold deposits (for example, Groves and others, 1998), which formed during a period of high crustal heat flow and rapid uplift associated with orogenic collapse. Veins show evidence of both brittle and ductile deformation, are most consistently anomalous in arsenic, antimony, and tungsten, and formed from a low-salinity, CO_2-rich ore fluid. The fluid and gold were likely liberated during devolatilization at depth during final stages of deformation and regional metamorphism, and subsequently formed veins at shallower levels in uplifting rocks of the eastern TGP. Pressure fluctuations during hydraulic fracturing and shear movements were the most probable cause for vein formation and gold deposition. Although controversial, many features of the large Pogo deposit also suggest that it is a relatively deeply formed orogenic gold deposit (Goldfarb and others, 2000, 2005).

A second genetic model of intrusion-centered mineralizing systems is most appropriate for other approximately 90 Ma gold resources in the eastern TGP, including the Fort Knox deposit near Fairbanks and those in Yukon (Hart and others, 2002; Hart and Goldfarb, 2005; Hart, 2007). These so-called intrusion-related gold systems (IRGSs) are similar to the orogenic gold deposits in that both deposit types are spatially and temporally associated with igneous rocks, may overlap in tectonic setting, have similar gangue mineralogy, can overlap in trace-element signatures (Ag, Au, As, Bi, Sb,

Table A2. Fluid inclusion and stable isotope geochemistry of ore-bearing samples from deposits in the Tintina Gold Province.

[Abbreviations and symbols are as follows: n.d., no data; °C, degrees Celsius; ≤, less than or equal to; ≥, greater than or equal to]

Deposit	$xCO_2 \pm N_2$, CH_4 (mole percent)	Salinity (weight percent equivalent NaCl)	Immiscible	Pressure (kilobars)	Temperature (°C)	$\delta^{18}O$ quartz (per mil)	$\delta^{34}S$ sulfide (per mil)	Reference
Clear Creek	15	12	Yes	1.4–1.8	300–350	14.0–18.7	-12.7– -9.5, -2.9–+0.4	Marsh and others, 2003
Scheelite Dome	20–60	≤4	No	2–3	290–380	14.1–19.0	-10.9– -7.1	Mair and other, 2006
Dublin Gulch	2–33	1.4–9.8	No	≥1.1	≥150– 271	n.d.	n.d.	Maloof and others, 2001
Fort Knox	22	2–8	Some	1.25–1.5	330–370	12.0–13.5	-3.4	Goldfarb and others, 1997; McCoy and others, 1997; Paul Jensen, Teck-Cominco, unpub. data, 2006
Ryan Lode	12	≤8	Yes	0.5–0.75	270–330	11.7–15.0	0.5–3.7	McCoy and others, 1997
Others—Fairbanks district	1–20	3–5	n.d.	n.d.	275–375	n.d.	0.3–4.1; 8.2–10.9	Metz, 1991; Goldfarb and others, 1997
Pogo	Highly variable	Highly variable	Yes	1.7–2.0	308–570	13.4–15.2	-2.5–+5.5	Smith and others, 1999; Rombach and others, 2002; C. Rombach, unpub. data, 2005
Others—Goodpaster district	Significant amounts	2.5–7.5	Yes	1.4–2.4	225–390	n.d.	n.d.	Dilworth, 2003; R.J. Goldfarb, unpub. data, 2005
Donlin Creek	3–7	3–6	Rare	0.3–0.6	275–300	14.3–24.7	-16– -10	Goldfarb and others, 2004
Shotgun	Variable	Moderate to high	Yes	0.5	280–630	16.4–17.1	-5.9– -5.0	Romach and Newberry, 2001

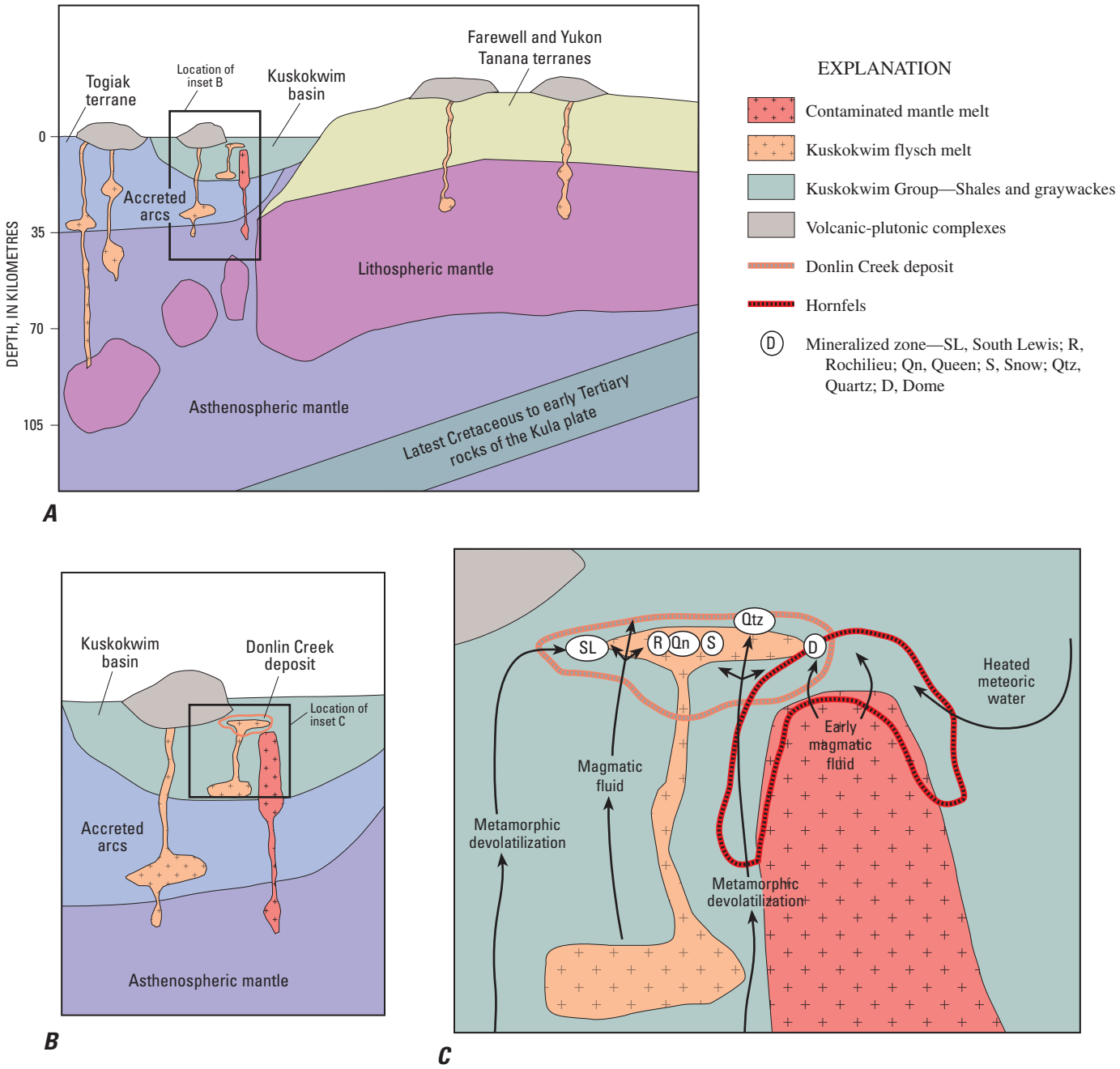

Figure A11. Genetic model for evolution of the Donlin Creek gold deposit. *A*, Small-scale, regional model showing location of inset *B*. Field of view is approximately 480 kilometers. *B*, Inset *B*, showing partial mantle melting above the subducting Kula plate leading to the emplacement of crustally contaminated intrusions and volcanic-plutonic complexes throughout the Kuskokwim basin. In a few locations (including at the site of the Donlin Creek deposit), small, almost pure flysch melts evolved. Shows location of inset *C*. *C*, Inset showing gold-transporting hydrothermal fluids released during devolatilization of flysch adjacent to the larger melts and (or) from the melts themselves. The fluids localized the gold ores in the already crystallized and structurally competent flysch melt dike-sill complex at Donlin Creek. (After Goldfarb and others, 2004.)

Te, and (or) W), and have formed from fluids with very similar chemistries. In fact, the low salinity and high CO_2 content of the IRGSs are very different from most other magmatic gold deposits and has led to much of the controversy regarding identification of IRGSs versus orogenic gold deposits (Groves and others, 2003). A key distinction is that an IRGS represents a zoned system centered around a causative pluton (fig. A10); a complete model would include (1) sheeted gold-bismuth-tellurium-tungsten-bearing quartz veins in the cupola of the intrusion; (2) gold-rich tungsten or copper skarns in any adjacent calcareous rocks; (3) gold-arsenic±antimony tension-vein arrays, disseminations, and breccias within 2- to 3-km-wide hornfels zones; and (4) distal low-temperature silver-lead-zinc veins (Hart and others, 2002). The IRGSs are also significantly lower in grade (less than 1 g/t gold) than orogenic gold deposits (greater than 1-2 g/t gold; commonly greater than 10 g/t gold). The zoned mineralization styles indicate an exsolved magmatic fluid that moved outward from the late-stage crystallizing magma. An abundance of aplites, pegmatites, vein dikes, miarolitic cavities, and unidirectional solidification textures in the igneous rocks is consistent with a fluid-rich melt and thus with a magmatic model. Potassic magmas released from the SCLM could have been the source of the gold that was further concentrated during magmatic evolution in the overlying crust (John L. Mair, Geoinformatics Exploration, Inc., unpub. data, 2008).

Two distinct ore deposit models also characterize the approximately 70 Ma gold deposits in the western TGP (Goldfarb and others, 2004). The gold-forming fluids at the giant Donlin Creek orogenic gold deposit may have been derived by broad-scale metamorphic devolatilization above rising mantle melts that were emplaced into the sediments at the base of the Kuskokwim basin. Alternatively, exsolution of fluids could have taken place from a magma that was dominated by a significant sedimentary rock melt component (fig. A11). Other gold occurrences in the Kuskokwim basin, best broadly classified as simply magmatic gold deposits (for example, Shotgun and Golden Horn), formed via fluid exsolution from fractionation of high-level intrusive systems dominated by a mafic to intermediate composition parent magma of lower crustal or lithospheric mantle origin. These gold deposits seem to be localized at the apices of the more fractionated porphyritic intrusive bodies in the region. The high degree of fractionation is important for preconcentration of metals and volatiles in these gold depositing magmatic-hydrothermal systems.

References Cited

Allegre, C.J., Staudacher, Thomas, and Sarda, Philippe, 1987, Rare gas systematics; Formation of the atmosphere, evolution and structure of the Earth's mantle: Earth and Planetary Science Letters, v. 81, no. 2–3, p. 127–150.

Allen, T.L., Hart, C.J.R., and Marsh, E.E., 1999, Placer gold and associated heavy minerals of the Clear Creek drainage, central Yukon; Past to present, *in* Roots, C.F., and Emond, D.S., eds., Yukon Exploration and Geology 1998: Whitehorse, Yukon, Canada, Indian and Northern Affairs Canada, Exploration and Geological Services Division, Yukon Region, p. 197–214.

Bakke, A.A., 1995, The Fort Knox "porphyry" gold deposit—Structurally controlled stockwork and shear quartz vein, sulphide-poor mineralization, hosted by a Late Cretaceous pluton, east-central Alaska, *in* Schroeter, T.G., ed., Porphyry deposits of the northwestern Cordillera of North America: Canadian Institute of Mining, Metallurgy and Petroleum Special Volume 46, p. 795–802.

Bakke, A.A., Morrell, B.G., Odden, J., Bergstrom, T., and Woodman, J., 2000, Kinross Gold USA's activities in the Fairbanks mining district, K2K, *in* Tucker, T.L., and Smith, M.T., eds., The Tintina gold belt—Concepts, exploration, and discoveries: British Columbia and Yukon Chamber of Mines, Special Volume 2, p. 89–98.

Bull, Katherine, 1989, Genesis of the Golden Horn and related mineralization in the Black Creek Stock, Flat, Alaska: Fairbanks, Alaska, University of Alaska, unpublished Master's thesis, 300 p.

Bundtzen, T.K., and Miller, M.L., 1997, Precious metals associated with Late Cretaceous-early Tertiary igneous rocks of southwestern Alaska, *in* Goldfarb, R.J., and Miller, L.D., eds., Mineral deposits of Alaska: Economic Geology Monograph 9, p. 242–286.

Day, W.C., Aleinikoff, J.N., Roberts, Paul, Smith, Moira, Gamble, B.M., Hennings, M.W., Gough, L.P., and Morath, L.C., 2003, Geologic map of the Big Delta B–2 quadrangle, east central Alaska: U.S. Geological Survey Geologic Investigations Series I–2788, 12 p., 1 sheet, scale 1:63,360. (Also available online at *http://pubs.usgs.gov/imap/i-2788/i-2788.pdf/*.)

Day, W.C., O'Neill, J.M., Aleinikoff, J.N., Green, G.N., Saltus, R.W., and Gough, L.P., 2007, Geologic map of the Big Delta B–1 quadrangle, east-central Alaska: U.S. Geological Survey Scientific Investigations Map SIM–2975, scale 1:63,360. (Also available online at *http://pubs.usgs.gov/sim/2007/2975*.)

Decker, John, Bergman, S.C., Blodgett, R.B., Box, S.E., Bundtzen, T.K., Clough, J.G., Coonrad, W.L., Gilbert, W.G., Miller, M.L., Murphy, J.M., Robinson, M.S., and Wallace, W.K., 1994, Geology of southwestern Alaska, *in* Plafker, George, and Berg, H.C., eds., The geology of Alaska, chapter G–1 *of* The geology of North America: Boulder, Colo., Geological Society of America, p. 285–310.

Dilworth, K.M., Mortensen, J.K., Ebert, Shane, Tosdal, R.M., Smith, M.T., and Roberts, Paul, 2007, Cretaceous reduced granitoids in the Goodpaster mining district, east central Alaska: Canadian Journal of Earth Sciences, v. 44, p. 1347–1373.

Dusel-Bacon, Cynthia, Hopkins, M.J., Mortensen, J.K., Dashevsky, S.S., Bressler, J.R., and Day, W.C., 2006, Paleozoic tectonic and metallogenic evolution of the pericratonic rocks of east-central Alaska and adjacent Yukon, *in* Colpron, Maurice, and Nelson, J.L., eds., Paleozoic evolution and metallogeny of pericratonic terranes at the ancient Pacific margin of North America, Canadian and Alaskan Cordillera: Geological Association of Canada Special Paper 45, p. 25–74.

Foster, H.L., Keith, T.E.C., and Menzie, W.D., 1994, Geology of the Yukon-Tanana area of east-central Alaska, *in* Plafker, George, and Berg, H.C., eds., The geology of Alaska, chapter G–1 *of* The geology of North America: Boulder, Colo., Geological Society of America, p. 205–240.

Goldfarb, R.J., Ayuso, Robert, Miller, M.L., Ebert, Shane, Marsh, E.E., Petsel, S.A., Miller, L.D., Bradley, Dwight, Johnson, Craig, and McClelland, William, 2004, The Late Cretaceous Donlin Creek gold deposit, southwestern Alaska—Controls on epizonal ore formation: Economic Geology, v. 99, no. 4, p. 643–671.

Goldfarb, R.J., Baker, Timothy, Dube, Benoit, Groves, D.I., Hart, C.J.R., and Gosselin, Patrice, 2005, Distribution, character, and genesis of gold deposits in metamorphic terranes, *in* Hedenquist, J.W., Thompson, J.F.H., Goldfarb, R.J., and Richards, J.P., eds., One Hundredth Anniversary Volume of Economic Geology 1905–2005: Littleton, Colo., Society of Economic Geologists, p. 407–450.

Goldfarb, R.J., Gray, J.E., Pickthorn, W.J., Gent, C.A., and Cieutat, B.A., 1990, Stable isotope systematics of epithermal mercury-antimony mineralization, southwestern Alaska, *in* Goldfarb, R.J., Nash J.T., and Stoeser, J.W., eds., Geochemical studies in Alaska by the U.S. Geological Survey, 1989: U.S. Geological Survey Bulletin 1950, p. E1–E9. (Also available online at *http://pubs.er.usgs.gov/usgspubs/b/b1950*.)

Goldfarb, R.J., Hart, C.J.R., Miller, M.L., Miller, L.D., Farmer, G.L., and Groves, D.I., 2000, The Tintina gold belt—A global perspective, *in* Tucker, T.L., and Smith, M.T., eds., The Tintina gold belt—Concepts, exploration, and discoveries: British Columbia and Yukon Chamber of Mines, Special Volume 2, p. 5–34.

Goldfarb, R.J., Miller, L.D., Leach, D.L., and Snee, L.W., 1997, Gold deposits in metamorphic rocks of Alaska, *in* Goldfarb, R.J., and Miller, L.D., eds., Mineral deposits of Alaska: Economic Geology Monograph 9, p. 151–190.

Gray, J.E., Frost, T.P., Goldfarb, R.J., and Detra, D.E., 1990, Gold associated with cinnabar- and stibnite-bearing deposits and mineral occurrences in the Kuskokwim River region, southwestern Alaska, *in* Goldfarb R.J., Nash J.T., and Stoeser, J.W., eds., Geochemical studies in Alaska by the U.S. Geological Survey, 1989: U.S. Geological Survey Bulletin 1950, p. D1–D6. (Also available online at *http://pubs.er.usgs.gov/usgspubs/b/b1950*.)

Groves, D.I., Goldfarb, R.J., Gebre-Mariam, M., Hagemann, S.G., and Robert, Francois, 1998, Orogenic gold deposits; A proposed classification in the context of their crustal distribution and relationship to other gold deposit types: Ore Geology Reviews, v. 13, no. 1–5, p. 7–27.

Groves, D.I., Goldfarb, R.J., Robert, Francois, and Hart, C.J., 2003, Gold deposits in metamorphic belts; Overview of current understanding, outstanding problems, future research, and exploration significance: Economic Geology, v. 98, no. 1, p. 1–29.

Hart, Craig, 2007, Reduced intrusion-related gold systems, *in* Goodfellow, W.D., ed., Mineral deposits of Canada; A synthesis of major deposit-types, district metallogeny, the evolution of geological provinces, and exploration methods: Geological Association of Canada, Mineral Deposits Division, Special Publication No. 5, p. 95–112.

Hart, C.J.R., and Goldfarb, R.J., 2005, Distinguishing intrusion-related from orogenic gold systems, *in* Realising New Zealand's mineral potential, Proceedings, Australasian Institute of Mining and Metallurgy, 2005 New Zealand Minerals Conference, Auckland, New Zealand, November 13–16, 2005: Wellington, New Zealand, Ministry of Economic Development Crown Minerals Group, p. 125–133.

Hart, C.J.R., Goldfarb, R.J., Lewis, L.L., and Mair, J.L., 2004, The northern Cordilleran mid-Cretaceous plutonic province—Ilmenite/magnetite series granitoids and intrusion-related mineralization: Resource Geology, v. 54, no. 3, p. 253–280.

Hart, C.J.R., Mair, J.L., Goldfarb, R.J., and Groves, D.I., 2004, Source and redox controls of intrusion-related ore systems, Tombstone-Tungsten belt, Yukon Territory, Canada: Royal Society of Edinburgh, Transactions–Earth Sciences, v. 95, no. 1–2, p. 339–356.

Hart, C.J.R., McCoy, D.T., Goldfarb, R.J., Smith, Moira, Roberts, Paul, Hulstein, Roger, Bakke, A.A., and Bundtzen, T.K., 2002, Geology, exploration and discovery in the Tintina gold province, Alaska and Yukon, *in* Goldfarb, R.J., and Nielsen, R.L., eds., Integrated methods for discovery, global exploration in the twenty-first century: Society of Economic Geologists Special Publication 9, p. 241–274.

Haynes, E.A., Fodor, R.V., Coleman, D.S., Goldfarb, R.J., and Jensen, P., 2005, Geochemical and isotopic compositions of the mid-Cretaceous Fort Knox and associated plutons, Fairbanks, Alaska—Implications for intrusion-related gold systems [abs.]: Geological Society of America Abstracts with Programs, v. 37, no. 7, p. 517.

Jia, Yiefei, Kerrich, Robert, and Goldfarb, Richard, 2003, Metamorphic origin of the ore-forming fluid for orogenic gold-bearing quartz vein systems in the North American Cordillera; Constraints from $\delta^{15}N$, δD, and $\delta^{18}O$: Economic Geology, v. 98, p. 109–123.

Kinross Gold Corporation, 2009, Fort Knox (100% ownership and operator)–USA: Kinross Gold Corporation Web site at *http://www.kinross.com/operations/usa-fort-knox.html*. (Accessed 1/7/2009.)

Mair, J.L., Goldfarb, R.J., Johnson, C.A., Hart, C.J.R., and Marsh, E.E., 2006, Geochemical constraints on the genesis of the Scheelite Dome intrusion-related gold deposit, Tombstone gold belt, Yukon, Canada: Economic Geology, v. 101, no. 3, p. 523–553.

Mair, J.L., Hart, C.J.R., Goldfarb, R.J., O'Dea, M., and Harris, S., 2000, Geology and metallogenic signature of gold occurrences at Scheelite Dome, Tombstone gold belt, Yukon Territory, *in* Emond, D.S., and Weston, L.H., eds., Yukon exploration and geology 1999: Whitehorse, Yukon, Canada, Indian and Northern Affairs Canada, Exploration and Geological Services Division, Yukon Region, p. 165–176.

Maloof, T.L., Baker, Timothy, and Thompson, J.F.H., 2001, The Dublin Gulch intrusion-hosted gold deposit, Tombstone plutonic suite, Yukon Territory, Canada: Mineralium Deposita, v. 36, no. 6, p. 583–593.

Marsh, E.E., Allan, M.M., Goldfarb, R.J., Jensen, Paul, Mair, J.L., and Shepherd, T.J., 2005, LA-ICP-MS microanalysis of single fluid inclusions from intrusion-related gold deposits, Tintina gold province, Alaska and Yukon [abs.]: Geological Society of America Abstracts with Programs, v. 37, no. 7, p. 501.

Marsh, E.E., Goldfarb, R.J., Hart, C.J.R., and Johnson, C.A., 2003, Geology and geochemistry of the Clear Creek intrusion-related gold occurrences, Tintina gold province, Yukon, Canada: Canadian Journal of Earth Sciences, v. 40, no. 5, p. 681–699.

Marsh, E.E., Hart, C.J.R., Goldfarb, R.J., and Allen, T.L., 1999, Geology and geochemistry of the Clear Creek gold occurrences, Tombstone gold belt, central Yukon Territory, *in* Roots, C.F., and Emond, D.S., eds., Yukon exploration and geology, 1998: Whitehorse, Yukon, Canada, Indian and Northern Affairs Canada, Exploration and Geological Services Division, Yukon Region, p. 185–196.

McCoy, D.T., Newberry, R.J., Layer, P., DiMarchi, J.J., Bakke, A.A., Mastermann, J.S., and Minehane, D.L., 1997, Plutonic-related gold deposits of interior Alaska, *in* Goldfarb, R.J., and Miller, L.D., eds., Mineral deposits of Alaska: Economic Geology Monograph 9, p. 191–241.

Metz, P.A., 1991, Metallogeny of the Fairbanks mining district, Alaska and adjacent areas: University of Alaska–Fairbanks, Mineral Industry Research Laboratory Report 90, 370 p.

Miller, M.L., Bradley, D.C., Bundtzen, T.K., and McClelland, W.C., 2002, Late Cretaceous through Cenozoic strike-slip tectonics of southwestern Alaska: Journal of Geology, v. 110, no. 3, p. 247–270.

Miller M.L., Bradley, D.C., Goldfarb, R.J., and Bundtzen, T.K., 2007, Tectonic setting of Late Cretaceous gold and mercury metallogenesis, Kuskokwim mineral belt, southwestern Alaska, USA, *in* Proceedings of the Ninth Biennial Meeting of the Society for Geology Applied to Mineral Deposits, Dublin, Ireland, August 20–23, 2007: Geneva, Switzerland, Society for Geology Applied to Mineral Deposits, p. 683–686.

Miller, M.L., and Bundtzen, T.K., 1994, Generalized geologic map of the Iditarod quadrangle, Alaska, showing potassium-argon, major-oxide, trace-element, fossil, paleocurrent, and archaeological sample localities: U.S. Geological Survey Miscellaneous Field Studies Map MF–2219–A, 48 p., 1 sheet in pocket, scale 1:250,000.

Moll-Stalcup, E.J., 1994, Latest Cretaceous and Cenozoic magmatism in mainland Alaska, *in* Plafker, George, and Berg, H.C., eds., The geology of Alaska, chapter G–1 *of* The geology of North America: Boulder, Colo., Geological Society of America, p. 589–620.

Mueller, S.H., Goldfarb, R.J., Hart, C.J.R., Mair, J.L., Marsh, E.E., and Rombach, C.S., 2004, The Tintina gold province, Alaska and Yukon—New world-class gold resources and their sustainable development, *in* Proceedings PACRIM 2004, Adelaide, Australia, September 19–22, 2004: Carlton, Victoria, Australia, Australasian Institute of Mining and Metallurgy, v. 5, p. 189–198.

Murphy, D.C., Heon, D., and Hunt, J., 1993, Geological overview of Clear Creek map area, western Selwyn basin (NTS 115P/14), *in* Yukon exploration and geology 1992: Whitehorse, Yukon, Canada, Indian and Northern Affairs Canada, Exploration and Geological Service Division, Yukon Region, p. 61–69.

Newberry, R.J., Allegro, G.L., Cutler, S.E., Hagen-Levelle, J.H., Adams, D.D., Nicholson, L.C., Weglarz, T.B., Bakke, A.A., Clautice, K.H., Coulter, G.A., Ford, M.J., Myers, G.L., and Szumigala, D.J., 1997, Skarn deposits of Alaska, *in* Goldfarb, R.J., and Miller, L.D., eds., Mineral deposits of Alaska: Economic Geology Monograph 9, p. 355–395.

Rombach, C.S., and Newberry, R.J., 2001, Shotgun deposit—Granite porphyry-hosted gold-arsenic mineralization in southwestern Alaska, USA: Mineralium Deposita, v. 36, no. 6, p. 607–621.

Rombach, C.S., Newberry, R.J., Goldfarb, R.J., and Smith, Moira, 2002, Geochronology and mineralization of the Liese zones, Pogo deposit, Alaska [abs.]: Geological Society of America Abstracts with Programs, v. 34, no. 6, p. 114.

Rhys, David, DiMarchi Jack, Smith, Moira, Friesen, Robert, and Rombach, Cameron, 2003, Structural setting, style and timing of vein-hosted gold mineralization at the Pogo deposit, east-central Alaska: Mineralium Deposita, v. 38, no. 7, p. 863–875.

Selby, David, Creaser R.A., Hart, C.J.R., Rombach, C.S., Thompson, J.F.H., Smith, M.T., Bakke, A.A., and Goldfarb, R.J., 2002, Absolute timing of sulfide and gold mineralization; A comparison of Re-Os molybdenite and Ar-Ar mica methods from the Tintina gold belt, Alaska: Geology, v. 30, no. 9, p. 791–794.

Selby David, Creaser, R.A., Heaman, L.M., and Hart, C.J.R., 2003, Re-Os and U-Pb geochronology of the Clear Creek, Dublin Gulch, and Mactung deposits, Tombstone gold belt, Yukon, Canada; Absolute timing relationships between plutonism and mineralization: Canadian Journal of Earth Scinces, v. 40, no. 12, p. 1839–1852.

Smith, Moira, 2000, The Tintina gold belt; An emerging gold district in Alaska and Yukon, *in* Tucker, T.L., and Smith, M.T., eds., The Tintina gold belt—Concepts, exploration and discoveries: British Columbia and Yukon Chamber of Mines, Special Volume 2, p. 1–3.

Smith, Moira, Thompson, J.F.H., Bressler, Jason, Layer, Paul, Mortensen, James, Abe, Ichiro, and Takaoka, Hidetoshi, 1999, Geology of the Liese zone, Pogo property, east-central Alaska: Society of Economic Geologists Newsletter, v. 38, no. 1, p. 12–21.

Thompson, J.F.H., and Newberry, R.J., 2000, Gold deposits related to reduced granitic intrusions, *in* Hagemann, S.G., and Brown, P.E., eds., Gold in 2000: Reviews in Economic Geology, v. 13, p. 377–400.

Tectonic Setting and Metallogenesis of Volcanogenic Massive Sulfide Deposits in the Bonnifield Mining District, Northern Alaska Range

By Cynthia Dusel-Bacon, John N. Aleinikoff, Wayne R. Premo, Suzanne Paradis, and Ilana Lohr-Schmidt

Chapter B of
Recent U.S. Geological Survey Studies in the Tintina Gold Province, Alaska, United States, and Yukon, Canada—Results of a 5-Year Project
Edited by Larry P. Gough and Warren C. Day

Scientific Investigations Report 2007–5289–B

U.S. Department of the Interior
U.S. Geological Survey

Contents

Figures

Tectonic Setting and Metallogenesis of Volcanogenic Massive Sulfide Deposits in the Bonnifield Mining District, Northern Alaska Range

By Cynthia Dusel-Bacon,[1] John N. Aleinikoff,[1] Wayne R. Premo,[1] Suzanne Paradis,[2] and Ilana Lohr-Schmidt[1]

Abstract

This paper summarizes the results of field and laboratory investigations, including whole-rock geochemistry and radiogenic isotopes, of outcrop and drill core samples from volcanogenic massive sulfide (VMS) deposits and associated metaigneous rocks in the Wood River area of the Bonnifield mining district, northern Alaska Range (see fig. 1 of Editors' Preface and Overview). U-Pb zircon igneous crystallization ages from felsic rocks indicate a prolonged period of Late Devonian to Early Mississippian (373±3 to 357±4 million years before present, or Ma) magmatism. This magmatism occurred in a basinal setting along the ancient Pacific margin of North America. The siliceous and carbonaceous compositions of metasedimentary rocks, Precambrian model ages based on U-Pb dating of zircon and neodymium ages, and for some units, radiogenic neodymium isotopic compositions and whole-rock trace-element ratios similar to those of continental crust are evidence for this setting. Red Mountain (also known as Dry Creek) and WTF, two of the largest VMS deposits, are hosted in peralkaline metarhyolite of the Mystic Creek Member of the Totatlanika Schist. The Mystic Creek Member is distinctive in having high concentrations of high-field-strength elements (HFSE) and rare-earth elements (REE), indicative of formation in a within-plate (extensional) setting. Mystic Creek metarhyolite is associated with alkalic, within-plate basalt of the Chute Creek Member; neodymium isotopic data indicate an enriched mantle component for both members of this bimodal (rhyolite-basalt) suite. Anderson Mountain, the other significant VMS deposit, is hosted by the Wood River assemblage. Metaigneous rocks in the Wood River assemblage span a wide compositional range, including andesitic rocks, which are characteristic of arc volcanism. Our data suggest that the Mystic Creek Member likely formed in an extensional, back-arc basin that was associated with an outboard continental-margin volcanic arc that included rocks of the Wood River assemblage. We suggest that elevated HFSE and REE trace-element contents of metavolcanic rocks, whose major-element composition may have been altered, are an important prospecting tool for rocks of VMS deposit potential in east-central Alaska.

Introduction

Devonian to Mississippian magmatism was widespread along the ancient Pacific margin of North America. Many of the volcano-plutonic complexes and associated sedimentary rocks contain volcanogenic massive sulfide (VMS) or sedimentary exhalative massive sulfide (SEDEX) syngenetic base-metal (zinc-lead-copper) mineral deposits, including several deposits in east-central Alaska (Newberry and others, 1997; Dusel-Bacon and others, 2006). (Syngenetic means that the deposit formed contemporaneously with the enclosing rocks.) The discovery in the mid-1990s of zinc-lead-silver massive sulfide deposits in the Finlayson Lake area of southeastern Yukon, Canada, prompted renewed interest in known and potential base-metal sulfide occurrences in similar rocks in Alaska. The potential for economic deposits provided the impetus for our investigations of the major known VMS deposits of the Bonnifield mining district and their host rocks. We summarize herein the results of our study to characterize the regional tectonic setting of the host rocks to the VMS deposits, the mineralogy and isotopic characteristics of the deposits, and the controls of mineralization in a submarine hydrothermal environment. The reader is referred to Dusel-Bacon and others (2004, 2005, 2006) for complete scientific referencing and more detailed results of our investigations.

Regional Geology

Greenschist-facies metavolcanic and metasedimentary rocks in the Bonnifield district form range-parallel, east-

[1]U.S. Geological Survey.

[2]Geological Survey of Canada.

trending belts (Wahrhaftig, 1968; Gilbert and Bundtzen, 1979). Protoliths (premetamorphic rock types) consist of varying amounts of predominantly felsic and mafic volcanic and shallow intrusive rocks that are interlayered with carbonaceous and siliciclastic sedimentary rocks indicating deposition in a submarine, basinal setting. U-Pb zircon ages from felsic rocks indicate a prolonged period of Late Devonian to Early Mississippian (373±3 to 357±4 Ma) magmatism (Dusel-Bacon and others, 2004, 2005, 2006; C. Dusel-Bacon and J.N. Aleinikoff, unpub. data, 2007).

Quartz-rich schists and subordinate carbonaceous schist and marble of the informally named Healy schist form the core of a regional anticline (fig. B1). Carbonaceous metasedimentary rocks and minor conglomerate and rhyolite of the Keevy Peak Formation crop out north of, and stratigraphically above, the Healy schist (fig. B1). Bimodal — having both silica-poor (mafic) and silica-rich (felsic) compositions — metaigneous rocks, and carbonaceous and siliceous metasedimentary rocks of the Totatlanika Schist overlie the Keevy Peak Formation. Totatlanika Schist is subdivided into the following five members (Wahrhaftig 1968), from bottom to top: (1) Moose Creek (felsic and minor mafic schist); (2) California Creek (augen gneiss, grading to metarhyolite porphyry); (3) Chute Creek (metabasalt, which interfingers with both California Creek and Mystic Creek Members); (4) Mystic Creek (metarhyolite—mostly metamorphosed crystal tuff); and (5) Sheep Creek (quartzofeldspathic schist derived from near-source, reworked volcanic deposits; metasiltstone, metatuff, and marble). Carbonaceous phyllite, indistinguishable from that in the Keevy Peak Formation, is found within all members of the Totatlanika Schist. These rocks form a syncline, with the Sheep Creek Member occupying its core (fig. B1).

The Wood River assemblage comprises a package of metavolcanic and metasedimentary rocks on the south flank of the anticline cored by Healy schist (fig. B1). This assemblage has gross lithologic similarities to the metavolcanic and carbonaceous sedimentary assemblages in the Totatlanika Schist and was proposed by Gilbert and Bundtzen (1979) to be equivalent to it. One of the goals of our study was to evaluate this hypothesis, and our conclusions regarding this correlation are given below.

Deposits

Two of the largest VMS deposits in the Bonnifield district, the Red Mountain (Dry Creek) deposit and the WTF deposit, are located approximately 90 kilometers (km) south of Fairbanks in the northeastern part of the Wood River area (fig. B1). Both deposits are hosted by the Mystic Creek Member of the Totatlanika Schist and occur near the contact between phyllitic felsic metavolcanic and subordinate carbonaceous rocks of the Mystic Creek Member and the overlying, predominantly metasedimentary rocks of the Sheep Creek Member (Newberry and others, 1997; Smit, 1999). Drilling of one of the massive sulfide horizons just north of Red Mountain, named for its distinctive 1,800-meter (m)-thick zone of quartz-sericite-pyrite footwall alteration (fig. B2), identified an estimated resource of 3.2 million tons averaging 4.4 percent zinc, 1.9 percent lead, 0.2 percent copper, 3.01 ounces per ton (oz/t) silver, and 0.018 oz/t gold (Szumigala and Swainbank, 1998).

The WTF deposit (fig. B1) is located about 3 km northeast of Red Mountain. The structural and stratigraphic relationship between the WTF and Red Mountain deposits is disputed. Smit (1999) placed the shallowly dipping host rocks of the WTF deposit and the steeply north-dipping host rocks of the Red Mountain deposit on the northern and southern limbs, respectively, of an east-west-trending syncline (within the broader syncline cored by the Sheep Creek Member; fig. B1). Newberry and others (1997), on the other hand, placed the Red Mountain deposit in a separate and lower stratigraphic interval. As discussed below, our geochemical and U-Pb zircon sampling addressed these two possibilities. WTF has an estimated resource of 3.09 million tons averaging 6 percent zinc, 2.5 percent lead, 0.1 percent copper, 5.73 oz/t silver, and 0.029 oz/t gold (Szumigala and Swainbank, 1998).

The Anderson Mountain VMS prospect, located 32 km southwest of the Mystic Creek deposits, is exposed on the south limb of the antiform cored by the Healy schist. This prospect occurs within felsic to mafic metavolcanic rocks and associated carbonaceous metasedimentary rocks of the Wood River assemblage (fig. B1).

Methods

We collected outcrop and drill core samples of sulfide-bearing and unmineralized rocks from the Wood River area (figs. B1, B3) of the Bonnifield district. We utilized sensitive high-resolution ion microprobe (SHRIMP) U-Pb dating of zircon crystals separated from felsic igneous rocks to determine the crystallization ages of volcanic and plutonic units in the Wood River area (fig. B1). This dating technique has the advantage of being able to analyze minute (about 30-micrometer-diameter) areas, allowing age determination and analysis of both inherited zircon cores (from incorporated crustal material) and magmatic rims of zircons. Whole-rock neodymium isotopic compositions helped us identify the relative abundance of mantle versus continental crust components in the parent magmas of the metaigneous rocks.

A major part of our study employed whole-rock trace-element geochemistry of metaigneous rocks to determine their origin and tectonic setting, particularly of those that are associated with the VMS deposits. Considerable care was taken to sample only the freshest, least altered material. Our conclusions are based on trace elements that have been shown to be immobile, except during high-temperature metamorphism or because of pronounced hydrothermal alteration, neither of which has affected the rocks of the Wood River area. Because

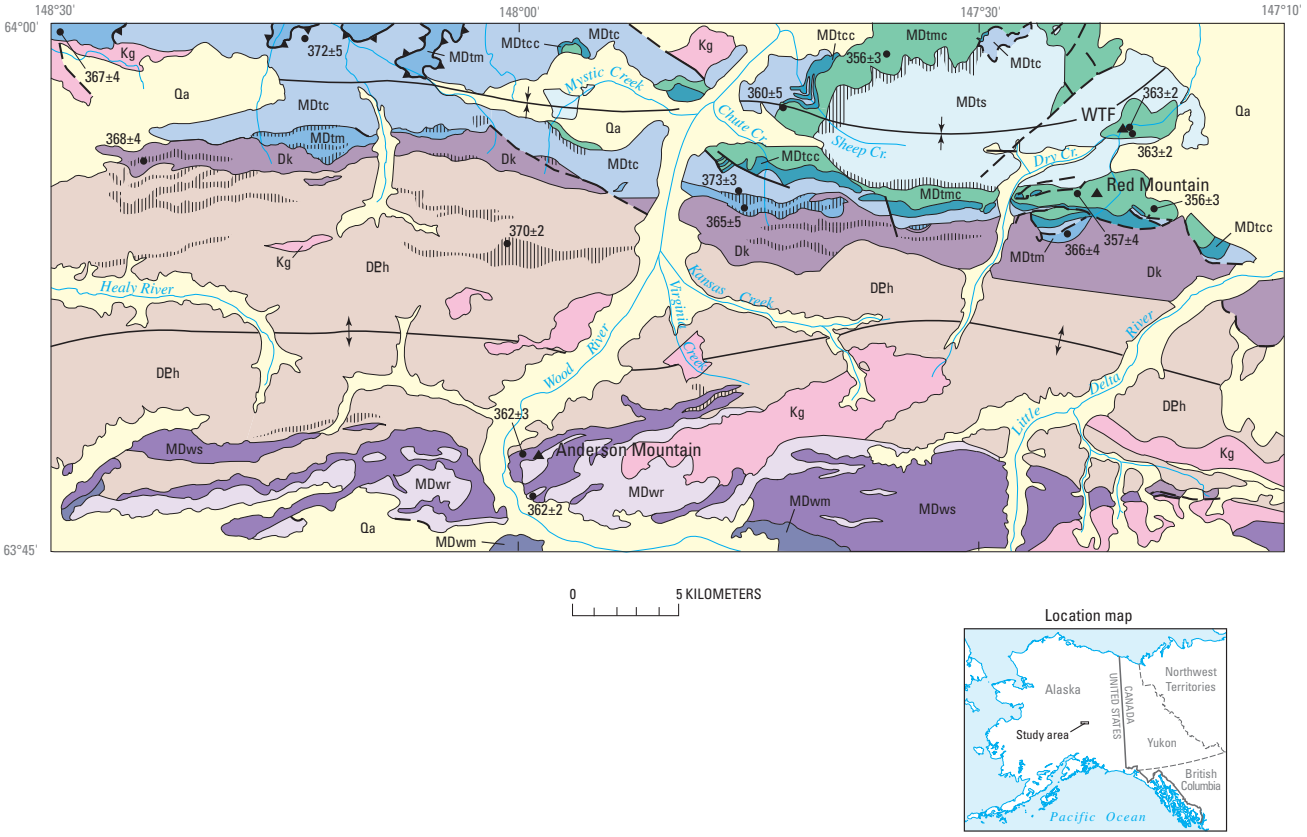

EXPLANATION

- Qa — Alluvium (Quaternary)
- Kg — Granite (Cretaceous)
- Totatlanika Schist (Early Mississippian to Late Devonian)— Individual members are mapped separately and listed below from youngest to oldest. Ages of individual members are based on SHRIMP U-Pb zircon ages and limited fossil age control. With the exception of the California Creek Member that yielded two Late Devonian ages, U-Pb zircon ages for all other dated members span the Late Devonian-Early Mississippian boundary (360±2 Ma; Okulitch, 2002); therefore, all members are assigned the map unit symbol of MD
  - MDts — Sheep Creek Member—Epiclastic quartz-feldspar-sericite schist and tuffaceous slate
  - MDtmc — Mystic Creek Member—Felsic metavolcanic schist
  - MDtcc — Chute Creek Member—Mafic metavolcanic schist
  - MDtc — California Creek Member—Quartz-potassium feldspar-sericite schist and augen gneiss
  - MDtm — Moose Creek Member—Quartz-potassium-feldspar gneiss, felsic schist, and mafic schist
- Wood River assemblage (Early Mississippian to Late Devonian)
  - MDwm — Metasedimentary rock—Includes marble, quartzite, and calcarenite
  - MDws — Green metavolcanic schist and carbonaceous schist
  - MDwr — Rhyolite schist
- Dk — Keevy Peak Formation (Devonian)—Quartz-sericite schist, carbonaceous quartz schist, slate, and stretched-pebble conglomerate
- DPh — Healy schist (informal) (Devonian and older)—Quartz-sericite schist, quartzite, chlorite schist, marble, and metagabbro
- Carbonaceous schist—Pattern superimposed on various units
- Contact
- Anticline
- Syncline
- Thrust fault—Sawteeth on upper plate
- Fault—Unclassified
- 362±3 — Location of sample and SHRIMP zircon age (in Ma)
- Major volcanogenic massive sulfide (VMS) deposit

Figure B1. Generalized geologic map of the Wood River area, northeastern Healy quadrangle, showing the location of the three main volcanogenic massive sulfide targets and U-Pb zircon ages. Abbreviations are as follows: SHRIMP, sensitive high-resolution ion microprobe; Ma, millions of years. Geology modified from Wahrhaftig (1968) and Gilbert and Bundtzen (1979); SHRIMP U-Pb zircon crystallization ages from Dusel-Bacon and others (2004, 2005) and C. Dusel-Bacon and J.N. Aleinikoff (unpub. data, 2007).

Figure B2. View of Red Mountain, looking west, showing quartz-sericite-pyrite alteration and north-dipping metarhyolite of the Mystic Creek Member. Cynthia Dusel-Bacon and Melanie Hopkins (U.S. Geological Survey (USGS)) in foreground. Photograph by Charlie Bacon (USGS).

Figure B3. Sampling drill core from the Dry Creek VMS deposit, stored at the Ester core facility, Alaska. Geologists from left to right: Rainer Newberry (University of Alaska), Curt Freeman (Avalon Development Corp.), Cameron Rombach (U.S. Geological Survey (USGS)), and Melanie Hopkins (USGS). Photograph by Charlie Bacon (USGS).

of major-element mobility, especially of alkalis and silica, magma compositions are identified utilizing a Zr/TiO_2 versus Nb/Y diagram (fig. B4).

Results

U-Pb zircon crystallization ages indicate a prolonged period of felsic magmatism from 373±3 to 357±4 Ma (fig. B1). Ages determined on felsic samples from the various map units overlap one another. Crystallization ages from throughout the Mystic Creek Member of the Totatlanika Schist overlap within the range of 363±3 to 357±4 Ma. Metarhyolites hosting both the WTF and Anderson Mountain deposits include SHRIMP U-Pb zircon ages of about 363 Ma, but their whole-rock compositions, trace-element signatures, and neodymium isotope compositions differ, as discussed below. U-Pb analyses of zircon cores from Totatlanika Schist and Healy schist felsic rocks yield Archean and Proterozoic ages (ranging from 2,681±16 to 981±31 Ma; Dusel-Bacon and others, 2004).

Epsilon neodymium isotope values (εNd_t; time-corrected to 360 Ma) are relatively elevated for the Mystic Creek Member metarhyolites (-1.0, -1.5, -1.6) and Chute Creek metabasalts (+1.7 and +5.3), indicating an enriched mantle component for both members of the bimodal suite. In contrast, metarhyolite from the Wood River assemblage and the Healy schist have lower εNd_t values (-4.5 and -13.5, respectively), reflecting a large continental crustal component. Proterozoic neodymium model ages of 1,030 to 2,010 Ma for metarhyolites (including samples from the Mystic Creek Member, Wood River assemblage, and Healy schist) and 570 to 910 Ma for Chute Creek Member metabasalt are consistent with a continental margin setting.

Trace-element analyses indicate that the metarhyolites of the Mystic Creek Member and the metabasalts of the Chute Creek, Sheep Creek, and Mystic Creek Members have high concentrations of high-field-strength and rare-earth elements, and yttrium and gadolinium, relative to average continental crust (for the metarhyolites) and primitive mantle (for the metabasalts). High-field-strength elements (HFSE) are those elements with a high charge to ionic radius ratio and include Zr, Hf, Nb, Ta, and Ti; rare-earth elements (REE) include La, Ce, Nd, Sm, Eu, Gd, Yb, and Lu. Rare-earth elements, not surprisingly, also are anomalously high in surface and water samples collected in the vicinity of Red Mountain, which is underlain by Mystic Creek metarhyolite (Eppinger and others, this volume, chap. I). The Zr/TiO_2–Nb/Y diagram (fig. B4) reveals the distinctive, highly alkaline ("peralkaline") composition of the Mystic Creek metarhyolites, which plot as comendites. In contrast, felsic rocks from the California and Moose Creek Members of the Totatlanika Schist have lower Nb/Y and Zr/TiO_2 ratios and plot as rhyodacite and dacite. Metabasalt from the Mystic Creek, Sheep Creek, and Chute Creek Members of the Totatlanika Schist also have high Nb/Y ratios and plot as alkali basalt. Compositions of the Wood River assemblage metavolcanic rocks differ from those of the Totatlanika Schist in that the former do not have alkaline compositions (that is, they do not fall within the alkali basalt, trachyandesite, trachyte, or comendite-pantellerite fields), with the exception of one sample that plots as a trachyte, and their compositions span a broad range that includes intermediate-composition andesite.

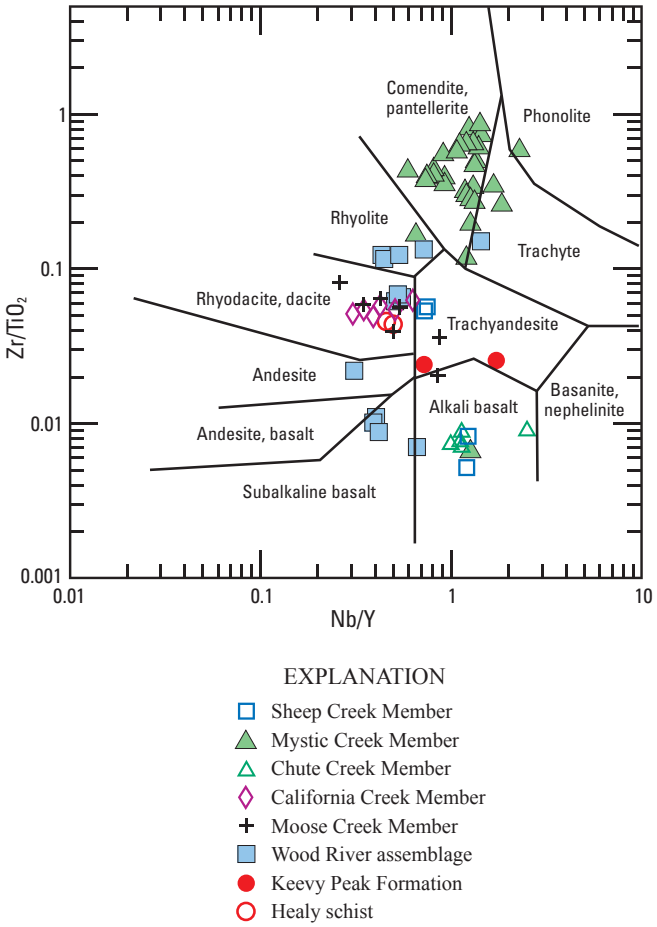

Figure B4. Metaigneous samples from the Wood River area plotted on the Zr/ TiO_2 versus Nb/Y discrimination diagram of Winchester and Floyd (1977).

Information about the tectonic setting in which magmas were generated can be attained from discrimination diagrams that utilize the immobile trace elements. The tantalum-ytterbium diagram (fig. B5) shows such information for our felsic igneous rocks (SiO_2 is 68–86 weight percent). The high tantalum and ytterbium contents of Mystic Creek peralkaline metarhyolites cause them to plot in the within-plate-granite field on the tantalum-ytterbium discrimination diagram (fig. B5). Within-plate rhyolites commonly are associated with rifting, an example being within-plate rhyolites from the Yellowstone Plateau volcanic field. Metarhyolites from the other members of the Totatlanika Schist and the Keevy Peak Formation plot in the field for volcanic-arc granites; however, the fact that their tantalum and ytterbium values are similar to the values for average upper continental crust (UCC, fig. B5) allows the possibility that the their chemical signatures could reflect involvement of continental crust during magma generation and ascent rather than being an indication of an arc (as opposed to a within-plate) setting. Wood River assemblage metarhyolites form a linear cluster that extends from the volcanic arc field into the transitional field between within-plate and anomalous ocean-ridge granites, in addition to having two samples that plot just inside the within-plate granite field.

The hafnium-thorium-tantalum diagram (fig. B6) shows the empirically determined magma types applicable to Bonnifield metabasalts (SiO_2 is 47–53 weight percent). Metabasalts from the Sheep Creek and Chute Creek Members of the Totatlanika Schist plot as ocean-island basalt (OIB), a magma type that is commonly associated with rifting and also is referred to as "within-plate basalt." Metabasalts from the Wood River assemblage plot in the calc-alkalic arc basalt and the enriched mid-ocean-ridge fields.

Conclusions

A continental margin setting and original proximity to the North American craton for the Late Devonian and Early Mississippian VMS host rocks of the Bonnifield district is indicated by (1) the quartz-rich compositions of many metasedimentary rocks; (2) the presence of Archean and Proterozoic inherited zircon cores and detrital zircons; (3) radiogenic neodymium isotopic compositions for the Healy schist and, to a lesser degree, the Wood River assemblage; (4) Proterozoic neodymium model ages for the Totatlanika Schist, Healy schist, and Wood River assemblage; and (5) the similarity in trace-element ratios between some of the felsic metaigneous samples and average upper continental crust.

Evidence for an extensional setting for the submarine eruption of the Mystic Creek Member metarhyolite consists of (1) its peralkaline composition and inferred within-plate tectonic setting; (2) its association with Chute Creek Member basalt, which also has alkalic, within-plate trace-element characteristics; and (3) elevated εNd_t values for Mystic Creek metarhyolite and Chute Creek metabasalts that indicate an enriched mantle component for both members of the bimodal suite. Dusel-Bacon and others (2004) speculated that the distinctly peralkaline, within-plate metarhyolites of the Mystic Creek Member may have been partial melts of underplated, deep crustal alkalic gabbros that also were the source of the alkalic, within-plate metabasite of the Chute Creek Member. Dark-gray shales interstratified with metarhyolite and massive sulfide horizons at WTF and Red Mountain show HFSE and light-REE enrichment similar to that in Mystic Creek metarhyolite, suggesting a significant peralkaline rhyolitic tuff component in the seafloor sediments that is consistent with their deposition in a synvolcanic, extensional basin. Similar U-Pb ages and geochemical characteristics for the WTF and Red Mountain deposits suggest that they occur in the same host-rock stratigraphic interval and support the syncline model of Smit (1999).

Mid-Paleozoic bimodal magmatic rocks, including mafic rocks that have within-plate geochemical characteristics, occur throughout much of the Yukon-Tanana Upland and northern Alaska Range. Dusel-Bacon and others (2004, 2006) proposed that this magmatism resulted from attenuation of the continen-

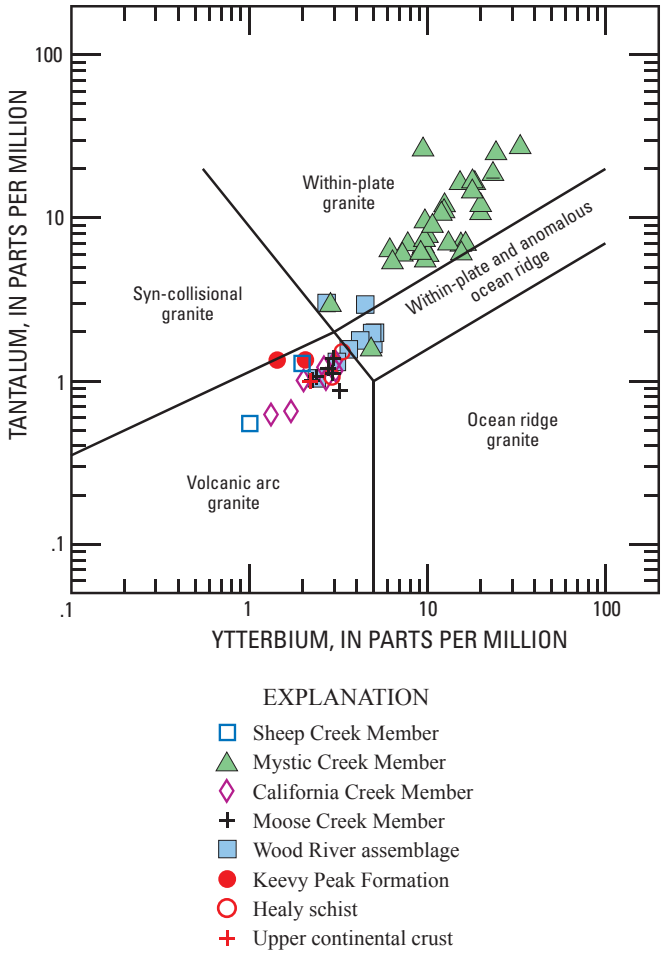

Figure B5. Felsic metaigneous samples from the Wood River area and the composition of average upper continental crust (values are those of McLennan, 2001) plotted on the tantalum-ytterbium (Ta-Yb) diagram of Pearce and others (1984).

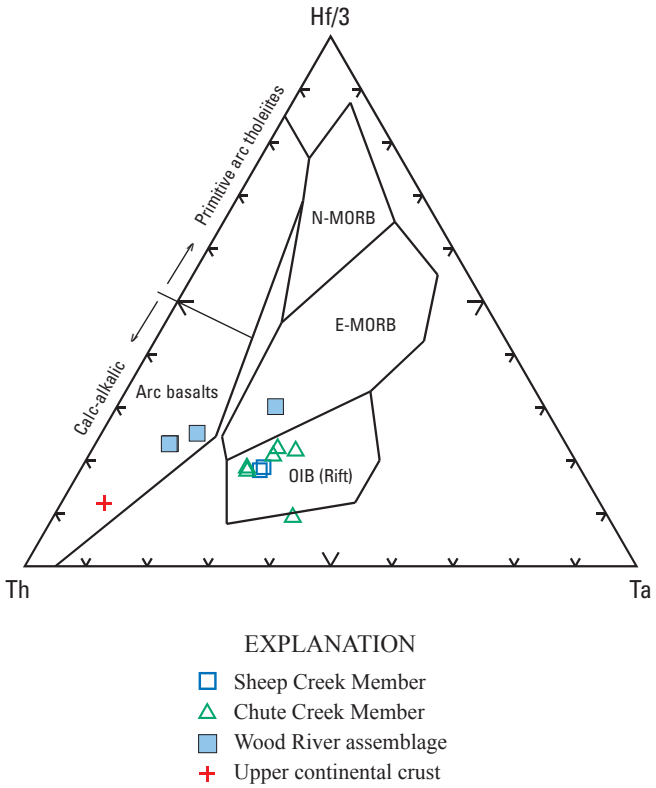

Figure B6. Mafic metavolcanic samples from the Wood River area plotted on the hafnium-thorium-tantalum (Hf-Th-Ta) diagram of Wood (1980). Abbreviations are as follows: E-MORB, enriched mid-ocean ridge basalt; N-MORB, normal mid-ocean ridge basalt; OIB, ocean-island basalt.

tal margin behind an east-dipping subduction zone. Evidence suggesting that the Wood River assemblage originated as an arc developed within continental crust above this subduction zone includes (1) metaigneous rocks that span a wide range of compositions, including andesitic rocks that are characteristic of arc magmatism; (2) some basalts that have trace-element arc signatures; and (3) an εNd_t value of -4.5 indicating a crustal component in the melt. This interpretation implies that the coeval Mystic Creek Member of the Totatlanika Schist formed an extensional (back-arc) basin that was associated with an outboard volcanic arc that included rocks of the Wood River assemblage (Dusel-Bacon and others, 2005).

Peralkaline metarhyolites of the Mystic Creek Member of the Totatlanika Schist that exhibit extreme within-plate geochemical characteristics host, or are associated with, the largest VMS deposits in the Bonnifield mining district. This association suggests that the presence of highly elevated HFSE and REE trace-element contents in metarhyolites, whose major-element compositions may have been altered, is an important prospecting tool for VMS deposits that formed in an extensional setting. Our trace-element data for Wood River assemblage metarhyolites that host the Anderson Mountain deposit further indicate that even slightly elevated HFSE and REE contents (for example, tantalum and ytterbium; fig. B5) can be prospective for VMS deposits formed in an arc setting.

Acknowledgments

We are indebted to Tom Bundtzen for introducing the senior author to the geology of the Wood River area. We also thank Pacific Alaska Resources Company geologists Barry Hoffmann, Jo Drechsler, Rob McLeod, Gary Andersen, and Ted Erdman; and Grayd Resource Corporation Vice President Hans Smit for providing access to drill core and company reports for the Bonnifield VMS deposits. Rainer Newberry, Sam Dashevsky, and Sean Bemis helped with drill core sampling. Curt Freeman, Cameron Rombach, Melanie Hopkins, and Charlie Bacon assisted during fieldwork, as well as drill core sampling. We thank Joe Wooden for re-analyzing one of the U-Pb zircon samples. This paper benefited from reviews by Marti Miller and Dave John.

References Cited

Dusel-Bacon, Cynthia, Hopkins, M.J., Mortensen, J.K., Dashevsky, S.S., Bressler, J.R., and Day, W.C., 2006, Paleozoic tectonic and metallogenic evolution of the pericratonic rocks of east-central Alaska and adjacent Yukon, *in* Colpron, Maurice, and Nelson, J.L., eds., Paleozoic evolution and metallogeny of pericratonic terranes at the ancient Pacific margin of North America, Canadian and Alaskan Cordillera: Geological Association of Canada, Special Paper 45, p. 25–74.

Dusel-Bacon, Cynthia, Premo, W.R., and Aleinikoff, J.N., 2005, Geochemical and Nd isotopic evidence for an extending continental-margin arc/back arc setting for peralkaline rhyolite-hosted massive sulfide deposits of the Bonnifield district, east-central Alaska [abs.]: Geological Society of America Abstracts with Programs, v. 37, no. 7, p. 97.

Dusel-Bacon, Cynthia, Wooden, J.L., and Hopkins, M.J., 2004, U-Pb zircon and geochemical evidence for bimodal mid-Paleozoic magmatism and syngenetic base-metal mineralization in the Yukon-Tanana terrane, Alaska: Geological Society of America Bulletin, v. 116, no. 7–8, p. 989–1015.

Eppinger, R.G., Briggs, P.H., Dusel-Bacon, Cynthia, Giles, S.A., Gough, L.P., Hammarstrom, J.M., and Hubbard, B.E., 2007, Environmental geochemistry at Red Mountain, an unmined volcanogenic massive sulphide deposit in the Bonnifield district, Alaska Range, east-central Alaska: Geochemistry: Exploration, Environment, Analysis, v. 7, no. 3, p. 207–223.

Gilbert, W.G., and Bundtzen, T.K., 1979, Mid-Paleozoic tectonics, volcanism, and mineralization in north-central Alaska Range, *in* Sisson, Alexander, ed., The relationship of plate tectonics to Alaskan geology and resources, Proceedings, Alaska Geological Society Symposium 6, Anchorage, Alaska, April 4–6, 1977: Anchorage, Alaska, Alaska Geological Society, p. F1–F22.

McLennan, S.M., 2001, Relationships between the trace element composition of sedimentary rocks and upper continental crust: Geochemistry, Geophysics, Geosystems, v. 2, no. 4, 24 p., available only online at *http://www.agu.org/journals/gc/gc0104/2000GC000109*. (Subscription may be required.) (*doi: 10.1029/2000GC000109*)

Newberry, R.J., Crafford, T.C., Newkirk, S.R., Young, L.E., Nelson, S.W., and Duke, N.A., 1997, Volcanogenic massive sulfide deposits of Alaska: Economic Geology Monograph 9, p. 120–150.

Okulitch, A.V., 2002, Geological time chart, 2002: Geological Survey of Canada, Open File 3040, 1 sheet.

Pearce, J.A., Harris, N.B.W., and Tindle, A.G., 1984, Trace element discrimination diagrams for the tectonic interpretation of granitic rocks: Journal of Petrology, v. 25, no. 4, p. 956–983.

Smit, H., 1999, The Dry Creek VMS project, Bonnifield district, central Alaska, *in* Pathways ‘99, Extended Abstracts Volume: Vancouver, British Columbia, Canada, British Columbia and Yukon Chamber of Mines, p. 17–18.

Szumigala, D.J., and Swainbank, R.C., 1998, Alaska’s mineral industry 1998: Alaska Division of Geological and Geophysical Surveys Special Report 53, 71 p.

Wahrhaftig, Clyde, 1968, Schists of the central Alaska Range: U.S. Geological Survey Bulletin 1254–E, p. E1–E22.

Winchester, J.A., and Floyd, P.A., 1977, Geochemical discrimination of different magma series and their differentiation products using immoble elements: Chemical Geology, v. 20, no. 4, p. 325–343.

Wood, D.A., 1980, The application of a Th-Hf-Ta diagram to problems of tectonomagmatic classification and to establishing the nature of crustal contamination of basaltic lavas of the British Tertiary volcanic province: Earth and Planetary Science Letters, v. 50, no. 1, p. 11–30.

Matching Magnetic Trends and Patterns Across the Tintina Fault, Alaska and Canada—Evidence for Offset of About 490 Kilometers

By Richard W. Saltus

Chapter C of
Recent U.S. Geological Survey Studies in the Tintina Gold Province, Alaska, United States, and Yukon, Canada—Results of a 5-Year Project
Edited by Larry P. Gough and Warren C. Day

Scientific Investigations Report 2007–5289–C

U.S. Department of the Interior
U.S. Geological Survey

Contents

Figures

Matching Magnetic Trends and Patterns Across the Tintina Fault, Alaska and Canada—Evidence for Offset of About 490 Kilometers

By Richard W. Saltus[1]

Abstract

Magnetic anomaly patterns on opposite sides of the mapped Tintina fault in eastern Alaska and western Canada show an apparent offset of about 490 kilometers (km), probably of Eocene age. This estimate is compared with previous geologically based estimates of 400 to 430 km and paleomagnetically based estimates of more than 1,100 km. The apparent geophysical alignments have geologic implications that deserve further study.

Introduction

The Tintina fault zone in eastern Alaska and western Canada (fig. C1) is a major tectonic boundary between cratonic North America and pericratonic rocks of the Yukon-Tanana and related terranes (Roddick, 1967; Gabrielse, 1985; Gabrielse and others, 2006). Numerous estimates have been made of the amount and timing of offset on this fault system (for example, Dover, 1994; Plafker and Berg, 1994; Gabrielse and others, 2006). Several of the latest estimates, based on matching of geologic elements across the fault, indicate probable offset of at least 400 kilometers (km), primarily during the Eocene (Dover, 1994; Gabrielse and others, 2006), although published displacement estimates based on paleomagnetic data have ranged as high as 1,100 to 2,400 km (Beck and others, 1981; Irving and others, 1985; Umhoefer and others, 1989).

Regional geophysical data, such as magnetic and gravity field maps, display patterns and trends that are representative of the composition of the crust (for example, Blakely, 1995). The amount of offset on crustal faults can be investigated by "cutting and sliding" the geophysical maps to evaluate pattern and trend alignment under various slip scenarios. In particular, the compiled aeromagnetic data portrayed on the Magnetic Anomaly Map of North America (North American Magnetic Anomaly Group, 2002) provide an excellent base map for this endeavor.

Regional magnetic anomalies reflect the amount and distribution of magnetic minerals, most notably magnetite, in regions of the crust and upper mantle at temperatures below about 580°C. Magnetic anomaly wavelengths are generally related to the depth to magnetic sources and show a geometric amplification of shallow-source amplitudes over those of deeper sources (Blakely, 1995; Sleep and Fujita, 1997). Thus, magnetic anomaly sources can arise from geologic features of varying depths within the crust and varying ages. Also, the magnetic properties of different sides of the fault may be modified by chemical and (or) thermal alteration before, during, or after fault slippage. Thus, the matching of magnetic anomaly patterns is somewhat subjective but can contribute to the larger body of evidence regarding the likely amount of displacement across a fault.

Methods

Regional geophysical data, specifically residual maps of the Earth's magnetic field, provide a complex proxy overview of crustal composition and structure as reflected in the occurrence of magnetic minerals, especially magnetite. Crustal magnetic field data are collected primarily from airborne platforms, usually by helicopter or fixed-wing aircraft. For the purpose of geological interpretation, the measured data are adjusted by the removal of a theoretical regional surface, the International Geomagnetic Reference Field (IGRF), which is created from ground-based observatory and satellite data (International Association of Geomagnetism and Aeronomy, 1992; Blakely, 1995). The IGRF is a model of the deep-seated and slowly varying geodynamic sources of the Earth's overall magnetic field. Once the IGRF is removed, residual magnetic field maps (frequently called "total field" maps) reflect anomalies (perturbations) in the regional field caused by magnetic material within the crust and upper mantle. The primary magnetic mineral, magnetite, has a Curie temperature

[1]U.S. Geological Survey.

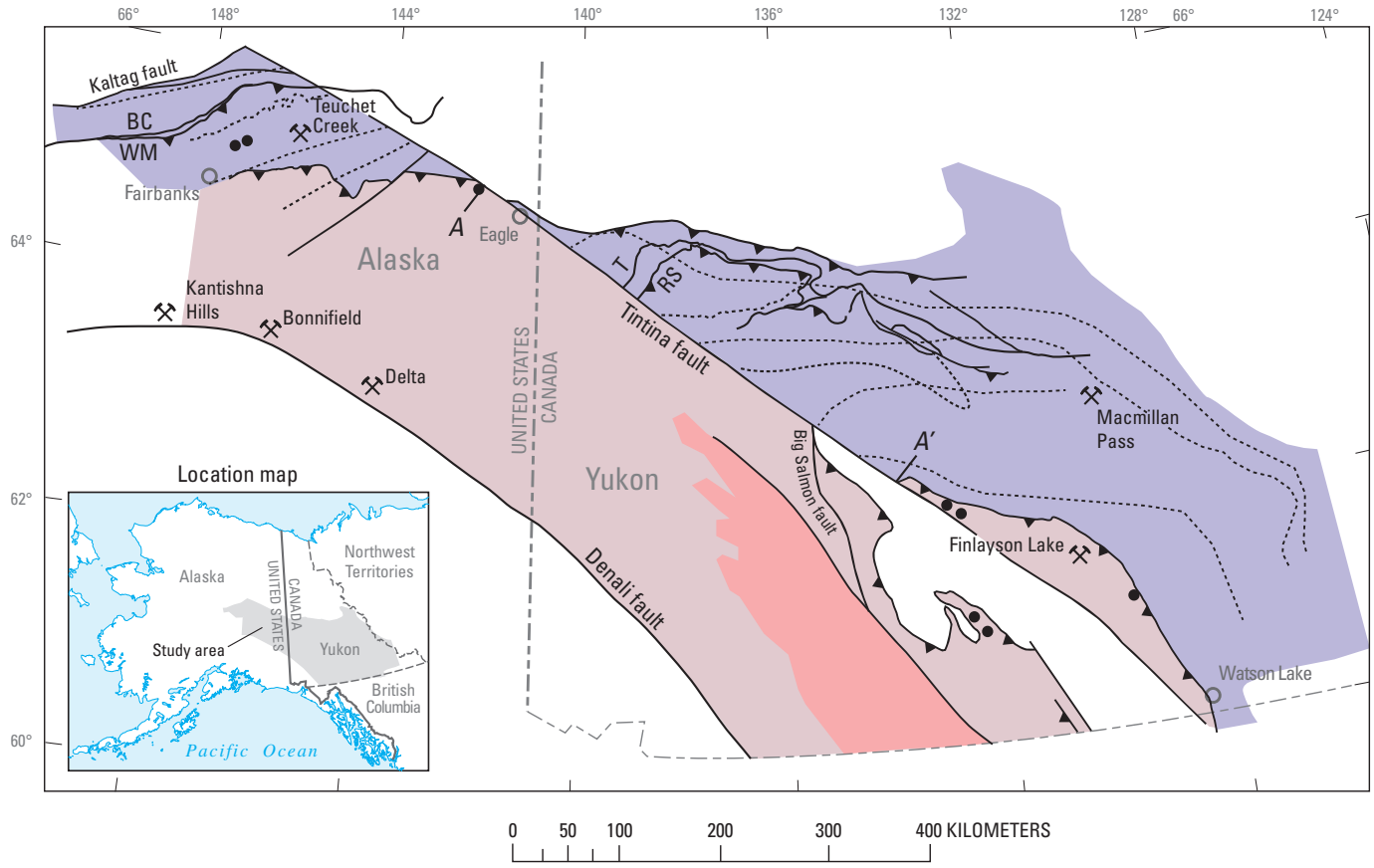

EXPLANATION

- Late Cretaceous plutons
- Yukon-Tanana terrane
- Paleozoic and Late Proterozoic off-shelf sedimentary rocks
- Selected geologic lineaments—Strain zones and boundaries between groups of plutonic rocks
- Major fault
- Thrust fault—Sawteeth on upper plate. BC, Brush Creek; RS, Robert Service; T, Tombstone; WM, White Mountains
- Mining district in Devonian to Mississippian rock
- Blueschist or eclogite occurrence

Figure C1. Regional geology with faults and features (adapted from Gabrielse and others (2006) and Dusel-Bacon and others (2006)). Markers *A* and *A′* are measurement points for proposed fault restoration.

of about 580°C, so magnetic sources have a thermal limit with depth that typically falls somewhere near the crust-mantle boundary, which is typically about 35 to 40 km deep.

The analysis and interpretation of magnetic anomalies typically involve some form of inversion to deduce the individual magnetic sources from their composite representation in the total field. In a strictly mathematical sense, this is a non-unique problem, which means that some assumptions must be made to constrain the solution. For the purpose of fault reconstruction by pattern matching, it is not required that the magnetic anomalies be inverted or interpreted. However, if the conclusions from geophysical pattern matching are to be evaluated geologically, it is useful to explore the possible geological associations of the geophysical features.

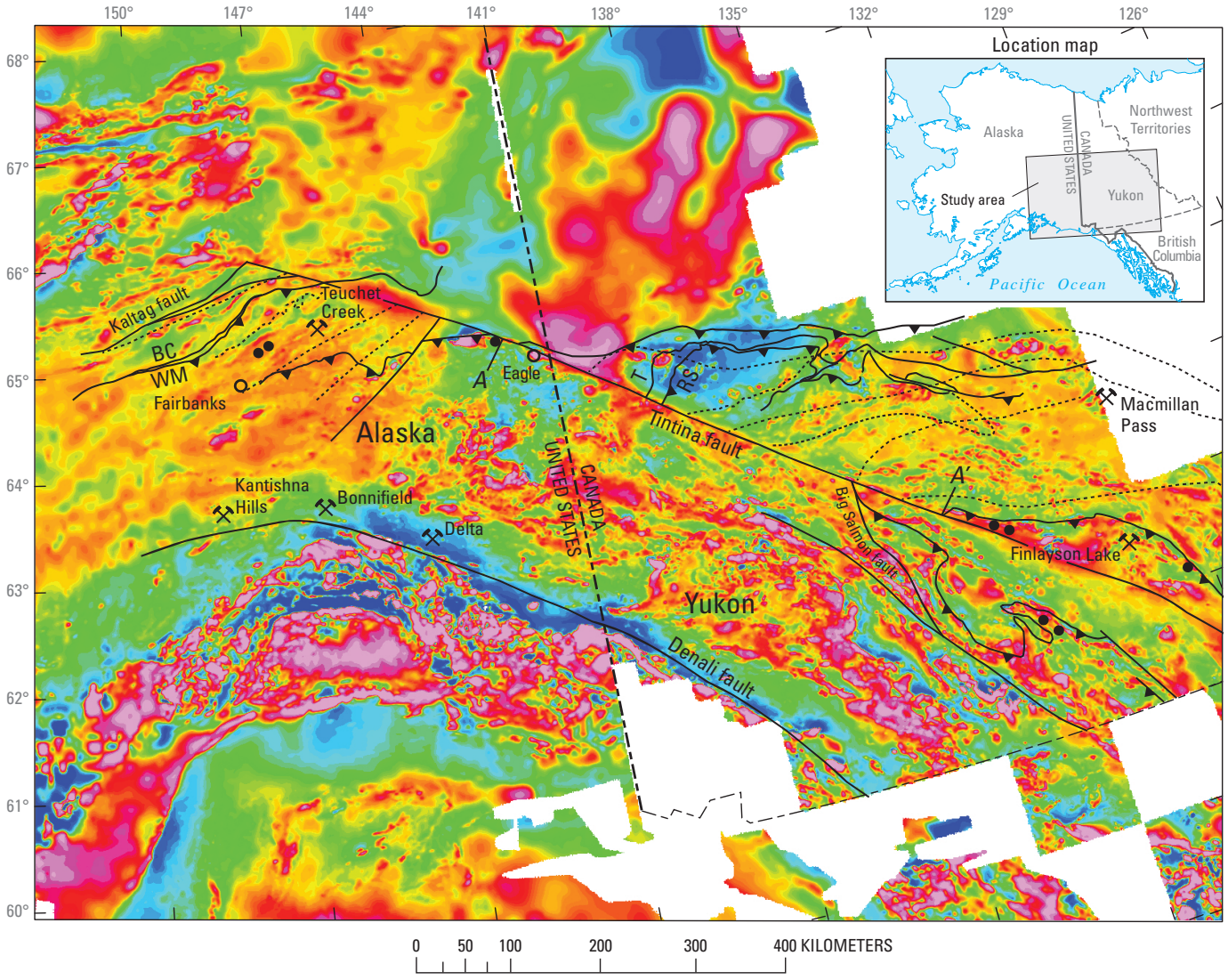

Figure C2. A subset of the Magnetic Anomaly Map of North America (North American Magnetic Anomaly Group, 2002) with selected geology elements (see fig. C1). Markers *A* and *A′* are reference points for proposed fault restoration.

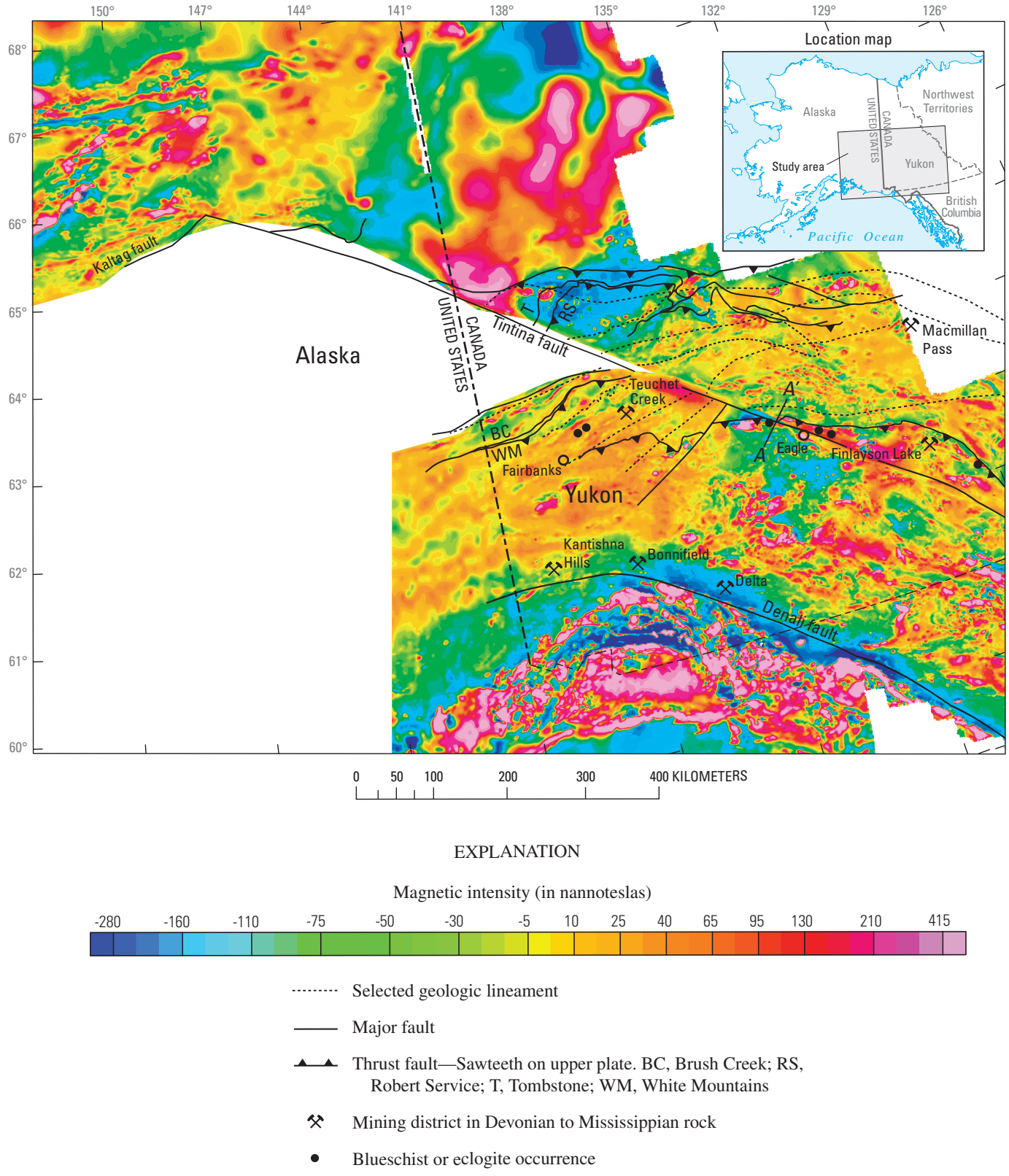

Figure C3. Proposed palinspastic restoration based on matching of magnetic anomalies across the Tintina fault. This figure is made by cutting and shifting figure C2. A shift of about 490 km from west to east aligns markers *A* and *A′* as shown.

This study involves a very simple visual approach to magnetic anomaly interpretation for this study. I selected a subset of the recently compiled Magnetic Anomaly Map of North America (North American Magnetic Anomaly Group, 2002). The Magnetic Anomaly Map of North America was created by carefully merging hundreds of individual aeromagnetic surveys into a single grid with uniform effective survey height. This compilation minimizes any artifacts related to individual magnetic survey boundaries and allows one to concentrate on geologically significant anomalies and patterns.

A visual image (fig. C2) of the selected grid subset was created using a histogram-stretched color scale adapted to the data ranges and statistics for the region. This coloring enhances subtle magnetic anomaly amplitude variations in the central part of the anomaly range. This is appropriate for identifying geologically significant variations that would otherwise be difficult to see if a linear color scale were used.

The colored magnetic anomaly image was then cut along the regionally mapped trace of the Tintina fault (Gabrielse and others, 2006) and slid by variable amounts along the fault trace to examine pattern and trend correlations for different slip scenarios. This pattern matching was based only on the magnetic anomalies and was done independent of geology. Our preferred matching of magnetic anomalies across the fault (fig. C2) requires about 490 km of total shift along the Tintina fault.

Results and Importance

What are the geologic implications of this hypothetical fault slip restoration on the Tintina fault system? Figure C3 shows the geologic base map from figure C1 cut along the Tintina fault and subjected to a 490-km shift. This shift produces a number of interesting geological alignments. Here we point out several implications of the proposed reconstruction, from southeast to northwest. For the purpose of discussion, the restored alignment points *A* and *A′*, located about 50 km northwest of the restored position of the town of Eagle, are used as the zero position for specifying features along the restored Tintina fault.

Perhaps the broadest scale geologic alignment is the matching of the separate strands of the Inconnu thrust fault (IT as shown by Gabrielse and others, 2006) at both ends of the orphaned Yukon-Tanana block that lies northeast of the Tintina fault. The southeastern edge of this block, near Watson Lake (about 400 km southeast of *A*-*A′*), ends up near the three-way intersection of the Inconnu fault, the Big Salmon fault, and the Tintina fault. The northwestern edge of the orphan Yukon-Tanana block connects at position *A*-*A′* with the thrust fault (thought to represent a continuation of the Inconnu thrust fault; Gabrielse and others, 2006) that separates the Yukon-Tanana terrane from off-shelf Late Proterozoic and Paleozoic sedimentary rocks to the northwest.

Another interesting alignment produced by this proposed restoration is the coincidence of eclogite and blueschist occurrences (as shown by Dusel-Bacon and others, 2006) near the restored position of the town of Eagle with those across the Tintina fault in the northwestern edge of the orphan Yukon-Tanana block. The restoration then puts these occurrences along the trend with two occurrences to the west near Fairbanks.

Several major Devonian to Mississippian mineral districts fall within the study area (fig. C1; Dusel-Bacon and others, 2006) and their relative locations are affected by the proposed restoration. The Kantishna Hills, Bonnifield, and Delta districts contain syngenetic volcanogenic massive sulfide deposits (see chapters B, E, I, and J in this volume). The proposed restoration brings these districts closer to the Finlayson Lake massive sulfide district in southeastern Yukon (fig. C3). The Teuchet Creek stratiform sedimentary exhalative (SEDEX) mineral district aligns along the geologic trend with the Macmillan Pass SEDEX district after restoration (fig. C3).

To the northwest of *A*-*A′*, several geologic trends are mapped on opposite sides of the Tintina fault. These include faults, strain zones, and Cretaceous plutonic belts (shown as dashed lines on figs. C1 and C3). The first set of matching features, as mentioned above, is the opposite strands of the Inconnu thrust fault that join up at *A*-*A′*. Proceeding to the northwest, two plutonic suite boundaries line up on opposite sides of the fault. Farther to the northwest, two strands of the strain zones line up approximately on opposite sides of the restored fault. Continuing northwest, the trends and zones on the Alaskan side appear to be increasingly compressed relative to the trends on the Canadian side. This is presumably the result of overall compression on the Alaskan side approaching the Kaltag fault and possibly of extension on the Canadian side. Up to 250 km of variation in relative offset due to compression and extension is suggested by the differential positions of the trends in the off-shelf sequence on opposite sides of the fault in this zone.

Discussion and Conclusions

The preliminary observations in this short paper are intended to stimulate continued comparative geologic study across the Tintina fault in Alaska and adjacent Canada. Correlations between magnetic anomalies and patterns can provide useful hypotheses about apparent fault slip but do not indicate timing of slip unless the individual anomalies and patterns are interpreted to associate them with geologic features with known ages. The significance of the geophysical alignments needs to be tested through geologic studies.

The most detailed analysis of the Eocene slip history of the Tintina fault to date is by Gabrielse and others (2006). They conclude that geologic evidence supports slip estimates

between 400 and 430 km. This amount of slip lines up the Beaver Creek-White Mountains thrust system on the Alaskan side with the Tombstone-Robert Service thrust system on the Canadian side of the Tintina fault. Their conclusions also depend on alignment of the Tombstone and McQuestern plutons across the fault.

The preferred restoration of between 400 and 430 km of fault slip (Gabrielse and others, 2006) results in a 60+ km mismatch of the two crossings of the Inconnu thrust fault from the Alaskan side to the Canadian side of the fault. Gabrielse and others (2006) interpret this as indication of extension on the Canadian side, presumably related to extensive Late Cretaceous magmatism in the region. This extension would have preceded the later Eocene movement of the Tintina fault yet used the trace of the Tintina as a bounding "transform" between zones of differential extension.

An alternate hypothesis to explain the difference in spacing of geologic features across this portion of the fault is that compressional deformation took place on the Alaskan side relative to the Canadian side. The amount of shortening might logically be expected to increase to the northwest toward the bend in the Tintina fault near its intersection with the Kaltag fault. This interpretation seems consistent with the character of magnetic anomalies along this part of the fault, although that conclusion is somewhat subjective.

The apparent slip estimates based on alignment of magnetic anomalies fall far short of published displacement estimates from paleomagnetic studies (for example, 1,900±700 km by Marquis and Globerman, 1988; Johnston and others, 1996; Wynne and others, 1998). I agree with Gabrielse and others (2006) that the burden for resolving this discrepancy appears to fall on the side of the paleomagnetic studies.

In conclusion, comparison matching of magnetic features on both sides of the Tintina fault in east-central Alaska and northwestern Canada indicates a good match of several key anomalies and magnetic patterns if slip of about 490 km is restored on the fault. This hypothetical fault slip restoration makes pre-slip predictions of the relation of geologic elements on opposite sides of the fault. The apparent relative compression of various thrust belts on the Alaskan side relative to the Canadian side may be due to tectonic compression or lateral ramps on the Alaskan side, possibly related to the geometry of the southwest bend of the Tintina fault near its intersection with the Kaltag fault.

Acknowledgments

The author is grateful for excellent and constructive reviews by Sue Karl and Dwight Bradley of the U.S. Geological Survey.

References Cited

Beck, M.E., Jr., Burmester, R.F., Engebretson, D.C., and Schoonover, R., 1981, Northward translation of Mesozoic batholiths, western North America; paleomagnetic evidence and tectonic significance: Geofisica Internacional, v. 20, no. 3, p. 143–162.

Blakely, R.J., 1995, Potential theory in gravity and magnetic applications: New York, Cambridge University Press, 441 p.

Dover, J.H., 1994, Geology of part of east-central Alaska, *in* Plafker, George, and Berg, H.C., eds., The geology of Alaska, chapter G–1 *of* The geology of North America: Boulder, Colo., Geological Society of America, p. 153–204.

Dusel-Bacon, Cynthia, Hopkins, M.J., Mortensen, J.K., Dashevsky, S.S., Bressler, J.R., and Day, W.C., 2006, Paleozoic tectonic and metallogenic evolution of the pericratonic rocks of east-central Alaska and adjacent Yukon, *in* Colpron, Maurice, and Nelson, J.L., eds., Paleozoic evolution and metallogeny of pericratonic terranes at the ancient Pacific margin of North America, Canadian and Alaskan Cordillera: Geological Association of Canada Special Paper 45, p. 25–74.

Gabrielse, Hubert, 1985, Major dextral transcurrent displacements along the northern Rocky Mountain Trench and related lineaments in north-central British Columbia: Geological Society of America Bulletin, v. 96, no. 1, p. 1–14.

Gabrielse, Hubert, Murphy, D.C., and Mortensen, J.K., 2006, Cretaceous and Cenozoic dextral orogen-parallel displacements, magmatism, and paleogeography, north-central Canadian Cordillera, *in* Haggart, J.W., Enkin, R.J., and Monger, J.W.H., eds., Paleogeography of the North American Cordillera; Evidence for and against large-scale displacements: Geological Association of Canada Special Paper 46, p. 255–276.

International Association of Geomagnetism and Aeronomy, 1992, Analysis of the main field and secular variation "International Geomagnetic Reference Field, 1991 revision": Geophysics, v. 57, no. 7, p. 956–959.

Irving, Edward, Woodsworth, G.J., and Wynne, P.J., 1985, Paleomagnetic evidence for northward motion of the Western Cordillera in latest Cretaceous to early Tertiary times: Geological Society of America Abstracts with Programs, v. 17, no. 6, p. 363.

Johnston, S.T., Wynne, P.J., Francis, Don, Hart, C.J.R., Enkin, R.J., and Engebretson, D.C., 1996, Yellowstone in Yukon; The Late Cretaceous Carmacks Group: Geology, v. 24, no. 11, p. 997–1000.

Marquis, Guy, and Globerman, B.R., 1988, Northward motion of the Whitehorse trough; Paleomagnetic evidence from the Upper Cretaceous Carmacks Group: Canadian Journal of Earth Sciences, v. 25, no. 12, p. 2005–2016.

North American Magnetic Anomaly Group, 2002, Digital data grids for the magnetic anomaly map of North America: U.S. Geological Survey Open-File Report 02–414, 1 sheet; scale 1:10,000,000. (Also available online at *http://pubs.usgs.gov/of/2002/ofr-02-414/*.)

Plafker, George, and Berg, H.C., 1994, Overview of the geology and tectonic evolution of Alaska, *in* Plafker, George, and Berg, H.C., eds., The geology of Alaska, chapter G–1 *of* The geology of North America: Boulder, Colo., Geological Society of America, p. 989–1021.

Roddick, J.A., 1967, Tintina Trench: Journal of Geology, v. 75, no. 1, p. 23–32.

Sleep, N.H., and Fujita, Kazuya, 1997, Principles of geophysics: Malden, Mass., Blackwell Science, 586 p.

Umhoefer P.J., Dragovish, Joe, Cary, Jeff, and Engebretson, D.C., 1989, Refinements of the "Baja British Columbia" plate-tectonic model for northward translation along the margin of western North America: Geophysical Monograph, v. 50, p. 101–111.

Wynne, P.J., Enkin, R.J., Baker, Judith, Johnston, S.T., and Hart, C.J.R., 1998, The big flush; Paleomagnetic signature of a 70 Ma regional hydrothermal event in displaced rocks of the northern Canadian Cordillera: Canadian Journal of Earth Sciences, v. 35, no. 6, p. 657–671.

The Black Mountain Tectonic Zone—A Reactivated Northeast-Trending Crustal Shear Zone in the Yukon-Tanana Upland of East-Central Alaska

By J. Michael O'Neill, Warren C. Day, John N. Aleinikoff, and Richard W. Saltus

Chapter D of
Recent U.S. Geological Survey Studies in the Tintina Gold Province, Alaska, United States, and Yukon, Canada—Results of a 5-Year Project

Edited by Larry P. Gough and Warren C. Day

Scientific Investigations Report 2007–5289–D

U.S. Department of the Interior
U.S. Geological Survey

Contents

Figures

The Black Mountain Tectonic Zone—A Reactivated Northeast-Trending Crustal Shear Zone in the Yukon-Tanana Upland of East-Central Alaska

By J. Michael O'Neill,[1] Warren C. Day,[1] John N. Aleinikoff,[1] and Richard W. Saltus[1]

Abstract

The Black Mountain tectonic zone in the Yukon-Tanana terrane of east-central Alaska is a belt of diverse northeast-trending geologic features that can been traced across Black Mountain in the southeast corner of the Big Delta 1°×3° degree quadrangle. Geologic mapping in the larger scale B1 quadrangle of the Big Delta quadrangle, in which Black Mountain is the principal physiographic feature, has revealed a continuous zone of normal and left-lateral strike-slip high-angle faults and shear zones, some of which have late Tertiary to Quaternary displacement histories. The tectonic zone includes complexly intruded wall rocks and intermingled apophyses of the contiguous mid-Cretaceous Goodpaster and Mount Harper granodioritic plutons, mafic to intermediate composite dike swarms, precious metal mineralization, early Tertiary volcanic activity and Quaternary fault scarps. These structures define a zone as much as 6 to 13 kilometers (km) wide and more than 40 km long that can be traced diagonally across the B1 quadrangle into the adjacent Eagle 1°×3° quadrangle to the east. Recurrent activity along the tectonic zone, from at least mid-Cretaceous to Quaternary, suggests the presence of a buried, fundamental tectonic feature beneath the zone that has influenced the tectonic development of this part of the Yukon-Tanana terrane. The tectonic zone, centered on Black Mountain, lies directly above a profound northeast-trending aeromagnetic anomaly between the Denali and Tintina fault systems. The anomaly separates moderate to strongly magnetic terrane on the northwest from a huge, weakly magnetic terrane on the southeast. The tectonic zone is parallel to the similarly oriented left-lateral, strike-slip Shaw Creek fault zone 85 km to the west.

Introduction

The Black Mountain tectonic zone, recently recognized and mapped in the Big Delta B–1 quadrangle, east-central Alaska, lies within the Yukon-Tanana Upland (YTU) (fig. D1; see also fig. 1 of the Editors' Preface and Overview). The YTU is restricted to the terrane between the Tintina and Denali dextral-slip fault zones and extends from central Alaska eastward into Yukon, Canada. The YTU is underlain mainly by complexly deformed greenschist to amphibolite-grade metamorphic rocks at least as old as Middle Devonian. The supracrustal metasedimentary and metavolcanic Paleozoic units were intruded during the Devonian by plutonic rocks of intermediate composition, which are now preserved as augen and biotite orthogneiss. After the tectonic assembly of the Paleozoic units during the regional early Mesozoic deformation, Jurassic, Cretaceous, and Tertiary plutonism flooded the area with mainly granodioritic batholiths (Dusel-Bacon and others, 2002).

The YTU between Fairbanks and Tok is cut by four prominent northeast-trending lineaments (Wilson and others, 1985). One such lineament is the Shaw Creek fault (fig. D1), a major left-lateral strike-slip fault that cuts across the Salcha River gneiss dome (Foster and others, 1979; Werdon and others, 2004). Two other lineaments to the east, the Sixtymile and Tok, are recognized by the alignment of physiographic features, mainly stream drainages and topographic highlands. The Mount Harper lineament, about 100 kilometers (km) east of the Shaw Creek fault and confined mainly to the Eagle 1°×3° quadrangle, directly east of the map area (see fig. D2), consists of mapped segments of faults, stratigraphic breaks, and physiographic alignments (Foster, 1976). The Mount Harper lineament appears to separate domains that have characteristic geochronologic signatures; Jurassic plutons do not occur west of this lineament (Foster, 1976).

The YTU between Fairbanks and Tok also is bisected by a major linear magnetic anomaly located between the Shaw Creek and Mount Harper lineaments (Saltus and Day, 2006). A steep, pronounced, northeast-trending magnetic gradient,

[1]U.S. Geological Survey.

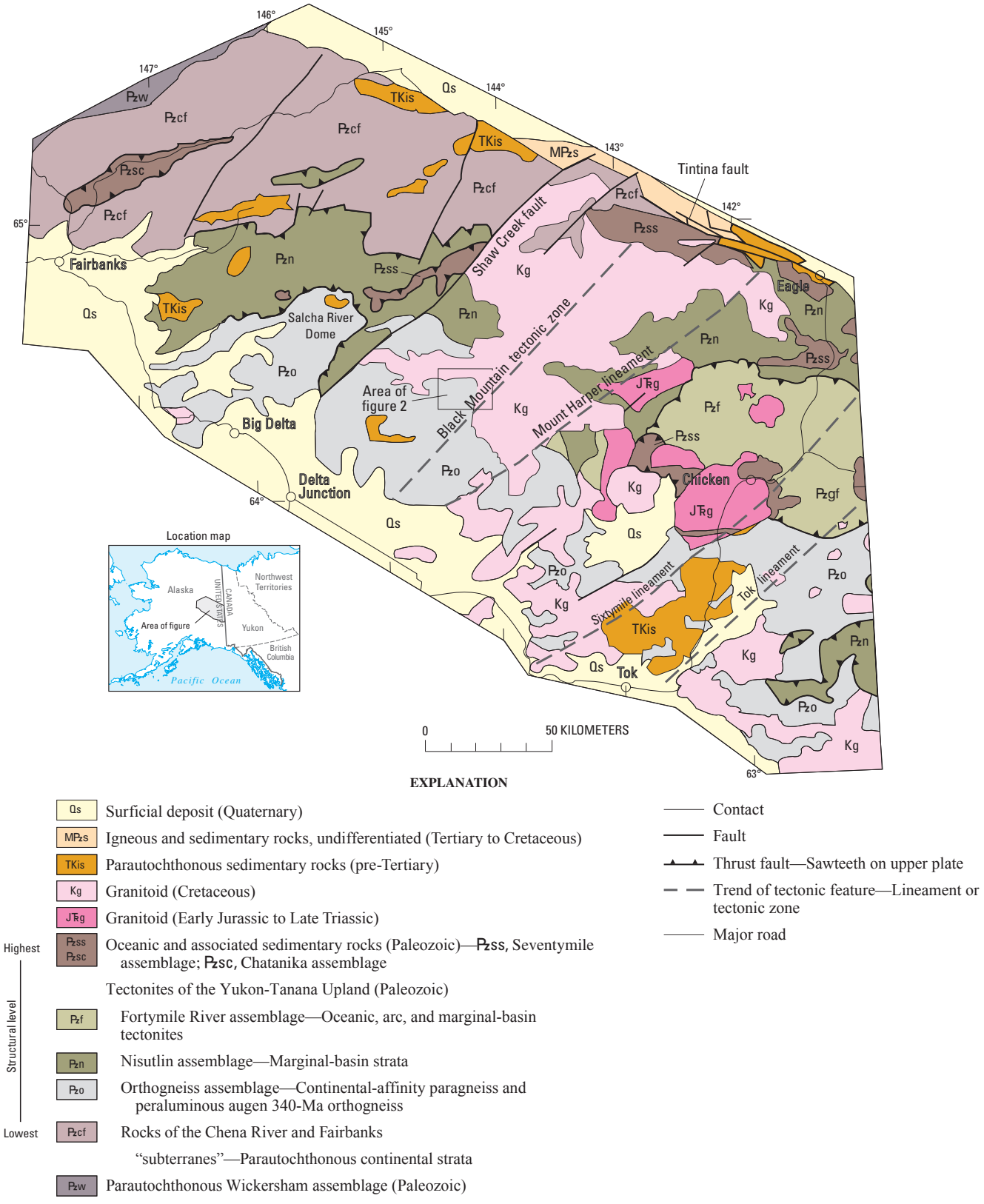

EXPLANATION

- Qs — Surficial deposit (Quaternary)
- MPzs — Igneous and sedimentary rocks, undifferentiated (Tertiary to Cretaceous)
- TKis — Parautochthonous sedimentary rocks (pre-Tertiary)
- Kg — Granitoid (Cretaceous)
- JTrg — Granitoid (Early Jurassic to Late Triassic)
- Pzss, Pzsc — Oceanic and associated sedimentary rocks (Paleozoic)—Pzss, Seventymile assemblage; Pzsc, Chatanika assemblage

Tectonites of the Yukon-Tanana Upland (Paleozoic)

Structural level: Highest → Lowest

- Pzf — Fortymile River assemblage—Oceanic, arc, and marginal-basin tectonites
- Pzn — Nisutlin assemblage—Marginal-basin strata
- Pzo — Orthogneiss assemblage—Continental-affinity paragneiss and peraluminous augen 340-Ma orthogneiss
- Pzcf — Rocks of the Chena River and Fairbanks "subterranes"—Parautochthonous continental strata
- Pzw — Parautochthonous Wickersham assemblage (Paleozoic)

- Contact
- Fault
- Thrust fault—Sawteeth on upper plate
- Trend of tectonic feature—Lineament or tectonic zone
- Major road

Figure D1. Simplified geologic map showing tectonic assemblage of the Yukon-Tanana tectonostratigraphic terrane of east-central Alaska. Shows approximate outline of map area (fig. D2), and location of major northeast-trending lineaments of Wilson and others (1985). Modified from Hansen and Dusel-Bacon (1998).

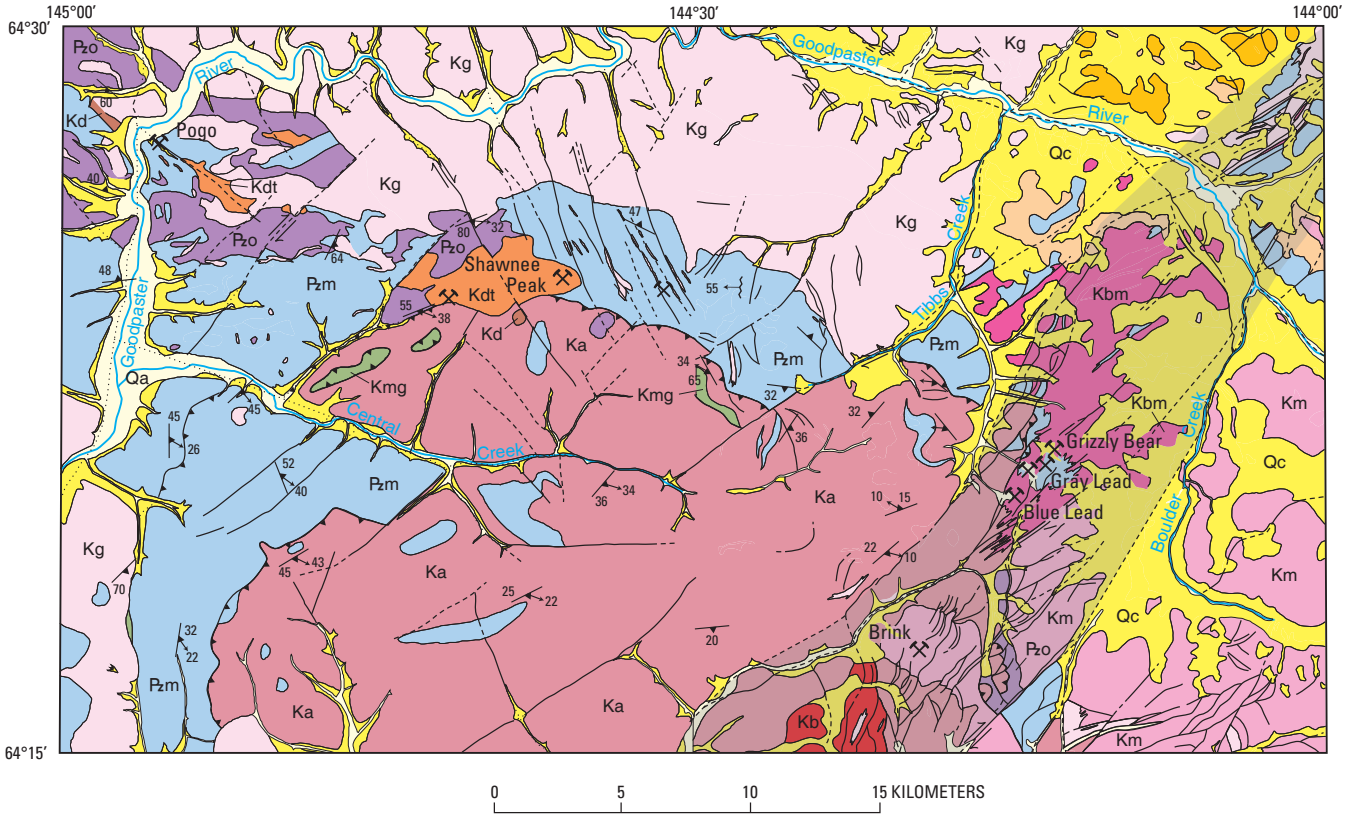

EXPLANATION

Qa	Alluvium (Quaternary)
Qc	Colluvium (Quaternary)
Tr	Rhyolite (Paleocene)
Tg	Gravel (Paleocene)
Kg	Granite, undifferentiated (Late Cretaceous)
Km	Rocks of the Mount Harper batholith (Late Cretaceous)
Kbm	Rocks of the Black Mountain intrusion (Late Cretaceous)
Kb	Rocks of the Brink intrusion (Late Cretaceous)
Kdt	Diorite and tonalite (Late Cretaceous)
Ka	Augen gneiss (Devonian)
Kd	Diorite gneiss (Paleozoic)
Kmg	Mafic and ultramafic gneiss (Paleozoic)
Pzo	Orthogneiss (Paleozoic)
Pzm	Metasedimentary rock, undivided (Paleozoic)
	Black Mountain tectonic zone—Shown by gray tint

Location map

Fault—Dashed where approximatly located, dotted where inferred. Arrows show sense of relative horizontal movment, where known

Thrust fault—Teeth on upper plate. Dashed where approximately located, dotted where inferred

20 Strike and dip of foliation

22 Trend and plunge of mineral lineation

55 Trend and plunge of minor fold

Gold deposit or occurence

Figure D2. Simplified geologic map of the Big Delta B–1 and B–2 quadrangles, east-central Alaska, showing location of gold mines and prospects and the surficial expression of the Black Mountain tectonic zone (shaded area).

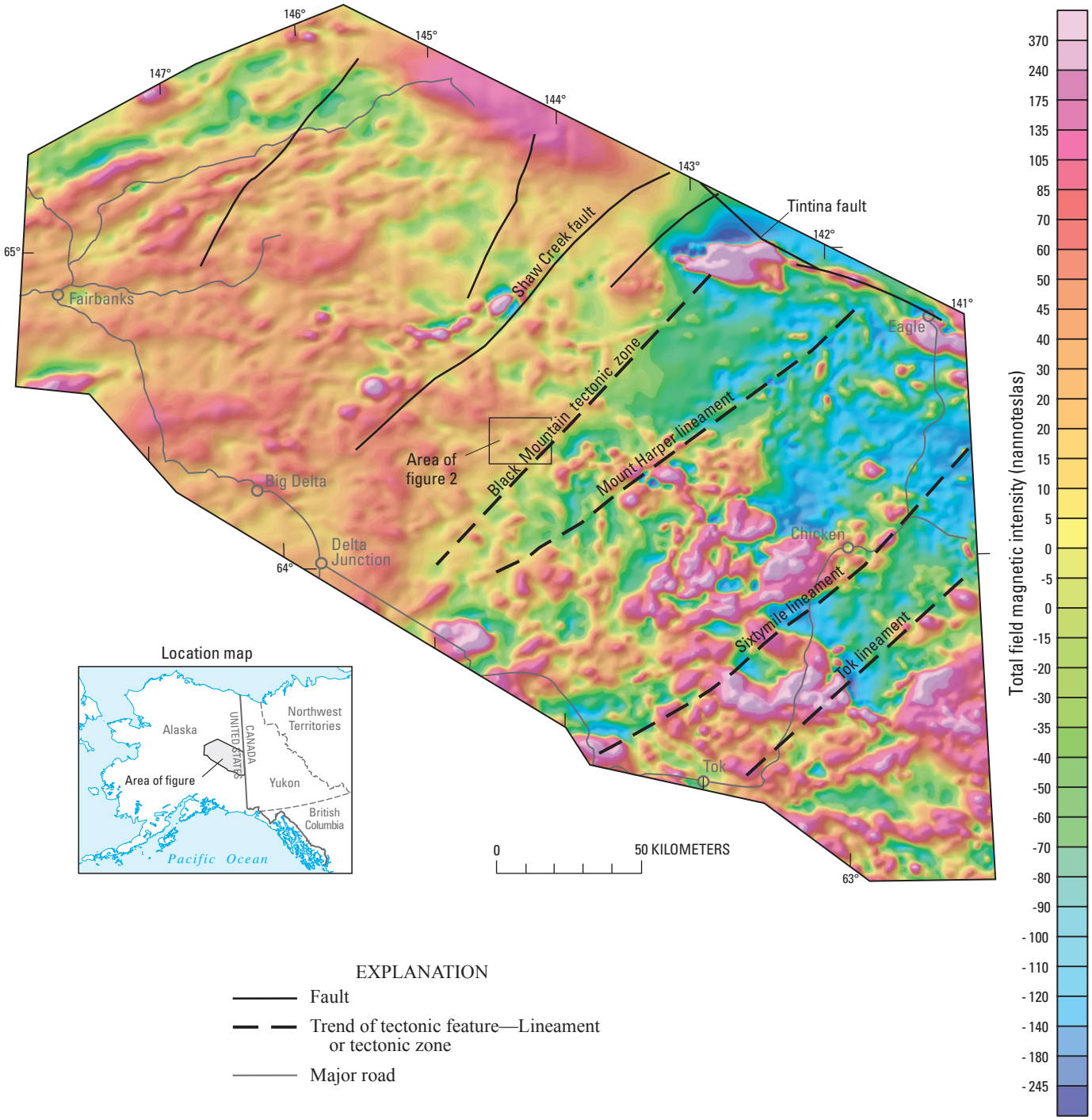

Figure D3. Regional aeromagnetic map of the Yukon-Tanana Upland of east-central Alaska showing location of the Black Mountain tectonic zone.

representing a 20-nanotesla (nT) step in mean magnetic anomaly values (as measured at a flight height of 300 meters, m) with higher values to the northwest, extends from the Denali fault to the Tintina fault and bisects the YTU (Saltus and Day, 2006) (fig. D3). In addition to the difference in mean values, there are distinct differences in the statistical character of the magnetic field on each side of the gradient, indicating that it is a fundamental boundary between magnetic source domains. Preliminary modeling of the magnetic boundary suggests that it represents a steeply east-dipping zone between contrasting crustal blocks that extend throughout the middle and lower crust (Saltus and Day, 2006). A gravity gradient coincides with a portion of the magnetic gradient in the Big Delta B–1 quadrangle (Saltus and Day, 2006; fig. D3). This gravity gradient is the eastern boundary of a 30-milligal (mGal) residual gravity high that occupies much of the western and

central portions of the Big Delta B–1 quadrangle. The adjacent lower gravity values to the east correlate, at least in part, with mapped postmetamorphic granitic rocks. Preliminary modeling of the gravity boundary suggests it also dips to the east as inferred for the magnetic feature (Saltus and Day, 2006). If a density contrast of 200 kilograms per cubic meter (kg/m^3) is assumed between the granitic intrusion (lower density) and the adjacent metamorphic rocks, the preliminary models suggest that the density contrast persists to depths of at least 8 km.

Geologic investigations in the Black Mountain area reveal a northeast-trending structural corridor, recognized as the Black Mountain tectonic zone by O'Neill and others (2005) (figs. D2 and D3), that coincides with the prominent magnetic and gravity anomalies described by Saltus and Day (2006). The tectonic zone and its associated faults and shear zones controlled the emplacement of Cretaceous (113–110 million years before present, Ma) granitoids and related felsic dikes, sills, elongate plugs, and quartz vein systems that carry gold deposits and occurrences. This high-angle tectonic zone formed a conduit along which subsequent basaltic to dioritic (109 Ma) dikes and dike swarms were emplaced and controlled the location and emplacement of a sulfide-bearing subvolcanic quartz-feldspar porphyry stock (99–95 Ma), and controlled the development of a Paleocene (57 Ma) rhyolite flow-dome complex. Reactivation and deformation along the Black Mountain tectonic zone has offset perched Tertiary erosion surfaces, and most recently, cut Quaternary alluvial deposits, indicating that tectonic activity along the zone is long-lived, complex, and ongoing (Day and others, 2007).

Black Mountain Tectonic Zone

Four distinct tectonic events are recorded in the bedrock of the Big Delta B–1 quadrangle that can be correlated to major regional magmatic-tectonic events that affected the YTU—Devonian (D_1) arc-related plutonism, Jurassic to Early Cretaceous (D_2) dynamothermal convergent tectonism, Early Cretaceous (D_3) ductile-brittle deformation and plutonism, and Paleocene to present (D_4) uplift and high-angle, northeast- and northwest-striking faulting related to strike-slip displacement on the Tintina-Denali fault systems. The third and fourth major tectonic events (D_3 and D_4) were concurrent with deformation observed in the 6.5- to 13-km-wide, northeast-trending Black Mountain tectonic zone.

The tectonic zone in the Big Delta B–1 quadrangle consists of five major left-lateral strike-slip faults spaced 1.6 to 4.8 km apart; they are, from west to east: the Last Chance-Goodpaster, Tibbs, Brink, and Serpentine faults, and the east-northeast-striking Porphyry fault zone (fig. D4). All faults strike northeast and have conspicuous left-stepping fault segments that accommodated extension along their traces.

Last Chance-Goodpaster Fault System

The Last Chance fault system marks the western boundary of the tectonic zone (fig. D2). The fault follows the northeast-trending Last Chance Creek on the southwest to Tibbs Creek, where a splay of the fault, the Goodpaster fault segment, steps left and trends north, following the creek to its intersection with the Goodpaster River. The eastern extent of the Last Chance fault system trends northeast to the map boundary, whereas the main strand of the fault trends north from Tibbs Creek to the northeastern corner of the map area. The Last Chance fault is a strike-slip structure and shows more than 4.8 km of sinistral displacement. On the northeast, the fault is marked by wide zones of shearing, by thin vertical screens of strongly deformed Paleozoic strata, and by dioritic to felsic dikes and dike swarms emplaced about 108 Ma. The area between the Goodpaster segment of the fault and the Last Chance fault on the north is unique; it is a graben underlain mainly by a Paleocene rhyolite flow-dome complex and is restricted to this part of the map area. The rhyolitic rocks were later partly covered and concealed by locally derived boulder gravel deposits of mid-Tertiary age. The Last Chance fault bounds the main body of the Black Mountain intrusive complex, a mixed granitic to granodioritic plutonic system, 109 to 107 Ma, confined to the core of the tectonic zone. No rocks related to the Black Mountain intrusive complex and no northeast-trending faults of significant size and magnitude are present northwest of this fault system (Day and others, 2003, 2007). The Last Chance fault separates markedly different rock types in the north part of the map area where Tertiary volcanic rocks and their extrusive centers on the east are juxtaposed against the Cretaceous Goodpaster batholith.

Tibbs Fault

The Tibbs fault is a complex structure within the tectonic zone. The Tibbs fault includes several interconnected splays along its central part characterized by a 1.6-km-wide zone of oblique-slip faulting and shearing. The Tibbs fault is subparallel to the Last Chance fault and, like the Last Chance fault, is a strike-slip structure; however, the Tibbs fault shows only about 1 km of left-lateral displacement. The Tibbs fault also includes left-stepping segments along its trace, the most profound and tectonically significant of which is in the south part of map area. Here the Tibbs fault is north trending and bounds the east margin of the Brink intrusion; this left-stepping segment of the fault accommodated a zone of extension during deformation and is interpreted to have provided a tectonic opening that influenced the localization and emplacement of the 113-Ma Brink granodiorite and its associated base- and precious-metal mineralization. On the northeast, the Tibbs and Last Chance faults are only about 1 km apart and may converge northeast of the map area where coalescing shear zones, dioritic dike swarms, and tectonic screens of strongly deformed Paleozoic strata are abundant.

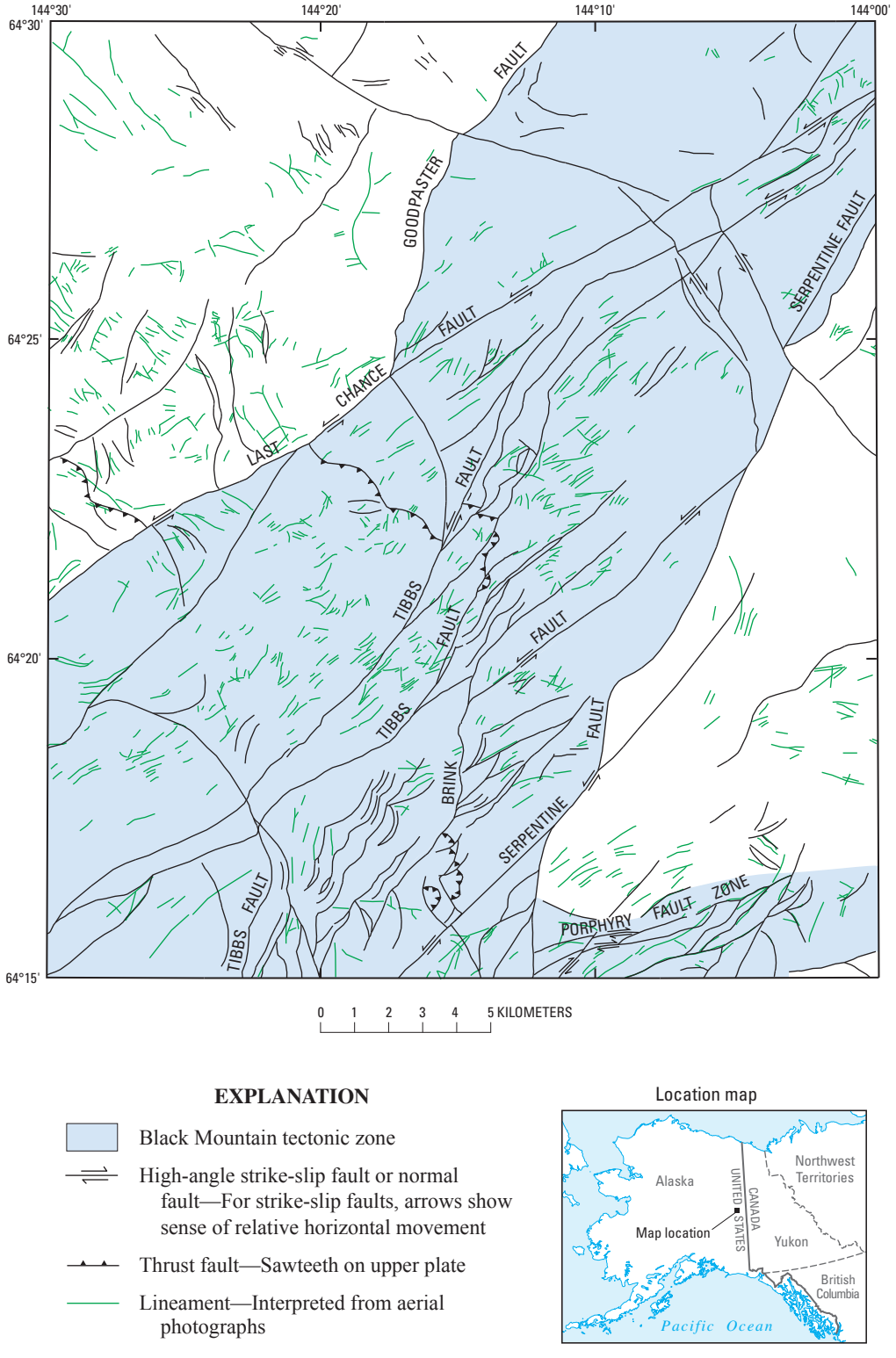

Figure D4. Structural geologic map of the Big Delta B–1 quadrangle showing major high-angle strike-slip and normal faults, thrust faults, and lineaments in the Black Mountain tectonic zone.

Brink Fault

The Brink fault is subparallel to the Tibbs fault and also has a major left-stepping segment along its trace in the southern part of the map area. The fault is clearly a strike-slip structure where a 50-m-wide gouge zone crosses the central part of Black Mountain, and it marks the southeast boundary of the Black Mountain intrusive complex. On the west side of Black Mountain, the fault turns abruptly south into the valley of the headwaters of the South Fork of Goodpaster River; there the fault is a profound down-to-the-west normal fault that is parallel to the left-stepping segment of the Brink fault on the west. In the area between the north-trending Brink and Tibbs fault segments is a leucocratic phase of the

Mount Harper batholith whose intrusion appears to have been accommodated along a pull-apart extensional zone created between these two faults (figs. D2 and D4). In this area only, the about 111 Ma Mount Harper pluton is sill-like, overlain by a metamorphosed, flat-lying carapace of augen gneiss; the pluton and the overlying gneissic rocks are also cut by a young, northeast-trending swarm of predominantly down-to-the-west normal faults that includes numerous small pull-apart grabens. These extensional faults and their scarps indicate ongoing left-lateral displacement and concomitant extension along and between the Tibbs and Brink fault systems (fig. D2). On the north, the Brink fault merges with the Serpentine fault directly south of the Eisenmenger Fork.

Serpentine Fault

The Serpentine fault in the southern part of the map area is marked by the juxtaposition of Paleozoic metasedimentary rocks against Devonian augen gneiss and underlying Devonian orthogneiss along a wide zone of strongly sheared rocks. The fault projects into the broad valley of Boulder Creek, where it is covered by widespread accumulations of Quaternary deposits. It follows Boulder Creek northward to its confluence with the Eisenmenger Fork, where it branches: the main segment continues northeastward across sheared, altered, and displaced metasedimentary and igneous rocks in the northeastern corner of the map; the northwest-trending segment of the fault, marked by normal faults that offset Quaternary deposits, appears to be a left-stepping tectonic link between the Serpentine fault and the converging Tibbs and Last Chance faults. This left-stepping link and the normal faults that define it outline a down-dropped zone of extension that has resulted in a northwest-trending graben that controls the course of the Eisenmenger Fork. Normal faults along the south side of this graben displace both older and younger Quaternary alluvial fan deposits, indicating that deformation along this graben has occurred in the recent past. Young fault displacements farther northwest along the Fork suggest that the tectonic linkage of the Serpentine fault with the Last Chance fault may actually extend farther northwest and connect with the Goodpaster segment of the Last Chance fault. The tectonic linkage of the Serpentine fault with the three strike-slip faults to the northwest, all within the Black Mountain tectonic zone and all accommodated along left-stepping normal fault segments, implies that the faults are coeval, are a part of the same kinematic movement picture, and have been recurrently active since the mid-Cretaceous.

The northernmost segment of the Serpentine fault has a more northerly trend and, like the Tibbs fault, may merge with the Last Chance and Tibbs faults northeast of the map area; the area is unique in that it is the most strongly sheared part of the Black Mountain tectonic zone and is characterized by thin, closely spaced vertical screens of metamorphic tectonites and sheared granodioritic plutonic rocks, all intruded by swarms of vertical dikes of all compositions.

Porphyry Fault Zone

The Porphyry fault zone is marked by a 1-km-wide zone of intense shearing, folding, and faulting, and associated dike swarms. The Porphyry fault zone is confined to rocks of the Mount Harper batholith; although there are no piercing points along the trace of the fault to indicate the magnitude of fault displacements, S-C mylonitic fabric (Lister and Snoke, 1984), and small-scale folds within the fault zone. These mesoscopic features are all consistent with dextral offset. The zone appears to have controlled the intrusion of a subvolcanic 99- to 95-Ma quartz-feldspar porphyry stock where it intersects and merges with the Serpentine fault at an acute angle along the south margin of the map area (fig. D3). This fault zone is marked by abundant normal faults and by swarms of subparallel granitic, aplitic, and pegmatitic dikes. This fault zone is also the locus of many sulfide-bearing dikes of quartz-feldspar porphyry and basaltic composition.

Lineaments

Linear features of various origins, mostly fractures and faults and less commonly dike swarms and geologic contacts, were mapped from aerial photographs of the Big Delta B–1 quadrangle. The major faults of the Black Mountain tectonic zone are visible on aerial photographs as are many of the mapped dike swarms; however, the vast majority of lineaments mapped from aerial photographs are fractures with no obvious offset. These fracture sets and other lineaments are ubiquitous and abundant across the quadrangle (fig. D4) (Day and others, 2007).

The northwest corner of the Big Delta B–1 quadrangle shows lineaments with a somewhat random pattern to preferred northwest-trending orientation. The fracture orientations appear to reflect the northwest-trending tectonic grain of small faults and dikes mapped in the adjacent Big Delta B–2 quadrangle (figs. D3 and D4) (Day and others, 2003).

The Last Chance strike-slip fault and associated Goodpaster fault segment separate the fracture pattern in the northwest corner of the quadrangle from a zone of consistently northeast-oriented fractures and recognizable faults east of the fault. The abrupt change in fracture patterns from random to dominantly northeast-striking across the Last Chance-Goodpaster faults coincides with the northwest boundary of the Black Mountain tectonic zone.

Southeast of the Last Chance fault, the predominant fracture orientation is northeast and continues uninterrupted to the southeast to the Serpentine fault. The width of this zone of consistently oriented fracturing, as much as 13 km wide, is inferred to define the scale, breadth, and tectonic continuity of the Black Mountain tectonic zone. The fracture pattern cuts rocks of the Mount Harper batholith southeast of the Serpentine fault; however, east of this fault, especially east of the Boulder Creek in the east-central part of the quadrangle,

the fracture patterns define intermixed, contiguous blocks or domains of randomly oriented fractures separated by northeast-trending zones of mixed fractures and faults.

Summary

Geologic investigations in the Black Mountain area reveal a northeast-trending structural corridor, described herein as the Black Mountain tectonic zone, that consists of five major strike-slip faults, spaced 1.6 to 4.8 km apart (fig. D2). The tectonic zone and its associated faults, fractures, and shear zones controlled the emplacement of 110- to 95-Ma Cretaceous granitoids and related felsic dikes, plugs, and quartz vein systems; formed a conduit along which subsequent basaltic to dioritic dikes and dike swarms were emplaced; and controlled the location and emplacement of a 57-Ma Paleocene rhyolite flow-dome complex erupted during the Paleocene. Reactivation and deformation along the Black Mountain tectonic zone have offset perched Tertiary erosion surfaces, and most recently, cut Quaternary alluvial deposits, indicating that tectonic reactivation of the zone is long-lived, complex, and ongoing. The tectonic zone coincides with fundamental geophysical crustal anomalies, suggesting that it is related to deep-seated crustal discontinuities; the tectonic zone is also a magmatic conduit that has a long-lived intrusive history and has localized gold deposits associated with igneous activity.

References Cited

Day, W.C., Aleinikoff, J.N., Roberts, Paul, Smith, Moira, Gamble, B.M., Henning, M.W., Gough, L.P., and Morath, L.C., 2003, Geologic map of the Big Delta B–2 quadrangle, east-central Alaska: U.S. Geological Survey Geologic Investigations Series I–2788, 12 p., 1 sheet, scale 1:63,360. (Also available online at *http://pubs.usgs.gov/imap/i-2788/*.)

Day, W.C., O'Neill, J.M., Aleinikoff, J.N., and Green, G.N., 2007, Geologic map of the Big Delta B–1 quadrangle, east-central Alaska: U.S. Geological Survey Scientific Investigations Map 2975, scale 1:63,360. (Also available online at *http://pubs.usgs.gov/sim/2007/2975/*.)

Dusel-Bacon, Cynthia, Lanphere, M.A., Sharp, W.D., Layer, P.W., and Hansen, V.L., 2002, Mesozoic thermal history and timing of structural events for the Yukon-Tanana Upland, east-central Alaska; $^{40}Ar/^{39}Ar$ data from metamorphic and plutonic rocks: Canadian Journal of Earth Sciences, v. 39, no. 6, p. 1013–1051.

Foster, H.L., comp., 1976, Geologic map of the Eagle quadrangle, Alaska: U.S. Geological Survey Miscellaneous Investigations Series I–922, 1 sheet, scale 1:250,000.

Foster, H.L., Albert, N.R.D., Griscom, Andrew, Hessin, T.D., Menzie, W.D., Turner, D.L., and Wilson, F.H., 1979, The Alaskan mineral resource assessment program; Background information to accompany folio of geologic and mineral resource maps of the Big Delta quadrangle, Alaska: U.S. Geological Survey Circular 783, 19 p. (Also available online at *http://pubs.er.usgs.gov/usgspubs/cir/cir783*.)

Hansen, V.L., and Dusel-Bacon, Cynthia, 1998, Structural and kinematic evolution of the Yukon-Tanana Upland tectonites, east-central Alaska—A record of late Paleozoic to Mesozoic crustal assembly: Geological Society of America Bulletin, v. 110, no. 2, p. 211–230.

Lister, G.S., and Snoke, A.W., 1984, S-C mylonites: Journal of Structural Geology, v. 6, no. 6, p. 617–638.

O'Neill, J.M., Day, W.C., Aleinikoff, J.N., and Saltus, R.W., 2005, The Black Mountain tectonic zone—A long-lived lithospheric shear zone in the Yukon-Tanana Upland of east-central Alaska: Geological Society of America Abstracts with Program, v. 37, no. 7, p. 82. (Also available online at *http://gsa.confex.com/gsa/2005AM/finalprogram/abstract_96201.htm*.)

Saltus, R.W., and Day, W.C., 2006, Gravity and aeromagnetic gradients within the Yukon-Tanana Upland, Black Mountain tectonic zone, Big Delta quadrangle, east-central Alaska: U.S. Geological Survey Open-File Report 2006–1391, poster, available only online at *http://pubs.usgs.gov/of/2006/1391/*. (Accessed March 9, 2009.)

Werdon, Melanie, Newberry, R.J., Athey, J.E., and Szumigala, D.J., 2004, Bedrock geologic map of the Salcha River-Pogo area, Big Delta quadrangle, Alaska: Alaska Division of Geological and Geophysical Surveys Report of Investigations 2004–1b, scale 1:63,360.

Wilson, F.H., Smith, J.G., and Shew, Nora, 1985, Review of radiometric data from the Yukon crystalline terrane, Alaska and Yukon territory: Canadian Journal of Earth Sciences, v. 22, no. 4, p. 525–537.

Mapping Known and Potential Mineral Occurrences and Host Rocks in the Bonnifield Mining District Using Minimal Cloud- and Snow-Cover ASTER Data

By Bernard E. Hubbard, Cynthia Dusel-Bacon, Lawrence C. Rowan, and Robert G. Eppinger

Chapter E of
Recent U.S. Geological Survey Studies in the Tintina Gold Province, Alaska, United States, and Yukon, Canada—Results of a 5-Year Project
Edited by Larry P. Gough and Warren C. Day

Scientific Investigations Report 2007–5289–E

U.S. Department of the Interior
U.S. Geological Survey

Contents

Figures

Mapping Known and Potential Mineral Occurrences and Host Rocks in the Bonnifield Mining District Using Minimal Cloud- and Snow-Cover ASTER Data

By Bernard E. Hubbard,[1] Cynthia Dusel-Bacon,[1] Lawrence C. Rowan,[1] and Robert G. Eppinger[1]

Abstract

On July 8, 2003, the Advanced Spaceborne Thermal Emission and Reflection Radiometer (ASTER) sensor acquired satellite imagery of a 60-kilometer-wide swath covering a portion of the Bonnifield mining district within the southernmost part of the Tintina Gold Province, Alaska, under unusually favorable conditions of minimal cloud and snow cover. Although rocks from more than eight different lithotectonic terranes are exposed within the extended swath of data, we focus on volcanogenic massive sulfides (VMS) and porphyry deposits within the Yukon-Tanana terrane (YTT), the largest Mesozoic accretionary terrane exposed between the Denali fault system to the south of Fairbanks and the Tintina fault system to the north of Fairbanks.

Comparison of thermal-infrared region (TIR) decorrelation stretch data to available geologic maps indicates that rocks from the YTT contain a wide range of rock types ranging in composition from mafic metavolcanic rocks to felsic rock types such as metarhyolites, pelitic schists, and quartzites. The nine-band ASTER visible-near-infrared region–short-wave infrared region (VNIR-SWIR) reflectance data and spectral matched-filter processing were used to map hydrothermal alteration patterns associated with VMS and porphyry deposit types. In particular, smectite, kaolinite, opaline silica, jarosite and (or) other ferric iron minerals defined narrow (less than 250-meter diameter) zonal patterns around Red Mountain and other potential VMS targets. Using ASTER we identified some of the known mineral deposits in the region, as well as mineralogically similar targets that may represent potential undiscovered deposits. Some known deposits were not identified and may have been obscured by vegetation or snow cover or were too small to be resolved.

Introduction

On July 8, 2003, the Advanced Spaceborne Thermal Emission and Reflection Radiometer (ASTER) sensor aboard the TERRA satellite acquired a 60-kilometer (km)-wide orbital swath of data covering parts of the 1:250,000-scale Healy quadrangle in east-central Alaska (fig. E1). The orbital swath of data continues on to include parts of the Talkeetna Mountains 1:250,000-scale quadrangle (see Hubbard and others, 2007) and areas to the south of Anchorage and the populated Matanuska Valley. Figure E1 illustrates the Healy and Bonnifield mining district portion of the ASTER data coverage used in this study, which was acquired under unusually low cloud- and snow-cover conditions (see also fig. 1 of Editors' Preface and Overview).

Mineral resource exploration throughout much of the State has been hampered by the large geographic distances, lack of roads, and paucity of detailed geologic maps at 1:63,360 scale or less. This leaves a large part of the State with possible undiscovered metallogenic resources. The purpose of this paper is to show the utility of ASTER for lithologic mapping of mineral deposit host rocks that define permissive tracts and for targeting hydrothermal alteration zones indicative of potential undiscovered occurrences.

Geologic Setting

Several important volcanogenic massive sulfide (VMS) deposits are located within the Yukon-Tanana terrane (YTT), and their metallogenesis is discussed by Nokleberg and others (1994) and Newberry and others (1997). The Healy quadrangle (fig. E1) contains a variety of rocks ranging from mafic metavolcanic rocks to felsic metavolcanic rocks with a range of intermediate compositions (Csejtey and others, 1986, 1992, and references therein). Felsic metavolcanic and metavolcaniclastic rocks are important host rocks for Kuroko-type VMS deposits (Lydon, 1984; Cox and Singer, 1986–deposit model

[1]U.S. Geological Survey.

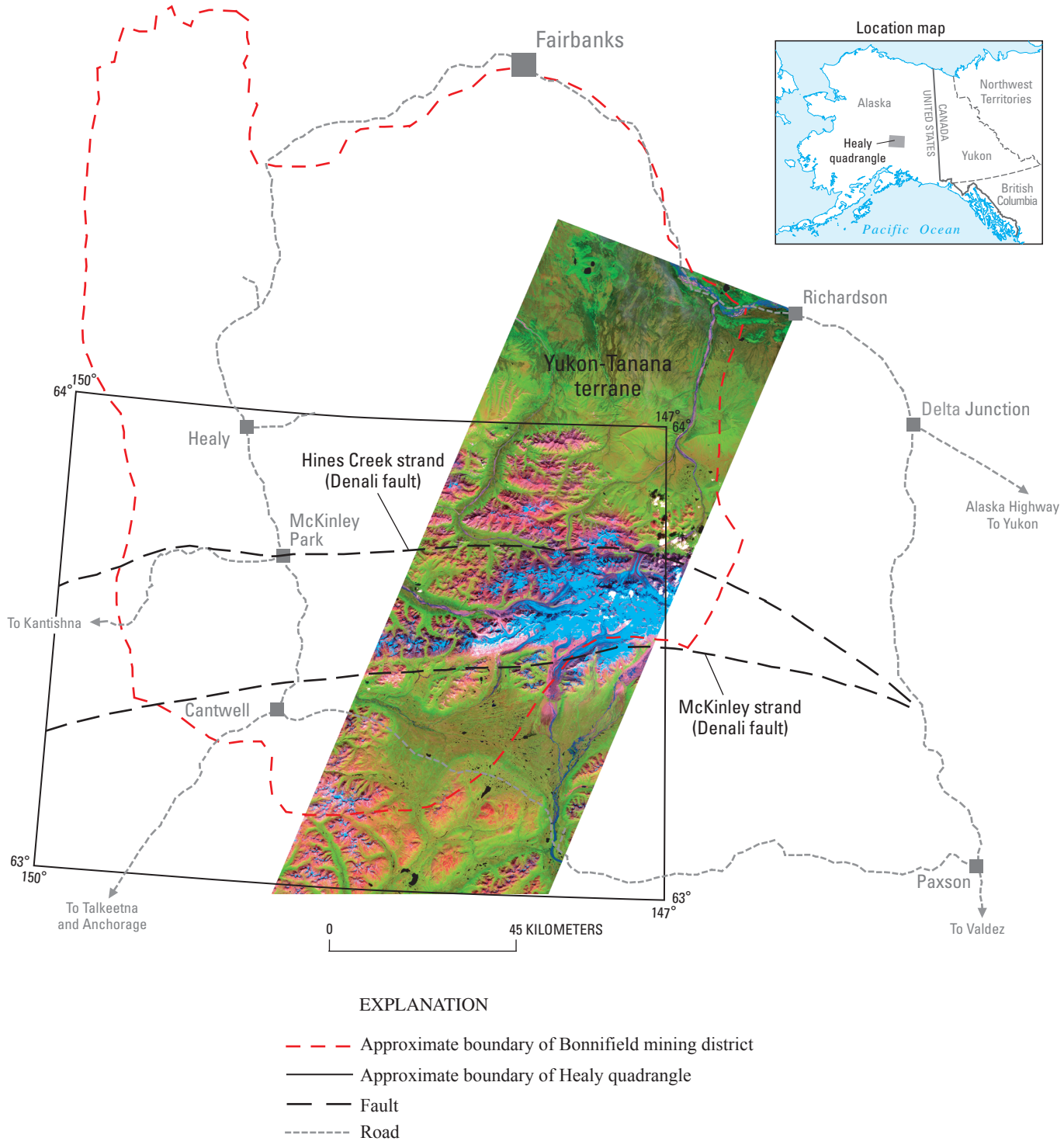

Figure E1. Map showing locations of the Bonnifield mining district south of Fairbanks, Alaska, and the 1:250,000-scale Healy quadrangle boundary. Also shown are the Hines Creek and McKinley strands of the Denali fault system and a false-color image (ASTER bands 6, 3 and 1, displayed as red, green, and blue respectively) showing the extent of minimal cloud- and snow-cover ASTER data for the area.

28a). Mafic metavolcanic and metavolcaniclastic rocks typically host Besshi-type VMS deposits (Cox and Singer, 1986–deposit model 24b), which are distinct from the Cyprus-type VMS deposits associated with ophiolites (Cox and Singer, 1986–deposit model 24a). Several of the VMS deposits mapped using ASTER are associated with greenschist-facies metamorphic host rocks (Dusel-Bacon and others, 1993; Hubbard and others, 2007; Dusel-Bacon and others, this volume, chap. B). Differences in host rock composition and metamorphic grade lead to differences in the phyllosilicate mineral assemblages associated with VMS deposits, potentially providing a remote sensing basis for their discrimination. For instance, greenschist-grade metamorphic rocks show enhanced crystallinity of clay minerals, both associated with hydrothermal alteration, and within the groundmass (for example, McLeod and Stanton, 1984; McLeod, 1985, 1987; McLeod and others, 1987). Higher metamorphic grades, such as amphibolite facies, will destroy clay minerals, such as kaolinite, unless these clay minerals are replenished through supergene alteration processes.

Background, Methodology, and Relevance

ASTER measures reflected radiation in the three wavelength bands between 0.520 and 0.860 micrometers (μm) (visible-near-infrared region, or VNIR) and in six bands from 1.00 to 2.43 μm (short-wave infrared region, or SWIR), with 15-m and 30-m spatial resolution, respectively (Fujisada, 1995). In addition, ASTER measures emitted thermal radiation in five bands in the 8.125- to 11.650-μm wavelength region (thermal-infrared region, or TIR) at 90-m resolution (Fujisada, 1995). Both standard calibrated ASTER data products (VNIR-SWIR reflectance, TIR emissivity, and TIR decorrelation stretch) and (or) their equivalents were used in this study (see Rowan and others, 2003; Rowan and Mars, 2003). Briefly, hydrothermal alteration minerals were mapped based on image spectral endmembers derived through principal component analysis (for example, Green and others, 1988; Boardman and others, 1995) of the nine ASTER VNIR-SWIR bands. These spectral endmembers (for example, Hubbard and others, 2007) were used as reference spectra in subsequent matched-filter image classification procedures (Harsanyi and Chang, 1994). The standard decorrelation stretch image product (fig. E2) shows ASTER TIR bands 10, 12, and 13 displayed as blue, green and red, respectively. Decorrelation stretch images are used to enhance the brightness variations between TIR bands related to compositional differences and emissivity, while suppressing correlated interchannel brightness values dominated by radiant temperature (Gillespie and others, 1986). Further processing details are discussed by Hubbard and others (2007).

Results

Host-Rock Mapping Using ASTER TIR Decorrelation Stretch Data

Within YTT and rocks south of the Hines Creek strand of the Denali fault, linear enhancement of the TIR decorrelation stretch data shows a variety of lithologic compositions ranging from the mostly mafic, such as the labeled Chute Creek Member of the Totatlanika Schist (of Csejtey and others, 1992; blue shades, fig. E2), intermediate (mixed red-blue, or purple through magenta shades, fig. E2), and quartz-rich rocks such as granitic intrusions and prominent quartzite exposures (red shades, fig. E2). Several of these rock types are grouped together into formations at a scale of 1:250,000 (such as the Totatlanika Schist) but also are shown as distinct lithological members in the more detailed 1:63,360 geologic maps (for example, from oldest to youngest, the Moose Creek, California Creek, Chute Creek, Mystic Creek, and Sheep Creek Members of the Totatlanika Schist; Wahrhaftig, 1970a,b; Gilbert, 1977). In particular, the metarhyolite-dominated Mystic Creek Member hosts the Red Mountain and WTF VMS prospects (figs. E3, E4). Spectral analysis of sampled ground truth areas is discussed in greater detail by Hubbard and others (2007).

Alteration Mineral Maps of Known and Undiscovered VMS and Porphyry Deposits

Figure E3 shows the resulting mineral maps generated using nine-band ASTER VNIR-SWIR data and spectral matched-filtering methods. Large areas of the upper two scenes of the ASTER mosaic (fig. E3*A*) were classified as containing zones of ferric-iron-rich minerals, chlorite and (or) epidote, and muscovite and (or) illite. Chlorite and (or) epidote are Fe,Mg-OH minerals that commonly occur in the predominantly greenschist and prehnite-pumpellyite facies of metamorphic rocks throughout the area. Muscovite and (or) illite can occur either as primary minerals in the groundmass of igneous and metamorphic rocks, within sericitic hydrothermal alteration zones, or as the weathering product of potassium-rich rocks.

Spectral analysis of fine-grained rock and soil samples collected at Red Mountain contain kaolinite, illite-muscovite, smectite, and goethite. These minerals were all mapped as distinct zoning patterns using ASTER data (fig. E3*B, C*). In addition, a variety of ferric-iron and aluminum oxy-hydroxide and sulfate mineral precipitates are found in and around the streams draining the mountain, reflecting natural acid-rock drainage conditions within the pristine (unmined) Red Mountain VMS deposit (Eppinger and others, this volume, chap. I).

Alteration mineral zones were mapped at a more detailed scale for the Red Mountain deposit and the location

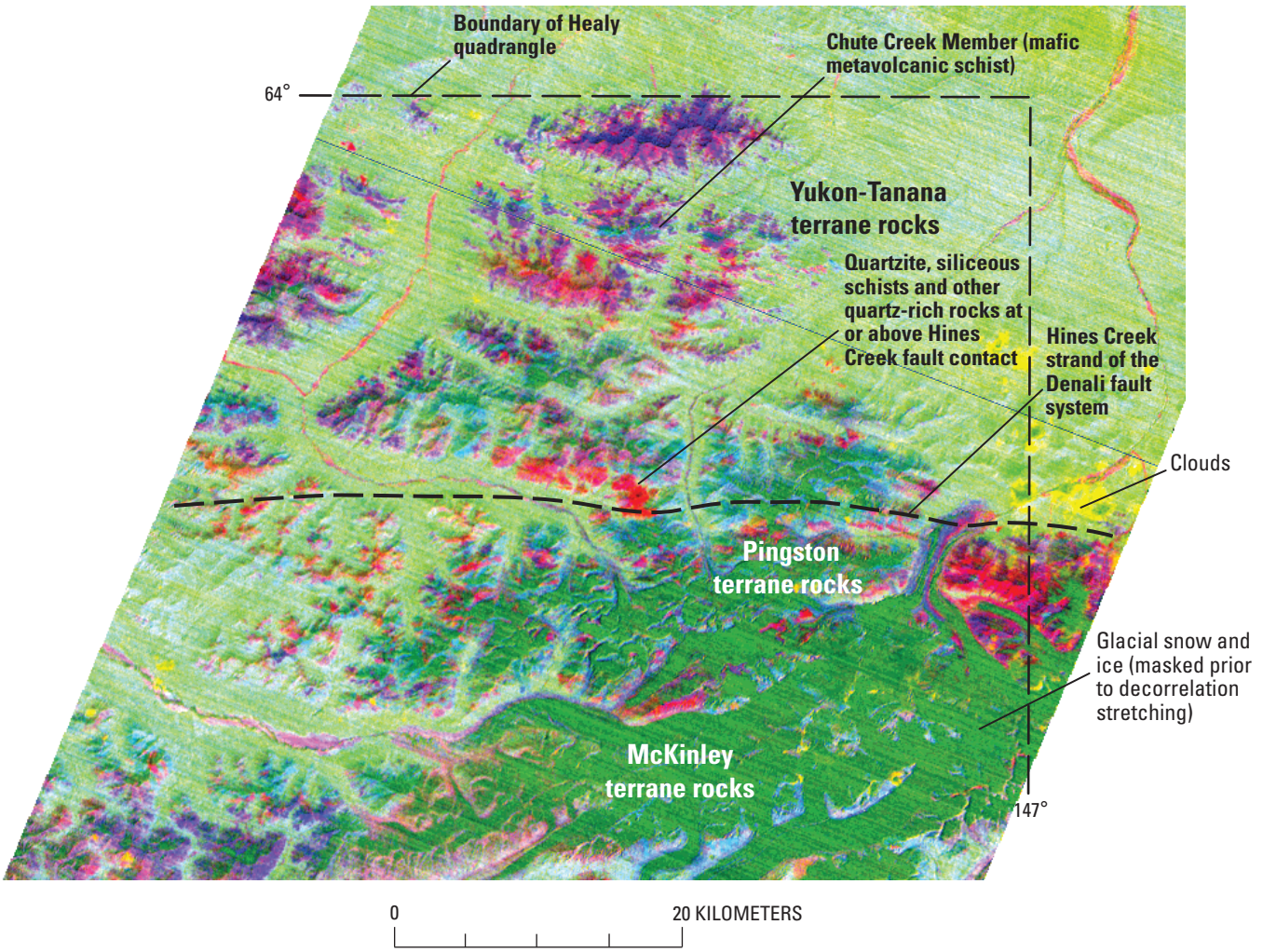

Figure E2. ASTER thermal-infrared decorrelation stretch image (ASTER bands 13, 12 and 10, displayed as red, green, and blue, respectively) covering the portion of the Healy quadrangle shown in figure E1, including maximum exposure of rocks from the Yukon-Tanana terrane. Snow and ice fields of glaciers south of the Denali fault have been masked prior to contrast stretching and appear as darkest shades to almost black. Vegetation appears mostly lighter green. Clouds and cloud shadows appear yellow. Red areas are exposed rocks that are more silicic in composition and blue areas depict rocks that are more mafic in composition. Colors in between (for example, purple, magenta, and cyan) represent mixtures of the aforementioned materials.

of the WTF massive sulfide deposit (fig. E3*B*), the Anderson Mountain massive sulfide deposits (fig. E3*C*), and an area of possible alunite occurrence at Nenana Mountain in rocks mapped as Tertiary granites and Quaternary Nenana Glacier lateral moraines (fig. E3*D*). The Nenana Mountain and Nenana Glacier distribution could represent argillic and propylitic alteration zones of a porphyry copper deposit which can extend from 1 to 4 km (Lowell and Guilbert, 1970; Cox and Singer, 1986–deposit model 17). This distribution differs in scale and mineralogy from what is expected in hydrothermal alteration zones associated with VMS deposits such as Red Mountain, which generally extends for less than a few hundred meters (Lydon, 1984). The red, orange, and yellow colors (fig. E4*A*) and related mineralogy (fig. E3*B*) displayed by the Red Mountain deposit are due mostly to supergene alteration of pyrite and other massive sulfide layers (figs. E4*B, C*), and exposed silica exhalite and chert deposits (figs. E4*B, C*).

Nearly 200 potential VMS deposits were mapped by Hubbard and others (2007) in portions of the Healy and Talkeetna Mountains quadrangles covered by ASTER. Their identification was based on small-scale (about 100–200-m diameter) mineral zoning patterns between hydrous silica, jarosite, kaolinite, and smectite, which graded into background rocks dominated by ferric iron, chlorite, and sericite. Potential porphyry deposits such as at Nenana Mountain and the Nenana Glacier are defined by larger scale (greater than 1 km diameter) argillic and propylitic alteration zones.

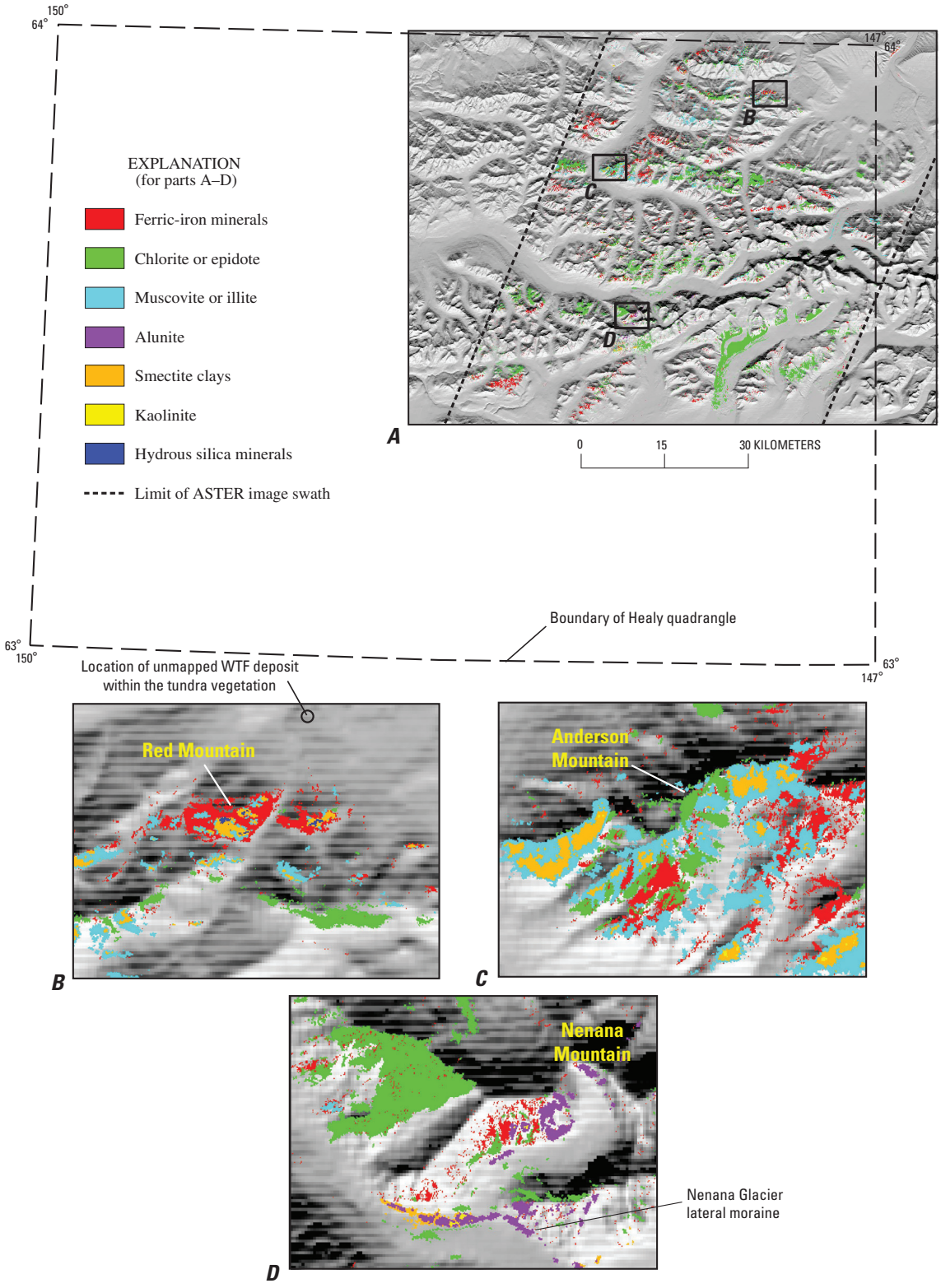

Figure E3. ASTER-derived images of portions of the 1:250,000-scale Healy quadrangle, Alaska, showing the distribution of host rocks and glacial sediments containing the three most abundant minerals. *A*, Overview map of a major portion of the Healy quadrangle showing locations of detailed hydrothermal alteration mineral zonation maps (*B*, *C*, and *D*). Shaded-relief base image was generated from U.S. Geological Survey digital elevation model dataset. *B*, Red Mountain and WTF massive sulfide deposits, with approximate northeastern (NE) and southwestern (SW) extents of profile shown in figure E4*B*. *C*, Anderson Mountain massive sulfide deposits. *D*, Area of possible alunite occurrence at Nenana Mountain in the McKinley terrane.

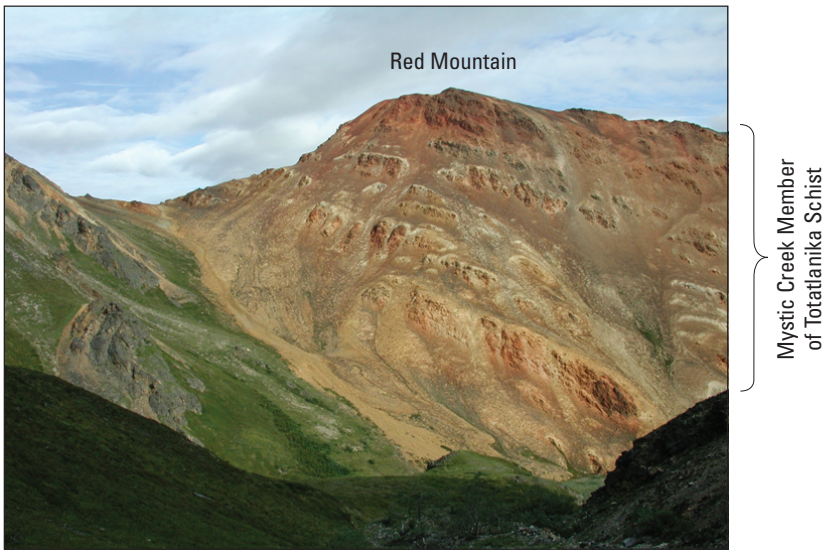

A

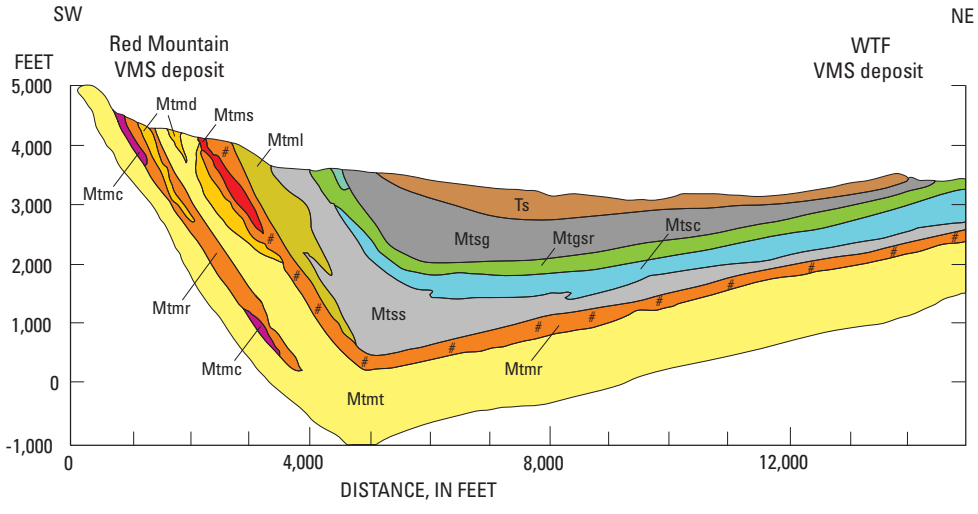

B

EXPLANATION

- Ts — Sandstone with coal (Tertiary)
- Totatlanika Schist (Mississippian?, as used by Csejtey and others, 1992)
- Sheep Creek Member
  - Mtsg — Graywacke
  - Mtsgr — Green shale
  - Mtsc — Calcareous shale
  - Mtss — Gray to black shale
- Mystic Creek Member
  - Mtml — Rhyodacite lapilli tuff
  - Mtmr — Rhyolite tuff
  - Mtms — Silica exhalatives and pyrite
  - Mtmd — Dacite tuff
  - Mtmt — Rhyodacite tuff
  - Mtmc — Chert (hydrous silica)
  - # # — Massive sulfide horizon

Figure E4. Photograph and stratigraphic section of the well-exposed Red Mountain deposit and the unmapped and poorly exposed WTF deposit. *A*, View of Red Mountain. *B*, Stratigraphic section showing geology, generalized and modified after Nokleberg and others (1994, fig. 6). Vertical scale is greatly exaggerated and topographic surface is generalized. Red Mountain is located in the higher and better exposed portion of the syncline structure. The southwestern and northeastern extents of the stratigraphic section correspond to the locations of Red Mountain and the WTF massive sulfide deposits mapped using ASTER as labeled on figure E3*B*. Note, however, that the minerals mapped at Red Mountain in figure E3*B* do not necessarily correspond to the individual stratigraphic units shown in the section.

Conclusions

We show in this study the utility of ASTER as an exploration tool for mapping potential occurrences of VMS and porphyry deposit types based on the deposit model characteristics such as host rock lithology and weathering characteristics, deposit size and scale, and hydrothermal alteration zonation patterns as described in Cox and Singer (1986). The results of this study show the utility of remote sensing, and in particular ASTER, for use in future mineral resource assessments. For example, such data are useful for the recognition of unknown deposits, definition of favorable or permissive tracts, and for providing basic rock composition data in geologically poorly known areas.

References Cited

Boardman, J.W., Kruse, F.A., and Green, R.O., 1995, Mapping target signatures via partial unmixing of AVIRIS data, *in* Proceedings of the Fifth JPL Airborne Earth Science Workshop, Jet Propulsion Laboratory, Pasadena, Calif., January 23–26, 1995: JPL Publication 95–01, p. 23–26.

Cox, D.P., and Singer, D.A., eds., 1986, Mineral deposit models: U.S. Geological Survey Bulletin 1693, 379 p.

Csejtey, Béla, Jr., Mullen, M.W., Cox, D.P., Gilbert, W.G., Yeend, W.E., Smith, T.E., Wahrhaftig, Clyde, Craddock, Campbell, Brewer, W.M., Sherwood, K.W., Hickman, R.G., Stricker, G.D., St. Aubin, D.R., and Goerz, D.J., III, 1986, Geology and geochronology of the Healy quadrangle, Alaska: U.S. Geological Survey Open-File Report 86–396, including 1:250,000-scale map (superseded by Csejtey and others, 1992). (Also available online at *http://pubs.er.usgs.gov/usgspubs/ofr/ofr86396/*.)

Csejtey, Béla, Jr., Mullen, M.W., Cox, D.P., and Stricker, G.D., 1992, Geology and geochronology of the Healy quadrangle, south-central Alaska: U.S. Geological Survey Miscellaneous Investigations Series Map I–1961, 63 p., 2 sheets, scale 1:250,000.

Dusel-Bacon, Cynthia, Csejtey, Béla, Jr., Foster, H.L., Doyle, E.O., Nokleberg, W.J., and Plafker, George, 1993, Distribution, facies, ages, and proposed tectonic associations of regionally metamorphosed rocks in east- and south-central Alaska: U.S. Geological Survey Professional Paper 1497–C, 73 p., 2 sheets, scale 1:1,000,000. (Also available online at *http://pubs.er.usgs.gov/usgspubs/pp/pp1497C*.)

Eppinger, R.G., Briggs, P.H., Dusel-Bacon, Cynthia, Giles, S.A., Gough, L.P., Hammarstrom, J.M., and Hubbard, B.E., 2007, Environmental geochemistry at Red Mountain, an unmined volcanogenic massive sulphide deposit in the Bonnifield district, Alaska Range, east-central Alaska: Geochemistry: Exploration, Environment, Analysis, v. 7, no. 3, p. 207-223.

Fujisada, Hiroyuki, 1995, Design and performance of ASTER instrument, *in* Fujisada, Hiroyuki, and Sweeting, M.N., eds., Advanced and next generation satellites, Proceedings of SPIE, December 15, 1995: International Society for Optical Engineering, v. 2583, p. 16–25.

Gilbert, W.G., 1977, General geology of the Healy D–1 and southern Fairbanks A–1 quadrangles and vicinity, Alaska: Alaska Division of Geological and Geophysical Surveys Open-File Report 105, 13 p., 2 sheets, scale 1:63,360.

Gillespie, A.R., Kahle, A.B., and Walker, R.E., 1986, Color enhancement of highly correlated images. I. Decorrelation and HSI contrast stretches: Remote Sensing of Environment, v. 20, no. 3, p. 209–235.

Green, A.A., Berman, M., Switzer, B., and Craig, M.D., 1988, A transformation for ordering multispectral data in terms of image quality and implications for noise removal: IEEE Transactions on Geoscience and Remote Sensing, v. 26, no. 1, p. 65–74.

Harsanyi, J.C., and Chang, C.I., 1994, Hyperspectral image classification and dimensionality reduction; An orthogonal subspace projection approach: IEEE Transactions on Geoscience and Remote Sensing, v. 32, no. 4, p. 779–785.

Hubbard, B.E., Rowan, L.C., Dusel-Bacon, Cynthia, and Eppinger, R.G., 2007, Geologic mapping and mineral resource assessment of the Healy and Talkeetna Mountains quadrangles, Alaska using minimal cloud- and snow-cover ASTER data: U.S. Geological Survey Open-File Report 2007–1046, 22 p. (Also available online at *http://pubs.usgs.gov/of/2007/1046/*.)

Lowell, J.D., and Guilbert, J.M., 1970, Lateral and vertical alteration-mineralization zoning in porphyry ore deposits: Economic Geology, v. 65, p. 373–408.

Lydon, J.W., 1984, Volcanogenic massive sulphide deposits, Part 1, A descriptive model: Geoscience Canada, v. 11, no. 4, p. 195–202.

McLeod, R.L., 1985, Preliminary observations of kaolinite in a volcanogenic massive sulphide deposit of Permian age: TMPM Tschermaks Mineralogische und Petrographische Mitteilungen, v. 34, no. 3–4, p. 261–269.

McLeod, R.L., 1987, Alteration associated with volcanogenic sulphide ores at Mount Chambers, Queensland, Australia: Institution of Mining and Metallurgy, Transactions (sect. B: Applied Earth Science), v. 96, p. B117–B127.

McLeod, R.L., and Stanton, R.L., 1984, Phyllosilicates and associated minerals in some Paleozoic stratiform sulfide deposits of southeastern Australia: Economic Geology, v. 79, no. 1, p. 1–22.

McLeod, R.L., Gabell, A.R., Green, A.A., and Gardavsky, V., 1987, Chlorite infrared spectral data as proximity indicators of volcanogenic massive sulphide mineralization, *in* Proceedings, Pacific Rim Congress 87, Gold Coast, Queensland, Australia, August 26–29, 1987: Parkville, Victoria, Australia, Australasian Institute of Mining and Metallurgy, p. 321–324.

Newberry, R.J., Crafford, T.C., Newkirk, S.R., Young, L.E., Nelson, S.W., and Duke, N.A., 1997, Volcanogenic massive sulfide deposits of Alaska: Economic Geology Monograph 9, p. 120–150.

Nokleberg, W.J., and others, 1994, Metallogeny and major mineral deposits of Alaska, *in* Plafker, George and Berg, H.C., eds., The geology of Alaska, chapter G–1 *of* The geology of North America: Boulder, Colo., Geological Society of America, p. 855–903.

Rowan, L.C., Hook, S.J., Abrams, M.J., and Mars, J.C., 2003, Mapping hydrothermally altered rocks at Cuprite, Nevada, using the Advanced Spaceborne Thermal Emission and Reflection Radiometer (ASTER), a new satellite-imaging system: Economic Geology, v. 98, no. 5, p. 1019–027.

Rowan, L.C., and Mars, J.C., 2003, Lithologic mapping in the Mountain Pass, California area using Advanced Spaceborne Thermal Emission and Reflection Radiometer (ASTER) data: Remote Sensing of Environment, v. 84, no. 3, p. 350–366.

Wahrhaftig, Clyde, 1970a, Geologic map of the Healy D–2 quadrangle, Alaska: U.S. Geological Survey Geologic Quadrangle Map GQ–804, scale 1:63,360.

Wahrhaftig, Clyde, 1970b, Geologic map of the Healy D–3 quadrangle, Alaska: U.S. Geological Survey Geologic Quadrangle Map GQ–805, scale 1:63,360.

Aufeis Accumulations in Stream Bottoms in Arctic and Subarctic Environments as a Possible Indicator of Geologic Structure

By Richard B. Wanty, Bronwen Wang, Jim Vohden, Warren C. Day, and Larry P. Gough

Chapter F of
Recent U.S. Geological Survey Studies in the Tintina Gold Province, Alaska, United States, and Yukon, Canada—Results of a 5-Year Project

Edited by Larry P. Gough and Warren C. Day

Scientific Investigations Report 2007–5289–F

U.S. Department of the Interior
U.S. Geological Survey

Contents

Figures

Aufeis Accumulations in Stream Bottoms in Arctic and Subarctic Environments as a Possible Indicator of Geologic Structure

By Richand B. Wanty,[1] Bronwen Wang,[1] Jim Vohden,[2] Warren C. Day,[1] and Larry P. Gough[1]

Abstract

Thick accumulations of ice, called "aufeis," form during winter along stream and river valleys in arctic and subarctic regions. In high-gradient alpine streams, aufeis forms mostly as a result of ground-water discharge into the stream channel. The ice occludes this discharge, perturbing the steady-state condition, and causing an incremental rise in the local water table until discharge occurs higher on the stream bank above the previously formed ice. Successive freezing of onlapping ice layers can lead to aufeis accumulations several meters thick.

The location and extent of aufeis in high-gradient streams may be useful to relate local hydrology to geologic structure. In the Goodpaster River basin study area, mineral deposits are known to occur, the location of which may be structurally controlled. Therefore, a more thorough understanding of regional geologic structures may facilitate a more detailed understanding of the genesis of the mineral deposits.

Extensive aufeis was observed during visits to the Goodpaster River basin in east-central Alaska during 1999, 2001, and 2002. Seeps from the sides of the valleys caused ice to build up, giving the ice surface a concave-upward shape perpendicular to the stream direction. This concavity is evidence for ground-water discharge along the length of the aufeis, as opposed to discharge from a single upstream point. During thaw, streamflow is commonly observed out of the normal channel, evidence that occlusion of the channel (and shallow sediments) by ice is a viable mechanism for causing the water table to rise.

The thickest (>3 meters) and most extensive aufeis (100's of meters to kilometers along valleys) coincided with locations of laterally extensive (>5 kilometers) mapped high-angle brittle fault zones, suggesting that the fault zones are hydraulically conductive. Additional evidence of water flow is provided by observed changes in stream-water chemistry in reaches in which aufeis forms, despite a lack of surface tributaries. Minor or no aufeis was observed in many other drainage valleys where no laterally extensive structures have been mapped, implying that aufeis formation results from more than a topographic effect or discharge from bank storage. Thus, the presence of thick, laterally extensive aufeis in high-gradient streams may be a useful aid to geologic structural mapping in arctic and subarctic climates.

Introduction

In high-latitude ecoregions, where prolonged subfreezing temperatures exist for a significant part of the year, thick accumulations of ice, called aufeis or naled, may form in areas of ground-water discharge, or where ice dams form in flowing rivers. For example, in our study area northeast of Delta Junction, Alaska, the average monthly temperature is below 0°C from October through April and the average January temperature is about -20°C (Weatherbase, 2007). Aufeis that forms as a result of ground-water discharge serves as an indicator of the location and extent of discharge. In areas with crystalline bedrock, ground-water flow is typically constrained by fractures. Aufeis that forms in such areas likely indicates locations of hydraulically conductive fractures. This paper demonstrates the coincidence of areas of aufeis formation in several alpine catchments with locations of regional-scale (from 1 kilometer (km) to 10's of kilometers) fractures. In physiographic settings such as the study area described herein, aufeis may be helpful to understand locations of geologic structures as well as to qualitatively indicate the possible hydraulic conductivity of those fractures.

Aufeis in high-gradient catchments tends to reform in the same locations year after year (Dean, 1986; Lauriol and others, 1991; Hu and Pollard, 1997a), perhaps due to relatively invariant geologic, geomorphic, and hydrologic circumstances. In such catchments, where soil cover is thin, geologic properties that control ground-water flow (for example, fractures in crystalline bedrock) may be more

[1]U.S. Geological Survey.

[2]Alaska Department of Natural Resources, Division of Mining, Land, and Water.

important to aufeis formation than the hydrologic properties of unconsolidated material overlying bedrock. In this context, aufeis may also serve as a guide to the existence of potential ground-water resources (Harden and others, 1977).

A useful genetic classification of aufeis that was proposed by Carey (1973) includes spring aufeis, ground aufeis, and river aufeis. Spring aufeis forms as a result of ground-water discharge from beneath a permafrost layer (Hall and Roswell, 1981; Yoshikawa and others, 2001) and is the primary focus of this study. Ground aufeis forms by discharge of shallow ground water from within the "active layer," which is that portion of seasonally frozen ground between permafrost and the ground surface. River aufeis forms as a result of fluvial processes, often related to ice dams and commonly found in areas where the river gradient abruptly decreases (Hu and Pollard, 1997a).

Hu and Pollard (1997a) describe the formation and buildup of aufeis using a three-stage model: freeze-up, obstruction, and overflow. Initial freeze-up is primarily responsible for aufeis location, while the latter two stages define the growth and abundance of individual icings. Hu and Pollard (1997b) developed a statistical model for aufeis growth during the overflow stage and found that ice thickness decreases away from the water source. In this study, relatively uniform ice thickness over distances of hundreds of meters to several kilometers implies numerous water sources or, more likely, a long continuous water source to the accumulating aufeis.

On an annual basis, aufeis serves as a reservoir for winter baseflow (Slaughter and Benson, 1986) that is released during late spring and early summer (Li and others, 1997). Aufeis formation during the winter quantitatively captures ground-water discharge, but because aufeis melts more slowly than regional snowpack, exceptionally thick (2 to 3 meters (m) or more) aufeis deposits may persist well into the summer months, continually releasing water to streams. Kane and Slaughter (1973) studied a watershed north of Fairbanks, Alaska, and found that the volume of water stored in the ice was only 4 percent of the total annual stream discharge but represented about 40 percent of the discharge for the winter months. They showed that if this ice melted within a 1-month period, there would be a significant increase in streamflow after snowmelt runoff was complete. Similarly, Osterkamp and others (1975) found significant (30–50 percent) reductions in streamflow just in the early stages of ice formation, implying temporary storage of the water as ice.

Previous studies have suggested links between aufeis formation and geologic properties of catchments. Lauriol and others (1991) noted that aufeis in the northern Yukon formed in spatial association with fault zones in carbonate bedrock. Hall and Roswell (1981) also noted a general spatial correlation between aufeis occurrences and locations of bedrock fracture zones, with greater density of aufeis in more heavily fractured areas. They proposed that the faults represent conduits along which ground water may flow between gaps in permafrost.

A baseline geochemical study was conducted in our study area (see fig. 1 of Editors' Preface and Overview) from 1999 to 2002, prior to new mining activity. New geologic mapping also was performed to complement concurrent sampling of surface water, soils, and plants, and to relate the chemical variations in the sampled media to surface or bedrock lithology. Because this study was conducted in a remote area, no possibility existed for sampling ground water other than by sampling springs in the area. During several visits to the area, thick aufeis accumulations were observed in some areas. These observations were used to investigate the spatial and causative relations between aufeis and local and regional hydrology. In contrast to earlier work, this study presents evidence for direct spatial correlations between streams that accumulate aufeis and specific fracture sets.

Description of Study Area

The study area is in the Goodpaster River drainage (fig. F1) about 70 km northeast of the town of Delta Junction, Alaska, and includes the entire Big Delta B–2 quadrangle (U.S. Geological Survey, 1958). Elevations range from 1,433 m above sea level atop Shawnee Peak to just less than 400 m, where the Goodpaster River flows along the southwest edge of the quadrangle. Drainages from the Shawnee Peak massif and an unnamed highland that spans the southern half of the quadrangle are the source of many of the streams sampled during this study.

Climate in the study area is characterized by long, cold winters, with an average of 223 days per year below 0°C. Average snowfall is about 1 m, with about 30 centimeters (cm) of rain between May and September (Weatherbase, 2007). The study area is located within the Intermontane Boreal Ecoregion (Nowacki and others, 2003), characterized by closed spruce hardwood forest over discontinuous permafrost. On south-facing slopes, where permafrost is less pervasive, the predominant forest species are white spruce, aspen, paper birch, and balsam poplar.

The geologic framework of the area is composed of Paleozoic to Tertiary crystalline rocks, with Devonian augen gneiss, Paleozoic biotite gneiss and paragneiss, and Cretaceous granitic plutonic rocks occupying most of the area of the quadrangle (Day and others, 2003). Through its complex geologic history, the Yukon-Tanana Upland, of which our study area is a part, has experienced a number of orientations of tectonic stresses, leading to metamorphism, foliation, and faulting of the rocks. Within the study area, the dominant direction of major fault zones is north-northwest in the northeastern part, northeast in the southern part, and northwest to east-northeast in the northwest part. Mapped structures have long strike lengths, in many cases in excess of 5 km.

The most important surface-water feature in the area is the Goodpaster River, which originates to the east of the

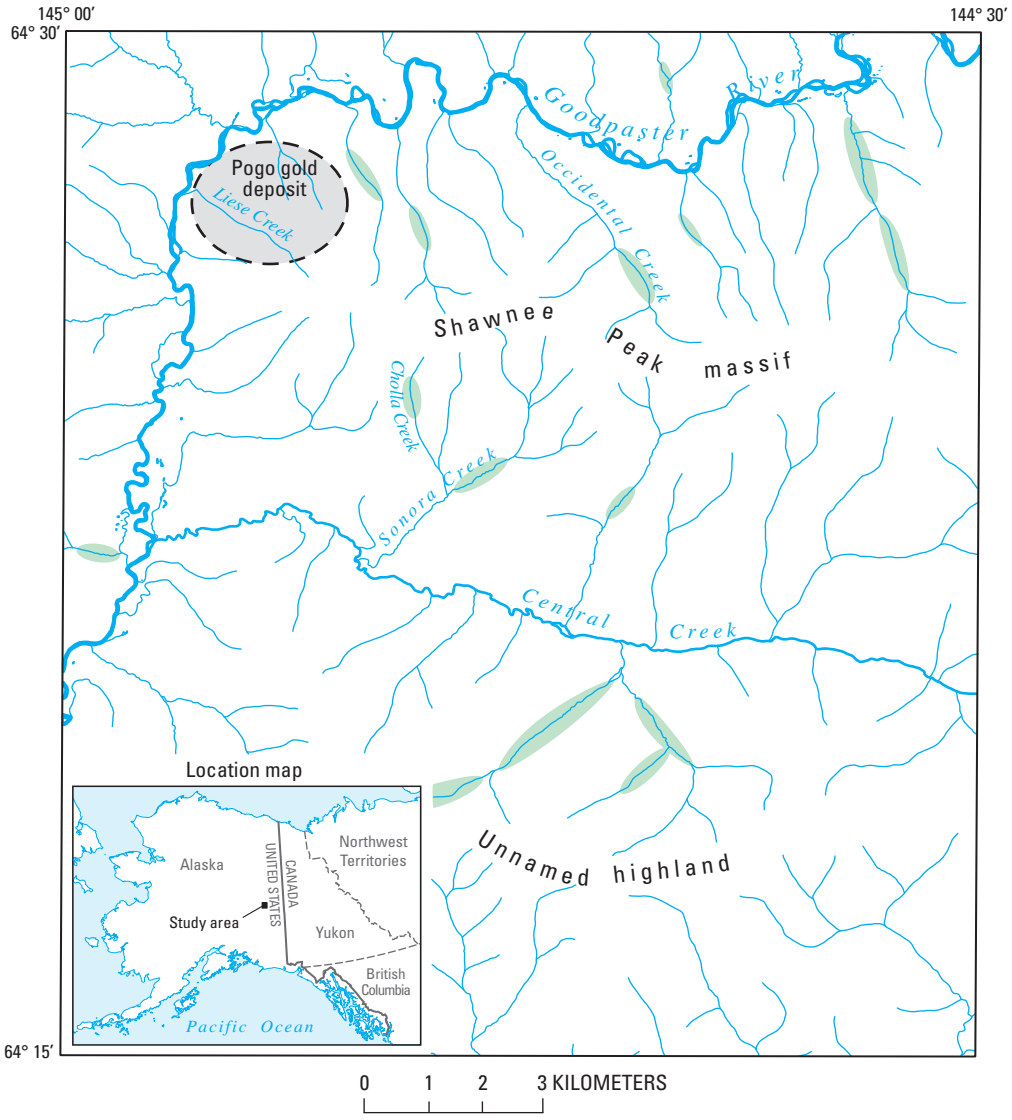

Figure F1. Map showing surface hydrologic features of the Big Delta B–2 quadrangle in east-central Alaska. Green areas show approximate extent of aufeis observed in satellite images or by ground observations. The approximate location of the Pogo gold deposit also is shown.

Big Delta B–2 quadrangle and follows the northern and western edges of the quadrangle. Central Creek flows from east to west through the middle of the study area and represents another major drainage feature. The focus of our study has been the numerous smaller streams that empty into either the Goodpaster River or Central Creek. This paper describes results of geochemical sampling along Cholla, Sonora, and Occidental Creeks (fig. F1), all of which accumulate aufeis in the winter.

Methods

Aufeis was located in stream valleys by a variety of means. In early July of 1999, remnant aufeis was observed in some stream bottoms. More aufeis was found by examining satellite images from early June 2001. In March of 2002, a low-altitude overflight of the area was made; then, in early June of 2002 fieldwork was conducted to examine aufeis locations in greater detail. Where aufeis has occluded stream channels, it commonly has led to the formation of braided immature channels in low-gradient sections of streams. It is therefore possible to infer the presence of aufeis on the basis of channel morphology.

An attempt was made to collect several water samples along each major stream drainage in the study area, including drainages with or without aufeis. Sampling was accomplished by walking the length of each stream to be sampled from the drainage divide to the confluence with the next higher order stream, usually Central Creek or the Goodpaster River. Along each stream length we sampled at the highest elevation of continuously flowing water and worked downstream, monitoring conductivity and temperature of the stream water along the way. If any change was observed, or if there were any tributaries, samples of the tributary and of the stream above and below the tributary were collected. Using this approach commonly resulted in collection of 2 to 10 samples per catchment.

At each sample site, field measurements were made for stream discharge, pH, conductivity, temperature, dissolved oxygen, and dissolved Fe^{2+}. If feasible, discharge was measured with a pygmy flow meter (U.S. Geological Survey, 2007). The pH was measured using a combination glass electrode with automatic temperature compensation. Each morning, the pH electrode was calibrated with buffers of pH 4.0, 7.0, and 10.0. Calibration was checked at least once in the afternoon by measuring the pH of a buffer solution. The measured value of the buffer was always within ±0.05 pH units of the accepted value for the buffer. Conductivity was not calibrated and was therefore used only for relative measurements during sampling. Temperature was measured using a digital thermometer traceable to thermometric standards of the National Institute of Standards and Technology (NIST). Dissolved oxygen and Fe^{2+} were measured using CHEMetrics self-filling ampoules.

In addition to the field analyses, samples were collected and preserved for later laboratory analyses. Samples were filtered through a 0.45-micrometer (µm) Gelman Supor filter and collected into acid-washed high-density polyethylene bottles and acidified to pH of approximately 1 with ultrapure HNO_3. These samples were analyzed for major and trace cations and rare earth elements using inductively coupled plasma–atomic emission spectroscopy (ICP–AES) and mass spectrometry (ICP–MS). A second sample was collected, which was filtered but not acidified, for anion analysis by ion chromatography. A raw sample was collected for alkalinity titration. The latter two samples were kept cool upon returning to the hotel each evening, whereupon they were refrigerated until analysis. Further details of the analytical methods can be found in Briggs (1996), Lamothe and others (1999), and Papp and others (1996).

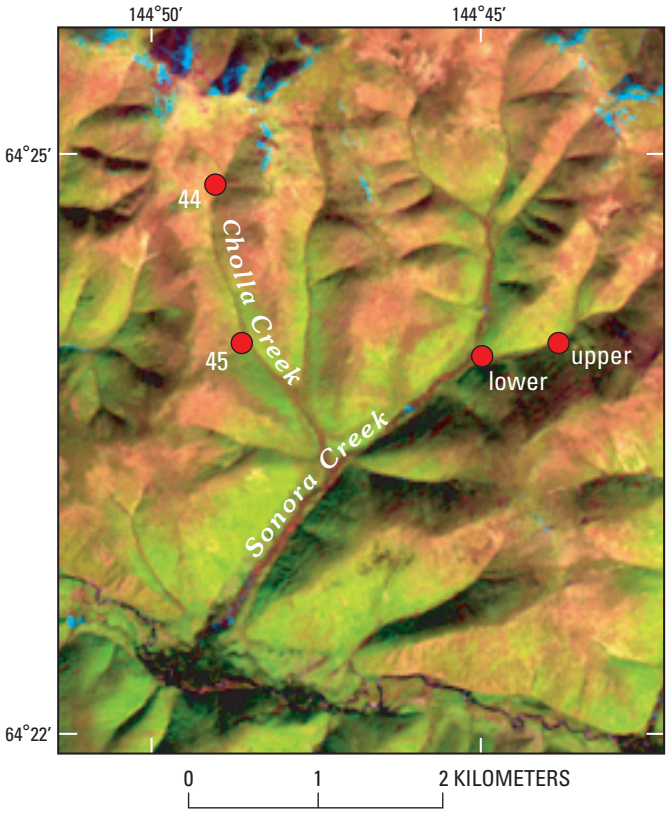

Figure F2. Landsat 7 satellite image (path 68, row 15) of the Cholla and Sonora Creek area, Big Delta B–2 quadrangle, taken June 2, 2001. Blue pixels are areas covered by ice or snow. Most of the blue area near the top of the image is snow, but some aufeis is visible along Sonora Creek just downstream from the lower site. Red dots are sample locations referenced in text.

Results and Discussion

This paper focuses on the Occidental, Cholla, and Sonora Creek catchments—all are high-gradient streams draining the flanks of the Shawnee Peak massif (fig. F1). Cholla and Sonora Creeks are located on south-facing slopes, where less permafrost is expected. Occidental Creek drains to the northwest on a north-facing slope, but the vegetation density is similar to the other two, suggesting an absence of permafrost, or incomplete permafrost in the shallow subsurface. In all three of these cases, the direct observation of aufeis extent is supported by stream-water chemical data and other measurements, including measurements of hydraulic head in the hyporheic zone at one of the sites.

Cholla Creek

Cholla Creek was sampled at two sites, numbered 44 and 45 (fig. F2), in July 1999. The two sites are about 1 km apart, with an elevation change of about 90 m. At the time of sampling, remnant aufeis was still present in the drainage from the previous winter at elevations above site 44. No aufeis was observed in the stream between these two sites, but in a March 2002 low-altitude overflight of the area, aufeis was observed between sites 44 and 45. Given the relatively small area of the Cholla Creek drainage, it is likely that smaller volumes of ice might form and that the 1999 sampling occurred after the aufeis melted from the Cholla Creek valley between the two sample sites.

Between the two sample sites, there were no surface-water tributaries, but the measured stream discharge increased from 1.1 to 2.5 liters per second (L/s) between sites 44 and 45. This observed increase in flow can be attributed only to ground-water discharge. Electrical conductivity of the stream water increased from 190 to 220 microsiemens per centimeter (µS/cm) between the two sites, which can be explained primarily by increases in calcium (34 to 42 milligrams per liter, mg/L), SO_4 (45 to 57 mg/L) and alkalinity (88 to 106 mg/L as HCO_3). Smaller increases were observed in concentrations of sodium, magnesium, and potassium. At both sites total dissolved iron was below detection (<0.02 mg/L).

On the basis of the observed changes in concentrations of dissolved constituents, the discharging ground water

must have greater total dissolved solids, and in particular, significantly higher alkalinity and concentrations of calcium and SO_4 than the stream water. The increases in calcium and alkalinity are expected, on the basis of the local aquifer material, a Paleozoic paragneiss that consists of biotite schist layers and quartzofeldspathic biotite schist layers. In an outcrop sample collected above site 44, fine-grained pyrite and possible marcasite were observed, suggesting that the incremental increase in SO_4 may be at least in part derived from the oxidation of sulfide-bearing minerals in the shallow subsurface.

Sonora Creek

Sonora Creek was sampled in July 1999 and early June 2002 at the sites marked "upper" and "lower" on figure F2. The same sites were sampled each time. In 1999, no aufeis remained along this reach of Sonora Creek, but during the 2002 sampling, aufeis covered the valley bottom continuously between the two sites, a distance of approximately 0.6 km. The vertical drop between the two sites is approximately 85 m.

The formation of aufeis in the Sonora Creek drainage is an indication of ground-water discharge throughout the winter. In July 1999, ground-water hydraulic potential in the shallow subsurface was measured using a device described by Wanty and Winter (U.S. Geological Survey, 2000). Several sites were tested, comparing the elevation of the water in the shallow subsurface (15 to 40 cm below the streambed) to that in the stream. In some cases, no head difference was observed, but in most cases, head differences between 1 and 5 cm were observed, with the ground-water potential always above the stream surface. This result indicates the tendency for ground-water discharge in this reach of Sonora Creek. In 1999, the stream discharge increased from 0.003 to 0.006 m^3/s between the upper and lower sites, with only one surface-water tributary between the sites. The discharge of that tributary was insufficient to make up the difference in discharge. At both times, the electrical conductivity (specific conductance, SpC) decreased slightly between the upper and lower sites, suggesting that discharging ground water had lower total dissolved solids. Chemical analyses indicated small but significant decreases in virtually all the major cations and anions. For example, in 1999, SpC decreased from 270 to 170 µS/cm, and decreases were observed for calcium (41 to 27 mg/L), magnesium (13 to 7 mg/L), sodium (3 to 2.5 mg/L), HCO_3 (140 to 80 mg/L), and SO_4 (53 to 38 mg/L) between the upper and lower sites.

Occidental Creek

Occidental Creek drains the north side of the Shawnee Peak massif (fig. F3). Occidental Creek was sampled in July 1999 and again in early June 2002 at the sites marked "upper" and "lower" on figure F3. The two sites are separated by a distance of approximately 1.6 km and an elevation drop of

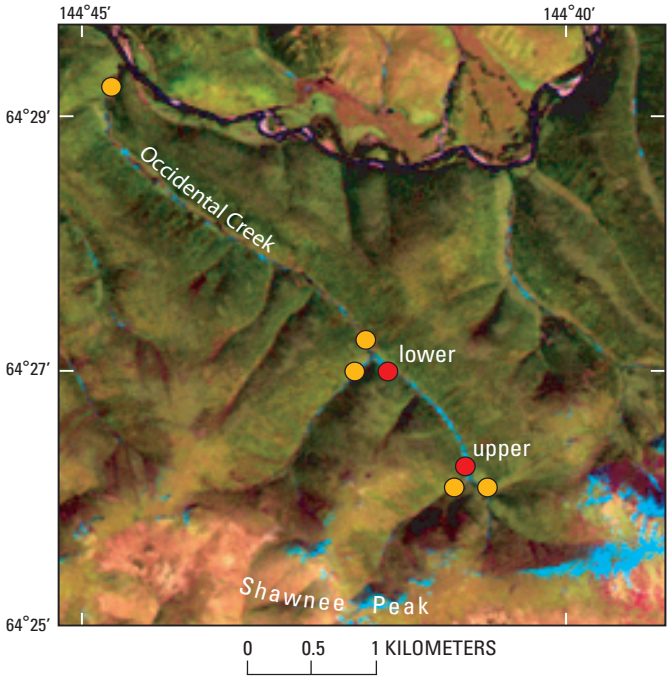

Figure F3. Landsate 7 satellite image (path 68, row 15) of the Occidental Creek area, Big Delta B–2 quadrangle, taken June 2, 2001. Blue pixels are areas covered by ice or snow. The blue areas along the southern part of the image are accumulated snow near the top of Shawnee Peak; nearly continuous aufeis is observed along Occidental Creek between the upper and lower sites. Red dots are sample sites discussed in text. Other sample sites along Occidental Creek are shown with yellow dots.

140 m. Aufeis was present at the upper site in July 1999, but in 2002, a thick (3 m or more) layer of aufeis extended continuously between the upper and lower sites. The satellite image in figure F3, taken June 2, 2001, shows the continuous aufeis in the Occidental Creek valley between the upper and lower sites.

In June 2002, the aufeis was beginning to melt but was still greater than 3 m thick at the upper site (fig. F4). Maximum thickness of the ice was probably about 1 m greater, based on observations of willows embedded in the ice that had their tops cut off at the same level, either by animals or by shearing of debris-laden water during the early stages of breakup. A notable feature of the aufeis at this location was its shape within the valley—viewed down the axis of the valley, the aufeis is concave upward and appears to climb up the valley walls. This morphology suggests that the source water for the aufeis came from spatially and temporally continuous discharge from the valley sides rather than from a point or series of points along the stream channel. A conceptual model for aufeis formation, used to explain this morphology in greater detail, is discussed later in this report.

The chemical changes observed in stream water in Occidental Creek between the upper and lower sites is similar to that in Cholla Creek in that discharging ground water is

Figure F4. Photograph of thick (2–3 meters) aufeis at the upper site on Occidental Creek, taken in early June 2002 after approximately 1 meter of the ice had melted. The flowing water that is visible at the bottom of the chasm is flowing on the ground, but in many areas, most of the streamflow was still over ice at the time our samples were collected.

likely to be a source of sulfate. Resolving the contributions of ground and surface water in Occidental Creek is complicated by the inputs of a surface-water tributary that has higher total dissolved solids and whose chemical contributions explain some of the changes observed between the upper and lower site. This tributary enters Occidental Creek from the southwest about midway between the upper and lower sites (fig. F3). Measured discharges were 0.03 m^3/s at the upper site, 0.006 m^3/s in the tributary, and 0.04 m^3/s at the lower site. Variations in stream discharge, sodium, magnesium, and conductivity can be explained by a conservative mixing model with about 85 percent of the water from Occidental Creek and 15 percent being added by the tributary. However, calcium is overestimated, and potassium, HCO_3, and SO_4 are underestimated by this mixing model, so we propose that discharging ground water has lower concentrations of calcium and greater concentrations of potassium, HCO_3, and SO_4 as compared to the surface-water tributary. The significance of this result is discussed in the next subsection.

Relation Between Aufeis Locations and Fractures

Much of the data presented on the three catchments can be explained by ground-water discharge causing aufeis formation in winter. One aspect of this phenomenon that has not been discussed is the control of ground-water flow in the bedrock aquifers. During the field studies, aufeis was observed in some stream drainages but not in all stream drainages. A spatial relation between the locations of aufeis and major fracture systems as mapped by Day and others (2003) was apparent. This relation is shown in figure F5, using an expanded view of the satellite image base from which figures F2 and F3 were taken. This relation is true for many of the locations where aufeis was studied. For example, one of the most laterally extensive fracture zones in the study area defines the Occidental Creek valley. This valley had some of the most extensive aufeis in the study area, in terms of both lateral extent and thickness. Another area with laterally extensive fractures lies in the southern part of the study area, south of Central Creek ("A" in figure F5). Extensive aufeis was observed along this creek. Ground-water discharge that leads to the formation of this aufeis continues through the summer months and serves as a significant water source to the base flow of these streams. Evaluating regional baseline geochemistry, and determining the chemical contribution of ground water to the streams, should give a "window" to the ground-water chemistry and a greater understanding of the water-rock interactions that take place in the subsurface.

An important distinction needs to be made between the depths of ground-water sources feeding the streams in the study area. It is likely that all the streams in the area are fed by ground-water discharge, but many of the streams in the area do not form aufeis. This difference may be explained by considering the depth from which the discharging ground water originates. Streams that do not form aufeis may be fed by shallower ground water, from within the "active layer." The active layer is that range of depth within the ground that undergoes seasonal freeze and thaw. In many areas, especially on north-facing slopes, the active layer sits atop permafrost. If ground water from the active layer is the primary source of stream water, then these streams would not be expected to form aufeis, as this water source freezes in winter. If the ground water discharging into the streams originates from a deeper source, such as flow within a laterally extensive fracture or fault system, there should be perennial flow, and thus aufeis formation in winter.

A Conceptual Model for the Mechanism of Aufeis Formation in Alpine Catchments

Streams aligned with hydraulically conductive fractures serve as discharge outlets for ground water. During summer months, ground-water discharge through the streambed is unimpeded ("A" in fig. F6). At the onset of winter, the streams freeze, occluding the channel and blocking the discharge of ground water. This blockage perturbs the steady state condition that was obtained over the summer months and leads to a small incremental rise in the potentiometric surface beneath the stream. As the water table rises above the level of ice in the stream, discharge resumes along the margins of the ice ("B" in fig. F6). Throughout the winter, the water table continually rises above the level of the previously formed ice, and discharge proceeds along the margins of the valley ("C" in fig. F6). By this mechanism, the sides of the valley represent a continuous locus of discharge; therefore, the highest elevation of the ice should be along the valley sides, as was observed. In the spring and summer as the ice melts, the potentiometric

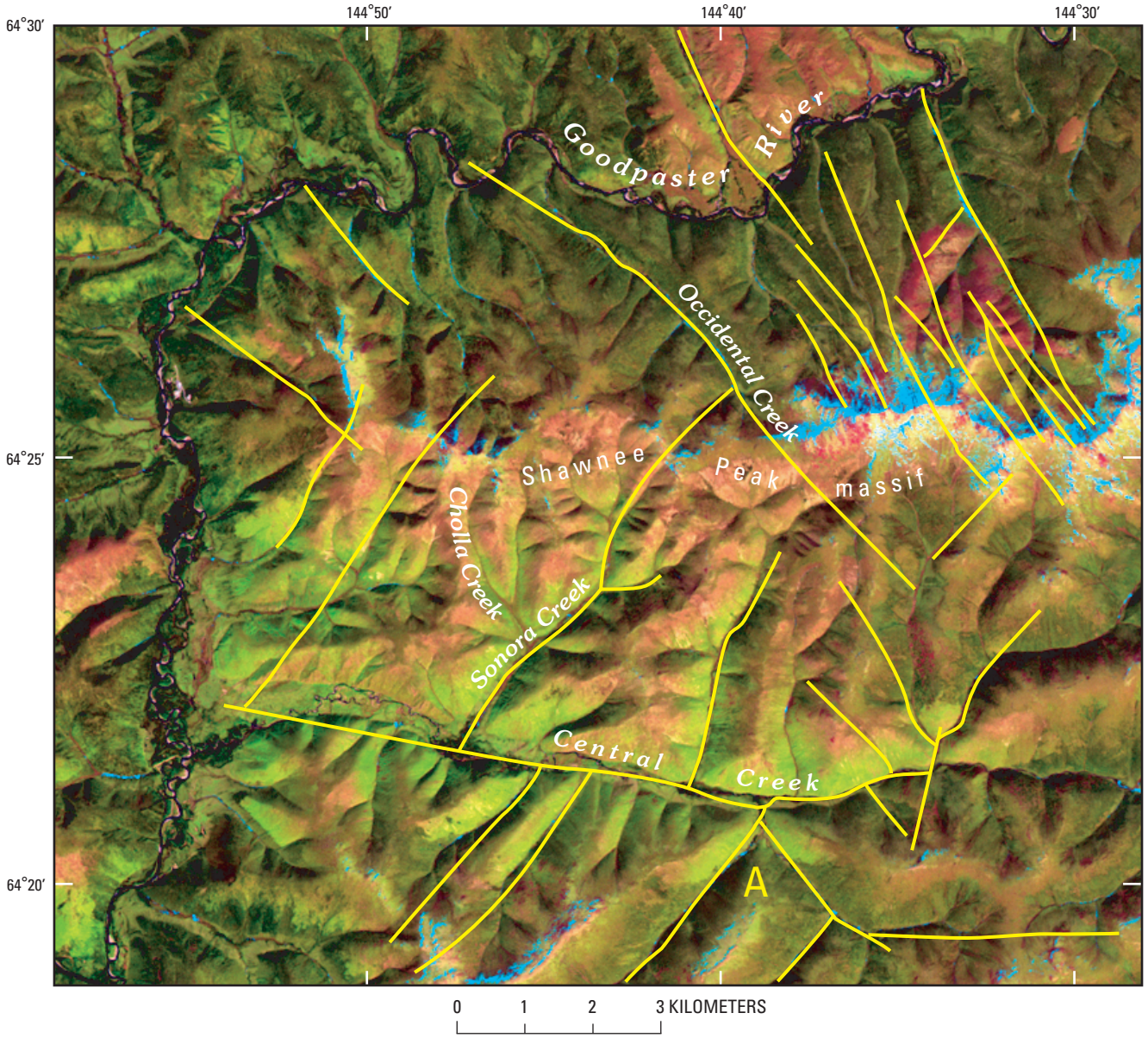

Figure F5. Landsat 7 satellite image (path 68, row 15) of the northern portion of the Big Delta B–2 quadrangle, taken June 2, 2001. Yellow lines show major faults as mapped by Day and others (2003). Location A is an additional area of laterally extensive fractures with aufeis.

surface retreats to the position of "A" in figure F6, and a new annual cycle begins.

Summary

Aufeis forms during the winter in high-gradient alpine streams in arctic and subarctic environments. There is a spatial correlation between streams that accumulate aufeis and regionally extensive fractures. Significant changes in stream-water chemistry were observed in stream reaches that accumulate aufeis. These changes can be explained on the basis of the chemistry of ground water in contact with local aquifer rocks.

The proposed conceptual model for aufeis formation begins with occlusion of normal ground-water discharge flowpaths as streams freeze solid at the beginning of winter. The ground-water level rises incrementally, and discharge proceeds throughout the winter by a succession of freezing of onlapping layers of ice followed by the next incremental rise in the water-table level.

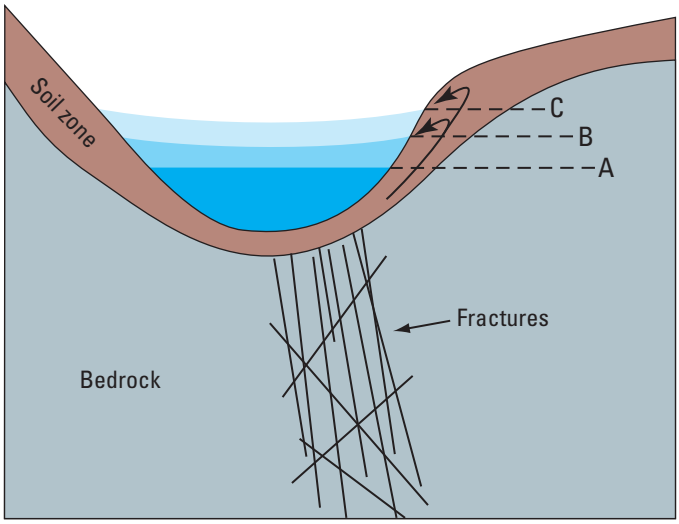

Figure F6. Schematic cross section of a stream fed by discharging ground water that is carried by regionally extensive fractures. See text for explanation.

Acknowledgments

The authors thank the Mineral Resources Program of the U.S. Geological Survey and the Alaska State Department of Natural Resources, Division of Mining, Land and Water, for funding this project. Thanks to Byron Berger and Ron Rickman for constructive reviews of earlier versions of this manuscript.

References Cited

Briggs, P.H., 1996, Forty elements by inductively coupled plasma–atomic emission spectrometry, *in* Arbogast, B.F., ed., Analytical methods manual for the Mineral Resource Surveys Program: U.S. Geological Survey Open-File Report 96–525, p. 77–94. (Also available online at *http://pubs.er.usgs.gov/usgspubs/ofr/ofr96525*.)

Carey, K.L., 1973, Icings developed from surface water and ground water: U.S. Army Cold Regions Research and Engineering Laboratory, Cold Regions Science and Engineering Monograph III–D3, 65 p.

Day, W.C., Aleinikoff, J.N., Roberts, Paul, Smith, Moira, Gamble, B.M., Henning, M.W., Gough, L.P., and Morath, L.C., 2003, Geologic map of the Big Delta B–2 quadrangle, east-central Alaska: U.S. Geological Survey Geological Investigations Series I–2788, 12 p., 1 sheet, scale 1:63,360. (Also available online at *http://pubs.usgs.gov/imap/i-2788/*.)

Dean, K.G., 1986, Regional distribution of stream icings in Alaska, *in* Cold Regions Hydrology Symposium, Fairbanks, Alaska: Bethesda, Md., American Water Resources Association, p. 339–344.

Hall, D.K., and Roswell, Charles, 1981, The origin of water feeding icings on the eastern north slope of Alaska: Polar Record, v. 20, no. 128, p. 433–438.

Harden, D.R., Barnes, P., and Reimnitz, E., 1977, Distribution and character of naleds in northeastern Alaska: Arctic, v. 30, no. 1, p. 28–39.

Hu, Xiaogang, and Pollard, W.H., 1997a, The hydrologic analysis and modeling of river icing growth, North Fork Pass, Yukon Territory, Canada: Permafrost and Periglacial Processes, v. 8, no. 3, p. 279–294.

Hu, Xiaogang, and Pollard, W.H., 1997b, Ground icing formation; Experimental and statistical analyses of the overflow process: Permafrost and Periglacial Processes, v. 8, no. 2, p. 217–235.

Kane, D.L., and Slaughter, C.W., 1973, Seasonal regime and hydrological significance of stream icings in central Alaska, *in* Role of Snow and Ice in Hydrology, Banff Symposium Proceedings: International Association of Hydrological Sciences Publication 107, v. 1, p. 528–540.

Lamothe, P.J., Meier, A.L., and Wilson, S.A., 1999, The determination of forty-four elements in aqueous samples by inductively coupled plasma–mass spectrometry: U.S. Geological Survey Open-File Report 99–151, 14 p. (Also available online at *http://pubs.er.usgs.gov/usgspubs/ofr/ofr99151*.)

Lauriol, Bernard, Cinq Mars, Jacques, and Clark, I.D., 1991, Localisation, genese et fonte de quelques naleds du nord du Yukon (Canada): Permafrost and Periglacial Processes, v. 2, no. 3, p. 225–236.

Li, Shusun, Benson, C.S., Shapiro, L., and Dean, K., 1997, Aufeis in the Ivishak River, Alaska, mapped from satellite radar interferometry: Remote Sensing of Environment, v. 60, no. 2, p. 131–139.

Nowacki, G.J., Spencer, Page, Fleming, Michael, Brock, Terry, and Jorgenson, Torre, 2003, Unified ecoregions of Alaska, 2001: U.S. Geological Survey Open-File Report 02–297, 1 sheet, scale 1:4,000,000. (Also available at *http://pubs.er.usgs.gov/usgspubs/ofr/ofr2297*.)

Osterkamp, T.E., Gilfilian, R.E., and Benson, C.S., 1975, Observations of stage, discharge, pH, and electrical conductivity during periods of ice formation in a small subarctic stream: Water Resources Research, v. 11, no. 2, p. 268–272.

Papp, Clara, Brandt, Elaine, and Aruscavage, Phillip, 1996, Carbonate carbon by coulometric titration, *in* Arbogast, B.F., ed., Analytical methods manual for the Mineral Resource Surveys Program: U.S. Geological Survey Open-File Report 96–525, p. 60–66. (Also available online at *http://pubs.er.usgs.gov/usgspubs/ofr/ofr96525*.)

Slaughter, C.W., and Benson, C.S., 1986, Seasonal snow and aufeis in Alaska's taiga, *in* Proceedings of the Cold Regions Hydrology Symposium, Fairbanks, Alaska: Bethesda, Md., American Water Resources Association, p. 101–109.

U.S. Geological Survey, 1958, Big Delta (B–2), Alaska, topographic map: Washington, D.C., U.S. Geological Survey, scale 1:63,360.

U.S. Geological Survey, 2000, A simple device for measuring differences in hydraulic head between surface water and shallow ground water: U.S. Geological Survey Fact Sheet 077–00, 2 p. (Also available online at *http://pubs.usgs.gov/fs/fs-0077-00*.)

U.S. Geological Survey, 2007, National field manual for the collection of water-quality data: U.S. Geological Survey Techniques of Water-Resources Investigations, Book 9, available only online at *http://water.usgs.gov/owq/FieldManual/*. (Accessed March 9, 2009.)

Weatherbase, 2007, Weatherbase: Canty and Associates LLC Web site at *http://www.weatherbase.com/*. (Accessed May 2, 2007.)

Yoshikawa, Kenji, Petrone, Kevin, Hinzman, L.D., and Bolton, W.R., 2001, Aufeis development and stream baseflow hydrology in the discontinuous permafrost region, Caribou Poker Creeks research watershed, interior Alaska [abs.], *in* 2001 American Water Resources Association Alaska Section Conference Proceedings, Fairbanks, Alaska, April 4–6, 2001: Anchorage, Alaska, American Water Resources Association, Alaska Section. (Available only online at *http://state.awra.org/alaska/proceedings/2001abstracts/yoshikawa.html/*.) (Accessed January 25, 2010.)

Surface-Water, Ground-Water, and Sediment Geochemistry of Epizonal and Shear-Hosted Mineral Deposits in the Tintina Gold Province—Arsenic and Antimony Distribution and Mobility

By Seth H. Mueller, Richard J. Goldfarb, Philip L. Verplanck, Thomas P. Trainor, Richard F. Sanzolone, and Monique Adams

Chapter G of
Recent U.S. Geological Survey Studies in the Tintina Gold Province, Alaska, United States, and Yukon, Canada—Results of a 5-Year Project
Edited by Larry P. Gough and Warren C. Day

Scientific Investigations Report 2007–5289–G

U.S. Department of the Interior
U.S. Geological Survey

Contents

Figures

Tables

Surface-Water, Ground-Water, and Sediment Geochemistry of Epizonal and Shear-Hosted Mineral Deposits in the Tintina Gold Province—Arsenic and Antimony Distribution and Mobility

By Seth H. Mueller,[1] Richard J. Goldfarb,[1] Philip L. Verplanck,[1] Thomas P. Trainor,[2] Richard F. Sanzolone,[1] and Monique Adams[1]

Abstract

Epigenetic mineral deposits in the Tintina Gold Province are generally characterized by high concentrations of arsenic and antimony in their mineral assemblage. A total of 347 samples (ground water, surface water, and stream sediment) were collected to investigate the distribution and mobility of arsenic and antimony in the environment near known mineral deposits. Samples were collected from east to west at Keno Hill and Brewery Creek, Yukon, Canada; and Cleary Hill, True North, Scrafford Mine, Fairbanks, Ryan Lode, Stampede Creek, Slate Creek, and Donlin Creek, all in Alaska. Surface- and ground-water samples are all slightly acidic to near-neutral in pH (5–8), have a wide range in specific conductance (surface water 17–2,980 microsiemens per centimeter and ground water 170–2,940 microsiemens per centimeter), and show elevated dissolved arsenic and antimony concentrations (arsenic in surface water is less than 1 to 380 micrograms per liter and in ground water is less than 1 micrograms per liter to 1.5 milligrams per liter; antimony in surface water is less than 2 to 660 micrograms per liter and in ground water is less than 2 to 60 micrograms per liter). Stream sediments downstream from these deposits have high concentrations of arsenic and antimony (arsenic median is 1,670 parts per million, maximum is 10,000 parts per million; antimony median is 192 parts per million, maximum is 7,200 parts per million). The mobility of arsenic and antimony is controlled by the local redox environment, with arsenic being less mobile in oxidized surface waters relative to antimony, and arsenic more mobile in reduced ground water. These factors suggest that both antimony and arsenic may be useful pathfinder elements in water and sediment for targeting similar style deposits elsewhere in the Tintina Gold Province.

Introduction

In recent years, trace elements such as arsenic and antimony have garnered significant attention from the scientific community and the general public due to their toxicity and our initially limited, but rapidly growing understanding of their geochemical behavior in the natural environment (Welch and others, 2000; Filella and others, 2002a,b; Smedley and Kinniburgh, 2002). Arsenic and antimony are strongly associated with both gold and base metals in epigenetic shear-zone-related mineral deposits within the Tintina Gold Province (TGP; Hart and others, 2002). We have carried out numerous investigations on the distribution, speciation, and mobility of arsenic and antimony in ground and surface waters as well as stream sediments in multiple environments (prior to, during, and after mining); and on their efficiency as pathfinder elements in exploration for similar, as of yet undiscovered gold deposits in the TGP. Studies of the speciation and mobility of trace metals, such as arsenic and antimony, are also critical to understanding the natural degradation of both mined and undisturbed mineral deposits and can provide empirical data necessary for the development of environmental geochemical models of epizonal shear- and shear zone-hosted mineral deposits.

Four primary areas within the TGP were studied. As shown in figure G1 (from east to west) our study included (1) Keno Hill and Brewery Creek in the Tombstone district of Yukon, Canada; (2) several deposits in the Fairbanks mining district, including Cleary Hill, True North, Scrafford, and Ryan Lode, as well as undeveloped shear- and fault-hosted zones of mineralization within the vicinity of the city of Fairbanks; (3) the Stampede and Slate Creek deposits in the Kantishna Hills mining district; and (4) the Donlin Creek gold deposit in the Kuskokwim district in southwestern Alaska.

[1]U.S. Geological Survey.

[2]University of Alaska—Fairbanks.

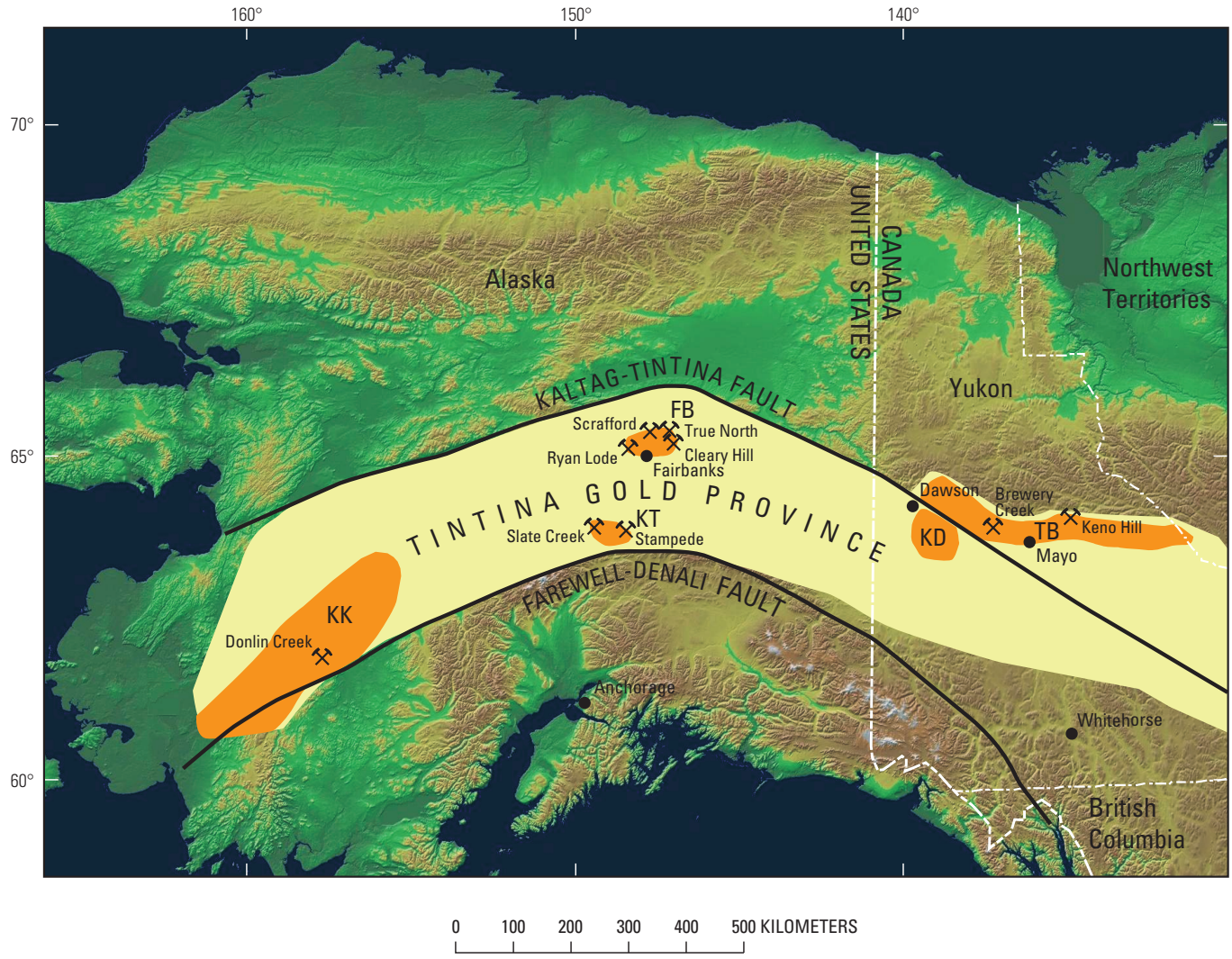

Figure G1. Landsat-based shaded-relief map showing the outline of the Tintina Gold Province, major faults, mining districts (KK, Kuskokwim; KT, Kantishna; FB, Fairbanks; KD, Klondike; TB, Tombstone Gold Belt), and study areas.

Geology of Mineral Deposits

The TGP is an arcuate east-west-trending belt of rocks made up of multiple and diverse geologic terranes generally bounded on the north by the Kaltag-Tintina fault system and on the south by the Farewell-Denali fault system (fig. G1). Three dominant geotectonic regimes lie within the TGP. They are, from east to west, (1) Neoproterozoic to middle Paleozoic turbidites, basinal clastic rocks, and limestones of the Selwyn basin continental margin sequence (Gordey and Anderson, 1993); (2) Neoproterozoic to Paleozoic polymetamorphosed metasedimentary and meta-igneous assemblages of the Yukon-Tanana Upland in east-central Alaska (Foster and others, 1994); and (3) Paleozoic to Mesozoic basement terranes overlapped by Cretaceous flysch sequences of the Kuskokwim basin (Decker and others, 1994).

The majority of the mineral deposits are shear zone- and (or) fault-hosted epizonal gold-bearing ores, typically containing as much as several volume percent arsenopyrite, pyrite, and (or) stibnite. The Keno Hill silver-lead-zinc deposit in the Tombstone district (fig. G1), although having a different metallogenic signature, was included for study because it is a similar style of epigenetic vein-type mineralization, and appears to have a spatial and temporal relationship with gold-bearing deposits in the eastern part of the TGP. Other gold deposits in the TGP with significantly lower sulfide volumes (for example, Fort Knox in Alaska and Scheelite Dome in Yukon), commonly termed intrusion-related gold systems (Hart and others, 2002), were not examined in these studies because arsenic and antimony mobility is less of a concern surrounding this deposit type. The following are brief summaries of the local geology of each study location from east to west across the TGP. For more detailed descriptions of the characteristics of these deposits, see Goldfarb and others (this volume, chap. A).

Keno Hill

The Keno Hill silver-lead-zinc deposits are located 270 kilometers (km) east of the Alaska-Yukon border, approximately 60 km northeast of the Brewery Creek deposit (fig. G1). This district is composed of about 70 subparallel veins (or vein systems) comprising a composite 6-km-wide by 30-km-long, east-west-trending mineralized zone. The vein deposits are hosted in the Carboniferous quartzite, carbonaceous phyllite, and calcareous quartzite of the informally named Keno Hill quartzite, and Middle to Late Devonian quartz-sericite-chlorite phyllite, carbonaceous phyllite, siliceous carbonaceous metasiltstone, and crystalline limestone of the Earn Group. These rocks are intruded by numerous granitic dikes and sills dated at about 90 million years before present (Ma) (Sinclair and Tessari, 1981; Franzen, 1986). Stibnite and arsenopyrite are associated with the silver-lead-zinc mineralization. Alteration and gangue minerals include quartz, calcite, and siderite. The majority of the historical mines in the Keno Hill district have been abandoned without reclamation.

Brewery Creek

The Brewery Creek deposit is located 60 km east of Dawson in east-central Yukon, in the hanging wall of the Jurassic to Cretaceous Robert Service thrust fault (Diment, 1996; Lindsay and others, 2000). The area is underlain by graptolitic shale, chert, mudstones, calcareous andesitic flows, tuffs and breccias, and siltstone of the Cambrian to Upper Devonian Road River Group, and argillite, silty shale, sandstone, graywacke, and limestone of the Earn Group (Diment and Craig, 1999; Lindsay and others, 2000). Granitic dikes and sills intrude these units and are the dominant ore host rocks. The deposit is characterized by an epizonal style of mineralization and is dated at 91 Ma (Lindsay and others, 2000). The ore-bearing quartz veinlets and disseminated sulfide zones are continuous along strike for 12 km. The ore contains a few percent arsenopyrite and pyrite, with gold-enriched rims. Stibnite postdates the main phase of gold mineralization (Diment and Craig, 1999; Lindsay and others, 2000). The mineralogical characteristics result in a gold-arsenic-antimony signature. Strong carbonate alteration occurs along the mineralized zone. The deposit is presently being reclaimed.

Fairbanks District

The deposits within the Fairbanks mining district included in this study are the Cleary Hill, True North, Scrafford, and Ryan Lode deposits. In addition, ground- and surface-water samples were collected throughout the city of Fairbanks, Alaska, area to determine the extent and environmental aspects of undeveloped fault- and shear-hosted disseminated sulfide zones concealed under Quaternary surficial materials. The mineral deposits of the Fairbanks mining district are hosted in a heterogeneous mixture of metasedimentary rocks that include quartz-muscovite schist, quartzite, chlorite quartzose schist, amphibolite schist, biotite schist, and marble of the Fairbanks Schist; slate, phyllite tuff, quartzite, calcareous schist, and marble of the Birch Hill sequence; and, in the case of True North, eclogite-bearing amphibolite and quartzite of the Chatinika terrane.

The Cleary Summit area is located 30 km northeast of the city of Fairbanks and contains about 30 small, high-grade (about 10 grams/ton gold) historical lode mining operations, including the Hi-Yu, Chatham Creek, and McCarty deposits. The deposits of Cleary Hill are best described as shear-hosted orebodies, with veins occurring as open-space fractures dominated by massive white quartz with variable sulfide content (Metz, 1991; McCoy and others, 1997). Alteration minerals include quartz, sericite, calcite, and ankerite.

The True North epizonal gold deposit is located 8 km north of the Cleary Hill mines. The ore zones are shallowly dipping and variably brecciated within the eclogitic rocks of the Chatinika terrane. Strong structural control is indicated by coincidence of ore zones with local thrust faults (Bakke and others, 2000). Gold occurs with fine-grained pyrite, arsenopyrite, and stibnite. In the developed oxidized zone, the pyrite and arsenopyrite have weathered to goethite and scorodite, respectively. Alteration minerals include quartz, manganese oxides, ankerite, mariposite, sericite, and graphite. The deposit is now abandoned and there is no reclamation.

The Scrafford deposit, located 18 km to the north of Fairbanks, was mined from 1915 to 1918 and was the second largest producing antimony mine in Alaska (Robinson and Bundtzen, 1982). Massive, fibrous stibnite occurs in blocks (about 3 m wide) within shear zones and in quartz stockwork veinlets (Robinson and Bundtzen, 1982). Minor arsenopyrite, gold, and galena are present within the lode. The shafts have since collapsed, leaving tailings piles and an open trench.

The Ryan Lode deposit is 13 km west of Fairbanks. The ore zone consists of northeast-striking, subparallel shear zones along the margin of a 90 Ma granodiorite plug (McCoy and others, 1997). The ore is mixed oxide-sulfide and contains several percent arsenopyrite and stibnite. Alteration minerals include albite, sericite, ankerite, and calcite.

Kantishna Hills

The Kantishna Hills mining district is located within the northwestern part of Denali National Park and Preserve. This district contains a number of gold- and antimony-bearing lode deposits, including Alaska's largest past antimony producer, the Stampede mine, as well as occurrences along Slate Creek. The host rocks consist of Precambrian to Paleozoic chlorite and graphite schists, marble, and metavolcanic rocks of the Spruce Creek sequence and calcareous schist, marble, slate, phyllite, tuff, and quartzite of the Birch Creek schist (Bundtzen, 1981). The district is defined by a number of

vein deposits that trend toward the northeast for greater than 60 km, from Slate Creek in the southwest to Stampede in the northeast. Individual veins that make up the bulk of the orebodies in the area are structurally controlled along faults and range in width from 8 cm to greater than 9 m and range in length from 30 m to greater than 500 m. The orebodies at both Stampede and Slate Creek are composed predominately of massive stibnite.

Donlin Creek

The Donlin Creek deposit is located 450 km northwest of Anchorage, in the Kuskokwim Mountains. The approximately 70 Ma deposit consists of a hypabyssal dike-sill complex that intrudes the Kuskokwim Group sedimentary rocks (Miller and Bundtzen, 1994; Bundtzen and Miller, 1997). The gold occurs in north- to northeast-striking, steeply dipping quartz veins and veinlets with lesser dolomite that fill brittle extensional fractures in the rhyolite-rhyodacite porphyry dikes and sills. The gold is contained in arsenopyrite and rarely pyrite, and is refractory in nature (Szumigala and others, 2000). Late-stage stibnite, orpiment, realgar, cinnabar, and native arsenic are also present in small quantities (Goldfarb and others, 2004). Sericite and carbonate are common alteration minerals.

Sample Collection and Methods

A total of 196 surface-water samples, 65 ground-water samples, and 86 stream-sediment samples were collected from sites surrounding active mines, exploration targets, and unreclaimed and partially reclaimed sites, and areas in the vicinity of Fairbanks previously identified as having elevated ground-water arsenic concentrations (table G1, fig. G2). Detailed information regarding sample collection, analysis, quality assurance, and quality control can be found in Mueller (2002), Mueller and others (2002, 2003, 2004), and Verplanck and others (2003).

Ground-Water Samples

Three types of ground-water sites were sampled: individual domestic supply wells, ground-water monitoring wells, and drilling water-supply wells. In the case of domestic supply wells, a flow-through cell was connected to the plumbing system upstream of any household filtration or treatment systems. Water pH, specific electrical conductance, and temperature were monitored until all three readings stabilized, then a composite sample was collected in a sterilized 5-gallon bucket, from which a subset of samples was transferred into polypropylene bottles. The subset included the following samples: unfiltered-acidified (ultrapure nitric), filtered-acidified (0.45-micrometer (µm) disposable capsule filter and ultrapure nitric acid), filtered-unacidified (0.45-µm disposable capsule filter), and filtered-acidified (0.45-µm disposable capsule filter and ultrapure hydrochloric acid). All samples were refrigerated until analysis.

Surface-Water Samples

At surface-water sites (springs, seeps, and streams), pH, specific conductance, and temperature measurements were taken after the readings stabilized. Then, a representative sample was collected and a subset of samples transferred to polypropylene bottles and refrigerated until analysis (see above).

Table G1. Sampling locations, sample types, and number of samples collected for each location in this study.

Mining district	Sample location	Number of samples		
		Surface water	Ground water	Stream sediment
Tombstone	Keno Hill	14		14
	Brewery Creek	13		7
Fairbanks	Fairbanks (city of)	27	[1]40	
	Cleary Hill	9		7
	True North	6	[2]10	
	Scrafford Mine	6		6
	Ryan Lode		132	
Kantishna	Slate Creek	22		22
	Stampede	18		[3]18
Kuskokwim	Donlin Creek	81	[4]2	12
	Total	196	65	68

[1] Ground-water samples not associated with known mineralization.

[2] Monitoring wells.

[3] Analyses have not been completed on these samples as of this publication.

[4] Drilling supply wells.

Figure G2. Photographs of geologists performing data collection at various locations. *A*, Sampling the reclaimed area of Slate Creek, Kantishna Hills mining district, Denali National Park and Preserve. *B*, Sampling streams near Keno Hill, Yukon. *C*, Monitoring well sampling setup, Ryan Lode mine, Fairbanks, Alaska. *D*, Examining the Ryan Lode shear zone, Fairbanks, Alaska.

Sediment Samples

Bedload stream-sediment samples (less than 63-µm wet sieved onsite) were collected using a variation of the method described in Shelton and Capel (1994). This size fraction includes high surface area, reactive materials such as clays and iron and aluminum hydroxides that are likely associated with downstream transport of adsorbed or co-precipitated arsenic and antimony. Samples were split, with one portion air dried at room temperature for inductively coupled plasma–mass spectrometry (ICP-MS) analysis.

Results and Discussion

The information described herein is partially drawn and summarized from Mueller (2002), Mueller and others (2002, 2003, 2004, 2005), and Verplanck and others (2003).

Water Geochemistry

Generally, both ground and surface water can be classified as Ca-Mg-HCO_3^--SO_4^{2+} dominated. Specific conductivity values show wide variation across the TGP (surface water 17–2,980 microsiemens per centimeter (µS/cm), ground water 170–2,940 µS/cm). Regardless of lithology, and absence or presence of permafrost, ground and surface waters associated with epizonal vein mineralization in the TGP have slightly acidic to slightly basic pH (5–8). Acid-rock drainage is generally not an issue with these types of deposits in the TGP because the metasedimentary host rocks are often calcareous; both gangue minerals and alteration products include calcite, ankerite, and dolomite, all of which contribute to a natural acid-neutralizing capacity within the vicinity of the deposits.

Sediment Geochemistry

Elemental concentrations in stream sediments collected downstream from the gold deposits vary greatly. Arsenic, antimony, iron, and aluminum occur in relatively high concentrations (arsenic median=1670 ppm, maximum=10,000 ppm; antimony median=192 ppm, maximum=7200 ppm; iron median=5.9 percent, maximum=43 percent; aluminum median=8 percent, maximum=15 percent). Median concentrations for arsenic and antimony downstream from known lodes are at least an order of magnitude greater than in sediments from streams draining unmineralized areas.

Arsenic and Antimony Distribution and Mobility

Arsenic concentrations in surface-water samples from different deposits in the TGP range from below detection (less than 1 microgram per liter, µg/L) up to 380 µg/L (fig. G3*A*). The sampling locations with the highest surface-water arsenic concentrations were downstream from deposits at Slate Creek, undeveloped sulfidized shear zones in the Fairbanks area, Scrafford, Cleary Hill, and Brewery Creek. Surface-water antimony concentrations ranged from below detection (less than 2 µg/L) to 660 µg/L (fig. G3*A*). Antimony concentrations were significantly higher in streams draining the Slate

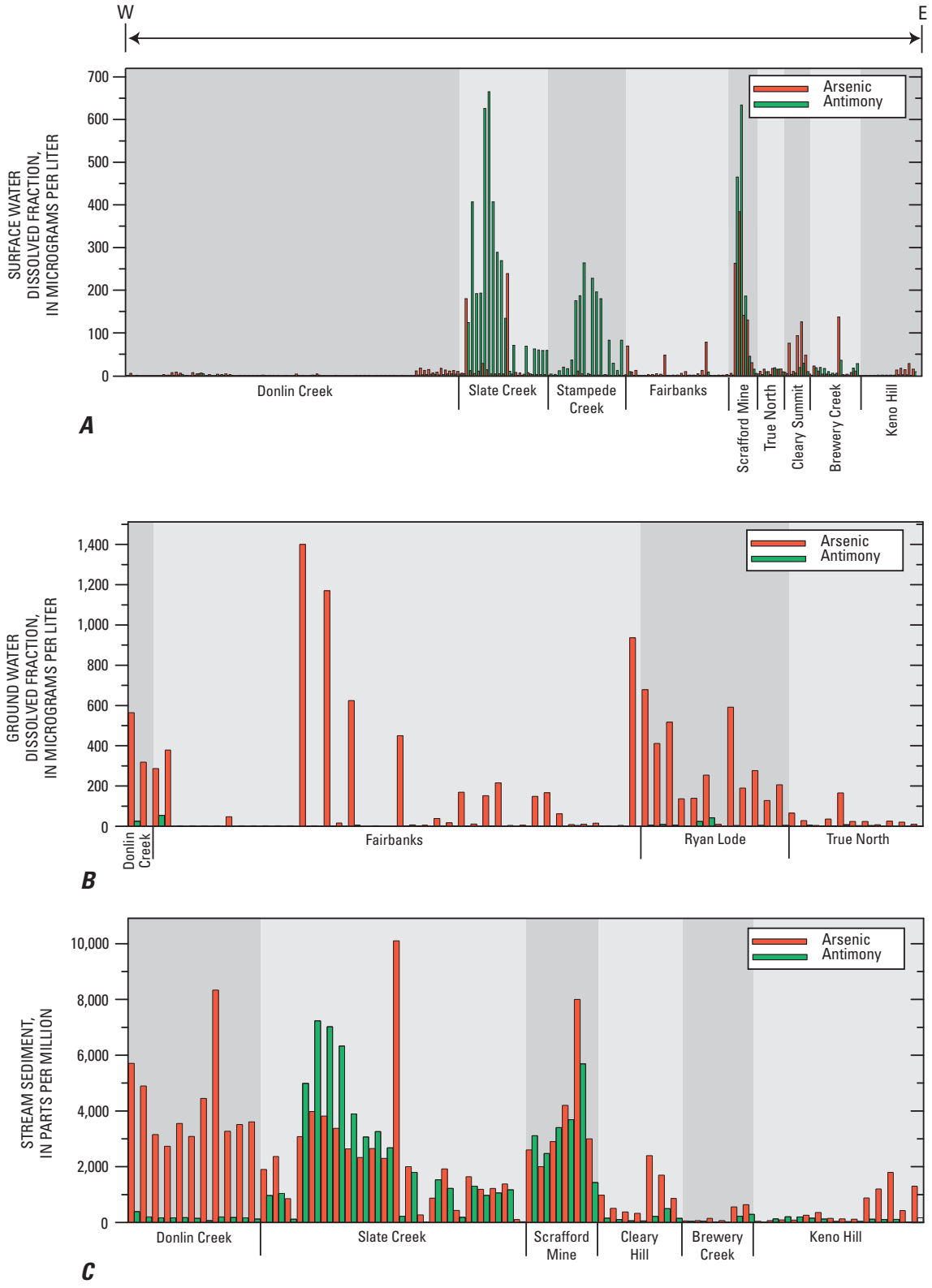

Figure G3. Graphs showing arsenic and antimony concentrations. *A*, Dissolved (less than 0.45-micrometer (μm) fraction) arsenic and antimony concentrations in surface water from west to east across the Tintina Gold Province (TGP). *B*, Dissolved (less than 0.45-μm fraction) arsenic and antimony in ground water from west to east across the TGP. *C*, Arsenic and antimony concentrations in the less than 63 μm fraction of stream-sediment samples from west to east across the TGP.

Creek, Stampede Creek, and Scrafford deposits. Arsenic concentrations in stream sediments are relatively elevated in stream channels downstream from the Donlin Creek, Slate Creek and Scrafford deposits (fig. G3*C*). Antimony is significantly enriched in sediment samples near the Slate Creek and Scrafford deposits (fig. G3*C*). Proximity to the sulfide source has the greatest effect on the relative concentration of arsenic and antimony. Generally, areas with exposed ore and (or) tailings at or near the surface (for example, Slate Creek and Scrafford Mine) have higher surface and stream-sediment concentrations of arsenic and antimony than do areas that have been revegetated naturally or by reclamation efforts (for example, Cleary Hill, Brewery Creek, and Keno Hill).

The absolute concentrations of arsenic and antimony in sediments are relatively similar from a given mineral deposit area (fig. G3*C*). In contrast, corresponding surface-water samples contain significantly less arsenic than antimony (fig. G3*A*, *C*). Surface-water arsenic concentrations are not as high as surface-water antimony concentrations due to the fact that in these near-neutral-pH oxidizing environments, arsenic undergoes oxidation from the more mobile arsenite (As(III)) to arsenate (As(V)) and adsorbs effectively onto iron hydroxides (Smedley and Kinniburgh, 2002). In contrast, antimony, even as oxidized Sb(V), has an apparent lower affinity for adsorption to iron or aluminum hydroxides and, therefore, remains mobile in solution. Surface-water arsenic concentrations commonly decrease significantly (to below detection limits) within less than 1 km from the source, whereas antimony concentrations can remain significantly above detection limit for as far as 8 km from the source.

Ground-water arsenic concentrations range from below detection (less than 1 µg/L) to 1.4 mg/L, with the highest concentrations being recorded in domestic water supply wells in the Fairbanks area (fig. G3*B*). Ground-water antimony concentrations are significantly lower than arsenic from all areas in the TGP, with concentrations ranging from below detection limit (less than 2 µg/L) to 60 µg/L. The highest concentrations of antimony in the Fairbanks area are in domestic supply wells and monitoring wells at the Ryan Lode deposit. The sources of the arsenic and antimony in the ground water are arsenopyrite and stibnite associated with subsurface shear- and fault-hosted sulfide zones. Both As(III) and As(V) are present in many of the ground-water samples. The presence of mixed arsenic species, along with the absence of acidic ground water, suggests that the source of arsenic in the ground waters is not the direct oxidation of arsenopyrite but rather the reductive dissolution of secondary oxide phases, such as arsenic adsorbed to iron hydroxides (see above discussion).

Ground-water arsenic concentrations in the Fairbanks area have been observed to vary by orders of magnitude over short distances (less than 500 m). The distribution of elevated arsenic concentrations in ground water in the Fairbanks area suggests that developed mineral deposits are not a major source of the arsenic; rather, it appears that undeveloped fault- and shear-hosted disseminated sulfides may extend in a northeast-striking trend several kilometers away from known lode deposits and may be a major contributor to the anomalous arsenic.

Exploration

This study not only provides valuable information on the distribution and mobility of arsenic and antimony but also provides information that can be used in exploration for disseminated and shear-hosted mineralization styles of epigenetic gold deposits in the TGP. We have demonstrated that regardless of the state of development of a given deposit (historical, exploration target, current production), both arsenic and antimony are relatively enriched in stream sediments within and downstream from mineralized areas when compared to background stream-water and sediment samples. Antimony may be detectable in surface waters several kilometers downstream of a mineralized source, whereas arsenic in surface waters will increase closer to the mineralized source.

Conclusions

Arsenic and antimony are typically highly anomalous in the Cretaceous epizonal and shear-zone-related gold deposits within the TGP. The geochemistry of surface-water and stream-sediment samples suggests that arsenic mobility is restricted by oxidation and adsorption processes. Antimony appears to be more mobile, remaining in solution at elevated concentrations for several kilometers downstream from a known source. The exposure and proximity of the mineralization to the surface environment directly affects the concentrations in the stream sediments and waters. The concentration of arsenic in ground water, particularly in the Fairbanks, Alaska, area, reflects proximity to numerous sulfide-rich fault and shear zones. Arsenic concentrations in ground waters are also controlled by the reduction-oxidation reaction (redox) state of the ground water, with the more strongly reduced ground waters having higher arsenic concentrations.

All of these aspects of arsenic and antimony geochemistry in the subsurface- and near-surface environment show that antimony and arsenic are useful pathfinder elements in exploration for epizonal and shear-related gold deposits within the TGP. Owing to the greater mobility of antimony, it could serve to more broadly target a mineralized zone, whereas arsenic could then conceivably be used to focus and target mineralized zones.

Acknowledgments

Vanessa Ritchie, Kunal Tanwar, Anastasia Ilgen, Dr. Rainer Newberry, Dr. Larry Hinzman (University of Alaska, Fairbanks), Dr. LeeAnn Munk (University of Alaska, Anchorage), Emily Youcha (Alaska Department of Environmental Conservation), Michael Lilly (GW Scientific), Marti Miller and Erin Marsh (U.S. Geological Survey), and Michelle Roller (formerly of Fairbanks Gold Mining, Inc.) provided assistance in planning and sample collection. Paul Briggs and Mike Anthony performed laboratory analyses. Additionally, we thank Fairbanks Gold Mining, Inc., NovaGold Resources, Inc., Avalon Gold Corp., Calista Corp., and Dr. Craig Hart and Mike Burke of the Yukon Geological Survey, and the National Park Service for property access and logistical support. We are grateful to the citizens of Fairbanks and Ester who volunteered their domestic wells for sampling.

References Cited

Bakke, A.A., Morrel, B.G., Odden, J., Bergstrom, T., and Woodman, J., 2000, Kinross Gold USA's activities in the Fairbanks mining district, K2K, *in* Tucker, T.L., and Smith, M.T., eds., The Tintina gold belt—Concepts, exploration, and discoveries: British Columbia and Yukon Chamber of Mines Special Volume 2, p. 89–98.

Bundtzen, T.K., 1981, Geology and mineral deposits of the Kantishna Hills, Mount McKinley quadrangle, Alaska: Fairbanks, Alaska, University of Alaska—Fairbanks, unpublished M.S. thesis, 238 p.

Bundtzen, T.K., and Gilbert, W.G., 1983, Outline of geology and mineral resources of upper Kuskokwim region, Alaska: Alaska Geological Society Journal, v. 3, p. 101–117.

Bundtzen, T.K., and Miller, M.L., 1997, Precious metals associated with Late Cretaceous-early Tertiary igneous rocks of southwestern Alaska, *in* Goldfarb, R.J., and Miller, L.D., eds., Mineral deposits of Alaska: Economic Geology Monograph 9, p. 242–286.

Decker, John, Bergman, S.C., Blodgett, R.B., Box, S.E., Bundtzen, T.K., Clough, J.G., Coonrad, W.L., Gilbert, W.G., Miller, M.L., Murphy, J.M., Robinson, M.S., and Wallace, W.K., 1994, Geology of southwestern Alaska, *in* Plafker, George, and Berg, H.C., eds., The geology of Alaska, chapter G–1 *of* The geology of North America: Boulder, Colo., Geological Society of America, p. 285–310.

Diment, Rick, 1996, Brewery Creek gold deposit, *in* Yukon exploration and geology, 1995: Whitehorse, Yukon, Canada, Indian and Northern Affairs Canada, Exploration and Geological Services Division, Yukon Region, p. 57–64. (Also available online at *http://www.geology.gov.yk.ca/publications/yeg/yeg95.pdf/*.)

Diment, Rick, and Craig, Sue, 1999, Brewery Creek gold deposit, central Yukon, *in* Roots, C.F., and Emond, D.S., eds., Yukon exploration and geology, 1998: Whitehorse, Yukon, Canada, Indian and Northern Affairs Canada, Exploration and Geological Services Division, Yukon Region, p. 225–230. (Also available online at *http://www.geology.gov.yk.ca/pulications/yeg/yeg98/diment_brewery_creek.pdf/*.)

Ebert, Shane, Miller, Lance, Petsel, Scott, Dodd, Stan, and Kowalczyk, Peter, 2000, Geology, mineralization, and exploration at the Donlin Creek project, southwestern Alaska, *in* Tucker, T.L., and Smith, M.T., eds., The Tintina gold belt—Concepts, exploration, and discoveries: British Columbia and Yukon Chamber of Mines Special Volume 2, p. 99–114.

Filella, Montserrat, Belzile, Nelson, and Chen, Y.W., 2002a, Antimony in the environment; A review focused on natural waters I. Occurrence: Earth-Science Reviews, v. 57, no. 1–2, p. 125–176.

Filella, Montserrat, Belzile, Nelson, and Chen, Y.W., 2002b, Antimony in the environment; A review focused on natural waters, II. Relevant solution chemistry: Earth-Science Reviews, v. 59, no. 1–4, p. 265–285.

Foster, H.L., Keith, T.E.C., and Menzie, W.D., 1994, Geology of the Yukon-Tanana area of east-central Alaska, *in* Plafker, George, and Berg, H.C., eds., The geology of Alaska, chapter G–1 *of* The geology of North America: Boulder, Colo., Geological Society of America, p. 205–240.

Franzen, J.P., 1986, Metal-ratio zonation in the Keno Hill district, central Yukon: Yukon Geology, v. 1, p. 98–108.

Goldfarb, R.J., Ayuso, Robert, Miller, M.L., Ebert, S.W., Marsh, E.E., Petsel, S.A., Miller, L.D., Bradley, Dwight, Johnson, Craig, and McClelland, William, 2004, The Late Cretaceous Donlin Creek gold deposit, southwestern Alaska; Controls on epizonal ore formation: Economic Geology, v. 99, no. 4, p. 643–671.

Gordey, S.P., and Anderson, R.G., 1993, Evolution of the northern Cordilleran miogeocline, Nahanni map area (1051), Yukon and Northwest Territories: Geological Survey of Canada Memoir 428, 214, 2 maps, scale 1:250,000 and 1:50,000.

Hart, C.J.R., McCoy, D.T., Goldfarb, R.J., Smith, Moira, Roberts, Paul, Hulstein, Roger, Bakke, A.A., and Bundtzen, T.K., 2002, Geology, exploration, and discovery in the Tintina gold province, Alaska and Yukon, *in* Goldfarb, R.J., and Nielsen, R.L., eds., Integrated methods for discovery, global exploration in the twenty-first century: Society of Economic Geologists Special Publication 9, p. 241–274.

Lindsay, M.J., Baker, T., Oliver, N.H.S., Diment, Rick, and Hart, C.J.R., 2000, The magmatic and structural setting of the Brewery Creek gold mine, central Yukon, *in* Emond, D.S., and Weston, L.H., eds., Yukon exploration and geology 1999: Whitehorse, Yukon, Canada, Indian and Northern Affairs Canada, Exploration and Geological Services Division, Yukon Region, p. 219–227.

McCoy, D.T., Newberry, R.J., Layer, P., DiMarchi, J.J., Bakke, A.A., Masterman, J.S., and Minehane, D.L., 1997, Plutonic-related gold deposits of interior Alaska, *in* Goldfarb, R.J., and Miller, L.D., eds., Mineral deposits of Alaska: Economic Geology Monograph 9, p. 191–241.

Metz, P.A., 1991, Metallogeny of the Fairbanks mining district, Alaska and adjacent areas: School of Mineral Engineering, University of Alaska Fairbanks, Mineral Industry Research Laboratory Report 90, 370 p.

Miller, M.L., and Bundtzen, T.K., 1994, Generalized geologic map of the Iditarod quadrangle, Alaska, showing potassium-argon, major-oxide, trace-element, fossil, paleocurrent, and archeological sample localities: U.S. Geological Survey Miscellaneous Field Studies Map MF–2219–A, 48 p., 1 sheet in pocket, scale 1:250,000.

Mueller, S.H., 2002, A geochemical characterization of ground water near Fairbanks, Alaska, with emphasis on arsenic hydrogeochemistry: Boulder, Colo., University of Colorado, unpublished M.S. thesis, 109 p.

Mueller, S.H., Goldfarb, R.J., Farmer, G.L., Sanzolone, R.F., Adams, Monique, Theodorakos, P.M., Richmond, S.A., and McCleskey, R.B., 2002. Trace, minor and major element data for ground water near Fairbanks, Alaska, 1999–2000: U.S. Geological Survey Open-File Report 02–90, 12 p.

Mueller, S.H., Goldfarb, R.J., Miller, M.L., Munk, L.A., Sanzolone, R.F., Lamothe, P.J., Adams, Monique, Briggs, P.H., McClesky, R.B., and Theodorakos, P.M., 2003, Surface and ground water geochemistry near the Donlin Creek gold deposit, southwestern Alaska: U.S. Geological Survey Open-File Report 03–492, 37 p. (Also available online at *http://pubs.usgs.gov/of/ofr-03-492/*.)

Mueller, S.H., Hart, C.J.R., Goldfarb, R.J., Munk, L. and Diment, R., 2004, Post-mining hydrogeochemical conditions, Brewery Creek gold deposit, central Yukon, *in* Emond, D.S., and Lewis, L.L., eds., Yukon exploration and geology 2003: Whitehorse, Yukon, Canada, Yukon Geological Survey, p. 271–280.

Mueller, S.H., Trainor, T.P., Goldfarb, R.J., Ritchie, V., Hart, C.J.R., and Newville, M., 2005, Antimony speciation and transport in streams and sediments in mine tailings and waste-rock environments, Alaska and the Yukon: Eos, Transactions, American Geophysical Union, v. 86, Fall Meeting Supplement, Abstract B33C–1053.

Robinson, M.S., and Bundtzen, T.K., 1982, Geology of the Scrafford antimony-gold lode deposit, Fairbanks mining district, Alaska: Alaska Division of Geological and Geophysical Surveys Open-File Report 173, 10 p., 1 plate in pocket.

Shelton, L.R., and Capel, P.D., 1994, Guidelines for collecting and processing samples of stream bed sediment for analysis of trace elements and organic contaminants for the National Water-Quality Assessment Program: U.S. Geological Survey Open-File Report 94–458, 20 p.

Sinclair, A.J., and Tessari, O.J., 1981, Vein geochemistry, an exploration tool in Keno Hill camp, Yukon Territory, Canada: Journal of Geochemical Exploration, v. 14, p. 1–24.

Smedley, P.L., and Kinniburgh, D.G., 2002, A review of the source, behaviour and distribution of arsenic in natural waters: Applied Geochemistry, v. 17, no. 5, p. 517–568.

Szumigala, D.J., Dodd, S.P., and Arribas, A., Jr., 2000, Geology and gold mineralization at the Donlin Creek prospects, southwestern Alaska: Alaska Division of Geological and Geophysical Surveys Professional Report 119, p. 91–115.

Verplanck, P.L., Mueller, S.H., Youcha, E.K., Goldfarb, R.J., Sanzolone, R.F., McClesky, R.B., Briggs, P.H., Roller, M., Adams, M., and Nordstrom, D.K., 2003, Chemical analyses of ground and surface waters, Ester Dome, central Alaska, 2000–2001: U.S. Geological Survey Open-File Report 03–244, 40 p. (Also available online at *http://pubs.usgs.gov/of/2003/ofr-03-244/*.)

Welch, A.H., Westjohn, D.B., Helsel, D.R., and Wanty, R.B., 2000, Arsenic in groundwater of the United States; Occurrence and Geochemistry Groundwater, v. 38, no. 4, p. 589–604.

Landscape Geochemistry Near Mineralized Areas of Eastern Alaska

By Bronwen Wang, Larry P. Gough, Richard B. Wanty, James G. Crock, Gregory K. Lee, Warren C. Day, and Jim Vohden

Chapter H of
Recent U.S. Geological Survey Studies in the Tintina Gold Province, Alaska, United States, and Yukon, Canada—Results of a 5-Year Project

Edited by Larry P. Gough and Warren C. Day

Scientific Investigations Report 2007–5289–H

U.S. Department of the Interior
U.S. Geological Survey

Contents

Figures

Tables

Landscape Geochemistry Near Mineralized Areas of Eastern Alaska

By Bronwen Wang,[1] Larry P. Gough,[1] Richard B. Wanty,[1] James G. Crock,[1] Gregory K. Lee,[1] Warren C. Day,[1] and Jim Vohden[2]

Abstract

The Pogo lode gold deposit was discovered in eastern Alaska in the early 1990s and provided the opportunity to study elemental distribution and mobility in the natural environment prior to mine development. Studying mineralized systems prior to mining allows us to compare the natural biogeochemical signature in mineralized versus nonmineralized areas. The resultant data and interpretation also provide a baseline for evaluating what, if any, changes in elemental distribution result from development. This report investigates the chemistry of stream water, streambed sediment, and soil in the context of regional bedrock geology. The major-ion chemistry of the waters reflects a rock-dominated aqueous system, and the waters are classified as Ca^{2+} and Mg^{2+} - HCO_3^- to Ca^{2+} and Mg^{2+} - SO_4^{2-} waters. Creeks draining the gneissic lithologies tend to be more sulfate dominated than those draining the intrusive units. Sulfate also dominated creeks draining mineralized areas; however, the underlying paragneiss unit could be contributing substantially to the sulfate concentration, and the sulfate concentration in these creeks may reflect a complex baltholith-paragneiss boundary rather than mineralization. Arsenic concentrations in bed sediments were elevated in mineralized areas relative to nonmineralized areas. Elevated concentrations of nickel, chromium, iron, manganese, and cobalt appear to reflect the presence of ultramafic rocks in the drainage. In general, aqueous metal concentrations were below the State of Alaska's Aquatic Life Criteria and Drinking Water Standards, with the exception of arsenic in stream water, which ranged in concentration from less than 1 to 14 micrograms per liter (µg/L) and exceeded the drinking water standard at one site. The arsenic and antimony concentration in the A, B, and C soil horizons ranged from 3 to 410 milligrams per kilogram (mg/kg), 6.1 to 440 mg/kg, and 2 to 300 mg/kg, respectively, for arsenic and 0.4 to 24 mg/kg, 0.6 to 25 mg/kg, and 0.2 to 16 mg/kg, respectively, for antimony. The arsenic and antimony concentrations in stream waters correlate well with the concentrations in soils. However, significantly less arsenic and antimony was extracted from C horizon soils in water leaching experiments, indicating that the arsenic and antimony in the C horizon is present in a less available form than in the A or B horizons. Arsenic and antimony uptake by grayleaf willow *(Salix glauca* L.) appears minimal, with arsenic concentrations ranging from less than 0.01 to 0.14 mg/kg and antimony concentrations ranging from less than 0.003 to 0.23 mg/kg in willow leaves. In general, the highest concentrations of both arsenic and antimony in water and soils were found near mineralized areas. Elevated arsenic concentrations were also found in bed sediments from mineralized areas. In these sample matrices, the presence of arsenic and (or) antimony was a good indicator of contact with mineralized rock units.

Introduction

The Pogo vein gold deposit was discovered in the early 1990s (Smith and others, 1999). Because our work was implemented before the mine was developed, we were able to study elemental distribution and mobility in the natural, undisturbed environment. The Tintina Gold Province (TGP) study area is located in the subarctic boreal forest of east-central Alaska (fig. H1; see fig. 1 of the Editors' Preface and Overview). The Pogo gold deposit, as well as other mineralized localities, is located within the study area. In 1999, we had the opportunity to compare the effect of the Pogo deposit mineralization type and other area mineralization on the soil, sediment, and water geochemistry relative to nonmineralized areas prior to active mining. Studying mineralized systems prior to mine development allows us to investigate the natural hydrogeochemical and biogeochemical signatures in mineralized versus nonmineralized areas. The resultant data and interpretation also provide a baseline for evaluating what, if any, changes in elemental distribution result from mineral development. Our goals were (1) to define geochemical

[1]U.S. Geological Survey.

[2]Alaska Department of Natural Resources, Division of Mining, Land, and Water.

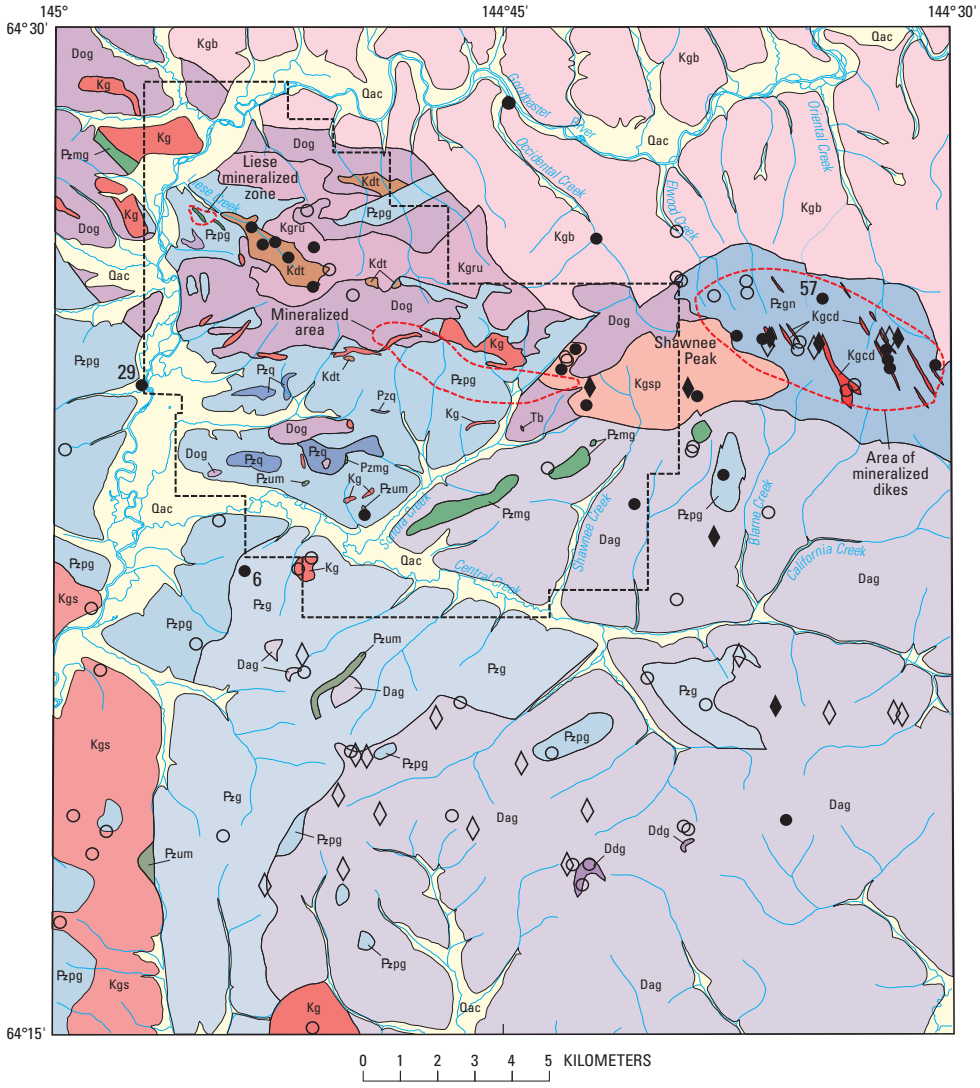

Figure H1. Site locations, simplified regional geology, and arsenic concentrations in bedrock and quartz veins, Pogo deposit region, eastern Alaska.

signatures imparted to the aqueous, soil, and biogeochemical environments from geologic (mineralized and nonmineralized) substrates, and (2) to provide a predevelopment snapshot of the geochemical signatures in selected drainages.

The Yukon-Tanana Upland has a continental climate with cold winters and warm summers and low to moderate annual precipitation (Gough and others, 2005). The area is characterized by heavily vegetated mountain drainages with alpine tundra and rounded barren peaks at higher elevation. The small river drainages are densely vegetated with alder and willow, whereas the larger rivers, such as the Goodpaster River and Central Creek, have broad meandering channels with forested banks and numerous sandbars. Boreal forest vegetation of the region is composed of closed spruce-hardwood subarctic forest containing white and black spruce, paper birch, aspen, and balsam poplar. Alpine tundra of the region is composed of low shrubs (willow, birch, spirea, and high bush cranberry) and a ground cover of forbs, mosses, and lichens.

The area soils are classified primarily as Cryepts (Inceptisols) and Orthels (Gelisols) (Gough and others, 2005). Discontinuous permafrost is found throughout the region and was typically observed at 15 to 50 centimeters (cm) below the surface at the soil sample sites (Gough and others, 2005). Soils in the study area typically had distinguishable A, B, and C horizons. The A and B horizons were usually less than 10 cm thick. The A horizon was typically dark brown with abundant root penetration, while the B horizon was lighter and more reddish than the A horizon and had moderate root volume. The C horizon was about 20 cm below the surface and consists of fine to coarse sand with blocks of angular bedrock and few roots (Gough and others, 2005).

The regional geology is described in detail in Day and others (2003) and condensed here as figure H1. Paleozoic gneisses are the predominant lithologies, although the Goodpaster batholith occupies much of the north to northeastern region of the Big Delta B–2 quadrangle study area. Gold mineralization, such as that found on the Pogo deposit, is associated with various phases of the Cretaceous plutonic rocks, which intrude the gneissic units (Smith and others, 1999; Day and others, 2003). Mineralization is also associated with dikes found in the eastern edge of the study area (Day and others, 2003).

Methods

Site selection, sampling, and analytical methods, as well as the complete analytical data for these samples, are given in detail in Gough and others (2005) and Wang and others (2006). Water and soil sites were selected on the basis of the regional geology and represent both mineralized and nonmineralized areas. Sites selected included (1) those that characterize the regional influence of the various lithologic units on the soil and water geochemistry and (2) downstream sequences designed to characterize the localized influence of mineralized areas, changes in lithology, or cross-cutting structural features.

Results and Discussion

The elements Sb, As, Ba, Be, Cd, Cr, Cu, Pb, Hg, Ni, Se, Ag, Tl, and Zn are all those for which either Water Quality Criteria for Priority Toxic Pollutants and (or) Primary Drinking Water Standards are available (State of Alaska, 2003). Of these fourteen elements, Be, Cr, Se, Ag, and Tl were not detected in any of our samples, and Hg concentrations were not determined (Wang and others, 2006). The concentration ranges for Sb, As, Ba, Cd, Cu, Pb, Ni, and Zn and their relevant standards are given in table H1. Samples collected from one site exceeded the drinking water standard for As. The spatial distribution of As concentrations in water samples is shown in figure H2. Those samples with detectable As concentrations were typically found near mineralized areas. A similar pattern was found for Sb and, in general, detectable concentration of As and Sb were found only in samples adjacent to, or downstream from, mineralized areas (Wang and others, 2005).

Bed sediments near mineralized areas also showed elevated As concentrations relative to nonmineralized areas. In bed sediments, Au and As correlated well, and the highest values of both were located along Liese and Occidental Creeks (fig. H3), Ni, Cr, Fe, Mn, and Co concentrations in bed sediment were also correlated. The greatest concentrations of these elements were located along Sonora Creek and may reflect the presence of ultramafic rock units in the area (Wang and others, 2005).

Aqueous Major-Ion Chemistry

On a plot of total dissolved solids versus the ratio of Na to Na plus Ca (Na/(Na+Ca)) in stream waters, the data points lie in the general region of rock-dominated systems as defined by Gibbs (1970) (fig. H4*A*), indicating that the composition of these samples is more rock dominated, as opposed to evaporation or precipitation dominated. The stream waters are classified primarily as Ca and Mg bicarbonate (Ca^{2+} and Mg^{2+} - HCO_3^-) to Ca and Mg sulfate (Ca^{2+} and Mg^{2+}- SO_4^{2-}) (fig. H4*B*). Waters draining the gneissic and intrusive lithologies of the study area can be differentiated on the basis of their major-ion chemistry (Wang and others, 2005). Stream waters draining gneissic units are more SO_4^{2-} dominated than those draining granitic units (fig. H5). Wang and others (2005) also found that the anionic composition of water in creeks draining the mineralized area was more SO_4^{2-} dominated. However, they concluded that the underlying paragneiss unit in this region could be contributing substantially to the SO_4^{2-} concentrations in these watersheds, and the increase in the SO_4^{2-} concentration

Table H1. Aqueous concentration ranges for selected regulated metals and corresponding State of Alaska Water Quality Criteria and Primary Drinking Water Standards.

[Abbreviations are as follows: mg/L, milligrams per liter; µg/L, micrograms per liter; mg/kg, milligrams per kilogram; –, not listed]

Element	Concentration range (µg/L)	Aquatic life criteria for fresh waters		Drinking water primary maximum contaminant level[1] (µg/L)
		Acute (µg/L)	Chronic (µg/L)	
Sb	<0.1– 0.7	–	–	6
As	<1– 14	340	150	10
Ba	5.4 – 31.8	–	–	2,000
Cd	<0.02–0.04	2.13*	0.27*	5
Cu	<0.5– 2	14*	9.33*	1,300*
Pb	< 0.09– 0.84	81.65*	3.18*	–
Ni	<0.45–3.3	469.16*	52.16*	–
Zn	<0.7–4.7	119.82	119.82	–

[1] Source: State of Alaska, Department of Environmental Conservation (2003).

*These aquatic life criteria (acute and chronic) are a function of the hardness of the water. Value given corresponds to a hardness of 100 mg/L calcium carbonate.

**Human health criteria for noncarcinogens, for consumption of water plus aquatic organisms.

may reflect a complex batholith/paragneiss boundary rather than sulfide oxidation.

Arsenic and Antimony in Soil and Selected Vegetation

The primary arsenic- and antimony-containing minerals in the mineralized areas are pyrite, loellingite, arsenopyrite, and other sulfide minerals (Smith and others, 1999). In soils, arsenic and antimony may be present in either residual primary mineral phases or in secondary weathering products formed during soil formation. The arsenic in the A, B, and C soil horizons ranged from 3 to 410 milligrams per kilogram (mg/kg), 6.1 to 440 mg/kg, and 2 to 300 mg/kg, respectively, whereas antimony concentrations in these horizons ranged from 0.4 to 24 mg/kg, 0.6 to 25 mg/kg, and 0.2 to 16 mg/kg, respectively. The concentrations of arsenic and antimony among the soil horizons were highly correlated, and the concentrations of both typically increased in the order A < B < C horizon. Consequently, higher concentrations of arsenic and antimony in the A horizon were generally found in those soils with high concentrations in the B and C horizons (fig. H6). The greatest concentrations of both elements were generally found near mineralized areas (Wang and others, 2007). The arsenic and antimony concentrations in stream waters collected near the soil sites correlate well with the total arsenic and antimony concentrations in the soils from all horizons (Wang and others, 2007); however, significantly less of the total arsenic and antimony in the C horizon was extractable in water leaching experiments compared to that extracted from the A and B horizon samples. The greater extractability of the arsenic and antimony in the A and B horizons indicates that a greater proportion in these horizons is present in more easily available forms. The lower extractability of the arsenic and antimony in the C horizon could arise if a greater proportion of the element is present in resistant primary mineral phases rather than on exchange surfaces (Wang and others, 2007).

The arsenic and antimony data for the willow samples are highly censored, with nearly half of the samples falling below the detection limit. Arsenic concentrations in willow ranged from less than 0.01 to 0.14 mg/kg (dry weight) for leaves and less than 0.01 to 0.16 mg/kg for twigs. The concentration range of arsenic in willows is consistent with arsenic concentrations of plants grown in uncontaminated soil (Kabata-Pendias and Pendias, 2001) and may indicate minimal plant uptake even in the mineralized regions. Antimony concentrations in both the willow leaves and twigs ranged from less than 0.003 to 0.23 mg/kg and less than 0.002 to 0.05 mg/kg, respectively. Arsenic and antimony concentrations in the leaves and twigs were correlated, but significantly more antimony is found in the leaves than in the twigs (Wang and others, 2007). Arsenic concentrations, however, did not differ between the twigs and leaves. Plant arsenic and antimony concentrations did not correlate with the A, B, and C soil horizon concentrations or the soil extractable concentrations. Lack of correlation between the plant concentrations and either the total or water-extractable soil concentrations also suggests the limited bioavailability of these elements within the system; however, the small number of data pairs coupled with the large amount of censored data made evaluation difficult.

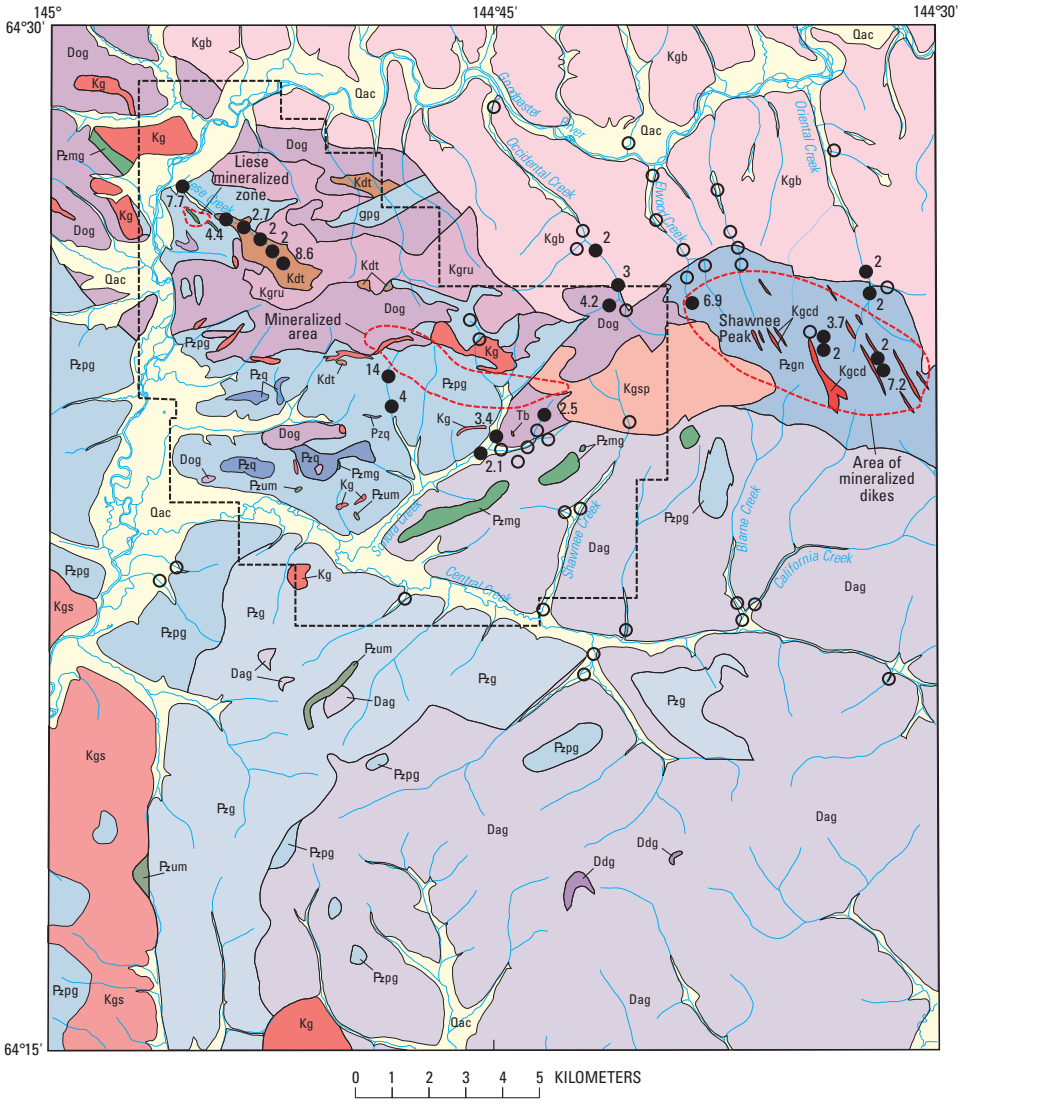

Figure H2. Concentration and distribution of arsenic in stream water plotted on a simplified regional geology map, Pogo deposit region, eastern Alaska.

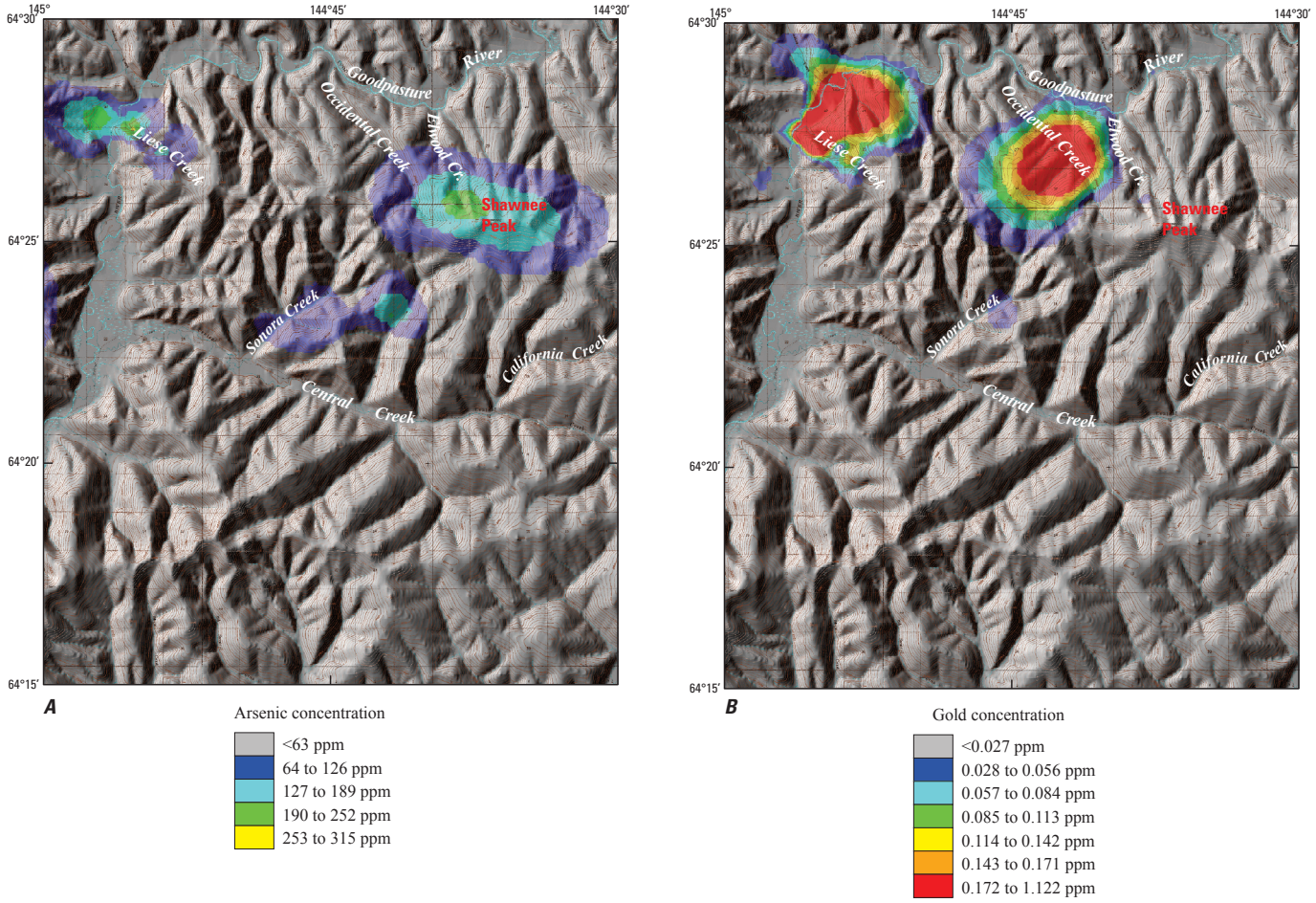

Figure H3. Shaded-relief maps showing the concentration and distribution of arsenic and gold in bed sediments, Pogo deposit region, eastern Alaska. *A*, Arsenic; *B*, Gold. ppm, parts per million.

Summary

In general, aqueous metal concentrations were below the Aquatic Life Criteria and Drinking Water Standards (State of Alaska, 2003); however, arsenic exceeded drinking water standards in one sample from a stream that drained a mineralized area. Both aqueous arsenic and antimony concentrations were greatest near mineralized areas, consistent with the oxidation of minerals, such as arsenopyrite, found in the region. The arsenic and antimony concentrations in stream waters correlated well with the total arsenic and antimony concentrations in the soils, but uptake by the vegetation examined appears minimal. Although the anionic composition of creeks draining the mineralized areas is also consistent with pyrite oxidation, the potential exists that the underlying paragneiss unit in this region is contributing substantially to the sulfate concentrations. Consequently, the presence of arsenic and (or) antimony in the water is the strongest indicator of a mineralizing influence in these waters. Bed sediments near mineralized areas also showed elevated arsenic concentrations relative to nonmineralized areas. Bed sediment arsenic concentrations were also highly correlated with gold concentrations, whereas nickel, chromium, iron, magnesium, and cobalt appear to reflect the presence of ultramafic rocks within the watershed.

References Cited

Day, W.C., Aleinikoff, J.N., Roberts, Paul, Smith, Moira, Gamble, B.M., Henning, M.W., Gough, L.P., and Morath, L.C., 2003, Geologic map of the Big Delta B–2 quadrangle, east-central Alaska: U.S. Geological Survey Geologic Investigations Series I–2788, 1 sheet, scale 1:63,360. (Also available online at *http://pubs.usgs.gov/imap/i-2788/*.)

Gibbs, R.J., 1970, Mechanisms controlling world water chemistry: Science, v. 170, no. 3962, p. 1088–1090.

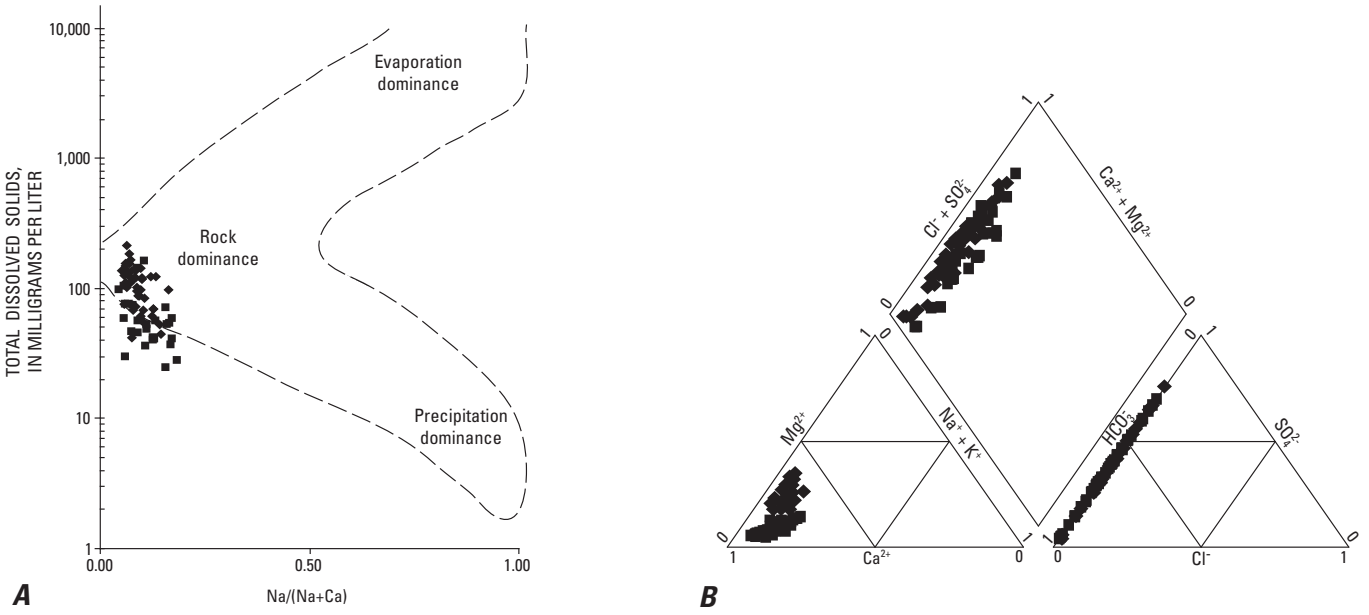

Figure H4. Graph and diagram showing the major-ion characteristics of the water. *A*, Graph showing total dissolved solids versus Na/(Na+Ca) ratio. "Boomerang" envelope approximated from Gibbs (1970). *B*, Trilinear diagram showing the range of major-ion composition. Diamonds and squares are samples collected in 1999 and 2001, respectively.

Gough, L.P., Day, W.C., Crock J.G., Gamble, B.M., Henning, M.W., Ager, C.M., Meirer, A.L., Briggs, P.H., Brown, Z.A., and Adams, Monique, 2005, Regional geochemistry results from the analyses of rock, soil, and vegetation samples—Big Delta B–2 quadrangle, Alaska: U.S. Geological Survey Open-File Report 2005–1431, 16 p., available only online at *http://pubs.usgs.gov/of/2005/1431/*. (Accessed August 13, 2007.)

Kabata-Pendias A., and Pendias H., 2001, Trace elements in soils and plants: Boca Raton, Florida, CRC Press, 413 p.

Smith, Moira, Thompson, J.F.H., Bressler, Jason, Layer, Paul, Mortensen J.K., Abe, Ichiro, and Takaoka, Hidetoshi, 1999, Geology of the Liese zone, Pogo property, east-central Alaska: Society of Economic Geologists Newsletter, v. 38, p. 1, 12–21.

State of Alaska, Department of Environmental Conservation, 2003, Alaska water quality criteria manual for toxic and other deleterious organic and inorganic substances as amended through 15 May, 2003: Juneau, Alaska, State of Alaska Department of Environmental Conservation, 51 p. (Also available online at *http://dec.state.ak.us/water/wqsar/wqs/pdfs/70wqsmanual.pdf*.)

Wang, Bronwen, Gough, Larry, Wanty, Richard, Vohden, Jim, Crock, Jim, and Day, Warren, 2006, Water and sediment chemical data and data summary for samples collected in 1999 and 2001 in the Goodpaster River basin, Big Delta B–2 quadrangle, Alaska: U.S. Geological Survey Open-File Report 2006–1131, 18 p. (Also available online at *http://pubs.usgs.gov/of/2006/1131/*.)

Wang, B., Gough, L., Wanty R., Crock, J., Day, W., and Vohden, J., 2007, Landscape geochemistry near mineralized areas of eastern Alaska with a focus on As and Sb, *in* Bullen, T.D., and Wang, Y., eds., Proceedings of the 12th International Symposium on Water-Rock Interaction: London, Taylor and Francis Group, p. 1513–1516.

Wang, Bronwen, Wanty, R.B., and Vohden, Jim, 2005, Geochemistry of surface-waters in mineralized and non-mineralized areas of the Yukon-Tanana Upland, *in* Walton, Raymond, ed., Impacts of global climate change, Proceedings of the 2005 World Water and Environmental Resources Congress, Anchorage, Alaska, May 15–19, 2005: Reston Va., American Society of Civil Engineers, p. 173–245.

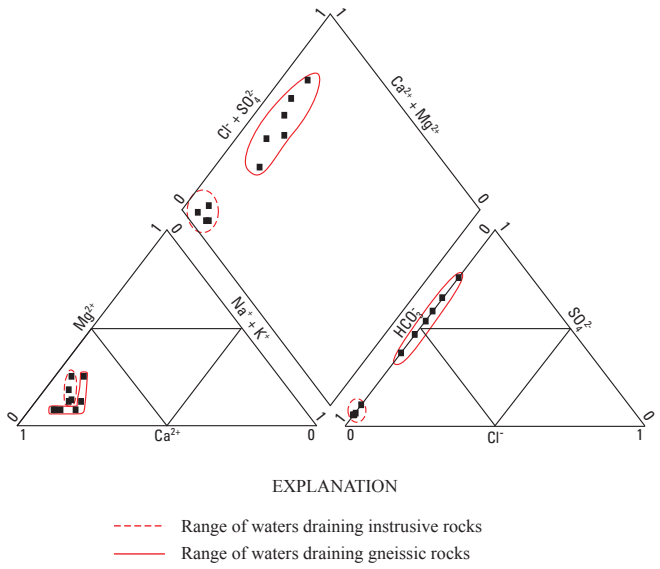

Figure H5. Trilinear diagram showing the compositional range of the major ions for waters draining the intrusive and gneissic rocks, Pogo deposit region, eastern Alaska.

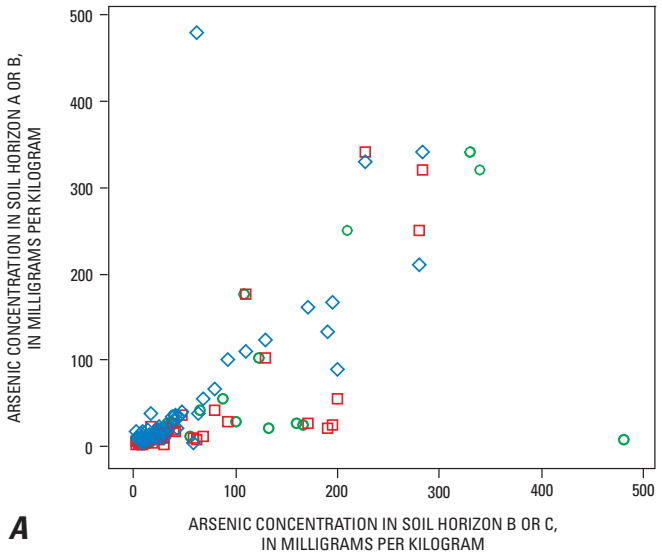

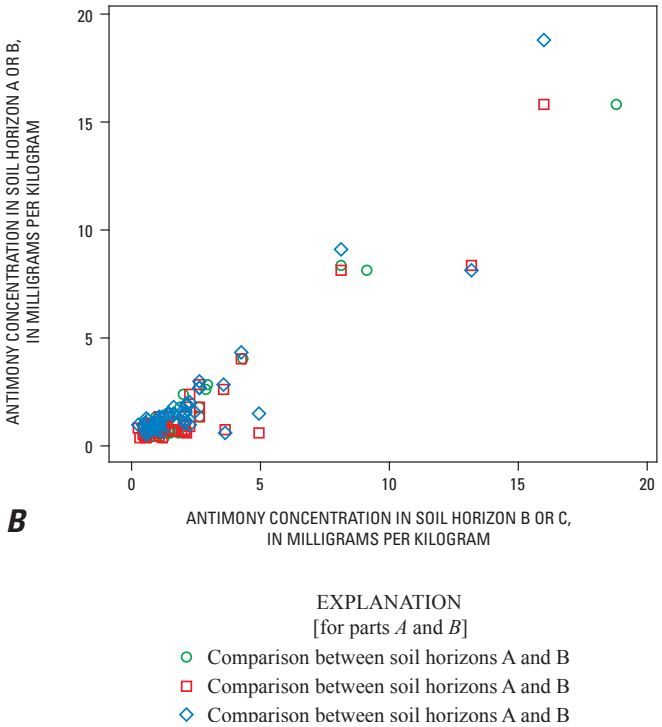

Figure H6. Graphs showing arsenic and antimony concentrations of soil horizons, Pogo deposit region, eastern Alaska. *A*, Arsenic, *B*, Antimony.

Environmental Geochemical Study of Red Mountain—An Undisturbed Volcanogenic Massive Sulfide Deposit in the Bonnifield District, Alaska Range, East-Central Alaska

By Robert G. Eppinger, Paul H. Briggs, Cynthia Dusel-Bacon, Stuart A. Giles, Larry P. Gough, Jane M. Hammarstrom, and Bernard E. Hubbard

Chapter I of
Recent U.S. Geological Survey Studies in the Tintina Gold Province, Alaska, United States, and Yukon, Canada—Results of a 5-Year Project
Edited by Larry P. Gough and Warren C. Day

Scientific Investigations Report 2007–5289–I

U.S. Department of the Interior
U.S. Geological Survey

Contents

Figures

Tables

Environmental Geochemical Study of Red Mountain—An Undisturbed Volcanogenic Massive Sulfide Deposit in the Bonnifield District, Alaska Range, East-Central Alaska

By Robert G. Eppinger,[1] Paul H. Briggs,[1] Cynthia Dusel-Bacon,[1] Stuart A. Giles,[1] Larry P. Gough,[1] Jane M. Hammarstrom,[1] and Bernard E. Hubbard[1]

Abstract

The Red Mountain volcanogenic massive sulfide (VMS) deposit exhibits well-constrained examples of acid-generating, metal-leaching, metal-precipitation, and self-mitigation (via co-precipitation, dilution, and neutralization) processes that occur in an undisturbed natural setting, a rare occurrence in North America. The unmined pyrite-rich deposit displays a remarkable environmental footprint of natural acid generation, high metal concentrations, and exceedingly high rare-earth-element (REE) concentrations in surface waters. Dissolution of pyrite and associated secondary reactions under near-surface, oxidizing conditions are the primary causes for the acid generation and metal leaching. The deposit is hosted in Devonian to Mississippian felsic metavolcanic rocks of the Mystic Creek Member of the Totatlanika Schist.

Water samples with the lowest pH values, highest specific conductances, and highest major- and trace-element concentrations are from springs and streams within the quartz-sericite-pyrite alteration zone. Aluminum, As, Cd, Co, Cu, Fe, Mn, Ni, Pb, Y, and particularly Zn and the REEs are all found in high concentrations, ranging across four orders of magnitude. Waters collected upstream from the alteration zone have near-neutral pH values, lower specific conductances, lower metal concentrations, and measurable alkalinities. Water samples collected downstream of the alteration zone have pH values and metal concentrations intermediate between these two extremes. Stream sediments are anomalous in Zn, Pb, S, Fe, Cu, As, Co, Sb, and Cd relative to local and regional background abundances. Red Mountain Creek and its tributaries do not support, and probably never have supported, significant megascopic faunal aquatic life.

Introduction

Environmental geochemical studies of a group of unmined volcanogenic massive sulfide (VMS) deposits in the Bonnifield mining district include a detailed study of the Red Mountain deposit, in the northern flank of the Alaska Range (see fig. 1 of Editors' Preface and Overview). The Red Mountain deposit (also known as the Dry Creek deposit) displays a significant environmental footprint of natural acid generation, high metal concentrations, and remarkably high REE concentrations in surface waters. The deposit and its associated alteration halo are well exposed, allowing for sample collection above, within, and downstream of the mineralized rocks and surrounding alteration zone. Details on the physiography and biota at Red Mountain are presented by Gough and others (this volume, chap. J).

This study is important because it establishes a premining geochemical baseline of an exposed, unmined VMS deposit, a rare occurrence in North America. Data and interpretations from this study may be useful as natural analog data to previously developed VMS deposits in similar climatic settings where premining data do not exist.

Geology, Alteration, and Mineral Deposit Setting

The 26 known VMS prospects in the district occur within a greenschist-facies assemblage of metavolcanic and metasedimentary rocks of the Yukon-Tanana terrane. The volcanic rocks are Late Devonian to Early Mississippian (376–353 million years old, Ma) in age, compositionally bimodal, and were emplaced in an extensional setting, inferred to be the attenuating continental margin of ancestral North America (Dusel-Bacon and others, 2004, 2005; Dusel-Bacon and others, this volume, chap. B).

At Red Mountain, a 4-square-kilometer (km^2) quartz-sericite-pyrite alteration zone (QSPAZ) is characterized

[1]U.S. Geological Survey.

by prominent shades of red, maroon, orange, and yellow in outcrop and colluvium and by a general lack of vegetation. Although actively explored through 1998, the Red Mountain deposit has never been mined. Mineralized rocks lie within the Mystic Creek Member of the Totatlanika Schist (fig. I1; Newberry and others, 1997; Smit, 1999).

Red Mountain is a pyrite-rich VMS deposit containing sphalerite, galena, chalcopyrite, and locally precious metals, as massive to semimassive sulfides. The deposit is tilted to the north, and subsequent erosion has exposed underlying quartz stockwork veins in pyrite-bearing altered footwall rocks and massive sulfide horizons in hanging wall rocks. Supergene oxidation of pyrite and ground-water flow are facilitated by the intensely fractured nature of the footwall and hanging wall rocks.

Methods

Bedload stream sediment, stream and spring water, or rock samples were collected at 36 sites in the vicinity of Red Mountain (fig. I1), under low-flow conditions during precipitation-free periods. Details on sample collection, analysis, quality assurance/quality control procedures used, and a listing of the analytical data are found in Giles and others (2007). Advanced Spaceborne Thermal Emission and Reflection Radiometer (ASTER) satellite data were used to identify the extent of altered bedrock at Red Mountain by indicating the distribution of ferric iron, illite-muscovite, kaolinite, smectite, and hydrous silica-jarosite (Eppinger and others, 2007; Hubbard and others, this volume, chap. E). Secondary efflorescent salts and mineral precipitates that form in streambeds were characterized by X-ray diffraction (XRD) and scanning electron microscopy (SEM).

At water sample sites, onsite measurements included pH, specific conductance, alkalinity, acidity, dissolved oxygen, water temperature, ferrous iron, turbidity, and a qualitative estimate of discharge. A representative water sample was collected at each site, filtered (0.45 micrometer, µm), and acidified with ultrapure nitric acid. Unacidified water samples were refrigerated prior to analysis. Samples were analyzed by inductively coupled plasma–atomic emission spectroscopy (ICP-AES), ICP-mass spectrometry (ICP-MS), and ion chromatography.

Bedload stream sediment samples were collected at 20 sites. Sieved samples were analyzed by ICP-AES, ICP-MS, and several element-specific methods. For the water and sediment samples, site duplicates, analytical duplicates, blanks, and reference standards comprised approximately 15 percent of the samples analyzed.

Results and Discussion

The information described herein is summarized from Eppinger and others (2004, 2007).

Waters

Surface and spring water samples were collected from within (19 samples), upstream of (8 samples), and downstream of the QSPAZ (6 samples). With respect to major ions, the waters are largely dominated by sulfate and intermediate with respect to calcium and magnesium. High concentrations of aluminum, iron, and sulfate are found in water samples within and downstream of the QSPAZ.

Water pH values range from 2.4 to 7.8. Waters upstream of the QSPAZ are all near-neutral, while those within the QSPAZ generally have pH values below 3.5. Specific conductances upstream of the QSPAZ are lowest, ranging from 370 to 830 microsiemens per centimeter (µS/cm), rise significantly in waters within the QSPAZ (commonly above 2,500 µS/cm; maximum = 4,800 µS/cm), and fall to 580 µS/cm upon mixing with surrounding streams. Below the QSPAZ, pH values remain low to the mouth of Red Mountain Creek (pH 4.2), about 2.5 kilometers (km) downstream, but pH quickly rises to 7.1 after mixing with the alkaline, glacial-silt-laden stream water of Dry Creek.

Trace elements in water that exhibit the widest variation, spanning four or more orders of magnitude, include Al, As, Cd, Co, Cu, Fe, Mn, Ni, Pb, Zn, La, Ce, Pr, Nd, Sn, and Y. Extremely high concentrations are found for Zn (median 13,000 micrograms per liter (µg/L), maximum=240,000 µg/L), Mn (median=4,200 µg/L, maximum=49,000 µg/L), and the summed REEs (median=3,200 µg/L, maximum=59,000 µg/L). In all cases, the highest trace-metal concentrations are found in springs and streams having low pH and high specific conductance, all within or downstream of the QSPAZ. Elements exhibit low concentrations above the QSPAZ, very high concentrations within and downstream of the QSPAZ, and rapid attenuation via co-precipitation, sorption, and dilution upon mixing with water from Dry Creek.

Sediments

Elemental abundances in stream sediments vary across one to two orders of magnitude. Zinc, Pb, S, and Fe are found in relatively high concentrations (Zn median=440 parts per million (ppm), maximum=2,300 ppm; Pb median=71 ppm, maximum=410 ppm; S median=0.39 percent, maximum=1.2 percent; Fe median=4.8 percent, maximum=30 percent), with median concentrations that are about an order of magnitude above those expected for average granitic or local Mystic Creek Member background rocks. Other elements found in high concentrations relative to these background rocks include As, Cd, Cu, Co, Mn, Mo, Sb,

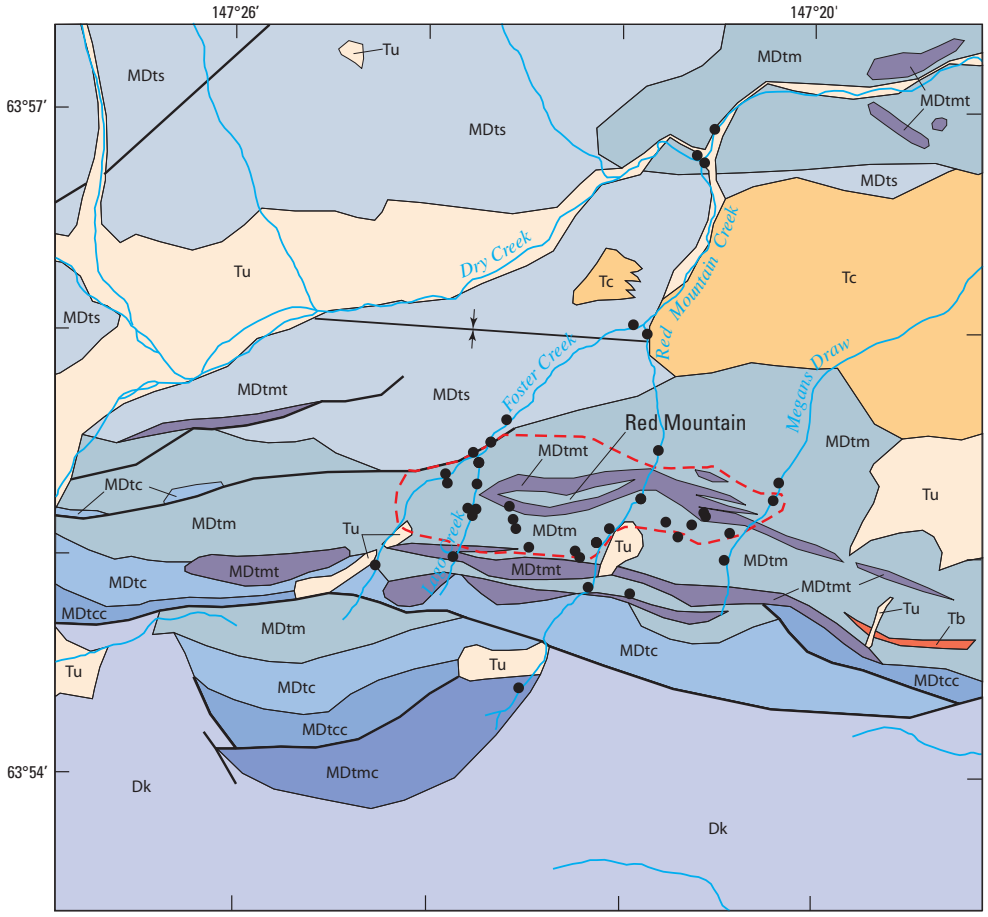

EXPLANATION

- Tu — Sedimentary rocks, undifferentiated (Tertiary)
- Tb — Basalt dike (Tertiary)
- Tc — Coal-bearing rocks, undifferentiated (Tertiary)

Totatlanika Schist (Lower Mississippian to Upper Devonian)

- MDts — Sheep Creek Member—Metasedimentary and metavolcanic rocks
- MDtm — Mystic Creek Member—Metavolcanic rocks and graphitic phyllites
- MDtmt — Rhyolite dike(?) and (or) welded tuff
- MDtc — Chute Creek Member—Mafic metavolcanic rocks
- MDtcc — California Creek Member—Felsic metaporphyry and augen gneiss
- MDtmc — Moose Creek Member—Felsic to mafic metavolcanic rocks and schist
- Dk — Keevy Peak Formation (Devonian)—Phyllite and quartzite
- Contact
- Fault
- Syncline
- Approximate extent of visible alteration
- Sample location

Figure I1. Generalized geologic map and sites for samples collected at the Red Mountain deposit, east-central Alaska. Regional geology from Gilbert (1977). Topographic map of this general area is provided elsewhere in this report (Gough and others, this volume, chap. J). The feature names, Foster Creek, Lago Creek, and Megans Draw are all local names.

Table I1. Sulfide, hydroxysulfate, and unusual minerals identified in samples from Red Mountain detected by X-ray diffraction and scanning electron microscopy.

Mineral	Formula
Sulfides	
Chalcopyrite	$CuFeS_2$
Galena	PbS
Pyrite	FeS_2
Sphalerite	ZnS
Hydroxysulfates	
Alunogen	$A1_2(SO_4)_3 \cdot 17H_2O$
Goslarite	$ZnSO_4 \cdot 7H_2O$
Gypsum	$CaSO_4 \cdot 2H_2O$
Halotrichite	$Fe^{2+}Al_2(SO_4)_4 \cdot 22H_2O$
Hexahydrite	$MgSO_4 \cdot 6H_2O$
Hydronium jarosite	$(H_3O)Fe_3(SO_4)_2(OH)_6$
Jarosite	$KFe_3(SO_4)_2(OH)_6$
Kalinite	$KAl(SO_4)_2 \cdot 11H_2O$
Melanterite	$FeSO_4 \cdot 7H_2O$
Natrojarosite	$NaFe_3(SO_4)_2(OH)_6$
Pentahydrite	$MgSO_4 \cdot 5H_2O$
Pickeringite	$MgAl_2(SO_4)_4 \cdot 22H_2O$
Schwertmannite	$(Fe^{3+})_{16}O_{16}OH_{12}(SO_4)_2$
Slavikite	$NaMg_2(Fe^{3+})_5(SO_4)_7(OH)_6 \cdot 33H_2O$
Oxyhydroxides	
Ferrihydrite	$5Fe_2O_3 \cdot 9H_2O$ or $Fe_2O_3 \cdot 2FeOOH \cdot 2.6H_2O$
Goethite	α-$Fe^{3+}O(OH)$
Carbonates/Halides/Oxifluorides	
Bastnäsite(?)[1]	$(Ce,La)(CO_3)F$
Häleniusite(?)[1]	(La,Ce)OF

[1]Identification uncertain.

Se, Tl, and V. This suite generally agrees with the anomalous metals found in mineralized rock samples. Cerium and La concentrations in stream sediments have moderately elevated medians that are near those for local background rocks, likely a reflection of the intrinsically high REE concentrations found throughout peralkaline metarhyolites of the Mystic Creek Member (Dusel-Bacon and others, 2004).

Precipitates

Efflorescent salt precipitates are common in protected bedrock areas within the QSPAZ and downstream along the edges of the creeks (fig. I2*A*, *B*). Mineral precipitates identified by XRD and SEM include a variety of Fe-, Al-, Mg-, K-, and Na-hydroxysulfate and oxyhydroxide minerals (table I1). These minerals are all compositional endmembers of pseudo-stable secondary minerals and are products of oxidative pyrite dissolution and coincident acid rock drainage. The presence of these various efflorescent salts indicates mobility of the above elements in the weathering environment. Ferricrete (Fe-oxyhydroxide-cemented alluvium) up to several meters thick actively cements alluvium in creek beds within lower pH portions of the QSPAZ (fig. I2*C*). As stream pH rises downstream from the low-pH zones, milky white to tan, amorphous aluminum floc forms centimeter-thick gels in calm stretches to the mouth of Red Mountain Creek (fig. I2*D*).

REE in Water

The summed (∑) REE concentrations in water samples upstream of the QSPAZ range from 0.5 to 10 times the average background concentration in river waters worldwide listed in Martin and Whitfield (1983). Extreme concentrations of ∑ REEs are found in waters within and downstream of the QSPAZ, where all but four of the water samples have ∑ REE concentrations that are greater than 10,000 times background. Several spring samples within the QSPAZ have ∑ REE concentrations of greater than 100,000 times background.

Profiles for REEs in waters from the QSPAZ, normalized to the North American shale composite (NASC), indicate moderately light REE enrichment but are overall exceedingly high at 0.01 to 0.5 times NASC. Normally, REE profiles for natural waters are around 10^{-6} times NASC, and mine drainage profiles rarely exceed 10^{-3} times NASC. Preliminary SEM investigation of the source of the REEs in the felsic metavolcanic rocks reveals a micron-scale Ce-La-F-O accessory mineral that is tentatively identified as the carbonate mineral bastnäsite (table I1; fig. I2*E*). Accessory bastnäsite likely is being preferentially dissolved by acidic ground water, resulting in light REE enrichment in the spring and stream waters in the QSPAZ. The premise that accessory minerals in host rocks rather than mineralized horizons are the source of the REEs is supported by two facts: (1) the waters containing high REE concentrations are widespread throughout the alteration zone, not confined to mineralized horizons, and (2) sulfide-rich rock samples from the mineralized horizons do not contain Ce and La in concentrations above those of local background rocks.

A plot of pH versus cerium illustrates the high light-REE concentrations in Red Mountain waters in a global context (fig. I3). Presented for comparison are data from 300 waters representing mine drainage, natural mineralized areas, and active volcanic systems, all from various mineral deposit types including VMS, sedimentary exhalative (SEDEX), copper-molybdenum porphyry, polymetallic vein, replacement, and skarn deposits, and from the hyperacidic (pH <1) Copahue Volcano in Argentina. Cerium concentrations from waters within and downstream of the QSPAZ at Red Mountain are at the upper end of the

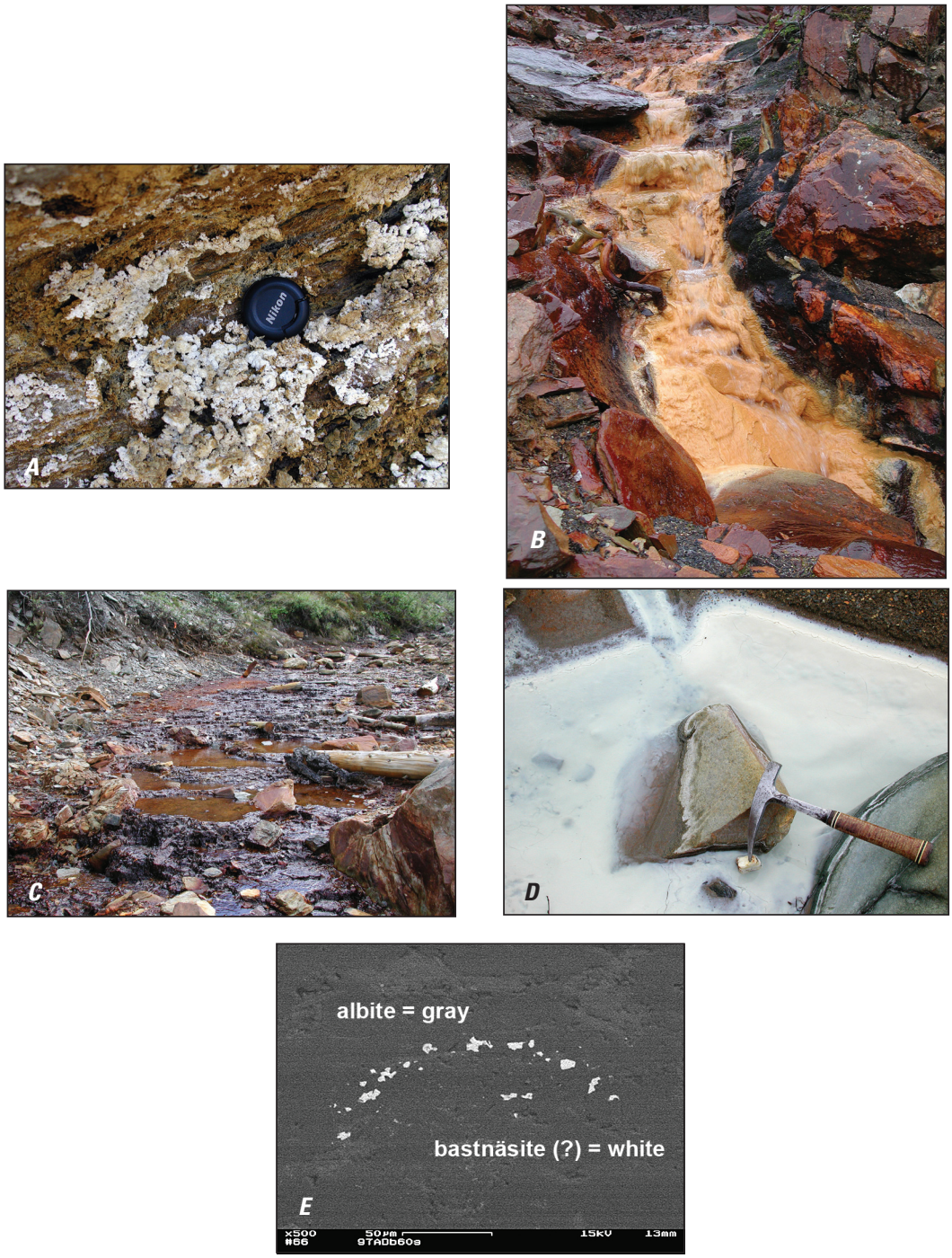

Figure I2. Photographs showing precipitates in outcrop and alluvium at Red Mountain. *A*, Salts under protected outcrop overhang adjacent to Red Mountain Creek. Minerals identified by X-ray diffraction include the water-soluble, acid-generating hydroxysulfates halotrichite (Fe, Al), pickeringite (Mg, Al), kalinite (K, Al), hexahydrite (Mg), melanterite (Fe), and alunogen (Al). *B*, Bright orange-tan precipitate is dominantly the metastable Fe-hydroxysulfate schwertmannite. This metalliferous spring along Lago Creek (local name) has a pH of 2.4 and specific conductance of 3,000 microsiemens per centimeter (µS/cm). The black organism growing just above the waterline is the unusual liverwort *Gymnocolea inflata*, which thrives in the low-pH waters (Gough and others, this volume, chap. J). *C*, Ferricrete-cemented alluvium in Foster Creek (local name) where spring merges with stream. Spring pH is 3.4 and specific conductance is 2,900 µS/cm. *D*, Amorphous aluminum floc settled in calm part of Red Mountain Creek below alteration zone. Stream pH is 4.6 and specific conductance is 1,200 µS/cm. Floc thickness locally reaches several centimeters. *E*, Scanning-electron microscopy photomicrograph of Ce-La-F-O accessory mineral (bastnäsite?) in polished thin section of Mystic Creek Member metarhyolite from the Red Mountain area.

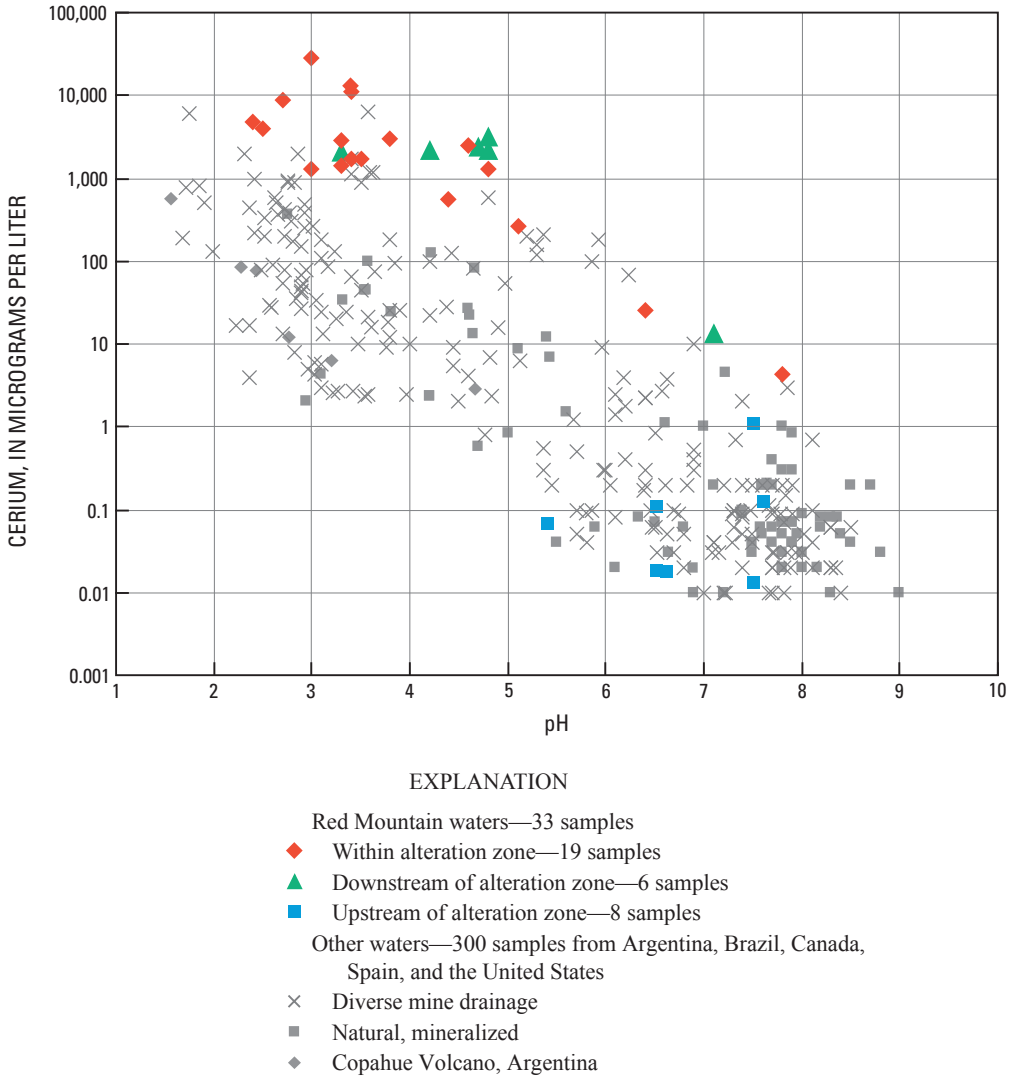

Figure I3. Cerium (in micrograms per liter) in Red Mountain filtered and acidified water compared to cerium from mine drainage and mineralized water from diverse deposit types from Argentina, Brazil, Canada, Spain, and the United States. For data references, see Eppinger and others (2007).

cluster of samples at all pH levels and are among the highest concentrations found in the literature. Clearly the REE concentrations at Red Mountain are unique and exceedingly high. More work is needed to identify additional REE-bearing mineral phases at Red Mountain.

Comparison With Mine Drainage Waters

Spring and stream waters from Red Mountain are similar in composition to mine drainage waters found elsewhere in the United States, as illustrated in the Ficklin diagram (Plumlee and others, 1999) of pH versus the sum of the metals Cd+Co+Cu+Ni+Pb+Zn (fig. I4). The 125 mine drainage waters in the figure are from the above-listed mineral deposit types. Samples collected upstream of the QSPAZ plot in the near-neutral and low-metal-concentration field, whereas samples collected within and downstream of the QSPAZ plot in the acid to high-acid and high- to extreme-metal concentration fields. Many of the comparison mine drainage samples that plot in the same portion of the diagram are from Kuroko and SEDEX massive sulfide deposits (Plumlee and others, 1999), emphasizing that the composition of the natural spring and stream waters at Red Mountain mimic metalliferous acid mine drainage.

Comparison With Water Quality Standards

Water samples were compared to established potable water maximum contaminant level (MCL) standards listed by the Alaska Department of Environmental Conservation (2003a,b) and U.S. Environmental Protection Agency (2003). The median concentrations in Red Mountain waters exceed the established MCLs for SO_4^{2-}, Al, Fe, Zn, Mn, Cd, Pb, total dissolved solids (TDS), and pH, indicating that most of the natural stream and spring waters are not potable. The water samples were also compared to freshwater quality standards for aquatic life listed by the Alaska Department of Environmental Conservation (2003a,b). Nearly all sampled streams and springs within and downstream of the QSPAZ exceed these standards for Al, Cd, Cu, Pb, and Zn and many exceed the standards for As, Fe, Ni, and Se. Element concentrations in stream sediment samples were compared to

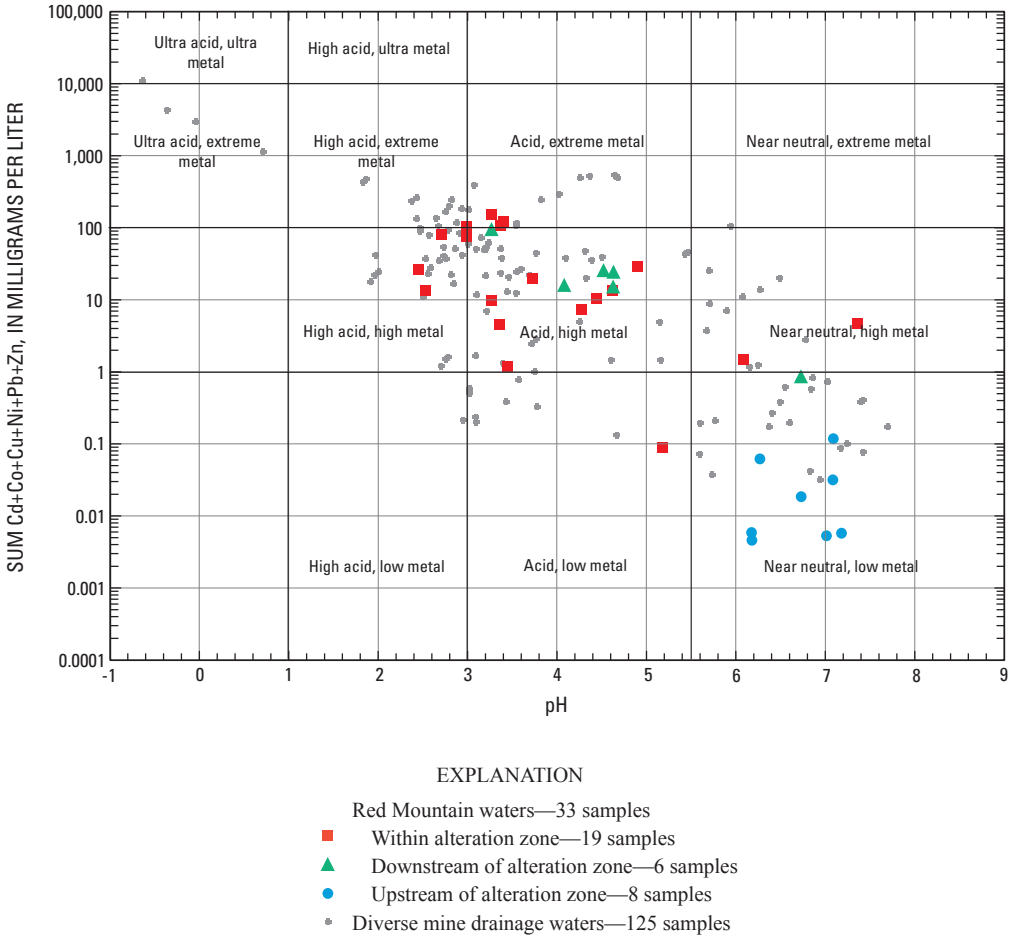

Figure I4. Ficklin diagram of pH versus the dissolved metals Cd+Co+Cu+Ni+Pb+Zn (in milligrams per liter) from filtered and acidified water samples. Comparison mine drainage waters are from diverse mineral deposits in the United States (data from appendix of Plumlee and others, 1999).

guidelines for freshwater ecosystems (MacDonald and others, 2000). The guidelines are exceeded for As, Cd, Cu, Ni, Pb, and Zn in most sediment samples, suggesting that the stream sediment is inhospitable to benthic organisms, using this standard.

Conclusions

The Red Mountain deposit is a well-constrained example of acid-generating, metal-leaching, metal-precipitation, and self-mitigation processes that occur in an undisturbed natural setting. Dissolution of pyrite and associated secondary reactions under near-surface, oxidizing conditions are the primary causes for the acid generation and metal leaching of the rocks at Red Mountain. However, the acidic waters mix with surrounding alkaline waters that have interacted with carbonate veinlets, resulting in self-mitigation (via dilution, neutralization, and attendant co-precipitation). This process limits downstream hydrogeochemical evidence of the deposit to within a few kilometers. Red Mountain Creek and its tributaries within the QSPAZ do not support, and probably never have supported, significant megascopic faunal aquatic life, except perhaps those organisms that have adapted to the extreme environment of low pH and very metalliferous conditions.

Water geochemistry varies widely, largely as a function of the local geologic setting. Samples with the lowest pH values, highest specific conductance, highest TDS concentrations, and highest major- and trace-element concentrations are all from springs and streams within the QSPAZ. Samples collected upstream of the QSPAZ have near-neutral pH values, lower specific conductance, lower metal concentrations, and measurable alkalinities. Water samples collected downstream of the QSPAZ have pH values and metal concentrations intermediate between these two extremes. As demonstrated here, an understanding of the local geologic setting is of first-order importance for environmental geochemical studies.

Some of the metals found enriched in waters within the QSPAZ, such as Fe, Zn, Pb, Cd, and Co, are directly related to dissolution of sulfides and associated secondary minerals. The high concentrations of REEs in these waters are a result of ground-water interaction with Mystic Creek Member felsic metavolcanic rocks that are intrinsically elevated in REEs due to their peralkaline composition. REE enrichment is considerably enhanced by the presence and selective dissolution of accessory REE minerals, such as bastnäsite, by dissociated sulfuric acid-rich ground water. High concentrations of Al,

Mg, F^-, K, Mn, and Si in the waters, and extensive mineral precipitates, ferricrete, and Fe and Al flocs in the lower reaches of the creeks are all indications of extensive supergene bedrock dissolution. The oxidation of pyrite and associated acid generation are enhanced by the dense fault and fracture network, the extensively exposed QSPAZ, and the relative abundance of shallow ground water. Any future exploration and exploitation of the Red Mountain VMS deposit needs to include a thorough recognition and understanding of the deposit's great acid-generating and metal-liberating potential.

At the mouth of Red Mountain Creek, about 2.5 km below the QSPAZ, stream water is acidic (pH is 4.2) and metalliferous. In contrast, Dry Creek, both upstream and just 0.3 km downstream of the confluence with Red Mountain Creek, is near neutral, alkaline, and relatively nonmetalliferous. The neutralization and reduction of metals are attributed to dilution by, and the acid-consuming capability of, Dry Creek, a relatively large, turbid, glacial flour-rich creek that drains rock types with high acid-neutralizing capacities. Red to orange iron-oxide staining on alluvium (with co-precipitated metals) is prominent along Red Mountain Creek within and downstream of the QSPAZ and continues down Dry Creek for about 1.5 km. Beyond this point, weaker hues of red and orange continue for another 0.5 km. The extreme hydrogeochemical and visual indications that characterize the Red Mountain VMS deposit appear to be largely self-mitigating within a few miles downstream of the deposit.

Acknowledgments

Thanks are given to the following U.S. Geological Survey employees: Melanie Hopkins and Cameron Rombach for help with sample collection; Monique Adams, Mike Anthony, Phil Hageman, Pete Theodorakos, and Ruth Wolf for laboratory analyses; Steve Sutley for X-ray diffraction; Phil Zelenak for drafting; and Robert Oscarson for SEM imaging and mineral identification. Ed and Megan Busby provided excellent food and lodging in a wilderness setting at Busby's Camp. Pilot Arnie Johnson of Johnson Flying Service provided helicopter logistical support. Reviews by David Fey and Bill Langer significantly improved the manuscript.

References Cited

Alaska Department of Environmental Conservation, 2003a, Water quality standards: Alaska Department of Environmental Conservation Report 18–AAC–70, 54 p. (Also available online at *http://www.dec.state.ak.us/regulations/pdfs/70mas.pdf*.)

Alaska Department of Environmental Conservation, 2003b, Alaska water quality criteria manual for toxic and other deleterious organic and inorganic substances: Alaska Department of Environmental Conservation, 51 p. (Also available online at *http://www.dec.state.ak.us/water/wqsar/wqs/pdfs/70wqsmanual.pdf*.)

Dusel-Bacon, Cynthia, Premo, W.R., and Aleinikoff, J.N., 2005, Geochemical and Nd isotopic evidence for an extending continental-margin arc/back arc setting for peralkaline rhyolite-hosted massive sulfide deposits of the Bonnifield district, east-central Alaska [abs.]: Geological Society of America, Abstracts with Program, v. 37, no. 7, p. 97.

Dusel-Bacon, Cynthia, Wooden, J.L., and Hopkins, M.J., 2004, U-Pb zircon and geochemical evidence for bimodal mid-Paleozoic magmatism and syngenetic base-metal mineralization in the Yukon-Tanana terrane, Alaska: Geological Society of America Bulletin 116, p. 989–1015.

Eppinger, R.G., Briggs, P.H., and Dusel-Bacon, Cynthia, 2004, Environmental geochemistry of an undisturbed volcanogenic massive sulfide deposit, Red Mountain, Bonnifield mining district, east-central Alaska, *in* Wanty, R.B., and Seal, R.R., II, eds., Water-rock interaction, Proceedings of the Eleventh International Symposium on Water-Rock Interaction, Saratoga Springs, N.Y., June 27–July 2, 2004: London, Taylor and Francis Group Publishers, p. 1483–1487.

Eppinger, R.G., Briggs, P.H., Dusel-Bacon, Cynthia, Giles, S.A., Gough, L.P., Hammarstrom, J.M., and Hubbard, B.E., 2007, Environmental geochemistry at Red Mountain, an unmined volcanogenic massive sulphide deposit in the Bonnifield district, Alaska Range, east-central Alaska: Geochemistry: Exploration, Environment, Analysis, v. 7, no. 3, p. 207–223.

Gilbert, W.G., 1977, General geology of Healy D–1 and southern Fairbanks A–1 quadrangles and vicinity, Alaska: Alaska Division of Geological and Geophysical Surveys Open-File Report 105, 13 p., 2 sheets, scale 1:63,360.

Giles, S.A., Eppinger, R.G., Granitto, Matthew, Zelenak, P.P., Adams, M.G., Anthony, M.W., Briggs, P.H., Gough, L.P., Hageman, P.L., Hammarstrom, J.M., Horton, J.D., Sutley, S.J., Theodorakos, P.M., and Wolf, R.E., 2007, Geochemical data for stream-sediment, surface-water, rock, and vegetation samples from Red Mountain (Dry Creek), an unmined volcanogenic massive sulfide deposit in the Bonnifield district, Alaska Range, east-central Alaska: U.S. Geological Survey Data Series DS–204, 64 p., 1 CD-ROM. (Also available online at *http://pubs.usgs.gov/ds/2006/204/*.)

MacDonald, D.D., Ingersoll, C.G., and Berger, T.A., 2000, Development and evaluation of consensus-based sediment quality guidelines for freshwater ecosystems: Archives of Environmental Contamination and Toxicology, v. 39, no. 1, p. 20–31.

Martin, J.M., and Whitfield, Michael, 1983, The significance of the river input of chemical elements to the ocean, *in* Wong, C.S., Boyle, E.A., Bruland, K.W., Burton, J.D., and Goldberg, E.D., eds., Trace metals in sea water: New York, Plenum Press, p. 265–296.

Newberry, R.J., Crafford, T.C., Newkirk, S.R., Young, L.E., Nelson, S.W., and Duke, N.A., 1997, Volcanogenic massive sulfide deposits of Alaska, *in* Goldfarb, R.J., and Miller, L.D., eds., Mineral deposits of Alaska: Economic Geology Monograph 9, p. 120–150.

Plumlee, G.S., Smith, K.S., Montour, M.R., Ficklin, W.H., and Mosier, E.L., 1999, Geologic controls on the composition of natural waters and mine waters draining diverse mineral-deposit types, *in* Filipek, L.H., and Plumlee, G.S., eds., The environmental geochemistry of mineral deposits, part B, Case studies and research topics: Reviews in Economic Geology, v. 6B, p. 373–432.

Smit, Hans, 1999, The Dry Creek VMS project, Bonnifield district, central Alaska, *in* Pathways ‘99, Extended abstracts volume: Vancouver, British Columbia, Canada, British Columbia and Yukon Chamber of Mines, p. 17–18.

U.S. Environmental Protection Agency, 2003, National primary drinking water standards: U.S. Environmental Protection Agency Report EPA 816–F–03–016. (Also available online at *http://www.epa.gov/safewater/mcl.html*.)

The Biogeochemistry and Occurrence of Unusual Plant Species Inhabiting Acidic, Metal-Rich Water, Red Mountain, Bonnifield District, Alaska Range

By Larry P. Gough, Robert G. Eppinger, and Paul H. Briggs

Chapter J of
Recent U.S. Geological Survey Studies in the Tintina Gold Province, Alaska, United States, and Yukon, Canada—Results of a 5-Year Project
Edited by Larry P. Gough and Warren C. Day

Scientific Investigations Report 2007–5289–J

U.S. Department of the Interior
U.S. Geological Survey

Contents

Figures

Tables

The Biogeochemistry and Occurrence of Unusual Plant Species Inhabiting Acidic, Metal-Rich Water, Red Mountain, Bonnifield District, Alaska Range

By Larry P. Gough,[1] Robert G. Eppinger,[1] and Paul H. Briggs[1]

Abstract

This report presents results on the occurrence and biogeochemistry of unusual plant species, and of their supporting sediment, in an undisturbed volcanogenic massive sulfide deposit in the Tintina Gold Province (see fig. 1 of Editors' Preface and Overview). The extraordinary plant assemblage found growing in the acidic metal-rich waters that drain the area is composed predominantly of bryophytes (liverworts and mosses). Ferricrete-cemented silty alluvial sediments within seeps and streams are covered with the liverwort *Gymnocolea inflata*, whereas the mosses *Polytrichum commune* and *P. juniperinum* inhabit the area adjacent to the water and within the splash zone. Both the liverwort-encrusted sediment and *Polytrichum* thalli have high concentrations of major- and trace-metal cations (for example, Al, As, Cu, Fe, Hg, La, Mn, Pb, and Zn). Soils in the area do not reflect the geochemical signature of the mineral deposit, and we suspect that they are most influenced by the chemistry of airborne dust (aeolian material) derived from outside the area.

Introduction

In June 2004, we began investigating the occurrence, general ecology, and biogeochemistry of plants growing in association with acidic metal-rich water associated with the Red Mountain volcanogenic massive sulfide (VMS) deposit (Gough and others, 2006; Dusel-Bacon and others, this volume, chap. B; Eppinger and others, this volume, chap. I, Hubbard and others, this volume, chap. E). These unusual plant assemblages included liverworts and mosses (bryophytes) as well as forbs, grasses and shrubs, especially willow (*Salix*).

Many terrestrial and aquatic bryophytes are known to accumulate large amounts of metals through direct ion exchange at the leaf surface and have been used in both mineral exploration studies and as biomonitors of airborne metal deposition. Some bryophytes are found most commonly on substrates that are high in particular bioavailable metals (for example copper or lead) and may actually be restricted to this type of substrate (Shacklette, 1967; Shaw, 1987). Field studies of these occurrences are important for understanding the habitat requirements of rare or unusual species and for a full appreciation of the ecology of mineralized areas.

Geological and Ecological Setting

The Bonnifield mining district, and the Red Mountain VMS deposit, are part of the Tintina Gold Province (TGP). Red Mountain (fig. J1) has been the target of past mineral exploration activity. A detailed discussion of the geology and mineral potential of the Bonnifield mining district is given

Figure J1. U.S. Geological Survey scientist examining alteration zone rocks of Red Mountain. Photograph by R.G. Eppinger.

[1]U.S. Geological Survey.

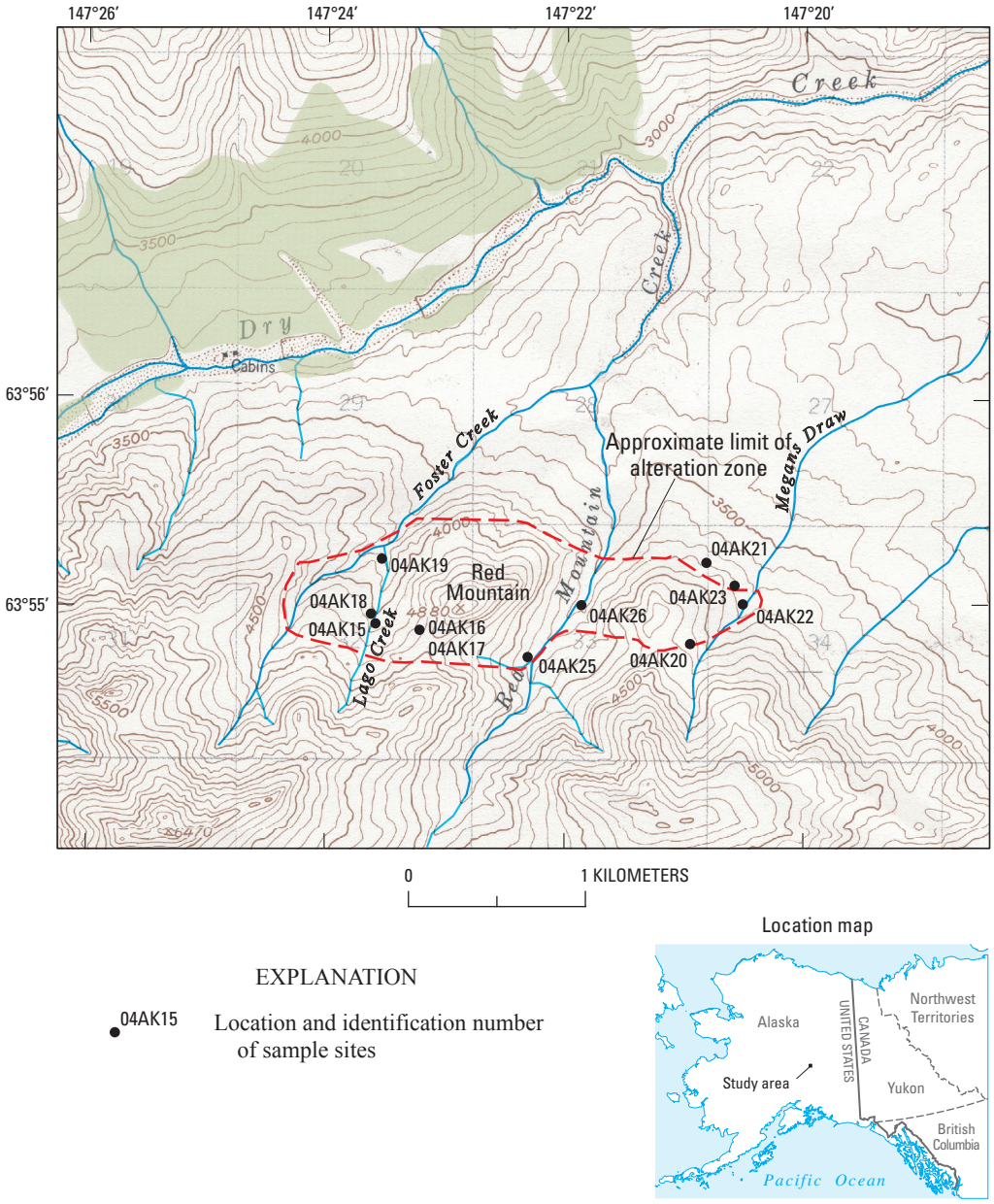

Figure J2. Map showing locations and identification numbers of sampling site locations within and near the Red Mountain volcanogenic massive sulfide deposit alteration zone. Red Mountain, Lago Creek, Foster Creek, and Megans Draw are all local names. Base map from U.S. Geological Survey Healy D–1 quadrangle, scale 1:63,360; contour interval 100 ft (30.48 m).

by Eppinger and others (2004), Dusel-Bacon and others (this volume, chap. B); and Eppinger and others (this volume, chap. I). In brief, Red Mountain is a pyrite-rich VMS deposit containing sphalerite, galena, chalcopyrite, and, locally, precious metals as outcropping and concealed massive to semimassive sulfides. A primary quartz-sericite-pyrite alteration zone (QSPAZ) is extensive, and pyrite oxidation is prevalent (fig. J2; see also fig. I1 in Eppinger and others, this volume, chap. I).

Red Mountain lies on the north slope of the Alaska Range foothills. The altitude of most of the Red Mountain study area (800 meters (m) to 1,800 m) is above the tree limit, and alpine tundra shrubs, grasses, sedges, and forbs dominate the vegetation. Many of the steep slopes are covered with scree and rubble whose stability is decreased by the rapid physical and chemical weathering of the extensive sulfidic alteration zone. Both permanent and intermittent streams, seeps, and springs permeate the slopes and ravines. In the mineralized areas, the submerged and emergent aquatic vegetation is dominated by bryophytes. Forbs and shrubs such as Labrador tea, spirea, cassiope, crowberry, and blueberry dominate the drier areas between the seeps, where there is a layer of soil. Willow, grasses, and sedges are common in the riparian zone immediately within and beside the several permanent streams that drain both the mineralized and nonmineralized areas.

Methods

We did not attempt to sample and analyze individual liverwort thalli (plant body), as they are very small (commonly

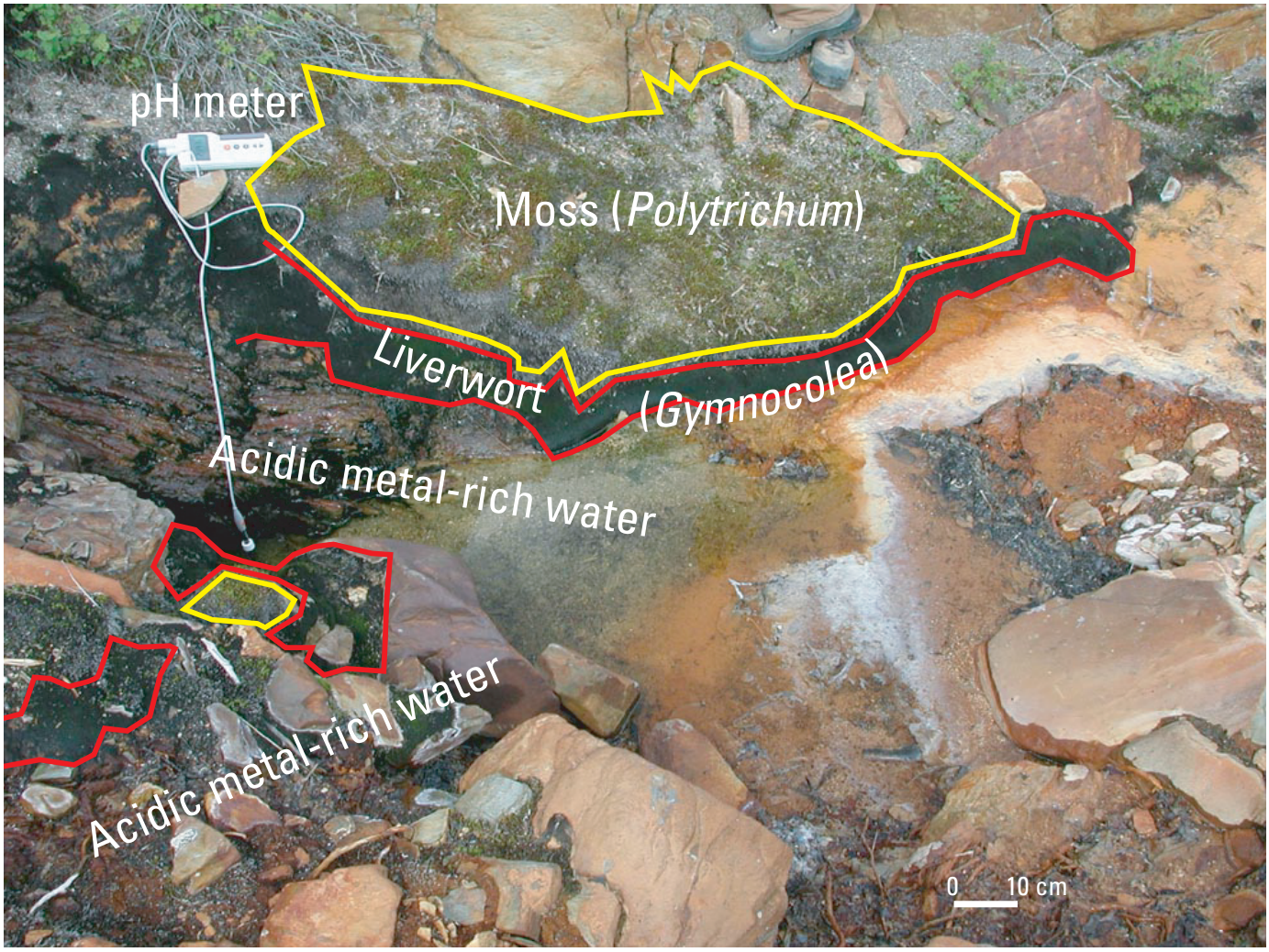

Figure J3. Liverwort and moss species growing in areas influenced by acidic waters. *Gymnocolea inflata*, *Pohlia obtusifolia* (not shown), and *Polytrichum juniperinum* mixed with *P. commune*. Photograph by R.G. Eppinger.

less than 1 millimeter, mm), compact, and grow in intimate association with the silty iron-rich sediments of the seeps and streams. We did, however, sample the composite iron- and organic-rich liverwort sediment substrate.

Samples of the mosses *Polytrichum commune* and *P. juniperinum*, nearby soils, and diamondleaf willow (*Salix pulchra*) leaves were collected for chemical analysis. The soils are poorly developed Gelisols that are dominated by silty colluvium. All geochemical data for this report can be found in Giles and others (2007).

Results and Discussion

Bryophyte Assemblage

The reader is referred to Gough and others (2006) for complete scientific referencing and more detailed results of our investigations. Figure J3 shows a typical bryophyte association found in or near acidic seeps and springs in the QSPAZ (fig. J2). From a distance, the stream or seep bryophyte-inhabited areas appeared black because of the visual dominance of the liverwort *Gymnocolea inflata*. At Red Mountain the liverwort occurred both in very damp sites and in areas with flowing water.

It is frequently observed that certain moss genera and a few liverworts are most common on, if not completely restricted to, substrates enriched with bioavailable heavy metals (Shaw, 1987). It is unclear, however, whether the bryophytes in this assemblage are simply acidophilic or actually require an abundance of a particular heavy metal such as copper. Also found in association with *G. inflata*, but much less common, was the moss *Pohlia obtusifolia*; we could find no mention in the literature of its association with acidic waters.

Of particular interest was the appearance of a mix of the haircap mosses *Polytrichum commune* and *P. juniperinum* within the splash zone of the seeps and small streams (fig. J3). At Red Mountain the acidic, metal-rich waters are an

important component of the *Polytrichum* habitat. When ice free, the water is introduced both through capillary upward movement and aerial spray deposition. The moss grows in polsters (small mounds) that are 10 to 20 centimeters (cm) high (fig. J3) and occurs in luxuriant mixed populations when present near the seeps. We found no mention in the literature of *Polytrichum* being associated with highly acidic mineralized substrates or waters.

Bryophyte Substrate Geochemistry

Eppinger and others (this volume, chap. I) characterize the waters within the quartz-sericite-pyrite alteration zone (QSPAZ) as sulfate dominant with high concentrations of Al, Cd, Co, Cu, Fe, Mn, Ni, Pb, Y, Zn, and the rare-earth elements; and to a lesser extent F^- and Si. Upstream of the alteration zone they found that all streams had pH values of 6.5 or greater and conductivities from 370 to 830 microsiemens per centimeter (µS/cm), whereas within the QSPAZ, pH values below 3.5 (as low as 2.4) and conductivities above 2,500 µS/cm (up to 3,400) were common. Within the portion of the QSPAZ where this bryophyte association was observed, the pH of the water in 2003 varied from 2.7 to 3.3 (with conductivities of 1,270 to 3,410 µS/cm) and in 2004 varied from 2.6 to 4.5 (with conductivities of 1,350 to 4,800 µS/cm).

The water within and immediately below the QSPAZ had extremely high concentrations of trace elements; for example, Zn (mean, 41,000 micrograms per liter (µg/L); median, 13,000 µg/L), Mn (mean, 8,500 µg/L; median, 4,200 µg/L), and the rare-earth elements (mean, 6,100 µg/L, median 3,200 µg/L). Other metals having high concentrations and associated high means include Al, Fe, Cd, and Cu, and to a lesser extent Co, Ni, and Pb.

Compared to both the Red Mountain soils and surficial materials throughout Alaska, the Red Mountain iron-rich sediment samples showed notably higher concentrations of As, Cu, Fe, Hg, La, Pb, S, and Sb (Gough and others, 1988, 2006). Concentrations of other elements in sediment associated with VMS deposits (Co, Cr, Mn, Ni, and Zn) either differed little from amounts found in Red Mountain soils and Alaska surficial materials or contained somewhat less. This is due to the predominance of aeolian dust, from outside the area, that is incorporated into these soils (Gough and others, 2001, 2005).

Element Concentrations of Moss

Concentrations of elements in the dry material of a *Polytrichum commune* and *P. juniperinum* mix are reported in table J1. Also listed for comparison are data for another terrestrial moss, *Hylocomium splendens*, collected in an unmineralized area of the Kenai Peninsula of Alaska (Severson and others, 1990). Although these two species have different growth habits, both are often found together in high latitude alpine and subalpine areas. We do not know how similar their inorganic chemistries would be if collected contiguously, but the concentration of some of the major elements in these two populations is quite similar (Mg, K, and P). The trace element and metal cation levels in *Polytrichum* from Red Mountain are considerably higher than the levels in *Hylocomium* (As, Cu, Fe, Hg, Mn, Pb, Zn, and the rare-earth elements La, Ce, as well as Y). We assume that

Table J1. Comparison of the average concentration of selected elements in haircap mosses (Red Mountain, volcanogenic massive sulfide deposit) and in feather moss from a nonmineralized area in Alaska (Severson and others, 1990).

[Concentrations are in parts per million, dry weight basis, except as noted; n.d., not determined.]

Element	Haircap mosses[1] mean (n=4)	Feather moss[2] geometric mean (n=21)
Ash yield[3]	7.5	7.5
Aluminum (Al)	7,870	3,740
Antimony (Sb)	0.4	n.d.
Arsenic (As)	2.3	0.14
Barium (Ba)	93	69
Cadmium (Cd)	2.2	n.d.
Calcium (Ca)	2,200	6,830
Cerium (Ce)	210	1.3
Chromium (Cr)	2.4	3.4
Cobalt (Co)	2.1	1.1
Copper (Cu)	290	4.6
Galium (Ga)	2.6	0.9
Iron (Fe)	6,170	1,740
Lanthanum (La)	75	1.2
Lead (Pb)	120	2.1
Magnesium (Mg)	1,590	1,620
Manganese (Mn)	130	450
Mercury (Hg)	0.25	0.09
Nickel (Ni)	2.9	2.0
Phosphorus (P)	920	1,200
Sodium (Na)	320	1,320
Selenium (Se)	0.26	0.06
Strontium (Sr)	8.6	44
Sulfur (S)	n.d.[4]	720
Titanium (Ti)	120	170
Vanadium (V)	6.2	5.3
Yttrium (Y)	20	0.94
Zinc (Zn)	570	34

[1] *Polytrichum commune* and *P. juniperinum* mix

[2] *Hylocomium splendens*

[3] percent

this difference is the direct result of element uptake from the large dissolved metal load in the water that bathes the moss and of the bioavailable forms of these metals in the sediment.

Conclusions

The Red Mountain quartz-sericite-pyrite alteration zone (QSPAZ), and the VMS deposit that it is part of, are characterized as having acidic (as low as pH 2.4) metal-rich, high sulfate waters, active ferricrete formation in the silty alluvial sediments, and an abundance of primary (pyrite) and secondary (sulfate) acid-generating minerals. Areas such as Red Mountain are an important ecological niche because they support the presence of rare or unusual species. The seep, spring, and stream habitats contain an extraordinary bryophyte community dominated by the liverwort *Gymnocolia inflata* in the areas with standing or flowing water and the mosses *Polytrichum commune* and *P. juniperinum* adjacent to, but elevated above, the water. Both the sediment upon which the liverwort grows and the *Polytrichum* thalli that receive acidic metal-laden spray have high concentrations of some major and trace metals, especially As, Cd, Cu, Fe, Hg, Pb, and Zn. We were unable to determine whether *G. inflata* requires an acidic environment or, alternatively, high concentrations of a specific dissolved metal, such as copper. The moss assemblage of *P. commune* and *P. juniperinum* that dominates the vegetation of the splash zone near the acidic metal-rich waters is truly unusual and we could find no report in the literature of similar observations.

The shallow Gelisol soils that are found throughout the QSPAZ alteration zone are, in general, similar in their major and trace element chemistry to soils found throughout Alaska due to the influx of airborne dust.

Acknowledgments

Dr. JoAnn W. Flock, University of Colorado, and Dr. Won S. Hong, University of Great Falls, aided in the identification of the mosses and liverworts. Chemical analyses were preformed by Monique Adams, Zoe Ann Brown, and Cathy Ager.

References Cited

Eppinger, R.G., Briggs, P.H., and Dusel-Bacon, Cynthia, 2004, Environmental geochemistry of an undisturbed volcanogenic massive sulfide deposit, Red Mountain, Bonnifield mining district, east-central Alaska, *in* Wanty, R.B., and Seal, R.R. II, eds., Water-Rock Interaction, Proceedings of the Eleventh International Symposium on Water-Rock Interaction, Saratoga Springs, N.Y., June 27–July 2, 2004: London, Taylor and Francis Group Publishers, p. 1483–1487.

Giles, S.A., Eppinger, R.G., Granitto, Matthew, Zelenak, P.P., Adams, M.G., Anthony, M.W., Briggs, P.H., Gough, L.P., Hageman, P.L., Hammarstrom J.M., Horton, J.D., Sutley, S.J., Theodorakos, P.M., and Wolf, R.E., 2007, Geochemical data for stream-sediment, surface-water, rock, and vegetation samples from Red Mountain (Dry Creek), an unmined volcanogenic massive sulfide deposit in the Bonnifield district, Alaska Range, east-central Alaska: U.S. Geological Survey Data Series DS–204, 64 p., CD-ROM. (Also available online at *http://pubs.usgs.gov/ds/2006/204/*.)

Gough, L.P., Crock, J.G., Day, W.C., and Vohden, Jim, 2001, Biogeochemistry of arsenic and cadmium, Fortymile River watershed, east-central Alaska, *in* Gough, L.P., and Wilson, F.H., eds., Geological studies in Alaska by the U.S. Geological Survey: U.S. Geological Survey Professional Paper 1633, p. 109–126. (Also available online at *http://pubs.usgs.gov/pp/p1633/*.)

Gough, L.P., Day, W.C., Crock, J.G., Gamble, B.M., Henning, M.W., Ager, C.M., Meier, A.L., Briggs, P.H., Brown, Z.A., and Adams, M., 2005, Regional geochemical results from the analyses of rock, soil, and vegetation samples—Big Delta B–2 quadrangle, Alaska: U.S. Geological Survey Open-File Report 2005–1431, available only online at *http://pubs.usgs.gov/of/2005/1431/*. (Accessed August 13, 2007.)

Gough, L.P., Eppinger, R.G., Briggs, P.H., and Giles, S., 2006, Biogeochemical characterization of an undisturbed highly acidic, metal-rich bryophyte habitat, east-central Alaska, U.S.A.: Arctic, Antarctic, and Alpine Research, v. 38, no. 4, p. 522–529.

Gough, L.P., Severson, R.C., and Shacklette, H.T., 1988, Element concentrations in soils and other surficial materials of Alaska: U.S. Geological Survey Professional Paper 1458, 53 p. (Also available online at *http://geopubs.wr.usgs.gov/prof-paper/pp1458/*.)

Severson, R.C., Crock, J.G., and Gough, L.P., 1990, An assessment of the geochemical variability for plants and soils and an evaluation of industrial emissions near the Kenai National Wildlife Refuge, Alaska: U.S. Geological Survey Open-File Report 90–306, 90 p. (Also available online at *http://pubs.er.usgs.gov/usgspubs/ofr/ofr90306*.)

Shacklette, H.T., 1967, Copper mosses as indicators of metal concentrations: U.S. Geological Survey Bulletin 1198–G, 18 p. (Also available online at *http://pubs.er.usgs.gov/usgspubs/b/b1198G/*.)

Shaw, J., 1987, Evolution of heavy metal tolerance in bryophytes II; An ecological and experimental investigation of the "copper moss," *Scopelophila cataractae* (Pottaceae): American Journal of Botany, v. 74, no. 6, p. 813–821.

U.S. Geological Survey Reports on the Tintina Gold Province—Products of Recent Mineral Resources Program Studies

By Larry P. Gough

Chapter K of

Recent U.S. Geological Survey Studies in the Tintina Gold Province, Alaska, United States, and Yukon, Canada—Results of a 5-Year Project

Edited by Larry P. Gough and Warren C. Day

Scientific Investigations Report 2007–5289–K

U.S. Department of the Interior
U.S. Geological Survey

U.S. Geological Survey Reports on the Tintina Gold Province—Products of Recent Mineral Resources Program Studies

By Larry P. Gough[1]

Crock, J.G., Briggs, P.H., Gough, L.P., Wanty, R.B., and Brown, Z.A., 2007, Regional geochemical results from the reanalysis of NURE stream sediment samples–Eagle 3° quadrangle, east-central Alaska: U.S. Geological Survey Open-File Report 2007–1075, available only online at *http://pubs.usgs.gov/of/2007/1075/*. (Accessed August 13, 2007.)

Crock, J.G., Seal, R.R., II, Gough, L.P., and Weber-Scannell, P., 2003, Results of elemental and stable isotopic measurements, and dietary composition of Arctic grayling (*Thymallus arcticus*) collected in 2000 and 2001 from the Fortymile River watershed, Alaska: U.S. Geological Survey Open-File Report 03–057, 28 p. (Also available online at *http://pubs.usgs.gov/of/2003/ofr-03-057/*.)

Day, W.C., Aleinikoff, J.N., Roberts, Paul, Smith, Moira, Gamble, B.M., Henning, M.W., Gough, L.P., and Morath, L.C., 2003, Geologic map of the Big Delta B–2 quadrangle, east-central Alaska: U.S. Geological Survey Geologic Investigations Series I–2788, 1 map plus text. (Also available online at *http://pubs.usgs.gov/imap/i-2788/*.)

Day, W.C., O'Neill, J.M., Aleinikoff, J.N., Green, G.N., Saltus, R.W., and Gough, L.P., 2007, Geologic map of the Big Delta B–1 quadrangle, east-central Alaska: U.S. Geological Survey Scientific Investigations Map I–2975, scale 1:63,360. (Also available online at *http://pubs.usgs.gov/sim/2007/2975/*.)

Dusel-Bacon, Cynthia, and Harris, A.G., 2003, New occurrences of late Paleozoic and Triassic fossils from the Seventymile and Yukon-Tanana terranes, east-central Alaska, with comments on previously published occurrences in the same area, *in* Galloway, J.P., ed., Studies by the U.S. Geological Survey in Alaska, 2001: U.S. Geological Survey Professional Paper 1678, p. 5–30. (Also available online at *http://pubs.er.usgs.gov/usgspubs/pp/pp1678*.)

Dusel-Bacon, Cynthia, Hopkins, M.J., Mortensen, J.K., Dashevsky, S.S., Bressler, J.R., and Day, W.C., 2006, Paleozoic tectonic and metallogenic evolution of the pericratonic rocks of east-central Alaska and adjacent Yukon, *in* Colpron, Maurice, and Nelson, J.L., eds., Paleozoic evolution and metallogeny of pericratonic terranes at the ancient Pacific margin of North America, Canadian and Alaskan Cordillera: Geological Association of Canada, Special Paper 45, p. 25–74.

Dusel-Bacon, Cynthia, Mortensen, J.K., and Fredericksen, R., 2003, Cretaceous epigenetic base-metal mineralization at the Lead Creek prospect, eastern Yukon-Tanana Upland, Alaska; Constraints from U-Pb zircon dating and Pb-isotopic analyses of sulfides, *in* Galloway, J.P., ed., Studies by the U.S. Geological Survey in Alaska, 2001: U.S. Geological Survey Professional Paper 1678, p. 31–40. (Also available online at *http://pubs.er.usgs.gov/usgspubs/pp/pp1678*.)

Dusel-Bacon, Cynthia, Slack, J.F., and Belkin, H.E., 2007, The magmatic to hydrothermal transition in peralkaline-hosted VMS systems—An example from the Bonnifield district, east-central Alaska, USA, *in* Andrew, C.J., ed., Proceedings of the 9th Biennial Meeting of the Society for Geology Applied to Mineral Deposits, August 20–23, 2007, Mineral Exploration and Research: Dublin, Ireland, Irish Association for Economic Geology, v. 2, p. 1045–1048.

[1]U.S. Geological Survey.

Dusel-Bacon, Cynthia, Wooden, J.L., and Hopkins, M.J., 2004, U-Pb zircon and geochemical evidence for bimodal mid-Paleozoic magmatism and syngenetic base-metal mineralization in the Yukon-Tanana terrane, Alaska: Geological Society of America Bulletin, v. 116, no. 7–8, p. 989–1015.

Dusel-Bacon, Cynthia, Wooden, J.L., and, Layer, P.W., 2003, A Cretaceous ion-microprobe U-Pb zircon age for the West Point orthogneiss; Evidence for another gneiss dome in the Yukon-Tanana Upland, *in* Galloway, J.P., ed., Studies by the U.S. Geological Survey in Alaska, 2001: U.S. Geological Survey Professional Paper 1678, p. 41–60. (Also available online at *http://pubs.er.usgs.gov/usgspubs/pp/pp1678*.)

Eppinger, R.G., Briggs, P.H., and Dusel-Bacon, Cynthia, 2004, Environmental geochemistry of an undisturbed volcanogenic massive sulfide deposit, Red Mountain, Bonnifield mining district, east-central Alaska, *in* Wanty, R.B., and Seal, R.R., II, eds., Water-rock interaction, Proceedings of the 11th International Symposium on Water-Rock Interaction, Saratoga Springs, N.Y., June 22–July 2, 2004: London, Taylor and Francis Group, p. 1483–1487.

Eppinger, R.G., Briggs, P.H., Dusel-Bacon, Cynthia, Giles, S.A., Gough, L.P., Hammarstrom, J.M., and Hubbard, B.E., 2007, Environmental geochemistry at Red Mountain, an unmined volcanogenic massive sulfide deposit in the Bonnifield district, Alaska Range, east-central Alaska: Geochemistry: Exploration, Environment, Analysis, v. 7, no. 3, p. 207–223. (Also available online at *http://geea.geoscienceworld.org/cgi/content/abstract/7/3/207*.)

Giles, S.A., Eppinger, R.G., Granitto, Matthew, Zelenak, P.P., Adams, M.G., Anthony, M.W., Briggs, P.H., Gough, L.P., Hageman, P.L., Hammarstrom, J.M., Horton, J.D., Sutley, S.J., Theodorakos, P.M., and Wolf, R.E., 2007, Geochemical data for stream-sediment, surface-water, rock, and vegetation samples from Red Mountain (Dry Creek), an unmined volcanogenic massive sulfide deposit in the Bonnifield district, Alaska Range, east-central Alaska: U.S. Geological Survey Data Series DS–204, 64 p. CD-ROM. (Also available online at *http://pubs.er.usgs.gov/usgspubs/ds/ds204*.)

Goldfarb, R.J., Ayuso, R.A., Miller, M.L., Ebert, S.E., Marsh, E.E., Petsel, S.A., Miller, L.D., Bradley, D.C., Johnson, Craig, and McClelland, William, 2004, The Late Cretaceous Donlin Creek gold deposit, southwestern Alaska—Controls on epizonal ore formation: Economic Geology, v. 99, no. 4, p. 643–671.

Goldfarb, R.J., Baker, Timothy, Dube, Benoit, Groves, D.I., Hart, C.J.R., and Gosselin, Patrice, 2005, Distribution, character, and genesis of gold deposits in metamorphic terranes, *in* Hedenquist, J.W., Thompson, J.F.H., Goldfarb, R.J., and Richards, J.P., eds., One Hundredth Anniversary Volume of Economic Geology, 1905–2005: Littleton, Colo., Society of Economic Geologists, p. 407–450.

Gough, L.P., ed., 2004, Selected geochemical and biogeochemical studies of the Fortymile River watershed, Alaska: U.S. Geological Survey Professional Paper 1685, 54 p. (Also available online at *http://pubs.er.usgs.gov/usgspubs/pp/pp1685*.)

Gough, L.P., Crock, J.G., Seal, R.R., II, Wang, Bronwen, and Weber-Scannell, Phyllis, 2004, Biogeochemistry, stable isotopic composition, and feeding habits of Arctic grayling (*Thymallus arcticus*) in the lower Fortymile River, eastern Alaska, *in* Gough, L.P., ed., Selected geochemical and biogeochemical studies of the Fortymile River watershed, Alaska: U.S. Geological Survey Professional Paper 1685, p. 21–43. (Also available online at *http://pubs.er.usgs.gov/usgspubs/pp/pp1685*.)

Gough, L.P., Day, W.C., Crock, J.G., Gamble, B.M., Henning, M.W., Ager, C.M., Meier, A.L., Briggs, P.H., Brown, Z.A., and Adams, Monique, 2005, Regional geochemical results from the analyses of rock, soil, and vegetation samples—Big Delta B-2 quadrangle, Alaska: U.S. Geological Survey Open-File Report 2005–1431, 16 p., available only online at *http://pubs.usgs.gov/of/2005/1431/*. (Accessed August 13, 2007.)

Gough, L.P., Eppinger, R.G., Briggs, P.H., and Giles, S.A., 2006, Biogeochemical characterization of an undisturbed highly acidic, metal-rich bryophyte habitat, east-central Alaska, USA: Arctic, Antarctic, and Alpine Research, v. 38, no. 4, p. 522–529.

Gough, L.P., Wang, Bronwen, Smith, D.B., and Gustavsson, Nils, 2005, Geochemical landscapes of Alaska—New map presentations and interpretations for 23 elements in surficial materials: U.S. Geological Survey Professional Paper 1716, 36 p. (Also available online at *http://pubs.usgs.gov/pp/2005/1716*.)

Groves, D.I., Goldfarb, R.J., Robert, Francois, and Hart, C.J.R., 2003, Gold deposits in metamorphic belts; overview of current understanding, outstanding problems, future research, and exploration significance: Economic Geology, v. 98, no. 1, p. 1–29.

Hart, C.J.R., and Goldfarb, R.J., 2005, Distinguishing intrusion-related from orogenic gold systems, *in* Realising New Zealand's mineral potential, Proceedings of the Australian Institute of Mining and Metallurgy, 2005 New Zealand Minerals Conference, Auckland, New Zealand, November 13–16, 2005: Wellington, New Zealand, Ministry of Economic Development Crown Minerals Group, p. 125–133.

Hart, C.J.R., Goldfarb, R.J., Lewis, L.L., and Mair, J.L., 2004, The northern Cordilleran mid-Cretaceous Plutonic province—Ilmenite/magnetite series granitoids and intrusion-related mineralization: Resource Geology, v. 54, no. 3, p. 253–280.

Hart, C.J.R., Mair, J.L., Goldfarb, R.J., and Groves, D.I., 2004, Source and redox controls on metallogenic variations in intrusion-related ore systems, Tombstone-Tungsten belt, Yukon Territory, Canada, *in* Ishihara, Shunso, Stephens, W.E., Harley, S.L., Arima, Makoto, and Nakajima, Takashi, eds., Fifth Hutton Symposium on the Origin of Granites and Related Rocks, Proceedings, Toyohashi, Japan, September 2–6, 2003: Transactions of the Royal Society of Edinburgh, v. 95, parts 1–2, p. 339–356.

Hart, C.J.R., Mair, J.L., Groves, D.I., and Goldfarb, R.J., 2003, The influence of source variations on redox state and metallogeny of a cross-orogen plutonic province, Yukon, Canada, *in* The origin of granites and related rocks, Hutton Symposium V: Geological Survey of Japan, Interim Report 29, 42 p.

Hart, C.J.R., Villeneuve, M.E., Mair, J.L., Goldfarb, R.J., Selby, D., Creaser, R.A., and Wijns, C., 2004, The duration of magmatic-hydrothermal ore systems—Comparative U-Pb SHRIMP & TIMS, Re-Os and Ar-Ar geochronology of mineralizing plutons in Yukon and Alaska, *in* Muhling, T., and others, eds., SEG 2004—Predictive Mineral Discovery Under Cover, Extended abstracts: University of Western Australia Publication 33, p. 347–349.

Hubbard, B.E., Rowan, L.C., Dusel-Bacon, Cynthia, and Eppinger, R.G., 2007, Geologic mapping and mineral resource assessment of the Healy and Talkeetna Mountains quadrangles, Alaska using minimal cloud- and snow-cover ASTER data: U.S. Geological Survey Open-File Report 2007–1046, 18 p. (Also available online at *http://pubs.usgs.gov/of/2007/1046/*.)

Jia, Yiefei, Kerrich, Robert, and Goldfarb, R.J., 2003, Metamorphic origin of the ore-forming fluid for orogenic gold-bearing quartz vein systems in the North American Cordillera; Constraints from $\delta^{15}N$, δD, and $\delta^{18}O$: Economic Geology, v. 98, p. 109–123.

Macalady, D.L., Ritter, Kaylene, Redman, A.D., and Skold, Magnus, 2004, Comparative characteristics of natural organic matter in the Fortymile River, Alaska, *in* Gough, L.P., ed., Selected geochemical and biogeochemical studies of the Fortymile River watershed, Alaska: U.S. Geological Survey Professional Paper 1685, p. 45–52. (Also available online at *http:/pubs.er.usgs.gov/usgspubs/pp/pp1685*.)

Mair, J.L., Goldfarb, R.J., Johnson, C.A., Hart, C.J.R., and Marsh, E.E., 2006, Geochemical constraints on the genesis of the Scheelite Dome intrusion-related gold deposit, Tombstone gold belt, Yukon, Canada: Economic Geology, v. 101, no. 3, p. 523–553.

Marsh, E.E., Goldfarb, R.J., Hart, C.J.R., and Johnson, C.A., 2003, Geology and geochemistry of the Clear Creek intrusion-related gold occurrences, Tintina gold province, Yukon, Canada: Canadian Journal of Earth Sciences, v. 40, no. 5, p. 681–699.

Mortensen, J.K., Dusel-Bacon, Cynthia, Hunt, Julie, and Gabites, Janet, 2006, Lead isotopic constraints on the metallogeny of middle and late Paleozoic syngenetic base metal occurrences in the Yukon-Tanana and Slide Mountain/Seventymile terranes and adjacent portions of the North American miogeocline, *in* Colpron, Maurice, and Nelson, J.L., eds., Paleozoic evolution and metallogeny of pericratonic terranes at the ancient Pacific margin of North America, Canadian and Alaskan Cordillera: Geological Association of Canada Special Paper 45, p. 261–279.

Mueller, S.H., Goldfarb, R.J., Hart, C.J.R., Mair, J.L., Marsh, E.E., and Rombach, C.S., 2004, The Tintina gold province, Alaska and Yukon—New world-class gold resources and their sustainable development: Australasian Institute of Mining and Metallurgy, v. 5, p. 189–198.

Mueller, S.H., Goldfarb, R.J., Miller, M.L., Munk, L.A., Sanzolone, R.F., Lamothe, P.J., Adams, Monique, Briggs, P.H., McClesky, R.B., and Theodorakos, P.M., 2003, Surface and ground water geochemistry near the Donlin Creek gold deposit, southwestern Alaska: U.S. Geological Survey Open-File Report 03–492, 37 p. (Also available online at *http://pubs.usgs.gov/of/ofr-03-492/*.)

Mueller, S.H., Hart, C.J.R., Goldfarb, R.J., Munk, L.A., and Diment, R., 2004, Post-mining hydrogeochemical conditions, Brewery Creek gold deposit, central Yukon, *in* Emond, D.S., and Lewis, L.L., eds., Yukon exploration and geology 2003: Whitehorse, Yukon, Yukon Geological Survey, p. 271–280.

Nelson, J.L., Colpron, Maurice, Piercey, S.J., Dusel-Bacon, Cynthia, Murphy, D.C., and Roots, C.F., 2006, Paleozoic tectonic and metallogenetic evolution of pericratonic terranes in Yukon, northern British Columbia and eastern Alaska, *in* Colpron, Maurice, and Nelson, J.L., eds., Paleozoic evolution and metallogeny of pericratonic terranes at the ancient Pacific margin of North America, Canadian and Alaskan Cordillera: Geological Association of Canada Special Paper 45, p. 323–360.

Oliver, D.H., and Dusel-Bacon, Cynthia, 2003, Kinematic analysis from tectonites in the northern part of the Big Delta quadrangle, east-central Alaska, *in* Galloway, J.P., ed., Studies by the U.S. Geological Survey in Alaska, 2001: U.S. Geological Survey Professional Paper 1678, p. 61–70. (Also available online at *http://pubs.er.usgs.gov/usgspubs/pp/pp1678*.)

Piercey, S.J., Nelson, J.L., Colpron, Maurice, Dusel-Bacon, Cynthia, Simard, R-L., and Roots, C.F., 2006, Paleozoic magmatism and crustal recycling along the ancient Pacific margin of North America, northern Cordillera, *in* Colpron, Maurice, and Nelson, J.L., eds., Paleozoic evolution and metallogeny of pericratonic terranes at the ancient Pacific margin of North America, Canadian and Alaskan Cordillera: Geological Association of Canada Special Paper 45, p. 281–322.

Saltus, R.W., and Day, W.C., 2006, Gravity and aeromagnetic gradients within the Yukon-Tanana upland, Black Mountain tectonic zone, Big Delta quadrangle, east-central Alaska: U.S. Geological Survey Open-File Report 2006-1391, poster, available only online at *http://pubs.usgs.gov/of/2006/1391/*.) (Accessed August 13, 2007.)

Verplanck, P.L., Mueller S.H., Goldfarb, R.J., and Nordstrom, D.K., 2007, Elevated arsenic in ground water, Ester Dome (Alaska), *in* Cidu, R., and Frau, F., eds., Water in mining environments, Proceedings, International Mine Water Association Symposium, Cagliari, Italy, May 27–31, 2007: Cagliari, Italy, University of Cagliari, p. 473–477.

Verplanck, P.L., Mueller, S.H., Goldfarb, R.J., Nordstrom, D.K., and Youcha, E.K., 2008, Geochemical controls of elevated arsenic concentrations in groundwater, Ester Dome, east-central Alaska: Chemical Geology, v. 255, no. 1–2, p. 160–172.

Verplanck, P.L., Mueller, S.H., Youcha, E.K., Goldfarb, R.J., Sanzolone, R.F., McCleskey, R.B., Briggs, P.H., Roller, M., Adams, Monique, and Nordstrom, D.K., 2003, Chemical analyses of ground and surface waters, Ester Dome, central Alaska, 2000-2001: U.S. Geological Survey Open-File Report 2003–244, 40 p. (Also available online at *http://pubs.usgs.gov/of/2003/ofr-03-244/*.)

Wang, Bronwen, Gough, L.P., Wanty, R.B., Vohden, Jim, Crock, J.G., and Day, W.C., 2006, Water and sediment chemical data and data summary of samples collected in 1999 and 2001 in the Goodpaster River basin, Big Delta B-2 quadrangle, Alaska: U.S. Geological Survey Open-File Report 2006–1131, 18 p. (Also available online at *http://pubs.usgs.gov/of/2006/1131/*.)

Wang, Bronwen, Wanty, R.B., and Vohden, Jim, 2004, Geochemical processes and geologic framework influencing surface-water and sediment chemistry in the Fortymile River watershed, east-central Alaska, *in* Gough, L.P., ed., Selected geochemical and biogeochemical studies of the Fortymile River watershed, Alaska: U.S. Geological Survey Professional Paper 1685, p. 3–19. (Also available online at *http://pubs.er.usgs.gov/usgspubs/pp/pp1685*.)

Tintina Gold Province Research Funded by the U.S. Geological Survey's Mineral Resources Program, External Research Program

For further information, see this Web site: *http://minerals.usgs.gov/mrerp/index.html/*.

Year 2005. Principal Investigator: G. Lang Farmer. Affiliation: University of Colorado, Boulder. Title: Petrogenesis of Cretaceous, gold-related plutons, eastern Tintina Gold Province (TGP), Alaska and Yukon–implications for ore genesis and resource distribution in the northern Cordillera.

Year 2006. Principal Investigator: Thomas Trainor. Affiliation: University of Alaska, Fairbanks. Title: Controls on antimony speciation and mobility in Legacy Mine tailings environments–a case study of mineral occurrences in the Tintina Gold Province, Alaska and Yukon.

Manuscript approved for publication December 27, 2007.
Prepared by the Reston and Raleigh Publishing Service Centers.
Edited by John M. Watson and Elizabeth D. Koozmin.
Graphics by Will R. Stettner.
Photocomposition by Cathy Y. Knutson.
For more information concerning the research in this report, contact the following
U.S. Geological Survey
Eastern Mineral Resources Science Center
12201 Sunrise Valley Drive, MS 954
Reston, VA 20192
703-648-6327
http://minerals.usgs.gov/east/index.html

USGS

Gough and Day, eds.—**Tintina Gold Province, Alaska, United States, and Yukon, Canada**—Scientific Investigations Report 2007–5289

ISBN 978-1-4113-2778-8